ORGANIC MATTER REMINERALIZATION IN COASTAL SEDIMENTS IN AND AROUND KANE‘OHE BAY, HAWAI‘I

A DISSERTATION SUBMITTED TO THE GRADUATE DIVISION OF THE UNIVERSITY OF HAWAI‘I AT MĀNOA IN PARTIAL FULFILLMENT OF THE REQUIREMENTS FOR THE DEGREE OF DOCTOR OF PHILOSOPHY IN OCEANOGRAPHY

AUGUST 2011

By:
Rebecca A. Briggs

Dissertation Committee:
Kathleen Ruttenberg (Chairperson), Brian Glazer, Fred Mackenzie, Margaret McManus, Megan Donahue

Keywords: biogeochemistry, coastal, sediments, redox, organic matter, porewater

"The cure for anything is salt water-sweat, tears, or the sea."

~Isak Dinesen

Acknowledgements

I would like to express my profound gratitude to my PhD advisor Kathleen Ruttenberg, who has been an exceptional role model and motivated me to become a better scientist. I am grateful for her guidance, patience and mentoring throughout my research.

I would also like to thank my thesis committee members, Brian Glazer, Fred Mackenzie, Margaret McManus, and Megan Donahue, for their support and supervision. I am fortunate to have worked with a group of exceptionally talented researchers that were generous with their time and advice, resulting in the success of the research presented in this dissertation.

The opportunity to become involved with the organization Paepae O He'eia, whose members maintain the historical and structural integrity of He'eia Fishpond, has been deeply appreciated. He'eia Fishpond is of cultural importance to the Hawaiian community and I was provided a unique experience in collaborating with the He'eia o'hana. The opportunity to conduct research at the fishpond and get to know the members of the o'hana has deeply impressed in me the importance of cultural understanding and mutual respect between science, tradition, and conservation.

I would also like to give a special thanks to my friends and fellow lab members: Marcie Grabowski, Dan Sulak, Chip Young, Danielle Hull, Jackie Padilla-Gamino, Jillian Ward, Karl Stein, and the numerous other volunteers who helped during fieldwork and within the laboratory making the completion of this study possible. I could not have conducted electrochemical work without the help of In-Chieh Chen and Amanda Ricardo, who spent countless hours polishing electrodes and collecting sediment porewater data.

Thanks are also due to the many others who have contributed indirectly to the success of the scientific work presented in this dissertation. Though the list is much too long to include in this space, without the support and generosity of my colleagues in the scientific community and the administrative staff of the Department of Oceanography and the University of Hawaii Seagrant Office, the research conducted would not have been possible. Within each chapter of this dissertation additional acknowledgements are given to the funding agencies and the people that directly contributed to that body of work.

And, most importantly, I owe my deepest gratitude to my close friends and family who have supported me through this incredible journey. **MAHALO**

Abstract

Nutrient cycles in shallow, near shore environments can be profoundly influenced by sediments, via the burial or release of nutrients through organic matter (OM) remineralization during diagenesis. The decomposition and burial of OM in sediments are key processes influencing biogeochemical cycles of nutrients (nitrogen, phosphorus) and carbon in coastal waters on time scales ranging from seasonal fluctuations to long, geologic timescales. This dissertation examines several aspects of OM remineralization in marine sediments, and addresses fundamental questions that link organic matter source, sediment redox state, and nutrient cycling. The studies described in this dissertation include development of new techniques that permit quantification and characterization of OM sources to marine sediments, which will be informative for OM preservation studies (Chapters 2-3); in the latter portion of this dissertation (Chapters 3-6), particular aspects of early diagenetic pathways of OM remineralization are examined. The studies described herein place constraints on sources and sinks of bioavailable nutrients in coastal sediments, including the flux of nutrients at the sediment-water interface. As such, the processes examined throughout this dissertation are essential to understanding coastal ocean biological productivity, and can shed light on transport of bioavailable nutrients from coastal waters to the open ocean. The research presented here was conducted in and around coastal Kane‘ohe Bay and, as such, reveals processes that may be unique to coastal systems adjacent to new, volcanogenic islands. However, many of the processes studied are more broadly operant, and insights into processes occurring within the coastal sediments of our study site can be readily extrapolated to other coastal systems.

Table of Contents

List of Tables

List of Figures

Chapter 1

Introduction and dissertation outline

1.1 Scope of work

The research described in this dissertation examines several aspects of organic matter (OM) remineralization in marine sediments, and addresses fundamental questions that link organic matter supply, sediment redox state, and nutrient cycling, including: (i) How does the quality versus the quantity of OM delivered to coastal marine sediments affect sediment redox state and rates of microbial mineralization of organic matter? (ii) How does the episodic delivery of OM to surface sediments, on a variety of time scales (daily, seasonally), impact sediment nutrient recycling, the magnitude of benthic nutrient efflux, and can it influence water column biological communities? (iii) Over what temporal and spatial scales do microbial respiratory pathways, and the consequent distribution of redox reactive chemical species, oscillate in response to shifts in benthic microbial activity. The research presented here was conducted in and around coastal Kane‘ohe Bay and, as such, reveals some processes that may be unique to coastal systems adjacent to new, volcanogenic islands. However, many of the processes studied in this dissertation are operant in all coastal marine sediments, and insights into processes occurring within the coastal sediments of our study site can be readily extrapolated to other coastal systems.

OM deposited in marine sediments is subjected to degradation and chemical alteration through a complex series of microbial respiratory pathways (e.g., Froelich et al 1979; Burdige 2006). A portion of degraded OM may be recycled into the overlying water as dissolved organic matter or inorganic nutrients, the products of OM remineralization. The residual material is incorporated into sediments, where it can be further degraded during burial. The decomposition and burial of OM in sediments are key processes influencing biogeochemical cycles of nutrients (nitrogen, phosphorus) and carbon in coastal waters on time scales ranging from seasonal fluctuations to long, geologic timescales. Nutrient cycling within coastal and continental margin sediments can account for 10-50% of the yearly primary production in overlying waters (Jorgensen 1983), and most of the organic carbon (94%) preserved in marine sediments is buried in continental margin sediments (Berner 1982; Hedges and Keil 1995). The results of the studies described in this dissertation provide novel insights into the factors controlling OM remineralization and the flux of nutrients at the sediment-water interface, which is

essential to understanding coastal ocean productivity and carbon cycling in the global ocean.

1.2 Dissertation research: Method development

Novel methods were developed as part of this dissertation research, without which it would not have been possible to address key hypotheses articulated in this dissertation. The first portion of this dissertation discusses the analytical method development work. Each new protocol underwent extensive testing using analog phases in order to ensure its applicability to natural marine sediments, as well as to rigorously document its precision and accuracy.

Organic carbon (OC) and total nitrogen (TN) concentration and isotopic composition are crucial parameters for interpreting source, quality, and degree of degradation of OM in marine sediments. Several of the coastal sediment sites examined in this study were enriched in carbonate phases (>50% carbonate minerals), and previously published methods, used to determine organic carbon concentrations and isotopic compositions (recently outlined in Komada et al. 2003), are inapplicable to carbonate-rich sediments. Specifically, the traditional acidification rinse method for preparing sediments results in a loss of labile OC from carbonate-rich sediments. **Chapter 2** describes a method that eliminates the loss of labile OC from carbonate-rich sediments using a combined coulometric-elemental analyzer-mass spectrometer approach for carbon and nitrogen quantification and isotopic analysis. The success of this method for quantifying OC concentration and isotopic composition in carbonate rich sediments permits use of a multi-tracer approach (OC and TN concentration and isotopic composition, and organic molar C:N:P ratios) to examine the source and degradation processes of OM within a range of depositional environments examined in this study.

Marine derived OM is generally more labile than its refractory, terrestrial counterpart (Aller et al. 1996; Cowie and Hedges 1992). In coastal marine environments, suspended particulates and deposited bottom sediments can be dominated by labile, cellular marine-derived OM. The ability to accurately quantify labile organic phosphorus (OP) is essential for quantifying living biomass phosphorus (P) and labile non-living OP, the pools most likely to generate mineralized P to support new cycles of primary

production. The SEDEX sequential extraction technique, used to separately quantify reservoirs of solid phase P in marine sediments, quantifies OP in the final step of the procedure. Therefore, the SEDEX method is not optimal for capturing and quantifying labile OP, which can be solubilized in prior steps and incorrectly quantified as inorganic P. In **Chapter 3** we evaluated the feasibility of inserting a Pre-Extraction step into the 'classical' SEDEX scheme, using the Bligh-Dyer (B-D) solution that solubilizes lipids and thus brings cellular OP into solution, in order to separately quantify labile OP in sediments.

1.3 Dissertation research: Field Studies

In **Chapter 4** variations in source (and therefore lability) of OM was systematically related to rates of OM degradation in coastal marine sediments. In this research, sediment cores collected along a shore-perpendicular transect were incubated and rates of microbial OM remineralization were estimated by examining O_2 consumption, H_2S production, and NH_4^+ accumulation in sediment porewaters. Combining estimates of the efficiency of OM remineralization with an analysis of OM sources, to depositional environments along a land-to-sea gradient, enables us to link the remineralization efficiency directly to OM source (e.g., terrestrial versus marine OM). Thus, providing insight into how OM source can impact preservation of organic carbon in marine sediments.

Depending upon the relative loading of different nutrients to an aquatic system, perturbations in nutrient ratios can shift phytoplankton community composition and influence water column productivity. Emplacement of OM to surface sediments during episodic events can alter sediment redox conditions and consequent nutrient retention/release. The impact of episodic input of labile OM in a coastal ecosystem is evaluated during a *Montipora capitata* coral spawning event in Kane'ohe Bay, Hawai'i. **Chapter 5** explicitly links the biogeochemical characteristics of spawning material to subsequent nutrient recycling pathways of spawn-derived organic material (SDOM). This study presents evidence for a water column phytoplankton bloom event triggered by the episodic input of labile SDOM and the subsequent recycling of nutrients from this OM source.

Finally, in **Chapter 6** we focus on OM remineralization pathways within sediments that influence the spatial distribution of reduction-oxidation (redox) reactive chemical species and dissolved metabolites generated from OM degradation. This research evaluates how the expansion and contraction of the oxygenated surficial sediment layer, driven by diurnal shifts between benthic photosynthesis and respiration, can influence the distribution and porewater accumulation of dissolved inorganic and organic nutrients. The shoaling of the oxic redox transition boundary alters down core distributions of redox reactive chemical species (such as ferrous iron), and influences the depth of the anoxic redox transition boundary (as identified by H_2S accumulation). Two distinct depositional environments were chosen for this research in order to examine the how OM source and physical sediment characteristics can influence these processes.

Chapter 7 concludes with a synthesis of the work presented throughout the dissertation, and examines how each research activity aids in our understanding of OM remineralization in coastal sediments.

Chapter 2

Quantifying organic carbon and nitrogen concentration and isotopic compositions in carbonate-dominated coastal marine sediments

with K. C. Ruttenberg, A. E. Ricardo, E. J. Gier, B. N. Popp

Abstract

Previous methods described for the quantification of organic carbon (OC) and total nitrogen (TN) concentrations in marine sediments using acidification for the removal of inorganic carbon (IC) are inapplicable to carbonate-rich (> 50 % by weight $CaCO_3$) sediments. Traditionally, an acidification rinse method has been applied to remove IC prior to quantification of OC and TN concentrations and isotopic composition. We show that application of this method to carbonate-rich sediments results in loss of labile OC (6.5-75.8 % loss) and nitrogen (0.9-27.9 % loss) during rinsing and, as a consequence, underestimates OC and TN. We describe a method that avoids OC loss using a combined coulometeric-elemental analyzer-mass spectrometer approach for carbon and nitrogen quantification and isotopic analysis. We quantified OC concentrations as the difference between TC and IC using coulometry to directly determine IC, and an elemental analyzer to determine total carbon (TC), thus avoiding problems associated with loss of labile OC during acidification and rinsing of carbonate-rich sediments. Total nitrogen (TN) and nitrogen isotopic values were determined on unacidified bulk sediment using an elemental analyzer-mass spectrometer. Although acidification rinse methods are not suitable for determination of OC and TN concentrations in carbonate-rich sediments, it is the only practical method for the determination of organic carbon $\delta^{13}C$ values. To evaluate whether bulk $\delta^{13}C$ values are compromised by OC loss during an acidification rinse treatment, we used the $\delta^{13}C$-$(C:P)_{org}$ metric for assessing organic matter source.

2.1 Introduction

Organic carbon and nitrogen concentration and isotopic composition are important and well-established parameters for interpreting source, quality, and degree of degradation of organic matter in marine sediments. Previously published methods used to determine organic carbon concentrations and isotopic compositions (recently outlined in Komada et al. 2003) are not appropriate for carbonate-rich (hereafter defined as >50% $CaCO_3$) sediments. In addition, previously published methods do not quantify total nitrogen concentrations and isotope composition in carbonate-dominated sediments. The absence of methods for determining organic carbon and nitrogen concentration and isotopic compositions in carbonate-dominated marine sediments represents a significant gap in our ability to quantify key carbon-cycle parameters in an important class of sedimentary environments. To redress this gap, we evaluated known methods for determining organic carbon and total nitrogen concentrations, as well as nitrogen isotopic values ($\delta^{15}N$) in marine sediments, and find that the most appropriate method for carbonate-rich sediments is a combined coulometeric-elemental analyzer-mass spectrometer approach. Organic carbon isotopic ($\delta^{13}C$) values must be determined on separate, paired splits of carbonate-rich sediment samples, using a suitable acidification rinse method (Komada et al. 2008).

Organic carbon in marine sediments is typically quantified via elemental analyzer after inorganic carbon is removed using a variety of acidification methods. Komada et al. (2008) outline three commonly used methods of acidification: i) the 'vaporous method,' in which samples are exposed to HCl vapor, ii) the 'aqueous method,' in which acid is directly applied to sediments without subsequent rinsing, and iii) the 'rinse method,' in which samples are acidified and then rinsed with Milli-Q ® deionized water (MQ-DI). These methods have significant limitations when applied to carbonate-rich sediments. The vaporous method does not completely remove carbonate minerals when sediments contain >33% carbonate (Hedges and Stern 1984; Komada et al. 2008). The most common method for the removal of inorganic carbon is the aqueous method (Hedges and Stern 1984), wherein samples are acidified, dried and reweighed post-acidification for analysis. However, the formation of hygroscopic salts ($CaCl_2$) occurs when the aqueous method is applied to carbonate-rich samples (see Assessment). Formation of $CaCl_2$

retains moisture and makes it impossible to obtain accurate weights for subsequent quantification of organic carbon and nitrogen contents via elemental analysis. Verardo et al. (1990) omitted drying prior to analysis by applying acid directly to pre-weighed sediments in analysis vessels. This method is impractical for carbonate-rich sediments, however, because the initial (pre-acidification) sample size required is too large to be accommodated by typical vessels used for elemental analysis. While the rinse method avoids the formation of hygroscopic salts and successfully removes inorganic carbon in carbonate-rich sediments, total organic carbon and nitrogen may be underestimated using this treatment due to loss of labile organic carbon (and nitrogen) during rinsing. Our study shows that although the rinse method is not suitable for determination of organic carbon and nitrogen concentrations in carbonate-rich sediments, it is the only practical method for determining organic carbon $\delta^{13}C$ values.

Isotopic data can be used to trace biogeochemical processes in marine environments (e.g., Lehmann et al. 2002), to assess sources and biological transformations of organic matter (e.g., McKee et al. 2002), and are useful in paleoecology studies (e.g., Wooller et al. 2003). $\delta^{15}N$ values are commonly determined on non-acidified sample splits via elemental analyzer coupled to a mass spectrometer. Organic C isotope values in sediments are routinely quantified by analysis of acidified samples. Despite the difficulty in obtaining organic C via acidification methods in carbonate-rich sediments (Komada et al. 2008), we are able to determine useful $\delta^{13}C$ values on acidified samples from our test sample sites using the rinse method of Komada et al. (2008). We discuss the impact of organic carbon loss, unavoidable when employing this rinse method, on resulting $\delta^{13}C$ values (see Assessment). It is worth noting that $\delta^{13}C$ and $\delta^{15}N$ values can not be quantified when employing alternative methods to analyze carbon concentration, such as on the residue of sediments that have been ashed to remove inorganic carbon (Gibbs 1977; Heath et al. 1977), or on evolved CO_2 resulting from oxidization and/or acidification methods (Mills and Quinn 1979).

In this paper we outline a method suitable for determining carbon and nitrogen concentration and nitrogen isotopic composition in carbonate-rich sediments. Because of the high total carbon to total nitrogen ratio (TC:TN) characteristic of carbonate-rich sediments we found it necessary to employ reference material with a high TC:TN ratio in

order to determine nitrogen concentrations. Our study-site transect included a gradient from terrestrial to marine dominated sedimentary organic matter (see Materials and Procedures section), enabling us to employ the coupled $\delta^{13}C$ -$(C:P)_{org}$ metric for identification of organic matter source (Ruttenberg and Goñi 1997a; Ruttenberg and Goñi 1997b) in order to evaluate the consistency of measured isotopic values with anticipated organic matter source.

2.2 Materials and procedures

Sediment collection: Sediment push cores were collected from a shore-perpendicular transect in Kane'ohe Bay, Hawai'i. Four sites with distinctly different sediment sites were sampled, and are hereafter defined as: i) Mangrove (collected under a mangrove canopy); ii) Terrigenous-Dominated (collected from a location proximal to riverine input); iii) Carbonate-Dominated (collected from a location distal to riverine input); and iv) Ocean (collected proximal to a coral reef within the bay). Sample sites were chosen to have distinct sources of organic matter and are characterized by systematically varying concentrations of $CaCO_3$ (see results Table 2.1). Sediment cores were sectioned at 0.25 to 1 cm intervals under an inert (N_2) atmosphere to prevent oxidation artifacts, and subsequently freeze-dried (Krall et al. 2009). From each site a surficial sediment sample and a sample from deeper within the cores (~8.5 cm) was ground with a mortar and pestle, sieved (<125 μm), and stored in a desiccator prior to analysis. The mortar and pestle were cleaned before and after each sample with dichloromethane and methanol to minimize cross-contamination of samples. Samples were analyzed at the Isotope Biogeochemistry Laboratory at the University of Hawai'i, Manoa.

Bulk sediment carbon and nitrogen analyses: Concentrations of inorganic carbon (IC) were quantified on untreated, ground samples using a Model 5011 Carbon Dioxide Coulometer coupled with a Model 5130 Acidification Module (UIC, Inc. Coulometrics) that detects carbon dioxide evolved after the addition of 5 mL 2 N perchloric acid. Optimal sample mass for each site was determined according to sample carbonate content (15-400 mg; Table 2.1) in order to keep CO_2 produced from the acidification of samples

Table 2.1 Method of analysis for carbon and nitrogen concentrations and isotopic compositions and approximate mass used for each analytical procedure. Sample mass for each analysis differs among sample sites due to the variable $CaCO_3$ content at each site.

		Ideal sample mass for analysis			
Method of Analysis	Parameter of Interest	**Mangrove Site (mg)**	**Terrigenous Dominated Site (mg)**	**Carbonate Dominated Site (mg)**	**Ocean Site (mg)**
CN[1]	TC, TN, $\delta^{15}N$	5	40	8	8
CN_{acid}[2]	$\delta^{13}C$, OC_{rinse}[4], TN_{rinse}[4]	5	25	10	10
Coulometer[3]	IC	400	100	20	15
		Calculated $CaCO_3$ (wt%)			
	$CaCO_3$[5]	*1.0*	*6.9*	*76.3*	*91.3*
		Gravimetric Correction Values			
	W_f/W_o[6]	*0.83*	*0.75*	*0.18*	*0.04*

[1] Unacidified samples analyzed with a Carlo Erba NA 2500 elemental analyzer coupled with a mass spectrometer (CN)
[2] Acidified samples analyzed with a Carlo Erba NA 2500 elemental analyzer coupled with a mass spectrometer (CN_{acid})
[3] Unacidified samples analyzed with a Model 5011 Carbon Dioxide Coulometer coupled with a Model 5130 Acidification Module
[4] Values obtained on acidified samples from which acid was removed via successive MQ-H_2O rinses, corrected for mass loss due to IC removed using gravimetric correction given by the following equation (for carbon): wt % OC_{rinse}= (ug carbon detected) / (ug sediment analyzed) * (W_f / W_o)
[5] Determined by converting coulometer IC concentration to wt% $CaCO_3$ assuming all IC is in the form of $CaCO_3$
[6] Initial, dry weights of bulk untreated sediments (W_o) and post acidification dry weights (W_f) allow gravimetric correction to OC_{rinse} and TN_{rinse} to account for mass lost during removal of IC (Hedges and Stern 1984). W_f/W_o values were empirically determined on each sediment interval. Reported values are averaged over surficial and deep intervals for each site and are provided solely as a guide for the application of this method to a different suite of sediment samples.

within the linear range of CO_2 produced from the acidification of pure calcium carbonate reference material, analyzed in parallel with the samples (Table 2.2).

Total carbon (TC) and total nitrogen (TN) concentrations and $\delta^{15}N$ values were quantified on untreated, ground samples using a Carlo Erba NA 2500 elemental analyzer, interfaced via a ConFlo II to a Delta Plus mass spectrometer (Finnigan, Inc), using the integrated signals of masses 44, 45 and 46 (for carbon) and masses 28, 29 and 30 (for nitrogen). Samples were weighed into 5 x 9 mm tin capsules (Costech Analytical ®), pre-cleaned by soaking in acetone. Sediment organic carbon concentrations (OC_{diff}) were determined as the difference between TC (measured by mass spectrometry) and IC (measured using coulometry).

Carbon and nitrogen isotopic values are reported using conventional δ-notation with respect to VPDB and atmospheric N_2, respectively. Sample weights were adjusted (5-40 mg; Table 2.1) so that abundances of C and N fell within the range of glycine and acetanilide laboratory reference materials. We found it difficult to obtain accurate

Table 2.2 Carbon and nitrogen contents and isotopic compositions of laboratory reference materials utilized for elemental (CN) analyzer (glycine, acetanilide, and peach leaves) and coulometer ($CaCO_3$) analyses.

	Glycine[1]	Acetanilide[2]	Peach Leaves[3]	$CaCO_3$[4]
Carbon (wt %)	32.0	71.0	45.3	12.0
$\delta^{13}C$ (‰)	-35.8	-30.9	-	-
Nitrogen (wt %)	18.7	10.4	2.8	-
$\delta^{15}N$ (‰)	11.3	-12.1	-	-
Carbon Range (ug C)[5]	20-150	100-1200	-	250-4800
Nitrogen Range (ug N)[5]	15-200	-	<1-15	-

[1]Glycine 99.5% Assay CAS #56-40-6
99% [2]Acetanilide Assay CAS #103-84-4
[3]NIST SRM 1547
[4] Reagent grade $CaCO_3$ CAS #471-34-1
[5]Suggested abundance range of reference material needed for instrument calibration for the samples analyzed in this study

weights of glycine and acetanilide needed for instrument calibration at low TN even using a 6-place balance (UMX2, Mettler Toledo). To extend the instrument calibration to low TN concentrations when analyzing carbonate-rich samples with high TC:TN, we used a National Institute of Science and Technology (NIST) certified reference material (peach leaves, NIST SRM1547; Table 2.2). The peach leaves reference material has a relatively high TC:TN, allowing u to weigh out measurable quantities of standard, with low nitrogen content, thus extending our standard curve to lower values.

Acidified samples for carbon isotopic analyses of organic matter were prepared using the rinse-acidification method modified after Komada et al. (2008). This analysis also provided organic carbon (OC_{rinse}) and nitrogen (TN_{rinse}) concentrations, which were utilized to assess quantity of OC and TN lost during acidification and rinsing. Dry, ground sediment samples from each location were weighed into pre-weighed centrifuge tubes (W_o). IC was removed by slowly adding 3 N hydrochloric acid, until no effervescence was detected. The required quantity of acid varied depending upon $CaCO_3$ concentration but was roughly between 10-50 ml for all samples (sample mass range: 300-2500 mg; Table 2.1). The acid and three consecutive MQ-H_2O rinses were removed via centrifugation and decanting. The acid-treated sediments were dried at 60ºC, re-weighed to determine final weight (W_f), and stored in a desiccator until analysis. Carbonate-free samples were weighed (5-25 mg; Table 2.1) and analyzed isotopically as above. Values were corrected for mass loss during acidification and IC removal by applying a gravimetric correction (Hedges and Stern 1984) using the following equation (given for carbon):

$$\text{wt\% } OC_{rinse} = (\mu g \text{ carbon detected}) / (\mu g \text{ sediment analyzed}) * (W_f / W_o) \quad (2.1)$$

Bulk sediment phosphorus analysis: Inorganic sedimentary phosphorus (IP) was determined utilizing the acid hydrolysis method of (Aspila et al. 1976) and total sedimentary phosphorus (TP) was determined using the high-temperature ashing/hydrolsis method of (Monaghan and Ruttenberg 1999). Organic phosphorus (OP) was determined as the difference between TP and IP.

End member analysis: The following samples were collected to characterize end member source material: (i) *Rhizophora mangle* propagules, seeds, leaves, and root material from a coastal mangrove forest in Kane'ohe Bay; (ii) *Acanthophora* sp. and *Gracilaria* sp., macroalgae found in Hawaiian coastal waters; and (iii) plankton collected from within Kane'ohe Bay using a 100 μm tow net. End member samples were freeze-dried and homogenized prior to analysis for organic carbon and total nitrogen concentrations and isotopic values, using the aqueous method described by Komada et al. (2008) to avoid soluble OC loss during rinsing. Inorganic and total phosphorus were analyzed using the previously discussed methods.

Error estimation: Errors were estimated using the following methods: (i) propagation of analytical errors, (ii) Monte Carlo simulation of analytical error, and (iii) calculation of precision based on duplicate sample analysis. Propagation of analytical error assumed uniform distribution of instrument standard deviations and resulted in the largest propagated uncertainties. In the Monte Carlo simulation we assumed normal distribution of instrument uncertainty, such that the mean value represented the most probable value, and instrument uncertainty was within the 95% confidence intervals of the distribution function. The Monte Carlo simulation was run over 100,000 iterations and yielded slightly lower uncertainties (Anderson 1976). Each sample was analyzed in duplicate and the uncertainty was estimated as the difference between the duplicate results. Calculation of precision over duplicate analysis, which implicitly includes instrument analytical uncertainty, produced the lowest estimate of analytical error. We chose to report here uncertainty based on Monte Carlo simulations, since these provided an intermediate value of uncertainty (Table 2.3).

Table 2.3: Carbon and nitrogen concentrations of sediment samples collected at two discrete depth intervals (near-surface and deep) at each site. All values reported are the average over duplicates; errors determined via Monte Carlo simulation are shown in parenthesis.

Site	Depth (cm)	TC (wt %)	IC (wt %)	OC_{diff}[1] (wt %)	OC_{rinse}[2] (wt %)	TN (wt %)	TN_{rinse}[2] (wt %)	% loss[3] OC	% loss[3] TN
Mangrove	1.3	7.89 (0.20)	0.12 (0.00)	7.77 (0.20)	7.12 (0.18)	0.494 (0.0012)	0.489 (0.012)	8.2	0.9
Mangrove	8.6	5.60 (0.14)	0.10 (0.00)	5.50 (0.14)	5.16 (0.13)	0.356 (0.009)	0.342 (0.009)	6.5	4.5
Terrestrial Dominated	1.3	1.78 (0.05)	0.70 (0.00)	1.08 (0.05)	0.81 (0.02)	0.054 (0.001)	0.039 (0.001)	25.2	27.7
Terrestrial Dominated	8.3	2.10 (0.05)	0.67 (0.01)	1.43 (0.05)	1.21 (0.03)	0.065 (0.002)	0.050 (0.001)	15.2	27.8
Carbonate Dominated	1.3	10.43 (0.26)	9.52 (0.10)	1.00 (0.28)	0.22 (0.01)	0.022 (0.001)	0.019 (0.000)	75.8	10.6
Carbonate Dominated	8.4	9.70 (0.24)	9.01 (0.09)	0.70 (0.26)	0.19 (0.00)	0.020 (0.000)	0.016 (0.000)	72.8	19.7
Ocean	2.1	11.29 (0.28)	10.97 (0.11)	0.33 (0.30)[4]	0.10 (0.00)	0.015 (0.000)	0.013 (0.000)	68.4	12.5
Ocean	8.5	11.17 (0.28)	10.95 (0.11)	0.23 (0.30)[4]	0.17 (0.00)	0.014 (0.000)	0.023 (0.001)	18.7	-

[1]Calculated as: $OC_{diff} = TC - IC$

[2]Organic carbon $(OC)_{rinse}$ and total nitrogen $(TN)_{rinse}$ values were obtained through analysis of acidified samples. Acid was removed via three successive MQ-H_2O rinses of sediments. Gravimetric correction for mass loss due to IC removal was calculated using equation 1.

[3]Values reflect estimates of OC and TN loss during acidification and subsequent rinses during IC removal prior to elemental analysis (see text for more complete discussion and equations).

[4]Error values obtained through analysis of duplicate samples yielded smaller uncertainties, indicating higher precision than expected based on reported Monte Carlo error propagation (see Comments and Recommendations)

2.3 Assessment

Carbon and nitrogen concentrations: Traditionally IC is calculated as the difference between TC and OC, measured using an elemental analyzer on untreated and acidified samples, respectively. We chose not to use acidified splits to determine OC concentrations because we were leery of OC loss during acidification and subsequent rinses. Instead we used coulometry to directly determine IC, and then used TC and IC to calculate OC by difference (OC_{diff}). As is the case for all difference methods, it is essential to obtain precise values for measured parameters (TC and IC in this case) in order to minimize error, and to propagate those errors when calculating the derived parameter and its uncertainty.

Figure 2.1 A typical nitrogen quantification curve for the Carlo Erba NA 2500 elemental (CN) analyzer. The linear range for mass of nitrogen obtained by integrating the peak area for masses 28, 29 and 30 for the glycine laboratory reference compound (15-100 μg N) is extended to lower values (1-15 μg N) using the NIST SRM1547 Peach Leaves certified reference material.

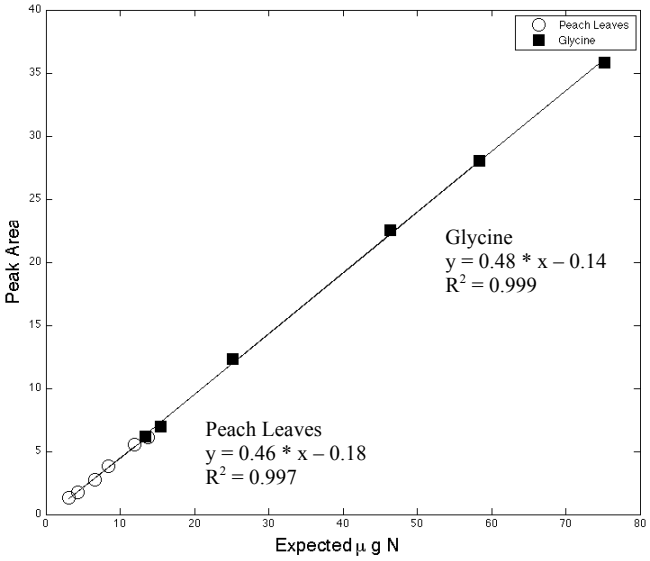

Quantification of total nitrogen proved challenging for carbonate-rich sediments because they typically have elevated TC:TN ratios, owing to the high IC content (Table 2.3). In order to achieve a sufficient instrument response necessary to determine N abundance and isotopic composition of the carbonate-dominated ocean sediments analyzed, large sample masses (35-45 mg) were required when using instrument response curves based only on the glycine and acetanilide reference materials. These large sample masses caused unacceptable increases in baseline between samples and inconsistent reproducibility. To address this problem, we extended the lower range of N quantification using a reference material with a high TC:TN ratio (NIST SRM1547, peach leaves; Figure 2.1) relative to the other reference materials. The low concentration of N in peach leaves, relative to C, allowed us to accurately weigh quantities of

SRM1547 needed to generate a reliable quantification curve, which allowed us to determine N concentrations of carbonate-rich sediments using a reasonable sample mass (~8 mg; Table 2.1). Although TN abundance could be determined reliably with this method on samples with less than ~15 μg N, the uncertainty in the measured $\delta^{15}N$ values of laboratory reference materials within this TN range became unacceptably large (>0.5‰).

Although samples prepared using the rinse method were used principally to allow measurement of $\delta^{13}C$ values, the OC_{rinse} and TN_{rinse} results allowed us to also evaluate the percent loss of carbon and nitrogen due to the post-acidification rinses (Table 2.3). After gravimetric correction (Equation 2.1), the % loss of OC was calculated using the following equation (given for carbon):

$$\% \text{ loss OC} = (OC_{diff} - OC_{rinse}) / OC_{diff} * 100 \quad (2.2)$$

Loss of organic carbon ranged from 6.5% in deep Mangrove sediment up to 75.8% of total OC in shallow carbonate sediments. Percent loss of carbon was greater in surficial sediment intervals (Table 2.3), which we attribute to the greater solubility of labile organic matter present within young surficial sediments relative to the more refractory organic matter found in more deeply buried sediments (Hedges and Keil 1995). The rinse method is known to cause loss of a fraction of organic matter (Froelich 1980), thus OC determined on acidified samples is underestimated (Table 2.3). The alternative method proposed here, in which IC determined directly via coulometry is subtracted from TC to derive OC, does not suffer from OC loss during sample preparation, and is therefore a more accurate method for the quantification of OC.

Carbon and nitrogen isotopic compositions: Although OC and TN losses during the rinse method are unavoidable, IC must be quantitatively removed from sediments via acidification prior to determination of $\delta^{13}C$ values of organic carbon. We found no practical alternative to the rinse method for the determination of $\delta^{13}C$ values of carbonate-rich sediments. Initial trials utilizing the vaporous method (Komada et al. 2008) on carbonate-rich samples did not completely remove all carbonate material. Trials of the aqueous method without MQ-H_2O rinses (Hedges and Stern 1984) required a large

Table 2.4 $\delta^{13}C$ and $\delta^{15}N$ values for sediment samples collected at two discrete depths from each site. All values reported are the average over duplicates; maximum instrumental error is ± 0.2‰. End member isotopic values are best estimates for local (Hawai'i) source organic material; elemental $(C:P)_{org}$ are also reported for end members.

Site	Depth (cm)	$\delta^{13}C$ (‰)	$\delta^{15}N$ (‰)
Mangrove	1.3	-25.7	1.4
Mangrove	8.6	-24.8	2.1
Terrestrial Dominated	1.3	-22.1	1.8
Terrestrial Dominated	8.3	-24.3	1.5
Carbonate Dominated	1.3	-15.3	1.8
Carbonate Dominated	8.4	-16.4	3.7
Ocean	2.1	-16.4	3.5
Ocean	8.5	-17.2	3.5

End member	$C:P_{org}$	$\delta^{13}C$ (‰)	$\delta^{15}N$ (‰)
Mangrove end member[1]	1321:1 to 782:1	-27.0 to -28.8	-0.3 to 2.6
Macroalgae end member[2]	5809:1 to 1572:1	-17.7 to -16.6	0.0 to 3.8
Phytoplankton end member[3]	268:1	-19.0 ± 0.1	6.8 ± 0.3

[1]Values from *Rhizophora mangle* in He'eia Fishpond.

[2]Values from macroalgae (*Acanthophora* sp. and *Gracilaria* sp.) found within He'eia Fishpond. High ratios are due to structural carbon found in fleshy marine algae.

[3]Values from a plankton tow conducted in Kane'ohe Bay. Phytoplankton $(C:P)_{org}$ ratios are markedly higher than the Redfield ratio for marine phytoplankton. We suspect that this elevated value is a consequence of inclusion of small fragments of high $(C:P)_{org}$ macroalgae and terrestrial vegetation in the net tow material that persisted despite our attempts to remove fragments of non-phytoplankton organic matter from this sample.

quantity of acid (see Method) to completely remove all carbonate material. This resulted in the formation of a hard, dry coating of hygroscopic salt ($CaCl_2$), which trapped moisture such that the bulk of the acidified sediments never dried, even at temperatures exceeding 160ºC for several days. Thus, rinse-acidification seems the only viable method for the removal of inorganic carbon in carbonate-rich samples, despite the fact that some organic carbon is lost due to solubilization and subsequent rinsing (Table 2.3).

Partial loss of organic carbon during rinsing after acidification could potentially alter $\delta^{13}C$ values. If the organic matter lost during acidification has a carbon isotopic composition distinct from the bulk organic matter within the sediments, the $\delta^{13}C$ values obtained after rinse-acidification may not be an accurate representation of bulk sediment $\delta^{13}C$ values. To investigate the extent to which $\delta^{13}C$ values obtained using the rinse method might have been impacted by organic carbon loss, we employed the coupled $\delta^{13}C$-$(C:P)_{org}$ metric (Ruttenberg and Goñi 1997a; Ruttenberg and Goñi 1997b) to evaluate whether sample

$\delta^{13}C$ values were consistent with end member source materials in the environments studied. Since our stations were arrayed along a transect that spanned a gradient from terrestrial- to marine-dominated organic matter, we can contrast sedimentary $\delta^{13}C$ values to the isotopic and elemental composition of end-member terrestrial and marine organic matter, and assess the extent of deviation from expected trends.

Marine phytoplankton have a mean molar organic $(C:P)_{org}$ of 106:1 (Redfield et al. 1963) in contrast to terrestrial, vascular plants, which have characteristic $(C:P)_{org}$ up to or exceeding 800 (Likens et al. 1981). Isotopic compositions of local marine phytoplankton and mangrove are reported (Table 2.4) for comparison against our sediment samples. A plot of $(C:P)_{org}$ versus $\delta^{13}C$ values of organic matter produces a hyperbolic trend characteristic of the mixing line between two-end member materials (marine phytoplankton vs. vascular plant) on a ratio-to-ratio plot, as described by Ruttenberg and Goñi (1997a; 1997b); Figure 2.2). This trend illustrates that the sediments along our shore-perpendicular transect reflect a smoothly varying progression between the two end-members. Thus, inadvertent removal of organic carbon during the rinse-acidification method did not measurably affect the characteristic isotopic signatures of the bulk sediments analyzed. It is preferable to determine total nitrogen concentration and $\delta^{15}N$ values on bulk, untreated sediment samples to avoid the complication of nitrogen loss during the acidification rinse method. We determined TN and $\delta^{15}N$ values on bulk sediments from our two sites that contained <50% $CaCO_3$, the mangrove and terrigenous dominated sites. Due to the high TC:TN ratios of the two sites with >50% $CaCO_3$, the TN concentrations of optimal sample mass fell below the threshold of accurate nitrogen isotopic analyses of reference materials (see previous discussion). Therefore, $\delta^{15}N$ values of carbonate-rich sediments, such as the carbonate-dominated and ocean site samples in this study were obtained from samples subjected to the acidification rinse method. Because the acidification rinse method results in loss of total nitrogen (Table 2.3), one must assume that loss of material does not result in a shift in the $\delta^{15}N$ value of bulk sediment. The $\delta^{13}C$-$(C:P)_{org}$ analysis discussed earlier (Figure 2.2) suggested that artifacts resulting from the acidification rinse method did not significantly alter sediment $\delta^{13}C$ values, so we make a similar assumption for $\delta^{15}N$ values. It was not possible to employ a similar analysis (e.g., $\delta^{15}N$-$(C:N)_{org}$) to evaluate the integrity of the nitrogen isotopic

compositions of samples (data not shown). TN concentrations and $\delta^{15}N$ values are significantly altered during early diagenesis (e.g., Freudenthal et al. 2001), and thus cannot be used to asses organic matter sources. The TN and $\delta^{15}N$ values are however useful to understand biogeochemical transformation in sediments (e.g., Lehmann et al. 2002).

2.4 Discussion

Previous methods described for the quantification of organic carbon and total nitrogen concentrations and isotopic composition are inapplicable to carbonate-rich (> 50% by weight $CaCO_3$) sediments. Our method overcomes the limitation of these published methods by employing a combined coulometric-elemental analyzer-mass spectrometer approach for carbon and nitrogen quantification and isotopic analysis. Using coulometry to directly determine IC, we quantified organic carbon concentrations as the difference between TC and IC, thus avoiding problems associated with loss of labile OC during acidification of carbonate-rich sediments. Use of a reference material with a high TC:TN ratio (NIST Peach Leaves) allowed quantification of TN in high TC:TN carbonate-rich samples using a workable sample mass. Because removal of inorganic carbon from sediments is required prior to analysis for organic carbon isotopic composition, it was necessary to use the acidification rinse method to determine organic

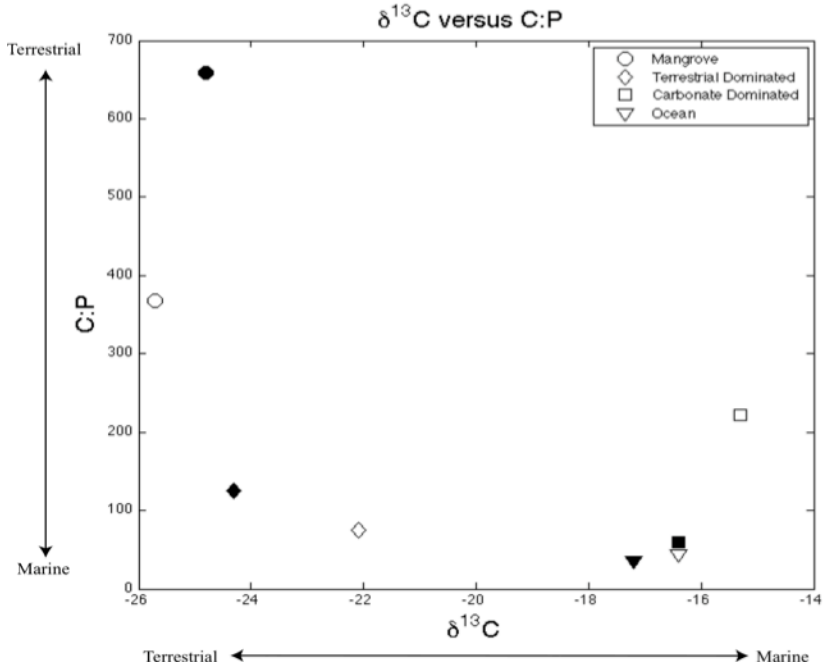

Figure 2.2 Organic carbon $\delta^{13}C$ values plotted against molar $(C:P)_{org}$ ratios permit evaluation of the source of organic matter to sediments. The upper left corner is representative of terrestrial material, characterized by high $(C:P)_{org}$ and low $\delta^{13}C$ values, whereas the lower right corner is indicative of marine material, characterized by low $(C:P)_{org}$ and higher $\delta^{13}C$ values (see Table 4). Open symbols represent surficial sediments at each site; filled symbols are taken from deeper within the sediment core (see Table 2.3

carbon $\delta^{13}C$ values. Application of the $\delta^{13}C$-$(C:P)_{org}$ metric for assessing source of organic matter suggests that the source signal of bulk $\delta^{13}C$ values was not compromised by OC loss during the acidification rinse method.

2.5 Comments and Recommendations

The ideal samples masses and W_f/W_o data presented in this paper were determined using trial and error (Table 2.1), and are specific to our sample sites. These values are provided solely as a guide for the application of this method to new sediment samples. Optimal values may vary based upon sample composition and organic matter lability as well as with the instrumentation used. Therefore, any analyst employing this method should independently verify ideal sample masses for optimal results.

Although it is not possible to independently quantify the effects of organic carbon loss on $\delta^{13}C$ values of sedimentary organic matter during the acidification rinse method, results of the $\delta^{13}C$-$(C:P)_{org}$ analysis (Figure 2.2) suggest that any losses did not obscure organic matter source information. However, it would be prudent to measure the percent loss of OC, and if possible its affect on bulk sediment $\delta^{13}C$ values, when applying the acidification rinse method to other environments. Such an assessment is likely to be particularly crucial for sediments containing labile organic matter, as a larger fraction of labile OC will likely be lost.

Recognizing the importance of obtaining accurate and robust estimates of analytical uncertainty of measurements, we compared the uncertainties obtained by 3 independent approaches (see Method section). In several instances the Monte Carlo approach yielded large uncertainties that may be unrealistic. The uncertainty obtained through analysis of duplicate samples typically yielded smaller uncertainties, indicating higher precision than expected based on Monte Carlo error propagation (data not shown). For example, OC_{diff} of the two ocean samples are reported as 0.33 ± 0.30 and 0.22 ± 0.30 wt% using the Monte Carlo simulation (Table 2.3); however, precision calculated from duplicate analysis of the same ocean samples yielded reproducibility of 0.33 ± 0.06 and 0.22 ± 0.00 wt%, respectively. Monte Carlo errors are reported to provide a conservative estimate of uncertainty. However, we suggest that error calculated over replicate analyses is equally valid, and may be a more realistic estimate of uncertainties.

Acknowledgements

Miguel Goñi supplied important suggestions that guided initial stages of method development, which we gratefully acknowledge. We thank Craig Glenn for access to his coulometer. This research was supported by a grant/cooperative agreement from the National Oceanic and Atmospheric Administration; project R/EL-42, which is sponsored by the University of Hawai‘i Sea Grant College Program, SOEST, under Institutional Grant NA05OAR4171048 from NOAA Office of Sea Grant, Department of Commerce. The views expressed herein are those of the authors and do not necessarily reflect the views of NOAA or any of its sub-agencies. UNIHI-SEAGRANT-xxxx. This is SOEST contribution #x

Chapter 3

Evaluation of Novel SEDEX Extraction Steps for Labile Organic Phosphorus and $CaCO_3$-bound Phosphorus in Aquatic Sediments

with K. C. Ruttenberg

Abstract

This study evaluates the merits of two proposed modifications to the 'classical' SEDEX scheme for sequential extraction of different forms of P from sediments, targeting labile organic phosphorus (L-OP) and calcium carbonate-bound phosphorus ($CaCO_3$-P). The selectivity and efficiency of a Bligh Dyer-type lipid extraction technique was analyzed for separately quantifying labile organic phosphorus in aquatic suspended particulate matter and bottom sediments. Monospecific phytoplankton cultures were used as 'analogues' for labile particulate organic matter. Our objective was to insert a step to precede the full SEDEX method that will remove the labile portion of the OP pool, prior to subjecting samples to the harsher extractants that make up the balance of the SEDEX scheme. Although the SEDEX method includes a step for quantifying OP, it is not optimal for capturing and quantifying labile OP because in the current scheme OP is quantified in the final step. Thus, labile OP can be solubilized in prior steps and incorrectly quantified as inorganic P. The ability to accurately quantify labile OP is essential for quantifying living biomass P and labile non-living OP, the pools most likely to generate mineralized P to support new cycles of primary production. This modification could be particularly important for aquatic suspended particulates or newly deposited bottom sediments, which may be dominated by labile, cellular material. The insertion of a tri-ammonium citrate extraction step prior to Step IIIA of the SEDEX method is evaluated for its ability to efficiently and selectively extract $CaCO_3$-P prior to extraction of other reactive Ca-P phases (authigenic carbonate fluorapatite and biogenic hydroxyapatite), which are targeted in SEDEX-Step III.

3.1 Introduction.

Selective, sequential extraction methods are widely used for separately quantifying different forms of phosphorus (P) in sediments and soils (e.g., Krall et al. 2009, Lukkarri et al. 2009, Monbet et al. 2009, Slomp et al. 2006). One method that has been particularly widely used in the study of marine sediments is the SEDEX method (Ruttenberg 1992; Ruttenberg et al. 2009), which separately quantifies five P reservoirs, in the following order: (Step I) exchangeable or loosely sorbed P, (Step II) ferric iron (Fe) bound P, (Step III) authigenic and biogenic apatite plus $CaCO_3$-bound P, (Step IV) detrital apatite and other inorganic P, and (Step V) organic P. As is the case with all selective extraction methods, the SEDEX method is operationally defined, and was exhaustively calibrated using analogue phases to confirm the specificity for the phase targeted for extraction in each step of the SEDEX scheme (Ruttenberg 1992).

Despite its careful standardization, the operationally defined nature of SEDEX leads to inherent uncertainties in the determination of sediment-P distribution and, where possible, it is valuable to refine the specificity of the method. Two SEDEX-defined P reservoirs have received such additional attention since the method was first proposed in 1992: The combined reactive Ca-P reservoir targeted in Step III, and the organic P (OP) reservoir targeted in Step V. For example, Shenau et al. (2000) introduced an additional step into the SEDEX scheme that permits the separate quantification of fish bones (biogenic, hydroxyapatite: HAP), which are otherwise extracted in tandem with authigenic apatite (CFA) plus $CaCO_3$-bound P in Step III. This step may be particularly important for coastal upwelling regions, where fish production can lead to large inputs of HAP to underlying sediments. Vink et al. (1997) proposed adding a step to enable extraction of OP earlier in the scheme, to avoid its premature extraction in Steps I-IV. Neither of these proposed modifications to the SEDEX method have been widely adopted, likely due to the work-intensive nature of each, as both involve multiple extractions. In this paper, we present results of experiments conducted to test two novel SEDEX steps to separately quantify these same two P-reservoirs: reactive Ca-P and labile-OP.

It has been previously recognized that because extraction of OP occurs as the final step of SEDEX (Step V), the potential exists for premature extraction of *labile* organic

Figure 3.1 SPExMan-SEDEX scheme for different forms of P in marine sediments (Ruttenberg et al. 2009) illustrating insertion of Pre-Extraction step for L OP recovery prior to Step I, and insertion of the TAC extraction for separate quantification of $CaCO_3$-P prior to Step IIIA

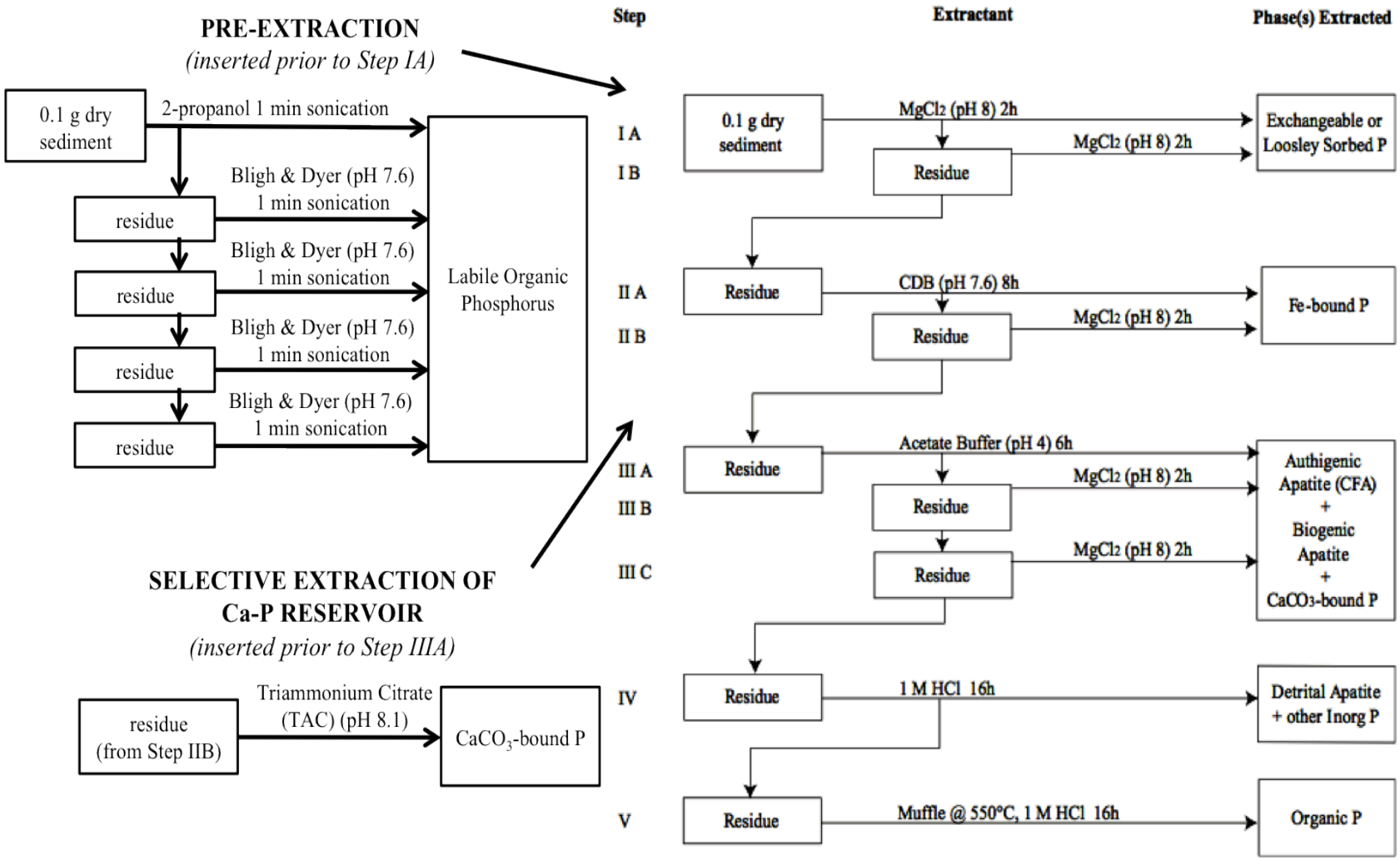

P (L-OP) in prior SEDEX steps. If solubilized and hydrolyzed, this dissolved organic P (DOP) would be erroneously included in one of the inorganic P (IP) reservoirs. If solubilized but not hydrolyzed, this prematurely extracted DOP would be unaccounted for in the final SEDEX P-distribution (Ruttenberg 1992; Vink et al. 1997). In its initial formulation the SEDEX method was developed for application to marine sediments, and Ruttenberg (1992) argued that the likelihood of significant OP loss in Steps I-IV was minimal because seabed sediments are more likely to be dominated by older, more degraded and refractory organic matter. In fact, solubilization of a portion of OP from in Steps I-IV was documented in test sediments (Ruttenberg 1992), but this quantity was fairly small (<10% of total-P (TP)) and, because it was solubilized without being hydrolyzed, did not contribute OP to the IP reservoirs solubilized in Step I-IV.

One cannot ignore the risk of premature extraction of L-OP, however, if the SEDEX method is applied to aquatic suspended sediments, which may be comprised in large part by cellular (planktonic) P, or to surface sediments that are the recipient of L-OP as the result of high overlying water primary productivity. This paper summarizes the evaluation of a Pre-Extraction step, inserted prior to Step I of the SEDEX scheme (Figure 3.1), designed to remove the labile portion of the OP pool prior to subjecting samples to the harsher extractants that make up the balance of the SEDEX scheme. In addition, we present results of experiments designed to evaluate the possibility of separately quantifying $CaCO_3$-bound P (hereafter $CaCO_3$-P), as distinct from CFA and HAP (Figure 3.1).

3.2 Materials and Methods

General strategy: Adopting the rationale of standardization experiments designed to evaluate the original SEDEX method (Ruttenberg 1992), three types of experiments were preformed: (i) efficiency experiments, designed to confirm the extent to which complete recovery of target phases (either L-OP or $CaCO_3$-P) was achieved, (ii) specificity experiments to examine the extent of dissolution of solid P reservoirs other than target phases in the proposed new extraction steps, and (iii) matrix effect experiments designed to examine the potential re-adsorption of P solubilized from target

phases onto surfaces of other (non-target, or matrix) phases that remain in tact during the extraction step.

Because of the operationally defined nature of SEDEX, it is critical to standardize the proposed extraction steps with materials that closely approximate naturally occurring materials (Table 3.1). Pure cultures of three algal taxa, grown under nutrient replete conditions, were used as analogues for L-OP. Cultured algae were washed with 1M ammonium formate solution prior to freeze drying to remove any non-cellular P and residual salts in the culture media. In addition to pure cultures, a mixed plankton assemblage recovered in a net tow from Long Island Sound (Ruttenberg 1992) was used as an analogue for field-collected, suspended particulate L-OP. Reagent grade $CaCO_3$ was used as an analogue for naturally occurring carbonate phases. Discrete mineral phases used for efficiency, specificity and matrix effect experiments are similar to those

Table 3.1 Analog phases used for Pre-Extraction experiments. (*) For specificity experiments pure minerals were pre-sorbed with P by shaking pure mineral phases in a saturated solution of inorganic P (10 mM P). Uncertainties are reported as standard error based on replicate analyses

Analog Phase	Total P (pre-sorption) µmol P/ g	Total P (sorbed to mineral) µmol P/ g	Source
Bulk Plankton	90.5 ± 0.7	N/A	Collected via net tow in Long Island Sound (Ruttenberg 1992)
Green algae	284 ± 3	N/A	*Tetraselmis chuii*; cultured at WHOI
Diatom	337 ± 13	N/A	*Thalassiosira pseudonana*; cultured at WHOI
Dinoflagellates	232 ± 10	N/A	*Heterocapsa* and *Lingulodinium polyedrum*; cultured at WHOI
Ferrihydrite*	N/A	279 ± 9	Synthesized according to Schewtmann and Cornell (1991)
Goethite*	N/A	54.4 ± 1.7	Synthesized according to Schewtmann and Cornell (1991)
Calcite*	N/A	0.34 ± 0.02	Baker analyzed pure $CaCO_3$
Aragonite*	N/A	1.25 ± 0.04	Collected in Kaneohe bay, Hawai'i; confirmed via XRD analysis
Smectite*	N/A	10.1 ± 0.8	Cutter Cermaics (Ruttenberg 1992)
Kaolinite*	N/A	17.7 ± 0.3	Fisher Scientifict kaolin, acid washed, Cat. No. K5-500 lot No. 761094 (Ruttenberg 1992)
CFA nodule	N/A	4106 ± 82	(Ruttenberg 1992)

used by Ruttenberg (1992), and for the purpose of efficiency and specificity experiments, were loaded with surface-sorbed phosphate by pre-equilibration in a 10 mM phosphate solution, as in Ruttenberg (1992).

Extractants and extraction approach: We have chosen to use the Bligh-Dyer (B-D) extractant, a well-proven medium for extracting lipids from particulate organic material (Bligh and Dyer 1959), to selectively solubilize L-OP from aquatic particulate material in the Pre-Extraction step. The B-D extractant is a single-phase water:methanol:chloroform (0.8:2:1) solution that efficiently extracts polar lipids. For this study, two modifications to the Bligh and Dyer method were adopted (Laarkamp 2000): (i) the sediment-solvent mixture was sonicated with a Tekmar® sonic disrupter probe to ensure complete recovery of intracellular OP, and (ii) a single 2-propanol extraction was conducted prior to B-D solvent extraction to deactivate lipases, preventing degradation of phospholipids during extraction. A 0.5 M solution of tri-ammonium citrate (pH 8.1), so called 'Silverman's Solution', was chosen for the selective dissolution of $CaCO_3$-associate P from carbonate fluorapatite because carbonate-fluorapatite is relatively insoluble (solubility = 0.012 g / 100 ml solution), as compared to calcium carbonate (solubility = 0.660 g / 100 ml solution) in this solution (Silverman et al. 1952).

The SPExMan extraction manifold (Ruttenberg et al. 2009) was used for all experiments in this study. Manifold reaction vessels, filter holders, stopcocks and caps are Teflon, which is essential in order to withstand exposure to the B-D solvent mixture, which would degrade other commonly-used plastics such as polycarbonate, polypropylene, polyethylene, etc. Reaction vessel diameter (20 mm) is large enough to accommodate the Tekmar sonic disrupter probe (10 mm), allowing samples to be sonicated within the reaction vessels.

GH polypropylene (GHP) filters (0.2 µm; Pall Life Sciences©), a hydrophilic universal membrane filter, were the filter of choice as they were expected to provide maximum chemical compatibility with both aqueous solutions and aggressive solvents; the polycarbonate (PC) filters recommended for the SPExMan-SEDEX protocol (Ruttenberg et al. 2009) are incompatible with the Pre-Extraction B-D solvent mixture. To verify the filter suitability, we examined the effects of physical sonication, as well as solvent and reagent exposure, on the integrity of the GHP filter. GHP filters were brought

through the Pre-Extraction step followed by the full SEDEX method (Figure 3.1), and also taken through the Pre-Extraction sonication and SEDEX steps replacing solutions with MQ-DI, as a control for effects of physical manipulation in the absence of solvent exposure. Filters were thoroughly rinsed with MQ-DI at the end of each experiment, dried at room temperature and cut in half. Half of the filter was prepared for Scanning Electron Microscope (SEM) viewing to visually ascertain filter integrity, and the other half was combusted according to Step V of SEDEX.

Phosphorus analysis of supernatants: Total Dissolved P (TDP) was quantified in Pre-Extraction solvents (both 2-proponal and the B-D solvent mix) using a modified high-temperature ashing method (Laarkamp 2000). Extractants (total volume: 13 mL) were adjusted to pH 1 with trace metal clean concentrated hydrochloric acid (HCl; 100 µL) and spiked with 50% (w/v) $Mg(NO_3)_2$ (560 µL). Samples were dried at 60˚C for several days. When samples appeared dry, the oven temperature was increased to 120˚C for 2 hours to ensure complete dryness, which is critical to prevent spattering during the muffling step. Each vial was tightly covered with muffled Al foil squares and combusted for 2 hours in a muffle furnace at 550˚C. Once cooled, 1M HCl (6.5 mL) was added to each vial, and vials were shaken on a horizontal shaker table at 300 rpm for 16 hours. After the 16-hour extraction was completed, 12 N NaOH was added (200 µL) to bring the solution to a final pH of 1. Samples were analyzed for TDP on a BioTek Synergy HT Multi-Mode microplate Reader using the molybdate-blue colorimetric method (Grasshoff, 1972). Because of citrate interference with colorimetric protocols for phosphorus (reviewed in He et al., 1998), TDP in Silverman's Solution was quantified using Inductively-Coupled Plasma-Optical Elemental Spectroscopy (ICP-OES). Extractants from Steps I-V were analyzed colorimetrically using a BioTek Synery HT multi-Mode microplate reader following protocols outlined in Appendix 4 of Ruttenberg et al. (2009), with the exception of P in Step-II, which was analyzed using a modification of the SepPak method for P-determination in CDB (Suzumura and Koike 1995) (see Appendix to this chapter for modified method).

3.3 Standardization experiments: Design and Procedure.

Efficiency experiments for L-OP: Adapting the work of Laarkamp (2000), the Pre-Extraction method includes a single 2-propanol extraction, followed by multiple B-D extractions. Ultrasonic cell disruption is employed during extraction to effect cell lysis, allowing for liberation and solubilization of intracellular P, and also to disrupt sorptive association of free phospholipids from particulate surfaces (Laarkamp 2000). It was necessary to determine both the number of B-D extractions as well as the optimal length of extraction time required to achieve maximal recovery of L-OP. Laarkamp (2000) found that 4-7 successive B-D extractions were necessary to exhaustively remove L-OP from marine sediments. Because we used cultured phytoplankton cells as our analogue for L-OP (Table 3.1), which we anticipated would be comprised entirely of L-OP, we expected 100% P-solubilization during the Pre-Extraction, and that possibly fewer than 6 successive B-D extractions would be required. In order to maximize OP recovery in a single Pre-Extraction step, the maximum possible volume of extractant permissible was used during each step (13 mL). Extractant volume was limited by the size of the SPEx-Man reaction vessel, which needed to accommodate not only the extractant volume, but insertion of the sonic probe as well, without causing overflow of solution during sonication. Efficiency of the Pre-Extraction for L-OP was determined by subjecting each L-OP analogue to a single 2-propanol extraction, followed by six sequential B-D extractions. Specifically, triplicate 5 mg splits of each plankton analogue phase (Table 3.1) were weighed into SPEx-Man reaction vessels and brought through the Pre-Extraction Step (2-prop extraction + 6 B-D extractions) using 1-minute extraction times. Supernatant of each extraction step was analyzed separately in order to determine the fractional recovery during each successive extraction.

After the optimal number of B-D extractions required for full recovery of OP was determined, the optimal extraction time was evaluated. Laarkamp (2000) used a 10-minute sonication time for B-D lipid-P recovery from marine seabed sediments. A significant drawback to such a lengthy sonication time is that the sample heats up during sonication, necessitating the use of cold-packs to cool the reaction vessel during sonication, which makes the procedure cumbersome and inconvenient. To evaluate whether extraction time could be reduced without sacrificing L-OP recovery, we

compared recovery of L-OP from analogue plankton phases using both 1- and 10-minute sonication times. Specifically, 5 mg splits of the bulk plankton analog phase (Table 3.1) were weighed into replicate reaction vessels and brought through the Pre-Extraction method (2-proponal + 4 B-D extractions) using 1-minute (n=3) and 10-mintue (n=5) sonication times.

Specificity experiments for L-OP: Sequential extraction techniques are operationally defined based on the solubility of target phases in a given extractant. To ensure that the Pre-Extraction method did not interfere with the standardized, operationally defined pools of SEDEX (Ruttenberg 1992; Ruttenberg et al. 2009) we evaluated extent of dissolution of potential sediment matrix phases in the Pre-Extraction method. A suite of naturally occurring minerals, similar to matrix phases used to standardize the original SEDEX method (Table 3.1), was subjected to the Pre-Extraction method followed by the entire SEDEX scheme (Figure 3.1). Matrix minerals artificially loaded with phosphate, as described previously, were assayed, permitting evaluation of matrix phase dissolution during Pre-Extraction, and the extent of release of exchangeable phosphate from non-organic particulate samples during the Pre-Extraction step, and during subsequent SEDEX steps. Specifically, duplicate splits of analogue phases with surface-sorbed phosphate (Table 3.1) were weighed (0.15-0.015 mg) into reaction vessels; optimal weights were determined based on the total P content of each mineral (Table 3.1) to ensure detectable P levels in extractants (data not shown). Samples were then taken through the Pre-Extraction Step (note: 10-min shake time at each Pre-Extraction step was used in this experiment), followed by the full SEDEX scheme.

Matrix effect experiments for L-OP: These experiments were designed to determine whether, subsequent to release of L-OP in natural samples, readsorption of P occurs onto surfaces of other sedimentary phases (hereafter called 'matrix phases') that remain in solid form throughout the Pre-Extraction. Bulk plankton (Table 3.1) was used as the target phase, acting as the 'P-source' material during matrix effect experiments. A split of bulk plankton was placed into a reaction vessel along with one pure matrix phase, and the Pre-Extraction was carried out, followed by the entire SEDEX scheme. By continuing to run the two-phase mixtures through the entire SEDEX scheme we were able to (i) ascertain whether any readsorption that may have occurred during the Pre-

Extraction step was reversed during SEDEX-Step I, which is designed to solubilize loosely-sorbed P (Figure 3.1), and/or whether additional secondarily sorbed P not recovered during SEDEX-Step I might be released in subsequent SEDEX steps. Analogue phases used in this experiments were pure phases of calcite, aragonite, smectite, kaolinite, goethite and ferrihydrite (Table 3.1). None of the matrix phases were expected to dissolve (see later discussion) during the Pre-Extraction step. We note that because the matrix phases are pure minerals, devoid of surface-sorbed phosphate, they are expected to display maximum sorption capacity for solubilized P, and thus may overestimate the potential matrix effect of natural sediments during the Pre-Extraction Step.

Comparison of SEDEX method with and without Pre-Extraction: Plankton analogue phases (Table 3.1) were subjected to the full SPExMan-SEDEX procedure, with and without the Pre-Extraction Step, to determine whether some fraction of OP in the L-OP analogue phases is not solubilized during the Pre-Extraction and, in that case, in which subsequent SEDEX steps this OP would be solubilized. Supernatants from SEDEX-Steps I and IV were analyzed for TDP as well as DIP, using a high-temperature ashing method (Monaghan and Ruttenberg 1999). Step II (CDB) and Step III (Na-acetate) are not amenable to TDP analysis via high-temperature ashing, and these data are unavailable. While bulk plankton is a good analogue for suspended particulate matter in aquatic systems, it is of interest to assay seabed sediments in these experiments in order to evaluate what fraction of sedimentary OP might be solubilized during the Pre-Extraction step, and thus be operationally identified as L-OP. To address this question, we also subjected seabed sediments from two well-studied sites, the Mississippi Delta and Equatorial Atlantic (Ruttenberg et al. 2009), as well as a seabed sample from Kaneʻohe Bay, Hawaiʻi (Briggs et al. 2011), to these standardization experiments.

Combined efficiency-specificity experiments for $CaCO_3$-bound P: To determine the efficiency and specificity of tri-ammonium citrate (TAC) for $CaCO_3$, both $CaCO_3$ and CFA analogue phases (Table 3.1) were subjected to a time-course dissolution experiment. Multiple splits of each analogue phase were weighed (0.3 g) into 50 mL centrifuge tubes and agitated on a shaker table (300 RPM) after addition of TAC (30 mL). Samples were sacrificed serially every hour for 8 hours to determine the dissolution rate, and extent of

dissolution, of each analogue phase. Calcium concentrations determined on supernatant filtrates, analyzed via ICP-OES, were used to determine the efficiency of TAC for dissolving $CaCO_3$, while at the same time evaluating its specificity for $CaCO_3$ over CFA. Phosphorus concentrations were also determined on supernatants via ICP-OES. Because results of these experiments indicated that TAC was not sufficiently specific for $CaCO_3$ over CFA, matrix effect experiments for TAC were not conducted.

3.4 Results and Discussion.

3.4.1 Standardization, Efficiency, and Matrix Experiments for L-OP determination

Filter durability assessment: SEM examination of GH polypropylene (GHP) hydrophilic membrane filters subjected to Pre-Extraction followed by SEDEX showed no evidence of filter degradation resulting from either reagents or physical sonication (data not shown), and thus were confirmed compatible for use with all SEDEX extractants as well as B-D solvents. During the Step V combustion, GHP filters were converted to CO_2, leaving behind no visible residue. PC filters (0.4 μm), successfully used in the 'classical' SEDEX method, dissolved upon exposure to the B-D solvents making them incompatible for the Pre-Extraction method. Thus, if Pre-Extraction is to be employed prior to SEDEX, use of GHP or comparable filters is required. PC filters remain useful for employment of the SEDEX method without Pre-Extraction.

Pre-Extraction efficiency determinations: The recovery of P from L-OP analogues was calculated by normalizing the μmoles of P extracted from each step in the Pre-Extraction Step to the total P extracted from all 7 steps (2-prop + 6 B-D). Between 10-20% of the P was solubilized during the 2-prop extraction, with most of the remaining labile OP (30-50%) recovered in the first B-D extraction (Figure 3.2). After the 4^{th} B-D extraction, recovery efficiency dropped to below 2%. Based on these results, we recommend a final Pre-Extraction Step consisting of a single 2-propanol extraction followed by four successive B-D extractions.

As described previously, 1-minute extractions were employed in the Pre-Extraction efficiency experiment summarized above, with results presented in Figure 3.2. In order to ascertain whether longer extraction times would improve efficiency enough to allow us to reduce the total number of B-D extractions to fewer than 4, and still maintain

Figure 3.2 Phosphorus extracted from each step in the Pre-Extraction method, normalized to the total P extracted from all 7 steps (2-prop + 6 BD). Data is displayed for 3 cultured plankton: dinoflagellates (squares), diatoms (triangles) and green algae (circles), as well as a bulk plankton analog phase (diamonds). See

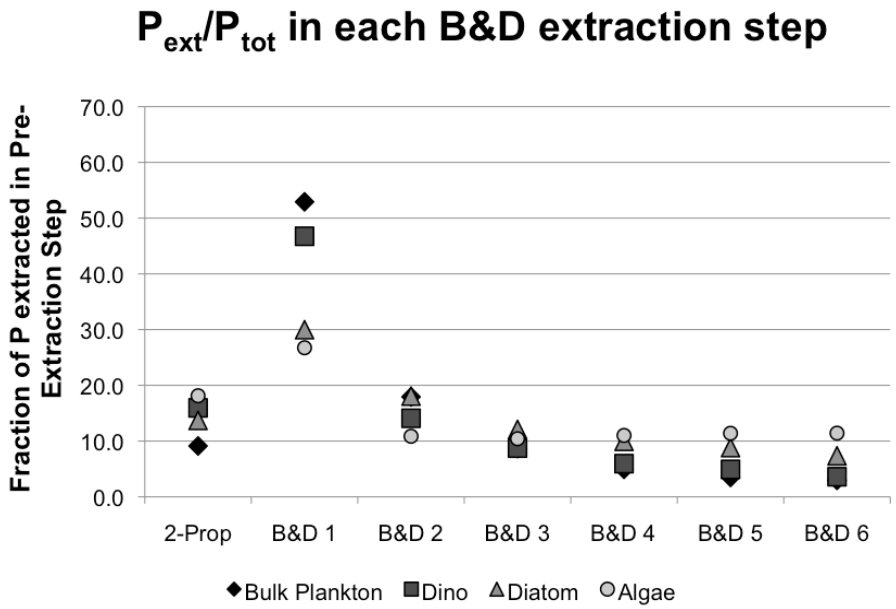

the same level of OP-recovery, we repeated the Pre-Extraction efficiency experiment using both 1- and 10-minute extraction times for each of the 4 B-D extraction steps. The quantity of P extracted during each step was summed to obtain a value for the total quantity of P extracted over the entire Pre-Extraction for each treatment (1- vs. 10-minute extraction) (Figure 3.3). We conclude from these results that the 10-min sonication time does not result in statistically superior P recovery during Pre-Extraction, and thus recommend 1-minute extraction times. Utilizing a 1-min extraction time offers advantages in that the shorter extraction time eliminates the need for cold pack wraps, as outlined by Laarkamp (2000), and it reduces the total time required to complete the Pre-Extraction.

Pre-Extraction specificity evaluation: The possibility of solubilization of P from non-organic sedimentary components (i.e. mineral phases) during the Pre-Extraction is most likely to affect the loosely-sorbed, or exchangeable P (P_{ex}) reservoir (Figure 3.1). The experiment designed to estimate the quantity of exchangeable phosphate that could be released from sediments during the Pre-Extraction Step involved subjecting pure minerals phases that had been loaded with surface-sorbed phosphate to the Pre-Extraction Step followed by the full SEDEX method (Figure 3.1). The fraction of Total P (TP) that

was extracted during the Pre-Extraction was calculated by summing the amount extracted in all 5 extractions (2-prop + 4 B-D extractions) of the Pre-Extraction Step, and normalizing to the quantity of P extracted in the Pre-Extraction plus subsequent SEDEX steps:

% P = (TP in 5 Pre-Ext steps) / (TP in all Pre-Ext plus SEDEX steps) *100 (3.1)

The P_{ex} that was solubilized from matrix mineral phases with surface-sorbed phosphate during the Pre-Extraction step ranged from 0 to 11% of TP, averaging 4 ± 4%, and was highly dependent upon the particular mineral phase onto which the phosphate was surface-sorbed (Table 3.2). For example, <1% of TP associated with aragonite, ferrihydrite, and CFA was solubilized during the Pre-Extraction step, while 6% was released from the goethite and smectite. The largest quantity of TP was released from kaolinite (11%), but it is important to consider the total quantity of P associated with each matrix phase in order to evaluate the impact of fractional solubilization during Pre-Extraction on the accuracy of L-OP determinations. For example, the TP associated with Kaolinite (17.7 ± 0.3 μmol P/ g) is small compared to the P associated with marine plankton (90.5 to 337 μmol P/ g) (Table 3.1). Thus, even if 11% of the P_{ex} associated with Kaolinite is included in the Pre-Extraction supernatant, this should not greatly impact the accuracy of the quantity of P attributed to the L-OP reservoir. Furthermore, it is important to point out that the values that resulted from this experiment likely overestimate of the quantity of P_{ex} released during Pre-Extraction because the minerals assayed were artificially loaded with phosphate. To summarize results of this experiment, P extracted during Pre-Extraction will likely

Figure 3.3 Recovery of OP from the bulk plankton analogue phase in the Pre-Extraction method (2-propanol + 4 B-D) using 1- minute (n=3) and 10-minute (n=5) sonication times. The P extracted was summed over all steps; the standard deviations from replicates are reported as error bars.

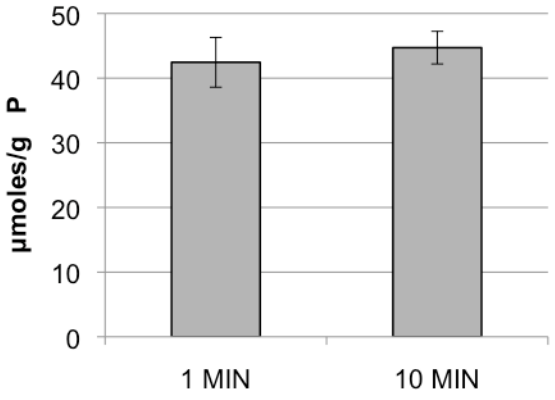

include a small portion of the P_{ex}-pool that is traditionally extracted in Step I of the 'classical' SEDEX method, but will most likely not affect subsequent steps of P extraction.

Table 3.2 Pure minerals with surface-phosphate were taken through the Pre-Extraction method (note: 10 min shaking time at each Pre-Extraction step was used in this experiment), followed by the SEDEX scheme. The percentage of P extracted during the Pre-Extraction method is reported and uncertainty calculated based on duplicate analysis is shown.

Minerals	Percent Dissolution
Aragonite	0.0 ± 0.0%
Smectite	5.8 ± 0.1%
Kaolinite	11.0 ± 2.8%
Geothite	6.2 ± 1.3%
Ferrihydrite	0.3 ± 0.2%
CFA	1.4 ± 0.7%

Evaluation of matrix effects: The goal of the matrix effect experiments was to evaluate the potential for re-adsorption of P released from the target phase (bulk plankton) onto other phases that likely will be present in actual aquatic particulate material. In order to isolate the specific effect of individual matrix phases, we assayed the target phase in isolation with matrix phase. Armed with knowledge of the effect of specific, individual matrix phases on P re-adsorption, one is in a position to evaluate whether a particular natural sediment may exhibit re-adsorption to a greater or lesser extent than is reflected in the experimental results presented here.

To create realistic composite samples that would be reflective of what might be found in natural aquatic systems, we considered the quantity of OP and matrix minerals that might reasonably be present in natural particulate samples. Where possible, we used quantities that reflected average natural conditions, but in some instances, practical considerations about analytical detection limits influenced our decision about quantities used in these experiments. Although the SPExMan-SEDEX method (Ruttenberg et al. 2009) suggests that ~0.1g of sediment is optimal for extraction, since we are using individual components of phases that would make up a bulk sediment, in all cases we used smaller quantities. The quantity of the target phase (bulk plankton) that was weighed into each reaction vessel for the matrix effect experiments was ~20 mg, because this quantity of bulk plankton was necessary to provide enough P such that re-adsorbed P would exceed P-detection limits. We realize that organic P content of typical marine sediments would never be expected to reach 20%; therefore, the matrix effect likely overestimates the re-adsorption of L-OP one might encounter in natural sediments.

The quantity of matrix phase used in each target-matrix phase pair was based upon the relative percentage of that phase in typical marine sediments. The carbonate content of sediments, either as calcite or aragonite, varies widely as a function of depositional environment, ranging from essentially 0 wt% in pelagic red clays to upwards of 90% in nearshore carbonate environments (e.g., Morse and Mackenzie 1990, Kennett 1982, Briggs et al. 2011 – or Chapter 2). Different clay minerals, such as smectite and kaolinite used as matrix phases in these experiments, also occur in widely varying proportions in different sediment environments, but can comprise upwards of 31 to 70% of sediment, respectively, on an organic- and carbonate-free basis (Morse and Mackenzie 1990).We chose to use a quantity of carbonate and clay mineral matrix phases that would be present in a sediment containing 50 wt% carbonate and/or clay on an average bulk sediment basis, and therefore added 0.05 g of pure calcite, aragonite, smectite and kaolinite as matrix phases to be combined with 20 mg of the target L-OP phase in each reaction vessel. (Note: Matrix phases used in these experiments do not have surface-sorbed P associated with them.)

Published values of sediment Fe:Fe-bound P ratios ($Fe:P_{Fe}$) in marine sediments were used as a basis for choosing the quantity of iron mineral matrix phases (goethite and ferrihydrite, Table 3.1) to be used in matrix effect experiments. We wanted to provide sufficient Fe-matrix phase material to ensure ample binding sites for the quantity of P provided by the target L-OP phase. While Slomp et al. (1996) found that $Fe:P_{Fe}$ ratios vary in different sediment environments, these authors suggest that an average ratio of 10 describes most marine sediments. Using an $Fe:P_{Fe}$ ratio of 10 and our choice of optimal target phase mass (≈20 mg), we determined that 3 mg of each Fe mineral would provide adequate number of surface sorption sites to accommodate phosphate solubilized by the bulk plankton target phase during the Pre-Extraction step. Given that if this quantity of Fe mineral were part of a 0.1 g bulk sediment aliquot subjected to SPExMan-SEDEX, this quantity falls within the range of average Fe content of marine sediments, estimated to vary between 2-10 weight percent (Hyacinthe and Van Cappellen 2004; Jensen and Thamdrup 1993). Considering both the average marine sediment Fe content and $Fe:P_{Fe}$ ratio discussed above, we chose to use 5 mg of each pure iron matrix phase, goethite and ferrihydrite, in matrix effect experiments.

Before discussing P re-adsorption onto matrix phases, it is important to evaluate the results shown for the target-phase only samples. Bulk plankton P-recovery was only 72 ± 3% in the Pre-Extraction (Figure 3.4, first blue bars; Figure 3.5). This is perhaps not surprising since, as a bulk surface water particulate sample collected during a plankton tow (Ruttenberg 1992), it may contain some particulate material other than 'pure' phytoplankton. Furthermore, even if the bulk plankton sample is dominated by phytoplankton, if diatoms are present their siliceous tests, which would not be expected to dissolve during the Pre-Extraction, could provide surfaces for P re-adsorption. An additional 13 ± 2% is recovered during Step-I, representing the quantity of secondarily adsorbed P that is recovered by $MgCl_2$, an extractant previously shown to reverse secondary P sorption occurring during SEDEX (Ruttenberg 1992), bringing the total P recovery up to 85 ± 4%. The remainder of the P associated with the bulk plankton

Figure 3.4 Matrix experiment results in which bulk plankton (Table 1) was used as the target phase, or source of labile organic P, and matrix phases were pure mineral analogs: aragonite, calcite, smectite, kaolinite, goethite and ferrihydrite. Each reaction vessel contained 20 mg of bulk plankton and 5-50 mg of the matrix phase. Values are reported as the % of total P extracted in each step. The bulk plankton sample (top bar) did not contain a matrix phase and shows the distribution of P extracted from bulk plankton in each step. Total P (IP + OP) extracted reported for Pre-Extraction and Steps I, IV, and V was analyzed using a high-temperature ashing method (Ruttenberg and Monaghan 1999). Inorganic P (IP) only is reported for Steps II and III.

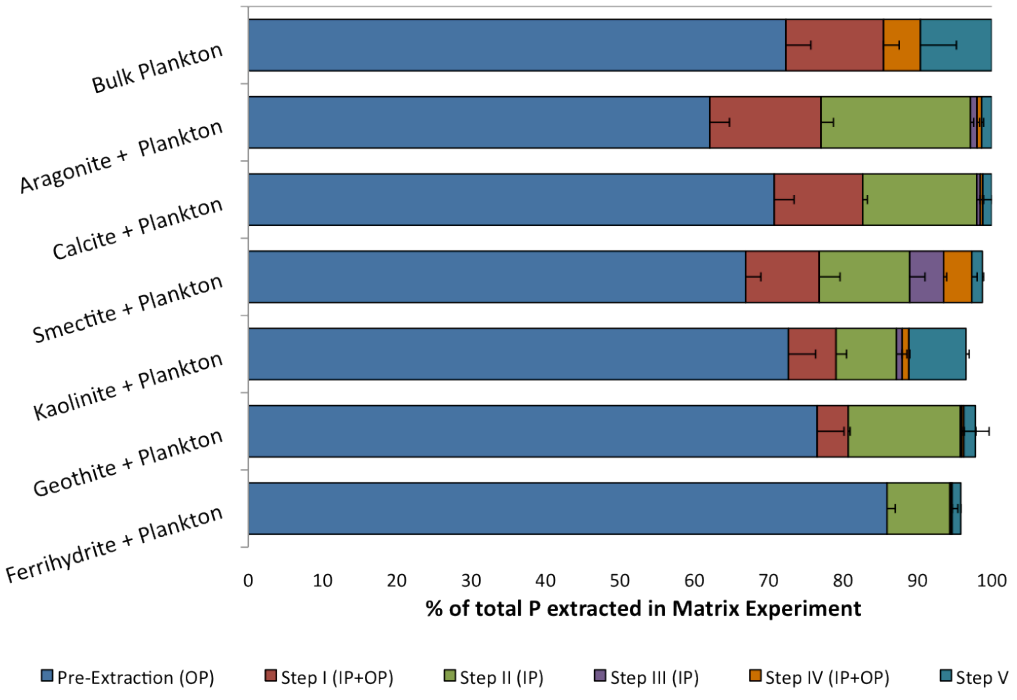

analogue phase is solubilized during SEDEX-Step IV (5 ± 3%) and Step V (10 ± 1%). P recovered in Step V represents a refractory component of organic matter, which may derive from phytoplankton (see discussion of pure plankton recovery, below), but could equally derive from terrestrial organic matter that might have been included in this bulk net-tow sample.

The quantity of P recovered in the Pre-Extraction step from the matrix plus target phase combinations ranged from 62-86% (Figure 3.4); average recovery was 72 ± 3%, which was equivalent to the expected P recovery in the Pre-Extraction step based on the quantity of bulk plankton L-OP (matrix phase alone) (Figure 3.5). The re-adsorption effect was determined as the difference between the P recovery expected (% based on bulk plankton matrix phase) and the actual percentage recovered in the Pre-Extraction step. Re-adsorption effects were most severe for aragonite, (10 ± 4 %) and calcite (5 ± 4%), with undetectable re-adsorption (within the range of uncertainties) occurring onto kaolinite, smectite, and goethite. All recoveries fall within the range observed for the target phase with the exception of ferrihydrite, which displayed higher recoveries of L-OP (86 ± 1%). Recent studies have shown that ferrihydrite can cause surface catalyzed DOP hydrolysis (Baldwin et al. 1995; Bladwin et al. 1996; Ruttenberg and Sulak 2011), thus the higher P recovery from ferrihydrite in the Pre-Extraction step be due to hydrolysis of surface associated OP.

Having observed incomplete recover of L-OP from bulk plankton in the matrix effect experiment, we examined the P recovery in the remaining SEDEX steps in order to evaluate where the un-recovered phytoplankton-associated P might be released (Fig. 3.4). As previously mentioned, P recovered from the bulk plankton analog (no matrix phase present) in the Pre-Extraction plus Step I was 85 ± 4%, which falls well in-line with the recovery of P when matrix phases were present (Figure 3.4). On average, for all matrix experiments, 38% of P associated with phytoplankton was not recoverable in the Pre-Extraction step, but between 4 to 15% of re-adsorbed P was recovered in Step I, bringing the total P recovery from both Pre-Extraction and Step I to 76-87% (Figures 3.4).

The majority of the remaining phytoplanktonic-P was released in Step II for all phases except for smectite, which displayed P release in Steps III and IV (consistent with Ruttenberg, 1992), and Kaolinite, which displayed release in Step V (Figure 3.4).

Figure 3.5 Partitioning of P extracted from bulk plankton, diatoms, dinoflagellates, and green algae analogue phases (Table 1) subjected to the full SEDEX procedure, with and without Pre-Extraction (dark and grey bars, respectively). Total P (IP + OP) extracted reported for Pre-Extraction and Steps I, IV, and V was analyzed using a high-temperature ashing method (Ruttenberg and Monaghan 1999). Inorganic P (IP) only is reported for Steps II and III. The sum of P extraction from Pre-extraction plus Step I is given below the graphic in italics. Values reported adjacent to bars in the bar graph report the percent of total P extracted in each step.

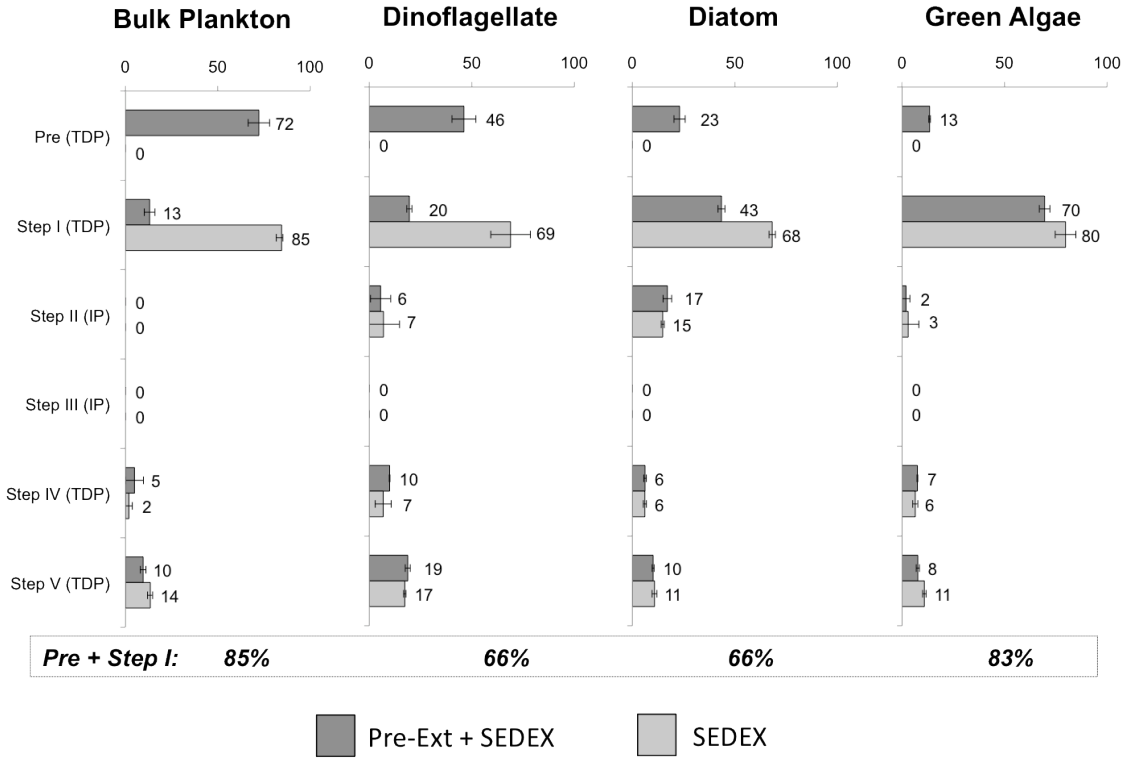

Recovery of the remaining phytoplanktonic-P appears to be influenced by the nature of the specific matrix phase present. For example, secondarily sorbed P may have become irreversibly sorbed onto matrix phases, to be released only when these matrix phases are solubilized; this is likely the case for P sorbed to Fe phases, goethite and ferrihydrite (see Ruttenberg (1992) and Ruttenberg and Sulak (2011) for a discussion of irreversible P sorption onto iron (oxy)hydroxides). In the case of P released from carbonate phases and clays during Step II, however, it is possible that the citrate in the Step-II extractant (CDB, Figure 3.1) effects partial dissolution of the matrix phases; this is particularly likely for the carbonate phases as Ca^{2+} forms stable soluble complexes with citrate (Stumm and Morgan 1981), but may also occur with clays, as Al^{3+} may be partially solubilized via chelation with citrate, as well. Partial solubilization will affect mineral surfaces, and thus may result in collateral solubilization of surface-sorbed P. We note that the fact that P

solubilized from kaolinite in Step V is consistent with results of Ruttenberg (1992), who reported P-recovery from another 1:1 clay, illite, after ashing during Step V, and suggests that solubility of some clay may be enhanced after ashing at high temperatures.

It is important to emphasize that the average recovery in the Pre-Extraction step for all matrix experiments was equivalent to the bulk plankton P recovery in the Pre-Extraction (without matrix phase present), and amounted to an average L-OP recovery of 72%. While some redistribution of the remaining phytoplanktonic-P onto matrix phases occurred via re-adsorption, overall recovery of 72% L-OP indicates that matrix effects do not impede recovery of the bulk of L-OP during the Pre-Extraction step.

3.4.2. Efficiency and specificity of TAC for $CaCO_3$-P.

Maximum $CaCO_3$ dissolution of ~55% was achieved after 8 hours in TAC with a solution:solid (s:s) ratio of 100 (ml:g) (Figure 3.6a). While it is possible that a higher s:s ratio would have enabled higher recoveries, this line of inquiry was not pursued further due to the fact that enough CFA dissolution occurred, even though it never exceeded 7% throughout the 8-hr time course (Figure 3.6a), to render successful separate quantification of $CaCO_3$-P via TAC unlikely. We use data from Ruttenberg (1992), who reported that shells used as $CaCO_3$ and CFA analog phases have associated with them 0.4 wt% and 11.66% P, respectively, to calculate the P yield expected from 55% dissolution of $CaCO_3$ in TAC, and compare this to the quantity of P expected to be released from 7% dissolution of CFA. Utilizing the wt% of P associated with each mineral and the s:s ratio of 100, 5-7 μmole P would be released from $CaCO_3$, while P release from CFA, experiencing only 7% dissolution, would release between 1500-2500 μmole P. Thus, although extent of CFA dissolution is relatively small compared with extent of $CaCO_3$ dissolution (Figure 3.6b), the quantity of P released from just 7% CFA dissolution could be enough to completely swamp any P release that might be expected to occur as a consequence of $CaCO_3$ dissolution.

We caution that the analysis of results from these dissolution experiments assumes that the quantity of $CaCO_3$ and CFA are equivalent in a given sediment sample, which grossly oversimplifies the natural variability in sediment composition that may be encountered in different depositional environments. In some sedimentary environments, the TAC method for separate quantification of $CaCO_3$-P may still be applicable. For example, if CFA concentrations are exceedingly low and $CaCO_3$ content is relatively large, 7% dissolution of CFA may not necessarily mask $CaCO_3$-bound P. Because our work focuses primarily on sediments with measurable quantities of CFA, the TAC method was judged not to be useful in our study, so no further standardization experiments were run with TAC.

3.4.3 Comparison of SEDEX method with and without Pre-Extraction.

Labile organic P (L-OP) analogue phase results: All phytoplankton analogue phases (Table 3.1) were subjected to the full SEDEX procedure, with and without Pre-Extraction, to evaluate the quantity of P liberated in each step. This experiment allows us to determine in which SEDEX-step the L-OP, solubilized from phytoplankton during the Pre-Extraction step, will be released during the 'classical' SEDEX scheme (e.g., SEDEX conducted without a Pre-Extraction step). Also, this test permits an assessment of

Figure 3.6 Results of $CaCO_3$ and CFA (Table 1) dissolution experiments using Triammonium citrate (TAC). (a) Percent yield of Ca^{2+} quantified via ICP-OES analysis. (b) Percent yield of phosphorus calculated utilizing wt% of P associated with $CaCO_3$ and CFA analog phases (0.4 wt% and 11.66% P, respectively; Ruttenberg 1992).

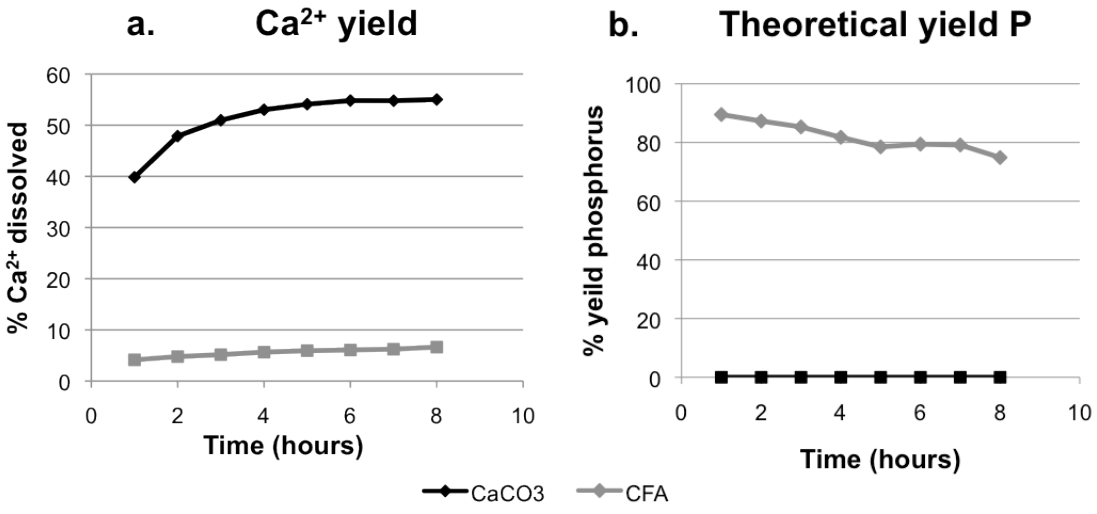

potential variability in L-OP recovery from different types of phytoplankton, including a diatom, a dinoflagellate, and a green alga, as well as the bulk plankton sample, which may be a mixed assemblage of phytoplankton and may contain non-phytoplankton material (as previously discussed).

Pre-Extraction followed by SEDEX: Triplicate splits of phytoplankton analogues (2-5 mg), weighed into SPExMan reaction vessels and subjected to the Pre-Extraction, released between 13 to 72 % of L-OP, with the largest fraction of L-OP released from the bulk phytoplankton analogue (72%) followed by the dinoflagellate (46%), diatom (23%) and the lowest quantity released from the green alga (13%) (Figure 3.5). The quantity of P released during Step I is operationally-defined as loosely-sorbed P (P_{ex}), and represents L-OP released during Pre-Extraction but sorbed onto solid-phase residue remaining after Pre-Extraction. When the quantity of P released during Step I is combined with that released during Pre-Extraction, the total released during Pre-Extraction + Step I is 85% from the bulk plankton, 66% from both the dinoflagellate and diatom, and 83% from the green alga (Fig. 3.5). The dissimilarities between algal taxa in partitioning of L-OP solubility are striking, and reflect either differences in the nature of DOP released during Pre-Extraction, or differences in the nature of the residual solid phase that provides surfaces for secondary P sorption, or both. Despite these differences, however, the bulk of P within these L-OP analogue phases, between 66 and 85% of L-OP, is accounted for by the P solubilized during Pre-Extraction and Step I.

Step V is the only other step where a consistently sizable fraction of P is recovered from all plankton analogue phases. Between 8 and 19% of phytoplankton cellular P are recovered in Step V (Figure 3.5). The fact that this quantity of P was not soluble until after ashing at 550°C suggests that, according to the operationally-defined nature of Step-V-solubilized P, this fraction of cellular phytoplanktonic P is refractory in nature. This surprising result will be discussed further, below. Smaller quantities (≤10%) of P were solubilized from all four L-OP analogue phases in Step IV, no detectable L-OP was released during Step III.

The quantity of P released during Step II, although small, merits some discussion because prior studies have found P extractable from cultured phytoplankton in extractants specific for reactive Fe-oxyhydroxides (Sanudo-Wilhelmy et al. 2004). Sanudo-Wilhelmy

et al. (2004) argued that P is present in phytoplankton as both surface-adsorbed and intra-cellular pools, and this result has been the basis for speculation about the integrity of the Redfield Ratio concept. The amount of P associated with cultured phytoplankton that is solubilized in Step II in our study, and is therefore operationally-defined as P associated with Fe-oxyhydroxides (P_{Fe}), ranges between 2 to 17% (Figure 3.5); no P_{Fe} was solubilized from the field-collected bulk plankton sample in Step II. Our results do not allow us to distinguish between L-OP originally associated with intact phytoplankton cells that was solubilized during the Pre-Extraction and secondarily sorbed onto phase(s) which were subsequently solubilized during Step II, from P_{Fe} that may have formed on surfaces of analog plankton cells during the culturing process. Because only cultured phytoplankton displayed a substantial quantity of P_{Fe}, it is unclear whether such a pool exists in natural phytoplankton populations. At this point, we can only concur with Sanudo-Wilhelmy et al. (2004) that this observation is intriguing, and that the possibility exists that a fraction of P, operationally defined as OP associated with phytoplankton, may not actually be organic in nature. If accurate, this result potentially undermines, to some extent, the valuation of the canonical Redfield Ratio of 106C:16N:1P, given that a portion of operationally-defined 'Redfieldian-P' might be surface sorbed P_{Fe} and not cellular OP.

Phytoplanktonic L-OP extracted in Pre-Extraction and Step I: The quantity of TDP (DIP + DOP) extracted from phytoplankton in SEDEX-Step I, without Pre-Extraction, is statistically equivalent to quantity of P extracted in Pre-Extraction + Step I (Figure 3.7). This result suggests that application of the 'classical' SEDEX method, without Pre-Extraction, will remove the bulk (66-85%) of L-OP prior to subjecting the residual sediments to the remaining SEDEX steps, so that most of the L-OP pool is recoverable in SEDEX-Step I. It is important to note, however, that quantification of the L-OP solubilized during SEDEX-Step I will only occur if this extract is subjected to TDP analysis, so that solubilized DOP will react colorimetrically and thus be detectable by the molybdate blue method (Monaghan and Ruttenberg 1999). If TDP analysis of SEDEX-Step I is not done, our results suggest (Fig. 3.7) that between 30-40% of the L-OP pool will remain undetected, and will be lost from the full accounting of P distribution in the sample.

Figure 3.7 The percentage of TDP (DIP + DOP) extracted in Pre-Extraction + Step I (first bar) from all analog phytoplankton phases, compared to the percentage of TDP extracted in Step I only (second bar). TDP and DIP were analyzed in all supernatants, and the distribution of P between DIP and DOP is shown as follows: Step I-DIP (blue), Step I-DOP (green), and Pre-Extraction TDP (red).

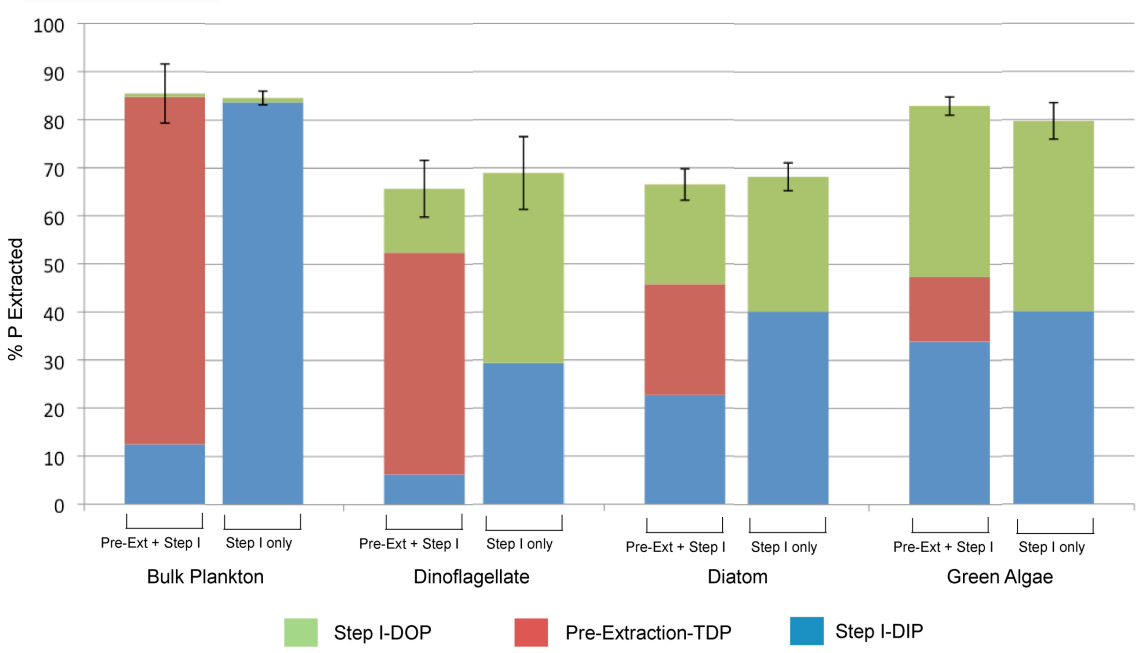

The quantity of DOP recovered from all cultured phytoplankton subjected to Step I but not Pre-Extraction exceeds the quantity of DOP recovered in Step I when Pre-Extraction was conducted (Fig. 3.7), indicating that the Pre-Extraction step recovers a portion of the L-OP pool that would otherwise be solubilized during Step I. Recovery of DIP in Step I when Pre-Extraction is not employed is always greater than the quantity of DIP recovered from Step I when it follows the Pre-Extraction step, suggesting either that hydrolysis of DOP occurs during the Step I extraction, or that P quantified as TDP in the Pre-Extraction solution is a combination of DOP and DIP. This latter could be the case if a portion of the intracellular phytoplanktonic P was phosphate or polyphosphate, as can happen under luxury P consumption conditions (Cembella et al. 1982). We are unable to distinguish between these two possible mechanisms that supply DIP from L-OP analogue phytoplankton phases during extraction, and can only state that it may represent either intracellular inorganic P, or be the result of hydrolysis of reactive DOP that may occur during cell-lysis and extraction.

To summarize, these results suggest that application of the Pre-Extraction method to sediments is not required if the objective is to quantify the combined pool of labile and

Figure 3.8 Comparison of P distributions obtained for marine sediment samples from three depositional environments as determined by the combined Pre-Extraction-SPExMan-SEDEX method (dark grey diamonds), as compared to the SPExMan-SEDEX method without Pre-Extraction (light grey squares). All values are reported in µmoles P g^{-1} sediment. Data for Mississippi Delta and Equatorial Atlantic sediments that were brought through the SPExMan-SEDEX method only are from Ruttenberg et al. (2009).

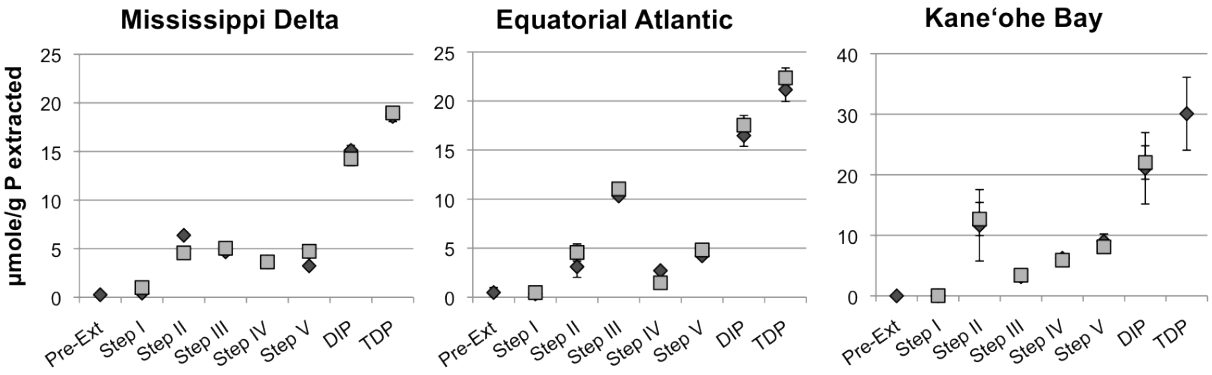

exchangeable P, without differentiating DOP from DIP. If the Step I supernatant is subjected to a TDP analysis, which will convert all DOP to DIP, then the quantity of TDP recovered in Step I will be equivalent to the combined (P_{ex} + L-OP) pool. If, on the other hand, the objective is to separately quantify L-OP, and potentially subject the L-OP pool to other analytical protocols to obtain further details about the nature of this pool (ie. Column chromatography, NMR, or other forms of spectroscopy), the Pre-Extraction step will permit the separate recovery of L-OP for its quantification and further investigation.

Comparison of SEDEX data from seabed sediments with and without Pre-Extraction: Sediment samples subjected to the Pre-Extraction Step did not display sizable quantities of L-OP relative to the quantities of P recovered in subsequent SEDEX steps (Figure 3.8). As a consequence, the concentrations of P recovered from each SEDEX reservoir are similar, to indistinguishable, whether or not the Pre-Extraction step was included (Figure 3.8). The absence of L-OP, as operationally defined by the Pre-Extraction, from seabed sediments from these three distinct depositional environments suggests that the OP reservoir in these surface sediments is relatively refractory. Unless surface sediments are collected immediately after deposition of a crashing phytoplankton bloom, or host a substantial layer of microphtyobenthos, it seems a good assumption that the organic P component of seabed organic matter is relatively refractory. Thus, unless the sediments have had a recent infusion of fresh (and therefore labile) organic matter, it

is probably safe to apply the SEDEX method without Pre-Extraction to seabed sediments, without risk of losing or mis-identifying L-OP, as originally argued in Ruttenberg (1992). Results from extraction of pure phytoplankton analogue phases (Figure 3.5), however, suggest that when analyzing water column suspended material that may be dominated by cellular OP, the Pre-Extraction method is useful for separately quantifying the labile OP pool.

Figure 3.9 The percentage of P extracted from two types of pure DNA (Sigma CAS #9007-49-2; Fisher CAS #BP25141, DNA-1 and DNA-2 respectively) by the Pre-Extraction method, Step I of SEDEX ($MgCl_2$ wash) and a final ashing step. Error bars represent the standard deviation calculated over triplicate analysis of each sample.

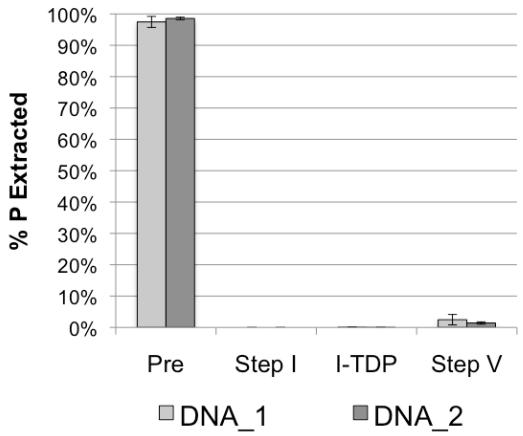

3.4.4 Further insight into 'Refractory phytoplanktonic-P'.

As previously discussed, the Step V recovery of a substantial fraction of OP from phytoplankton analogue phases raises the possibility that a portion of cellular P may, in fact, be refractory in nature. This is an intriguing possibility as it runs counter to our preconceived notions about the nature of cellular OP. In addition, it is tempting to align these results with the often-speculated upon refractory OP pool that could be responsible for the low organic C:P ratios observed in environments characterized by low concentrations of refractory organic matter, such as pelagic and certain deltaic environments (e.g., Ingall and Van Cappellen 1990; Ruttenberg and Goñi 1995). Another possibility is that this apparently refractory OP is an artifact, and may result from failure to solubilize DNA, a highly insoluble molecule that will only dissolve in polar-to-neutral solutions. We considered the possibility that the non-polar nature of the solvents in the B-D reagent might inhibit the solubilization of DNA during Pre-Extraction and subsequent the SEDEX extractions, but that DNA would decompose during muffling at 550°C, and could then be solubilized during Step V.

To test the possibility that L-OP recovered in Step V may result from failure to extract and solubilize cellular DNA in prior steps, two types of DNA (Sigma CAS #9007-

49-2; Fisher CAS #BP25141) were taken through the Pre-Extraction method, Step I of SEDEX ($MgCl_2$ wash), and subjected to a final ashing step equivalent to SEDEX-Step V. The fact that DNA was fully recovered (98-99%) in the Pre-Extraction Step (Figure 3.9) allows us to conclude that the OP that is recovered from phytoplankton analogue phases in SEDEX-Step V, while it remains insoluble during Pre-Extraction, cannot be attributed to failure to solubilize cellular DNA from phytoplankton. Thus, the mystery of the nature of the 'refractory' phytoplanktonic P pool persists, and awaits further work to reveal the nature of this highly refractory OP pool that is rendered soluble only after ashing at high temperature (550°C).

Appendix 3.1 Sep-Pak analysis of SEDEX-Step II (CDB) supernatants for quantification of Fe-bound P.

Step II of SEDEX utilizes a citrate dithionite bicarbonate (CDB) solution to selectively dissolve Fe-bound P. The CDB solution cannot be analyzed via the standard molybedenum blue method due to interferences from citrate with color formation. The butanol extraction method of Watanabe and Olsen (1962) was previously used to separate liberated soluble reactive phosphorus (SRP) from the CDB solution in the Step II of the SEDEX method (Ruttenberg 1992). This analysis yields variable precision, ~10-20% and can sometimes be as poor as 50%. Therefore, finding a new, precise method for the determination of P in Step II extracts was necessary.

We utilized a solid-phase extraction technique by Suzumura and Koike (1995) to replace the Watanbe and Olsen pretreatment of CDB solution. The method works by converting SRP in solution to a 12-molybdophosphric acid (12-MPA), which is adsorbed from the aqueous solution onto a non polar solid-phase cartridge. The 12-MPA is then eluted off the column and analyzed for SRP by the standard molybedenum blue method of Koroleff (1983). Our method employs several modifications to the method outlined by Suzumura and Kioke (1995), which to increase the efficiency of this method, as well as tests the reusability of seppak cartridges.

The sep-pak technique utilizes a Waters© Sep-Pak cartridge packed with polystyrene divinylbenzen (PSDVB). In the original sep-pak manuscript, Suzumura and Koike (1995) utilize a PS-1 cartridge by Waters. This cartridge has since been replaced by a PS-2 cartridge, which we find works with the same efficiency. The cartridge is manufactured by Waters, Japan, but can be ordered through the US Waters Corp (Part # JJAN20151); there is no US manufactured replacement part. The cartridge was equipped with a make-shift reservoir by attaching the seppak cartridge to the barrel of a luer-lok 20cc syringe, which fit snugly together. The cartridge and adapted reservoir were attached to a PTFE manifold stopcock needles (AllTech) on a 24-port SPE glass column processor (JT Baker). The glass rig was connected to a vacuum pump, which allowed simultaneous filtration of multiple samples through the sep-pak columns.

Standard solutions were made (0-150 μM range) using 10 μmol ml^{-1} phosphate stock solution in a CDB matrix. All standards were brought through the procedure

identical to samples. The procedure, as described below, results in a 10-fold dilution therefore final concentration ranges of standards were 1-15 μM (note: the procedure does not have to result in a 10-fold dilution, if you start with 10ml of solution and scale prior to elution, there will be no dilution). Samples from the SEDEX method are typically highly concentrated so the 10-fold dilution works well and eliminates both the production of waste when utilizing larger sample size and dilution prior to analysis. Additionally, diluting the CDB extractant prior to sep-pak recovery of SRP assisted in the complete recovery of liberated P. A 10-fold dilution of CDB samples (or standards) with MQ-DI water (1mL CDB and 9mL MQ-DI) was employed immediately following the recovery of filtrate from Step II in the SEDEX method. The CDB solution is not stable, due to the volatility of dithionite in its aqueous form, thus it is suggested to pretreat and analyze CDB extracts immediately after completion of Step II. CDB extracts that were treated and analyzed several weeks later resulted in slightly lower recovery of SRP (data not shown).

A pretreatment with $FeCl_3$ prevents the interference of citrate with the reduction of the molybdate complex (Lucotte and D'Angeljan). After the 10-fold dilution, samples were reacted with 1% v/v 1M $FeCl_3$ solution (initial color is a dark yellow). Analytical grade $FeCl_3$ has a 0.01% maximum PO_4 blank. If larger volumes of $FeCl_3$ are used the P blank from $FeCl_3$ can result in a final P signal that masks the signal of SRP solubilized in CDB. After the addition of $FeCl_3$, samples are allowed to react overnight (final color is a pale light yellow).

The next morning samples were mixed with acid-molybdenum solution (Suzumura and Koike 1995) at a volume ratio of 3:1 to convert SRP to 12-MPA. Prior to running samples through the cartridge, the sep-pak was prepped and washed according to Suzumura and Koike (1995) using 3 mL of methanol and 5 mL of 1N sulfuric acid. After the sample was passed through the cartridge a yellow plug appeared, indicating retention of the 12-MPA complex. Cartridge and reservoir were then washed with 5 ml of 1N sulfuric acid to remove all residual citrate dithionite. The 12-MPA was eluted off the column and collected using 5 ml of 0.5M ammonium solution (yellow plug disappears). An additional 3 mL of 1N sulfuric acid and 2 ml of MQ-DIW was passed through the column and collected with the 5 ml of 0.5M ammonium solution, bringing the solution to

Appendix Figure 3.1 Reusability test on the Sep-Pak cartridges to examine carry over on each column. Standards were run through the same Sep-Pak cartridge 5 times; all standards were within 5% error.

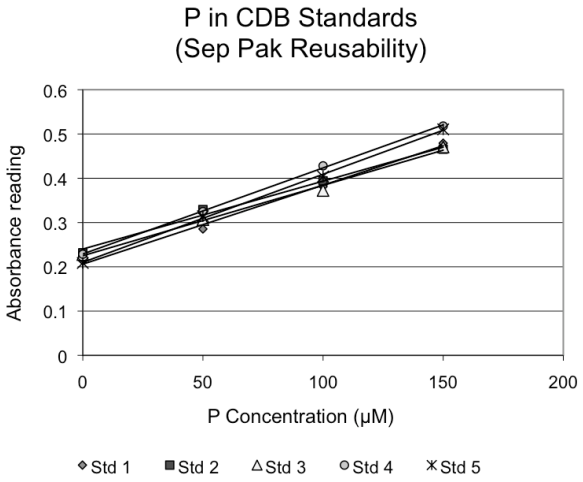

a final volume of 10 ml at pH 1. Samples were then analyzed using the standard molybdenum blue method with a BioTek Synergy HT Multi-Mode Microplate Reader (Grasshoff, 1972).

Cartridges are reused multiple times during analysis. A simple reusability test was conducted to examine carry over on each column. We ran standards through the same sep-pak cartridge 5 times and found all standards were within 5% error. This experiment demonstrates the high reproducibility of this method and also suggests no carry over during re-use of the cartridge even at high (150 µM P) concentrations (Appendix Figure 3.1).

Appendix-3.2 Miscellaneous analytical details regarding Pre-Extraction.

We were surprised and perplexed that during a first attempt to test the specificity of the Pre-Extraction for L-OP large quantities of P were extracted from each pre-sorbed mineral phase with the B-D solvent mix. Closer examination revealed that the B-D reagent used in this first test was extremely acidic (pH~2). We learned that chloroform ($CHCl_3$) degrades to hydrochloric acid over time, and it turned out that the particular bottle of chloroform we initially used to make up our B-D reagent had decomposed substantially and, as a result, had become acidic. When new, non-degraded chloroform is used, the final pH of the B-D solution should be between pH 7 to pH 8.5. Thus, prior to using the B-D reagent, pH should be measured, to guard against employing an inadvertently acidic Pre-Extraction solution, which will actively dissolve non-organic, mineral-P that will normally comprise the operationally defined pools of SEDEX-Steps I-IV.

Acknowledgments

Mashiro Suzumura supplied important suggestions that guided initial stages of method development for the $CaCO_3$ extraction, as well as information and assistance with the Sep-Pak method, which we gratefully acknowledge. Sonya Dyhrman and Sheehan Haley at WHOI provided cell cultures, which we gratefully acknowledge. We would like to thank Marcie Grabowski and Kathryn MacDonald for laboratory assistance and James Cowen for access to the SEM. This work was funded grant/cooperative agreement from the National Science Foundation. The views expressed herein are those of the authors and do not necessarily reflect the views of NSF or any of its sub-agencies. This is SOEST contribution #xxxx.

Chapter 4

Linking source, abundance and lability of sedimentary organic matter to remineralization efficiency

with A.E. Ricardo, K.C. Ruttenberg, B.T. Glazer

Abstract

This study systematically relates how variations in source (and therefore lability) of organic matter (OM) affects rates of OM degradation in marine sediments. Molar OC:TN:OP ratios are used in tandem with carbon isotopic values to constrain sources of OM to sediments. OC:TN ratios are a weaker indicator of OM source than OC:OP ratios, because: (i) the more restricted dynamic range of OC:TN ratios prevents clear distinction of terrestrial- from marine-derived OM, and (ii) post-depositional changes in OC:TN ratios occur during diagenesis, obscuring the source signature of initially deposited OM. Whole sediment cores collected along a shore-to-bay transect were embedded with voltammetric microelectrodes and incubated in the laboratory. Rates of O_2 consumption, H_2S production, and NH_4^+ accumulation in porewaters were quantified as proxies for microbial OM remineralization. Higher remineralization rates were observed at sites located farthest from the shore where sediments were characterized by more labile, marine-dominated OM; progressively slower remineralization rates were observed as the fraction of terrestrial (more refractory) OM increased in sites proximal to the shore. Although larger quantities of OM were deposited at the most landward site, resulting in larger quantities of regenerated inorganic nutrients per unit time and greater benthic nutrient fluxes, specific remineralization rates were lower at this site. This contrast makes clear the importance of distinguishing between quantity versus quality of OM when assessing remineralization rates.

4.1 Introduction

Organic matter (OM) in coastal aquatic sediments derives from marine sources, such as seagrasses, micro- or macroalgae and phytoplankton, as well as terrestrial sources that are principally delivered by rivers. In areas where mangrove forests are present, mangrove litter can contribute OM to coastal sediments, as well. If OM is not respired within the water column or physically transported out of the system, it settles to the sediment, where it is subjected to degradation and chemical alteration by the benthic community. A portion of degraded OM may be recycled into the overlying water as dissolved organic matter or inorganic nutrients, the products of OM remineralization. The residual material is incorporated into sediments, where it can be further degraded during burial. Most of the organic carbon (94%) preserved in marine sediments is buried in continental margin sediments (Berner 1982; Hedges and Keil 1995). Therefore, understanding the sources, lability and subsequent preservation of OM in coastal sediments is essential to understanding carbon cycling in the global ocean.

Marine derived OM is generally more labile than its refractory, terrestrial counterpart (Aller et al. 1996; Cowie and Hedges 1992). The principle tools for distinguishing marine versus terrestrial OM are elemental ratios and isotopic composition. While marine phytoplankton have a mean molar organic carbon to total nitrogen to organic phosphorus (OC:TN:OP) ratio of 106:16:1 (Redfield et al. 1963), terrestrial, vascular plants have characteristic OC:OP up to or exceeding 800, and OC:TN ratios ranging up to or exceeding 1000 (Likens et al. 1981). Bulk sediment stable isotope signatures provide an additional, independent tool for the identification of OM sources to sediments (e.g., Hedges and Parker, 1976, as cited by Goñi et al. 1997). Organic compounds derived from marine OM are enriched in ^{15}N and ^{13}C relative to compounds originating as terrestrial OM (Gearing et al. 1977; Goñi et al. 1998; Ogrinc et al. 2005). Isotopic composition is a robust tracer of OM source because isotopic fractionation during digenesis of OM appears to be small, typically less than 2% (Meyers 1997).

OM in surface sediments is metabolically degraded through a complex series of microbial respiratory pathways (e.g., Froelich et al 1979; Burdige 2006). The quality and quantity of OM deposited in coastal sediments will determine rates of OM respiration.

Complete characterization of OM remineralization rates is hindered by our inability to directly measure all of the oxidation pathways in marine sediments (Canfield et al. 1993; Kostka et al. 1999; Thamdrup and Canfield 1996). Due to these constraints, characterization and direct quantification of the dominant microbial OM respiration pathways is often incomplete, and relies heavily on thermodynamic modeling (Nedwell et al. 1993; Rysgaard et al. 1996). An alternative approach to the separate quantification of individual metabolic pathways is to estimate total rates of OM remineralization via changes in oxidant concentrations and the products of OM remineralization (e.g., Canfield et al. 1993). We adopt this latter approach in the present study.

The purpose of this study was to systematically relate how variations in source (and therefore lability) of OM affect rates of OM degradation in marine sediments. Whole sediment cores embedded with voltammetric microelectrodes were incubated in the laboratory and rates of O_2 consumption, H_2S production, and NH_4^+ accumulation were quantified as proxies for microbial OM remineralization. Solid-state Au/Hg glass voltammetric microelectrodes used in this study are a unique tool for estimating sediment redox conditions, as they can simultaneously measure multiple dissolved species, such as O_2 and H_2S (e.g., Luther III et al. 2008 for review). In order to capture a gradient in OM sources, sediment cores for our incubation study were collected along a terrestrial-to-marine gradient from sites located in a protected coastal marine embayment in Kane‘ohe Bay, Oahu, Hawai‘i. We utilize sediment molar OC:TN:OP ratios in tandem with bulk sediment carbon isotopic values to constrain sources of OM to sediments from each site. This multi-tracer approach allows tighter constraints to be placed on the source of OM to coastal sediments than either parameter alone (Middelburg and Nieuwenhuize 1998; Ruttenberg and Goñi 1997a; Ruttenberg and Goñi 1997b). A component of our study included an examination of the effects of diagenesis on the preservation of source signatures of terrestrial and marine OM. Combining estimates of the efficiency of OM remineralization with an analysis of OM sources to depositional environments along a land-to-sea gradient enables us to link the remineralization efficiency directly to OM source, and thus provides insight into how OM source can impact preservation of organic carbon in marine sediments.

4.2 Study Site

Figure 4.1 Aerial photograph of He‘eia Fishpond with study sites marked as white boxes.

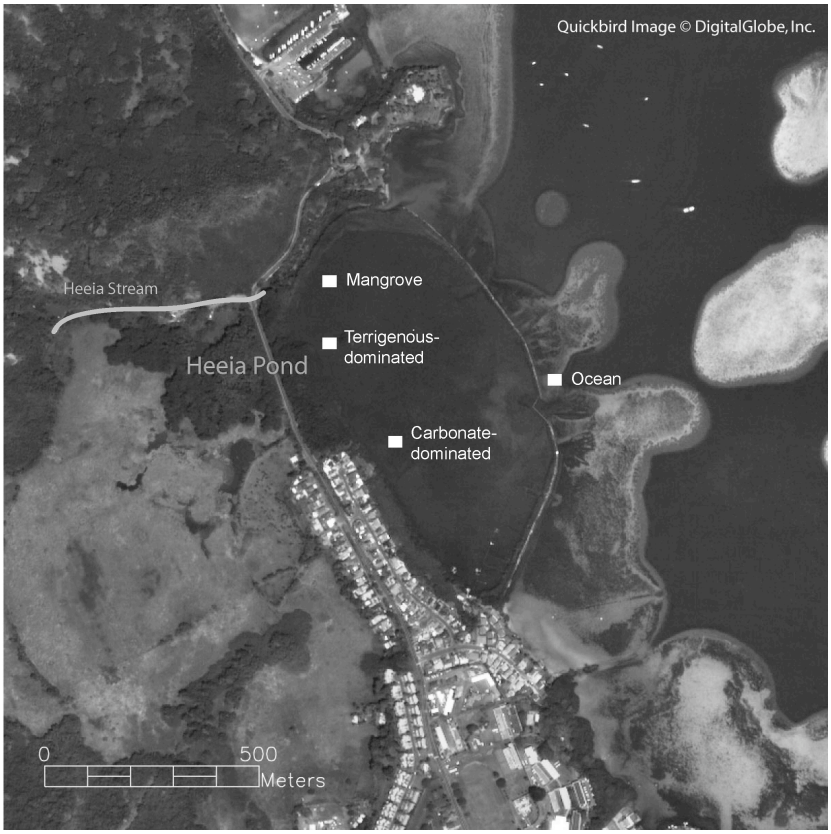

Sediment push cores were collected along a shore-to-bay transect in He‘eia Fishpond, an 88-acre coastal pond located on the eastern side of Oahu, adjacent to Kane‘ohe Bay at the land-sea boundary of the He‘eia watershed (Figure 4.1). The fishpond is a low-energy, shallow coastal system influenced by an influx of both riverine freshwater and seawater from Kane‘ohe Bay, and is ringed by a mangrove forest along its terrestrial periphery. Water flow into and out of the pond is controlled by gates, which are typically left open, rendering the pond analogous to a large mesocosm embedded in a natural coastal environment, making it an ideal site for coastal biogeochemical studies (Young 2011).

In order to study sediments characterized by distinct OM sources and redox conditions, four depositional environments were sampled along a transect extending from the shoreline to progressively more marine-dominated sites. These sites are hereafter defined as: i) Mangrove (collected under the mangrove canopy); ii) Terrigenous-Dominated (collected from a location proximal to riverine input); iii) Carbonate-Dominated (collected from a location distal to riverine input); and iv) Ocean (collected outside He‘eia Fishpond, proximal to the coral reef in Kane‘ohe bay; Figure 4.1).

4.3 Methods

Sample Collection: Two sediment push cores were taken at each site along the terrestrial-to-marine transect. One core was collected for sediment sectioning and porewater extraction and a second core for laboratory incubation experiments. The mangrove and terrigenous-dominated sites were sampled and incubations were initiated on 17 April 2008; four days later the experiment was repeated at the carbonate-dominated and ocean sites. Weather patterns remained constant during this 4-day sampling period, and all cores were collected within the same tidal regime. Thus, cores from all 4 study sites were collected under similar initial physical conditions. Immediately after collection, cores were placed in a bucket of ice to reduce metabolic activity, and covered to inhibit photosynthetic activity during transport to the laboratory.

Tissue samples were collected from terrestrial and aquatic plants that are likely sources of OM to He'eia Fishpond, including mangroves and macroalgae. A surface-water plankton tow (100 μm mesh) was conducted from a small boat, both inside the fishpond and outside, in Kane'ohe Bay. Plankton samples and plant tissues were freeze-dried and analyzed for elemental and isotopic composition to characterize end member sources of OM to the study site.

Core processing and analysis: Cores from each site used to determine initial conditions were sectioned at 0.25 to 1 cm intervals under an inert (N_2) atmosphere to prevent oxidation artifacts (Bray et al. 1973). Porewater was separated from bulk sediment via centrifugation. In order to maximize porewater collection in sandy sediments, we adapted Whatman VectaSpin 20 ® centrifuge tubes that allow filtration during centrifugation by replacing the manufacturer installed polypropylene filter with a coarse (1.2 μm) GF/F filter. The coarse GF/F filter allowed maximum recovery of sediment porewater, which was subsequently filtered using a 0.4 μm Pall Life Sciences GHP acrodisc ® filters. Filtered porewater was split into two subsamples: a frozen, untreated split and a refrigerated-acidified split. Samples were analyzed for dissolved inorganic phosphate (DIP) and ammonium (NH_4^+) using established colorimetric protocols on a BioTek Synergy HT Multi-Mode Microplate Reader (Grasshoff et al. 1983); all reported data have a 2% standard error associated with them. Colorimetric detection on small porewater sample volumes (300 μL) can be conducted using the

microplate reader, which allowed for the analysis of multiple dissolved constituents on a single porewater interval, despite the small volumes of porewater collected from each interval. We used Nunc 96-well Optical Bottom Plates ®, which have a 1-cm path length, comparable to that of standard spectrophotometric detection. However, analyses conducted on the plate reader have a slightly higher detection limit than traditional spectrophotometers (0.2 μM for PO_4^{3-} and NH_4^+).

After removal of porewater, sectioned sediments were frozen under an inert atmosphere until freeze-dried under vacuum to prevent oxidation artifacts (Bray et al. 1973; Krall et al. 2009). Sediments were ground with an agate mortar and pestle, sieved (<125 μm) and stored in a sealed vessel prior to analysis. Inorganic sedimentary phosphorus (IP) was determined utilizing acid hydrolysis and total sedimentary phosphorus (TP) was determined using the high-temperature ashing/hydrolysis method of Aspila et al. (1976). Organic phosphorus (OP) was estimated as the difference between TP and IP. Total carbon (TC), organic carbon (OC), inorganic carbon (IC), and total nitrogen (TN), as well as carbon and nitrogen isotope values ($\delta^{13}C$ an $\delta^{15}N$, respectively), were determined using a combined coulometric-elemental analyzer-mass spectrometry method adapted for high carbonate sediments (Briggs 2011). Samples were analyzed for carbon and nitrogen at the Isotope Biogeochemistry Laboratory at the University of Hawai‘i, Manoa. Carbon and nitrogen isotopic values are reported using conventional δ-notation with respect to VPDB and atmospheric N_2, respectively.

Incubation set-up: Sediment cores were incubated in the dark for 3 days with constant stirring of the overlying water. The net O_2 consumption and H_2S production were measured using electrochemical analysis of porewater throughout the incubation experiment. Solid-state Au/Hg glass microelectrodes were custom fabricated by sealing a 0.1 mm diameter gold wire into drawn glass tubing and plating mercury on the polished gold surface (Brendel and Luther 1995). Prior to use, electrodes were calibrated using a suite of laboratory standardization methods (e.g. Luther III et al. 2008). For each incubation experiment we operated two voltammetric analyzers (Analytical Instrument Systems, Inc. Model DLK 100a), which utilized a standard three-electrode cell and multiplexed 4 replicate working electrodes in each incubated core. A programmable scan sequence was used to switch between microelectrodes at each depth. Scans were

programmed in a 7.5 min sequence, resulting in a total of four scans per electrode every 7.5 minutes for 3 days.

Each core had one counter and one reference electrode positioned in the overlying water and four working Au/Hg microelectrodes positioned at fixed depths relative to the sediment-water interface (SWI): 2 cm above the SWI, at the SWI, 6 cm below the SWI, and 13 cm below the SWI (Figure 4.2). The depth of each microelectrode was selected based on knowledge of likely positions of redox transition zones from prior work. The overlying water and SWI electrodes were placed in initially oxic regions, the 6 cm electrode was placed in the suboxic zone and the deepest electrode was placed below the suboxic zone (e.g., in anoxic sediments) to capture hydrogen sulfide buildup resulting from sulfate reduction. Changes in detectable concentrations of O_2 and H_2S were measured at each depth throughout the three-day incubation experiment. At the end of the incubation experiment, the sediment core was sectioned and analyzed for solid phase and porewater constituents following the procedures outlined previously.

Figure 4.2 Incubation setup and schematic. Microelectrodes are attached to the micromanipulator and lowered into paired sediment cores. Each core had one counter and one reference electrode positioned in the overlying water and four working Au/Hg microelectrodes positioned at fixed depths relative to the sediment-water interface (SWI) attached to a voltammetric analyzer. Electrodes were placed 2 cm above the SWI, at the SWI, 6 cm below the SWI, and 13 cm below the SWI.

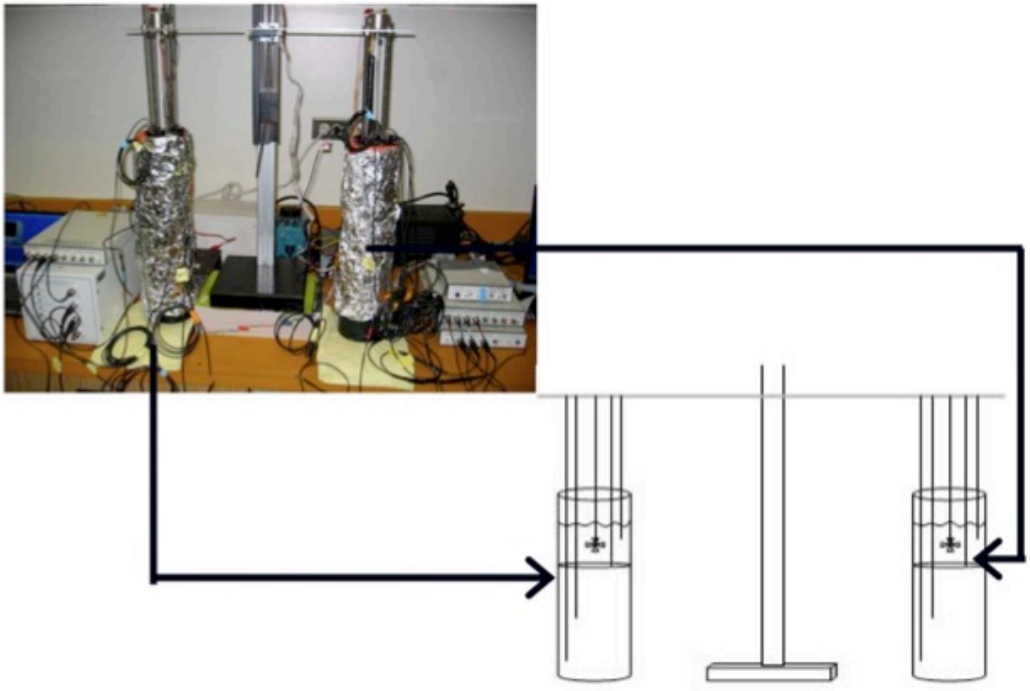

4.4 Estimation of Mineralization Efficiency

Conceptual Framework: The spatial distribution of redox reactive species in marine sediments is dictated by the dominant microbial respiratory pathways employed to oxidize organic carbon at any given point in the sediment, through the reduction of inorganic electron acceptors (i.e., O_2, NO_3^-, oxides of Mn and Fe, and SO_4^{2-}) (Thamdrup and Canfield 1996). For the purposes of this paper we will refer to redox zonations by the classical terms: oxic (the zone with detectable O_2), suboxic (the zone with no detectable O_2 or H_2S), and anoxic (the zone with detectable H_2S from sulfate reduction). We recognize that broadly applying this classification scheme may lead to confusion due to the overlap of metabolic processes within each designated zone (Canfield and Thamdrup 2009); however, because this study examines total combined OM remineralization rates via several metabolic pathways, our adherence to this classical classification of redox zonations should cause no confusion.

OM decomposition rates were estimated via two approaches. The first approach was to measure and calculate rates of O_2 consumption and H_2S production using microelectrodes positioned at the sediment-water interface and at 13 cm within each sediment core, respectively. O_2 is the terminal electron acceptor in respiration pathways, thus rates of O_2 consumption can be utilized to represent the integrated rates of OM oxidation in oxic and suboxic sediment layers. In other words, O_2 is utilized (i) directly in heterotrophic respiration of OM and (ii) as an oxidant for the products of anaerobic OM oxidation by other pathways (i.e., NH_4^+, H_2S, Fe^{2+} and Mn^{2+}); therefore, O_2 consumption rates are directly proportional to total OM oxidation by both aerobic and anaerobic pathways in the oxic and suboxic redox zones (Canfield et al. 1993; Jahnke et al. 2005). Sulfate reduction rates in the anoxic zone of sediments can be estimated by quantifying the production of H_2S, a product of sulfate reduction. Specific rates of H_2S production provide a minimum estimate of OM remineralization via sulfate reduction because abiotic reactions, such as secondary re-oxidation of sulfide or reactions with reduced iron that consume H_2S, were not constrained. Nevertheless, differences in H_2S production rates between sites allowed us to evaluate the impact of organic matter source on mineralization rates at depth in sediment cores from each location.

The second approach used to estimate OM decomposition rates utilized the buildup of porewater NH_4^+, a product of OM remineralization. Porewater profiles of NH_4^+ from pre- and post-incubation sediment cores were integrated and the differences between the integrated profiles were used to estimate rates of NH_4^+ accumulation. This approach provides a minimum estimate of NH_4^+ production from organic matter remineralization over the course of the incubation. In addition to integrating whole sediment core accumulation of NH_4^+, we calculated differences in the diffusional benthic efflux of NH_4^+ from the porewater gradient exhibited in pre- and post-incubation porewater NH_4^+ profiles. Measuring the buildup of inorganic nutrients such as NH_4^+, and the subsequent diffusional fluxes of inorganic nutrients, does not inform us about specific metabolic pathways; however rates calculated this way can be used to compare total OM oxidation rates in different sedimentary environments (Jahnke et al. 2005).

Rates of O_2 consumption, H_2S production, and NH_4^+ accumulation, calculated using the assumptions outlined above, were normalized to the quantity of OM available for remineralization at each site. We define the normalized, absolute rate per mole of OM as the 'specific rate' of remineralization. By normalizing to the quantity of OM, we can directly compare rates (per mole of OM) at each site, and thus remove the effect that quantity of OM has on bulk rates of oxidant consumption or metabolite build-up. The specific rates are thus characteristic of lability of the bulk OM at each location, and reflect the different mixture of terrestrial and marine organic matter present. For instance, although the total rate of NH_4^+ accumulation (not normalized to OM) in the mangrove site is greater than that observed at the ocean site, after normalizing to the quantity of OM at each site, it is clear that the absolute rate per mole of OM (e.g., the specific rate of remineralization) is lower at the mangrove site than at the ocean site. Thus, we will report specific rates at each location, so that we can evaluate relative differences in the efficiency OM remineralization (which is directly related to the inherent lability of the bulk OM in sediments) at each site.

Calculations: Microelectrode detection of O_2 in surface sediments and H_2S at depth within sediment cores was used to calculate specific rates of O_2 consumption and H_2S production according to equation 4.4 (given for O_2 consumption):

$$O_2 \text{ consumption} = (\Delta [O_2]_{SWI}) * (\varphi) * (t)^{-1} * ([OC]_{PRE})^{-1} \quad (4.1)$$

where $\Delta [O_2]_{SWI}$ is the change in oxygen concentration measured at the electrode positioned at the SWI, $[OC]_{PRE}$ is the concentration of organic carbon at the depth of electrode placement in the pre-incubation core (e.g., the SWI), t is the time over which consumption occurred, and φ is porosity.

Matlab Curve Fitting Toolbox™ was used to integrate profiles of NH_4^+ and OC from pre- and post-incubation sediment cores using an integrated smoothing spline. The integrated areas under the curves were used to determine the standing crop (μmole cm^{-2}) of NH_4^+ and OC in pre- and post-incubation cores using the following equations:

$$\text{Standing crop of } NH_4^+ = (\text{Integrated } [NH_4^+]) * (\varphi) * (z) \quad (4.2)$$

$$\text{Standing crop of OC} = (\text{Integrated [OC]}) * (1 - \varphi) * (z) \quad (4.3)$$

where z is the depth over which the sediment profile was integrated (e.g., see Ruttenberg and Berner 1993). Pre- and post-incubation standing crop values were then used to determine specific rates of NH_4^+ accumulation according to equation 4.4:

$$NH_4^+ \text{ accumulation} = (\Delta NH_4^+ \text{ standing crop}) * (t)^{-1} * (\text{OC standing crop})_{PRE}^{-1} \quad (4.4)$$

where t is the time interval between pre- and post-incubation cores (72 hours). Dividing by the standing crop of OC allows calculation of specific rates of NH_4^+ accumulation.

The standing crop of NH_4^+, determined using whole-core profiles of incubated sediment cores, represents a balance between biotic and abiotic production and consumption pathways. Because consumption pathways were not quantified in this study, the specific rates reported are considered minimum estimates of microbial OM decomposition. Nevertheless, these minimum estimates provide insight into the relative OM liability and therefore the ease of OM remineralization at each study site (see Discussion).

Sediment porewater NH_4^+ profiles were used to estimate the diffusional flux of NH_4^+ across the sediment-water interface using Fick's first law of diffusion.

$$J_{sed} = -(\varphi) * (D_{sed}) * (\partial C/\partial x) \quad (4.5)$$

where J_{sed} is the diffusional flux, D_{sed} is the whole sediment diffusion coefficient and $\partial C/\partial x$ is the changes in concentration over depth calculated from porewater profiles. The whole sediment diffusional constant (D_{sed}) was estimated using sediment tortuosity (calculated using the porosity of sediments at each study site) and a molecular diffusional constant for seawater for each analyte (see Boudreau 1997 for equations and average diffusion coefficient values). The D_{sed} value of NH_4^+ calculated for this study was 1.85e-9. The $\partial C/\partial x$ gradient used in these calculations is defined by the difference between the peak concentration of porewater NH_4^+ at depth and the NH_4^+ concentration in the overlying water.

4.5 Results

End member OM source compositions, plotted as property-property box plots, are consistent with previously published values for mangrove and plankton end member tissues (Table 4.1; Figure 4.3). Molar OC:TN:OP ratios and $\delta^{13}C$ values of bulk sediments from pre- and post-incubation cores, plotted in property-property plots (Figure 4.4a and 4.4b), display a transition from lighter $\delta^{13}C$ values (-27 to -22‰), typical of terrestrial OM in mangrove and terrestrially-dominated sites, to heavier marine-like $\delta^{13}C$ values (-16 to -11‰) in carbonate-dominated and ocean sites. OC:OP values drop from high ratios at sites dominated by terrestrial OM, to low ratios in the sites dominated by marine OM; OC:TN ratios do not display a similarly systematic trend along the transect. Open-symbols represent sediment samples from pre-incubation cores; closed symbols represent post-incubation sediment cores that have undergone early diagenetic transformation. Post-incubation samples from the terrigenous-, carbonate-dominated, and ocean sites display lower OC:TN ratios relative to pre-incubation samples (Figure 4.4b); no systematic alteration in OC:OP ratios is observed (Figure 4.4a). Post-incubation samples from the terrigenous-dominated site display a clear shift toward less negative $\delta^{13}C$ values. Ocean and mangrove sites also display a shift to less negative values after the incubation.

Table 4.1 Carbon, nitrogen and phosphorus concentrations and isotopic composition of potential end member contributors to marine sedimentary OM. The n values represent the number of distinct samples analyzed in each study, excluding replicates. Bold values are averages over reported data for each end member type (excluding values from this study). Values from this study are averaged and listed in italics.

Terrestrial End members	n	$\delta^{13}C$	$\delta^{15}N$	C:N	C:P	N:P	Source
Mangrove		**-27.4**	**2.7**	**87**	**9983**	**66**	
Mangrove Green Leaf	3	-	-	50	3298	66	*Reviewed in Lee et al (2008)*
Mangrove Green Leaf	6	-26.7	-	41	-	-	*Hemminga et al 1994*
Mangrove Senescent Leaf	9	-	-	110	16668	66	*Reviewed in Lee et al (2008)*
Mangrove Senescent Leaf	5	-	-	152	-	-	*Hemminga et al 1994*
Mangrove Coarse Root	10	-	-	103	-	-	*Reviewed in Lee et al (2008)*
Mangrove Fine Root	10	-	-	65	-	-	*Reviewed in Lee et al (2008)*
Mangrove	2	-28.0	2.7	-	-	-	*Loneragan et al 1997*
Mangrove	*4*	*-28.1*	*1.1*	*53*	*1583*	*40*	*this study*
Terrestrial and Saltmarsh C3 Plants		**-27.6**	**5.2**	**49**	**1826**	**27**	
C3 Plants	4	-29.3	0.4	-	-	-	*Reviewed in Peterson and Howarth (1987)*
C3 Plants		-28.5	-	100	1000	8	*Ruttenberg and Goni (1997); Likens (1981)*
C3 Plants	6	-26.1	-	55	-	-	*Reviewed in Meyers (1994)*
C3 plants	2	-26.4	10.6	18	-	-	*Decottignies et al 2007*
C3 plants	4	-27.4	10.3	31	-	-	*Cloern et al 2002*
Terrestrial angiosperms	4	-28.1	1.5	-	-	-	*Decottignies et al 2007*
Terrestrial foliage	55	-	-	44	1334	28	*McGroddy et al 2004*
Terrestrial litter	106	-	-	66	3144	46	*McGroddy et al 2004*
Terrestrial plants	4	-27.6	3.0	26			*Cloern et al 2002*
Land based C4 Plants and Seagrass		**-12.2**	**5.8**	**51**	1137	60	
C4 plant	2	-14.9	9.7	27	-	-	*Cloern et al 2002*
C4 Plants	4	-12.1		107	-	-	*Reviewed in Meyers (1994)*

Terrestrial End members	n	$\delta^{13}C$	$\delta^{15}N$	C:N	C:P	N:P	Source
C4 plants	1	-14.0	8.7	-	-	-	*Decottignies et al 2007*
Seagrass	1	-	-	19	1137	60	*Fourqurean et al 1992*
Seagrass	1	-8.8	1.7	-	-	-	*Anderson and Fourqurean 2003*
Seagrass	48	-11.5	-	-	-	-	*Hemminga and Mateo 1996*
Seagrass	6	-12.0	3.2	-	-	-	*Loneragan et al 1997*
Freshwater Algae		**-28.5**	**5.0**	**7**			
Freshwater Plankton	30	-28.6	5.0	7	-	-	*Cloern et al 2002*
Lake Algae	3	-28.3	-	7	-	-	*Reviewed in Meyers (1994)*

Marine End members	n	$\delta^{13}C$	$\delta^{15}N$	C:N	C:P	N:P	Source
Macroalgae		**-17.3**	**4.2**	**21**	**482**	**37**	
Macroalgae	9	-	-	-	-	66	*Larned 1998*
Macroalgae	92	-	-	20	700	35	*Atkinson (1983)*
Macroalgae	41	-	-	22	263	10	*Lapointe et al 1992*
Macroalgae	3	-14.9	8.4	21	-	-	*Decottignies et al 2007*
Macroalgae	1	-22.0	1.2	-	-	-	*Loneragan et al 1997*
Macroalgae	1	-15.0	3				*Cornelisen et al 2007*
Macroalgae	*3*	*-17.0*	*3.9*	*29*	*3054**	*109*	*this study*
Benthic Algae		**-18.6**	**3.7**	**8**	**464**	**43**	
Benthic Microalgae		-	-	7	119	17	*Reviewed in Hillibrand and Sommer (1999)*
Benthic Diatoms	2	-22	7.0	8	-	-	*Cloern et al 2002*
Benthic Diatoms	1	-12.9	5.3	7	-	-	*Decottignies et al 2007*

Marine End members	n	$\delta^{13}C$	$\delta^{15}N$	C:N	C:P	N:P	Source
Microbial Mat	20	-	-	12	809	68	*Reviewed in Lee et al (2008)*
Marine Algae	4	-21.6	-	5	-	-	*Reviewed in Meyers (1994)*
Marine Algae	1	-17.8	-1.2	7	-	-	*Wild et al 2008*
Marine Plankton		**-22.9**	**7.5**	**7**	**106**	**16**	
Estuarine Plankton	31	-21.5	8.0	6	-	-	*Cloern et al 2002*
Marine Plankton	56	-21.3	8.6	-	-	-	*Reviewed in Peterson and Howarth (1987)*
Marine Plankton	-	-28.5	-	7	106	16	*Ruttenberg and Goni (1997); Redfield (19XX)*
Marine Plankton	9	-20.4	5.8	-	-	-	*Loneragan et al 1997*
Marine Plankton	*2*	*-16.3*	*5.7*	*6*	*223*	*38*	*this study*
Coral		**-14.0**	**5.3**	**11**	**203**	**18**	
Coral Tissue	2	-16.0	5.0	-	-	-	*Grottoli et al 2004*
Coral Tissue	2	-11.4	3.8	7	-	-	*Ove Hoegh-Guldberg et al 2004*
Coral Tissue	26	-13.8	4.4	-	-	-	*Muscatine et al 2005*
Coral Tissue	1	-	-	6	172	27	*Parker et al 1994*
Coral Symbiont	2	-16.0	5.0	-	-	-	*Grottoli et al 2004*
Coral Symbiont	2	-11.7	3.1	6	-	-	*Ove Hoegh-Guldberg et al 2004*
Coral Symbiont	26	-18.4	6.3	-	-	-	*Muscatine et al 2005*
Coral Tissue and Symbiont	7	-13.9	5.0	-	-	-	*Yamamuro et al 1995*
Coral Symbiont	1	-	-	20	365	21	*Parker et al 1994*
Coral Eggs	1	-9.5	4.8	17	-	-	*Wild et al 2008*
Coral Sperm	1	-11.2	5.6	7	-	-	*Wild et al 2008*
Coral Mucus	1	-18.2	10	12	72	6	*Wild et al 2004; 2005; 2008a*

** The large C:N and C:P values for these samples are driven by the high concentrations of structural carbon that characterizes Kappaphycus spp.*

Pre- and post-incubation depth profiles of OC (weight percent), OC:TN and OC:OP ratios are shown in shown in Figures 4.5a-c. OC is significantly higher at all depths at the mangrove site (5.0-8.8%), with progressively lower quantities OC observed in sediments along the transect towards the ocean site (<1%). OC:TN ratios fall within the same range for all sites (~10-60), whereas OC:OP ratios are significantly higher in the mangrove site (~400) compared to the other study sites (~50-200). Post-incubation sediment OC:TN profiles (closed-symbols) are nearly 2-fold lower at all sites, with the exception of the mangrove site. By contrast, OC:OP sediment profiles from post-incubation cores show no systematic shift from pre-incubation cores.

Porewater NH_4^+ accumulates with depth at all sites (Figure 4.6a). By contrast, porewater DIP concentrations are at or below the detection limit at all sites except the mangrove site (Figure 4.6). NH_4^+ concentrations from pre-incubation sediment cores display typical diffusional profiles, with lower concentrations in surface sediments building up to progressively higher concentrations at depth. Maximum concentrations in the pre-incubation cores from all sites are around 80 μM NH_4^+ whereas the post-incubation cores show significant increases in NH_4^+ concentrations above pre-incubation levels, particularly at the ocean site (up to ~500 μM). The post-incubation NH_4^+ porewater profiles from the carbonate-dominated and ocean sites both display discrete maxima in concentrations with distinct reversals at depth.

Overlying water NH_4^+ concentrations (ranging from 3-6 μM) were significantly lower than porewaters, setting up conditions that favor a diffusional flux of NH_4^+ from the sediments to overlying water. With the exception of the terrigenous-dominated site, calculated benthic efflux of NH_4^+ from each sediment core displays higher diffusional fluxes in post-incubation cores (Table 4.2). The calculated benthic flux of NH_4^+ from pre-incubation cores ranges from 23-167 μmoles m^{-2} d^{-2}, while post incubation benthic NH_4^+ fluxes range from 31-301 μmoles m^{-2} d^{-2} (Table 4.2).

While DIP concentrations reached 11.0 μM in at the mangrove site, concentrations were <1 μM at all depths in the other sites (Figure 4.6b). Porewater samples that fell below the detection limit (marked by a dashed line) were omitted from the porewater profiles. All values for DIP within the 0-6 cm interval at the terrigenous

Table 4.2 Calculated benthic flux of NH_4^+ ($\mu moles*m^{-2}*d^{-1}$) across the sediment-water interface

Incubation Core	Mangrove	Terrestrial Dominated	Carbonate Dominated	Ocean
Pre-incubation	167	68	70	23
Post-incubation	301	31	296	187

dominated site were below the detection limit; porewater samples below 6 cm were unavailable. Only at the mangrove site did we observe DIP accumulation during the incubation, reaching a maximum of 11.0 μM at depth in the sediment core.

Representative voltammetric microelectrode scans of O_2 consumption at the SWI (ocean site), and H_2S production at 13 cm depth (mangrove site) display consumption of O_2 and production of H_2S during the first 12-24 hours of the incubation (Figure 4.7a-b). Oxygen at the ocean site, measured at the -0.2 V peak, was consumed to below detectable limits after 12 hours of incubation. H_2S at 13 cm depth in the mangrove site, as detected by the peak at -0.62 V, continually increased throughout the incubation. A plot of sulfide evolution at the 13 cm electrode at all sites reveals the continuous production of H_2S in the first 12 hours of the incubation within the mangrove, terrigenous-, and carbonate-dominated sites, with no detectable H_2S production at the ocean site (Figure 4.7c). O_2 consumption rates at the SWI of each core during the first 12 hours of the incubation ranged from -4.0 to -121.4 (mM O_2 * μM OC^{-1} * hr^{-1}), and H_2S production rates at 13 cm depth within each core ranged from 1.2 to 4.3 (mM H_2S * μM OC^{-1} * hr^{-1}) (Table 4.3).

4.6 Discussion

Sources and degradation of OM end members: In traditional models assessing OM sources to marine sediments, sedimentary OM is characterized by two primary sources: labile, marine-derived OM and refractory, terrestrial-derived OM; source is determined by the distinctive isotopic composition and elemental ratios of marine versus terrestrial OM (e.g., Hedges and Parker 1976; Ruttenberg and Goñi 1994a; Ruttenberg and Goñi 1994b). OC:TN:OP and $\delta^{13}C$ values of source OM from our study sites, determined as part of this study, are consistent with previously published values of OM source material, reviewed and summarized in Table 4.1 and Figure 4.3. It has been shown that sediments dominated by terrestrial sources generally contain less OP and TN relative to OC and are characterized by

lighter $\delta^{13}C$ values than sediments dominated by marine sources (Ruttenberg and Goñi, 1997a; Ruttenberg and Goñi, 1997b) (Table 4.1). A closer inspection of published and new end member data, however, reveals considerable heterogeneity in these signature parameters for both terrestrial and marine OM. In some cases, the elemental ratios and isotopic signatures of terrestrial and marine OM overlap. For instance, relatively high OC:TN and OC:OP in marine macroalgae (Table 4.1), as a consequence of high concentrations of structural carbon associated with some marine macroalgae, prevent clear distinction between marine macroalgae and terrestrial vascular plants to be made solely on the basis of OC:TN and OC:OP ratios (Figure 4.3). However, the same two end members display distinctive $\delta^{13}C$ values, allowing marine macroalgae (-14.0‰) to be distinguished from C3 plants (-27.6‰) on the basis of their stable carbon isotopic compositions (Table 4.1; Figure 4.3). Likewise, marine plankton can be characterized by heavy enough $\delta^{13}C$ values (-22.9‰) to be indistinguishable from some terrestrial sources, such as mangrove or C3 plants, but have distinctively low marine-like OC:TN and OC:OP

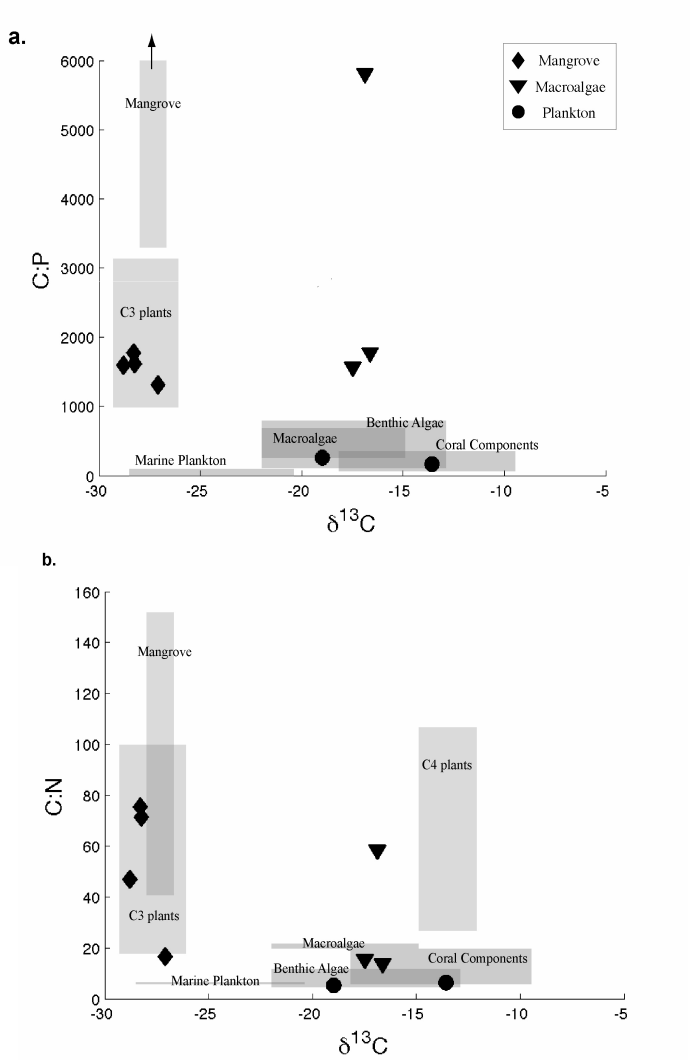

Figure 4.3 End member box plot of (a) molar OC:OP ratios versus $\delta^{13}C$ and (b) molar OC:TN ratios versus $\delta^{13}C$. Mangrove end members analyzed in this study are represented by diamonds, macroalgae by triangles, and plankton by circles. Boxes represent the range of OC:OP and $\delta^{13}C$ (a) and OC:TN and $\delta^{13}C$ (b) values for each end member source based on literature review summarized in Table 1. Note: The high OC:OP value for macroalgae from this study is a consequence of the high structural carbon content characteristic of Kappaphycus spp. No published OC:OP data for C4 plants is available.

ratios (7 and 106, respectively) relative to the higher ratios characteristic of terrestrial plants (Table 4.1). These two examples illustrate the importance of using a multi-tracer approach, including OC:OP and OC:TN ratios, as well as $\delta^{13}C$ values, to evaluate sources of OM to marine sediments (Ruttenberg and Goñi 1997a; Ruttenberg and Goñi 1997b).

Sources and degradation of OM sediments: We expected $\delta^{13}C$ values from sediments at the ocean site to reflect dominantly, or even exclusively marine sources of OM, classically believed to be comprised primarily of marine plankton. However, heavy $\delta^{13}C$ values (-11‰) were observed in sediments from the carbonate dominated and ocean sites, which could not be reconciled with typical $\delta^{13}C$ values of marine plankton (-22.9‰). While more positive $\delta^{13}C$ values in sites dominated by marine sources of OM could be explained by contributions from seagrasses (-9‰ to -12‰, Table 4.1) (Goñi and Hedges 1995; Goñi et al. 1997), seagrasses are absent from our study sites. Recognizing that an additional end member, characterized by a heavy isotopic signature, must be contributing OM to sediments at the marine-dominate sites of our study area, we evaluated the OM derived from coral reef ecosystems. OM from adult tissue die-off in fragmented coral skeleton, coral symbionts, eggs/sperm material, and mucus derived from the coral reef ecosystem can contribute OM to sediments with $\delta^{13}C$ values ranging from -10‰ to -18‰ (Table 4.1), and thus are a likely candidate to explain the unusually heavy $\delta^{13}C$ values in OM from our marine-dominated study sites. Our analysis suggests that it may be important to consider the contribution of OM from coral reef ecosystems in evaluating sources and subsequent preservation of OM in sediments deposited in tropical environments.

The hyperbolic trend that results when OC:OP ratios are plotted versus $\delta^{13}C$ values is characteristic of the mixing line between these signature ratios in terrestrial and marine sources of OM (Ruttenberg and Goñi 1997a; Ruttenberg and Goñi 1997b). This hyperbolic trend is seen clearly in the end-member box plots (Figure 4.3a), and we also observe a systematic progression from terrestrially derived material at the mangrove site ($\delta^{13}C$ -26‰; OC:OP ~700) to marine derived material in the ocean site ($\delta^{13}C$ -11‰; OC:OP ~13) along our study transect (Figure 4.4a). Post-incubation sediment cores from the terrigenous-dominated site display $\delta^{13}C$ values ~2‰ higher than pre-incubation cores, indicating preferential degradation of OM with lower $\delta^{13}C$ values at this sites, leaving behind an isotopically heavier sedimentary OM reservoir. Systematic fractionation of carbon isotopes

Figure 4.4 Sediment (a) OC:OP ratios versus $\delta^{13}C$ and (b) OC:TN ratios versus $\delta^{13}C$. Sites are designated by different symbols: mangrove (diamonds), terrigenous-dominated (circles), carbonate-dominated (squares) and ocean (stars). Open symbols: pre-incubation, closed symbols: post incubation.

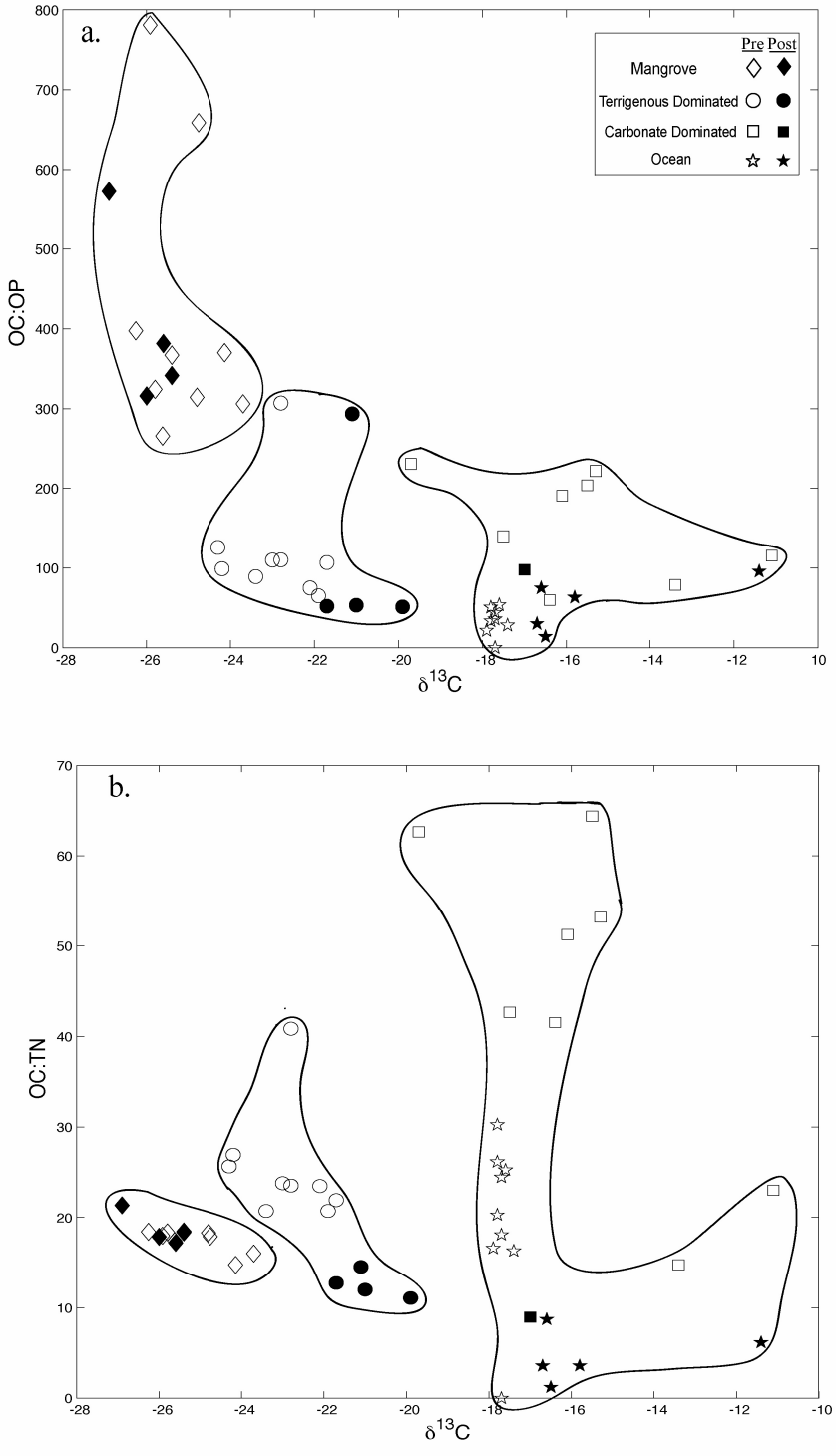

during diagenesis is not as clear at the ocean and mangrove sites, where there is an indication of smaller shifts in post-incubations cores. Meyers (1997) reported that shifts of 2‰ in $\delta^{13}C$ of organic matter during diagenesis did not represent a significant isotopic fractionation of the source organic material. Thus, $\delta^{13}C$ and OC:OP source signatures of end member OM are discernible and a clear separation exists between sediments dominated by terrestrial versus marine end member OM (Figure 4.4a).

Post-incubation sediment cores did not display significant changes in OC:OP ratios at any of the four sites compared to the pre-incubation sediments (Figure 4.4a). Thus, despite the early diagenetic transformations that occurred throughout the 3-day incubation, OC:OP values from all depths within the sediment cores retain the signature of OM source material. This suggests that OC:OP ratios are a robust indicator of organic source material.

OC:TN data is far more common than OC:OP data due to analytical ease of measuring TN. However, consistent with other studies (Ruttenberg and Goñi 1997b), we find that OC:TN ratios are not as robust an indicator of OM source as OC:OP ratios. The lower fidelity of OC:TN ratios as indicators of OM source is a consequence of: (i) the low dynamic range of OC:TN ratios over terrestrial and marine sources of OM, and (ii) post-depositional changes in OC:TN ratios that occur during diagenesis.

Unlike the OC:OP versus $\delta^{13}C$ plots (Figure 4.4a), we do not observe a systematic trend in OC:TN ratios along the land-to-sea transect that our study sites describe (Figure 4.4b). Thus, the progression from terrestrially- to marine-dominated sources of OM is not evident in the plot of OC:TN versus $\delta^{13}C$ values for sediments from the four study sites. We attribute this failure of OC:TN as a source signature to the low dynamic range of OC:TN ratios in source OM (7-87; Table 4.1). However, our study examined bulk sediment only, and analysis of OC:TN versus $\delta^{13}C$ in size fractionated sediments could improve the utility of OC:TN as an OM source indicator (Hedges and Keil 1995).

It is important to consider whether the decrease in post-incubation OC:TN ratios could be due to post-depositional changes in OC:TN ratios that are distinct from OM remineralization. We consider two possible scenarios that could drive accumulation of solid phase N during diagenesis. An increase in bacterial biomass during the incubation could result in progressively lower OC:TN ratios because bacteria are characteristically enriched in nitrogen (Rice and Hanson 1984; Ruttenberg and Goñi 1997b). Alternatively, recognizing

that the TN reservoir includes organic nitrogen (ON) and inorganic nitrogen (IN), the potential exists for fixation of IN by clays, which would result in a decrease in OC:TN ratios during diagenesis. This latter scenario is most likely to be important in the ocean site, which is characterized by low OM (< 0.3%), and where the IN component may thus be an important fraction of the TN (e.g., Ruttenberg and Goñi 1997a). This complication is less likely to occur in sediments with higher OM (reviewed in Meyers 1997).

Contrasting down-core variations in OC:TN and OC:OP in post-incubation cores (filled symbols) to pre-incubation cores (open symbols) (Figure 4.5b and 4.5c) permits us to examine the effect of short-term remineralization, occurring during the 3-day incubation, on sediments at different depths below the SWI that have experienced different extents of diagenetic transformation. Post-incubation OC:TN and OC:OP ratios are indistinguishable from pre-incubation ratios in sediment profiles from the mangrove site, indicating minimal fractionation of TN and OP from OC in OM source material due to diagenetic transformations which occurred during the incubation. However, post-incubation sediments from the terrigenous dominated, carbonate dominated and ocean sediment cores are characterized by OC:TN values that are systematically lower than OC:TN in pre-incubation cores. We attribute the greater susceptibility of the latter three sites to short-term diagenetic modification of OC:TN to the low quantities of OM at these sites (ranging from <0.1% to 1%) relative to the mangrove site (4-8 % OC, Figure 4.5a). The magnitude of the shift observed, up to 2-fold increase in OC:TN ratios, will obscure the source signature OC:TN ratio these sites. The OC:OP ratios in the post-incubation cores from all sites were not significantly different from pre-incubation ratios, indicating that sedimentary OM more faithfully retains the OC:OP ratios of initially deposited OM, even after significant remineralization has occurred, and even in sediments with low wt% OC.

Quality versus quantity of OM: By linking measured indices of OM source (elemental ratios and isotopic signatures) to measured rates of OM remineralization, we are able to discern the effects of OM source and lability on OM degradation rates. The rate of sedimentary OM remineralization was estimated using 4 independent approaches: (i) calculating O_2 consumption and (ii) H_2S production during the incubation at the depth of microelectrode placement (at and 13 cm below the SWI, respectively), (ii) calculating of integrated NH_4^+ production rates in sediment cores, and (iii) calculating rates of benthic

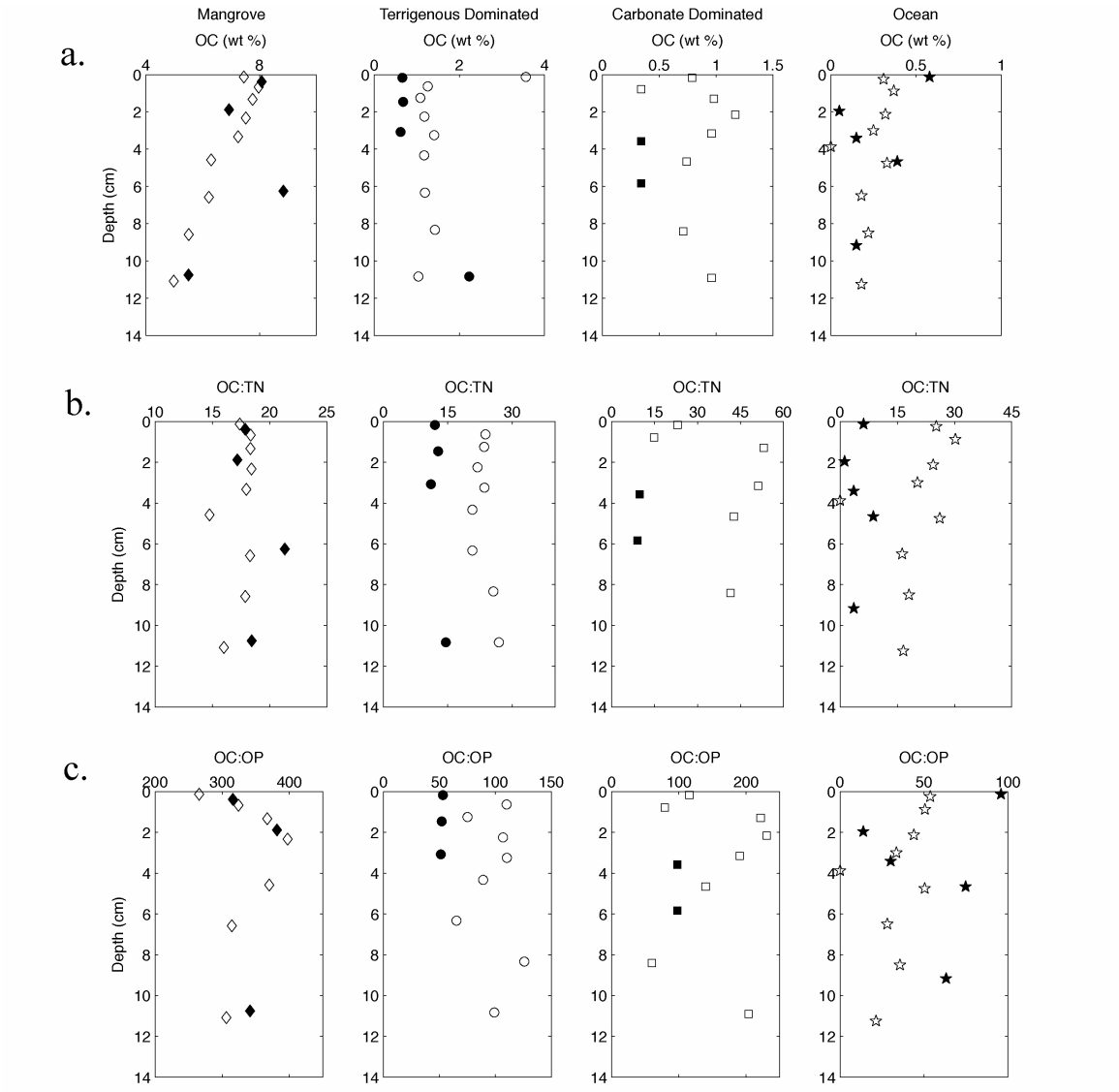

Figure 4.5 Down core sediment profiles of (a) OC:TN ratios, (b) OC:OP ratios, and (c) wt% OC. Sites are designated by different symbols: mangrove (diamonds), terrigenous-dominated (circle), carbonate-dominated (square) and ocean (star). Open symbols: pre-incubation, closed symbols: post incubation. Note different scales on x-axes.

efflux of NH_4^+. In each approach, we utilize the specific rates of reactive species in the degradation pathways to estimate the relative efficiency of OM remineralization at each study site. By using specific rates (e.g., rates per mole of organic matter), we are able to factor out the effect of OM quantity, which varies significantly from site to site (Figure 4.5a), and thus can discern the inherent rates characteristic of the particular mix of organic matter sources at each site.

It is well established that microbially mediated OM degradation proceeds by successive use of oxidants beginning with those that yield the greatest quantity of free energy per mole of organic carbon, to progressively less energy efficient metabolic pathways (e.g., Froelich et al. 1979; Canfield et al. 1993; Burdige 2006). We focused on two of these pathways in this study: aerobic respiration utilizing O_2, the most energetically favorable oxidant, and SO_4^{2-} reduction, one of the least energetic metabolic pathways, as represented by the following equations (Tsandev 2010):

$$OM + a\ O_2 \rightarrow a\ CO_2 + b\ NH_4^+ + c\ H_3PO_4 + a\ H_2O \quad (4.6)$$

$$OM + a/2\ SO_4^{2-} + a\ H^+ \rightarrow a\ CO_2 + b\ NH_4^+ + c\ H_3PO_4 + a/2\ H_2S + a\ H_2O \quad (4.7)$$

Contrasting the specific rates of O_2 consumption (Eq. 4.7) and H_2S production, a by-product of sulfate reduction (Eq. 4.7), at each site on our transect provides insight into the efficiency of OM remineralization at each study site (approach 1 and 2). Because NH_4^+ is a direct product of OM remineralization (Eq. 4.6 and 4.7), calculating the rate of NH_4^+ accumulation in porewaters (approach 3), and the subsequent benthic flux of NH_4^+ out of sediments (approach 4), provides two additional approaches for estimating relative rates of OM remineralization at each site. A comprehensive assessment of OM mineralization by the full suite of metabolic pathways is beyond the scope of the present study. Instead we utilize estimated remineralization rates as proxies for OM lability, which is linked to the relative importance of terrestrial versus marine OM at each study site along the land-to-sea transect.

Specific rates of O_2 consumption are calculated at the SWI over the initial 12 hours of the incubation experiment and therefore represent both the rapid, oxic remineralization of OM, as well as the kinetically fast re-oxidation of reduced species. As previously mentioned, O_2 is considered the terminal electron acceptor and thus represents the specific rate of oxic and suboxic remineralization pathways. Sediments in close proximity to land, and thus dominated by terrestrial OM, are characterized by slower rates of O_2 consumption (Table 4.3). We attribute the observed lower rates to the more refractory nature of terrestrial OM. In contrast, sediments proximal to the ocean, which are dominated by marine OM, are characterized by more rapid O_2 consumption rates at the SWI (Table 4.3). Thus, sites

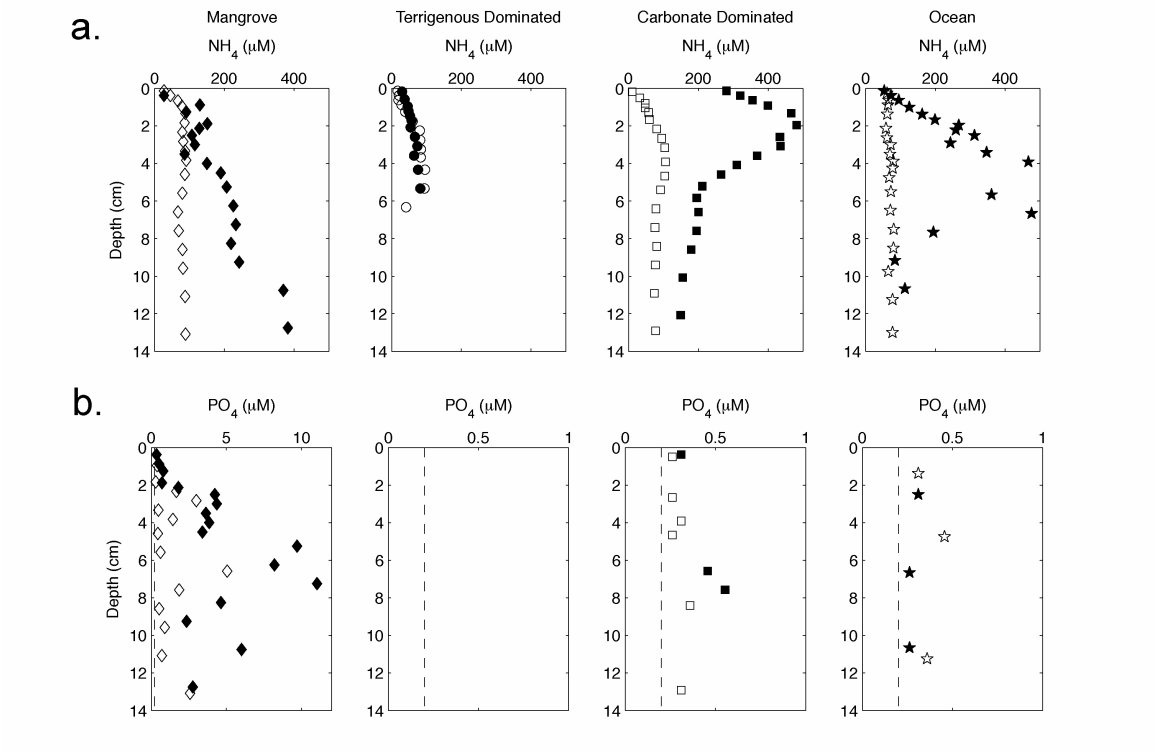

Figure 4.6 Down core porewater profiles of (a) NH_4^+ and (b) PO_4^{3-} (DIP). Sites are designated by different symbols: mangrove (diamonds), terrigenous-dominated (circles), carbonate-dominated (squares) and ocean (stars). Open symbols: pre-incubation, closed symbols: post-incubation. Dashed line represents the detection limit for DIP (0.2 μM). Note different scales on x-axes.

dominated by labile, marine OM sources have higher OM remineralization efficiencies compared to sites characterized by terrestrial sources of OM.

The mangrove site is characterized by high quantities of OM available for biological remineralization (5 to 10% by weight, Figure 4.4a) yet, as previously mentioned, the mangrove site displays lower rates of OM oxic remineralization in surface sediments than the ocean site (Table 4.3). However, more rapid production of H_2S is observed at the mangrove site than the ocean site (Table 4.3). We can reconcile the apparent paradox of low oxic respiration rates yet high sulfide production rates at the mangrove site by considering the influence of quantity over quality of OM. Due to the large quantity of OM at the mangrove site (Figure 4.5a), a significant fraction escapes remineralization in surface sediments and is buried below the zone of oxic respiration. The large quantity of OM buried below the zone of oxic respiration in sediments at the mangrove results in a substantial standing stock of OM that is available for respiration via sulfate reduction. The accumulation of H_2S within these sediments indicates that the rate of sulfate reduction exceeds that of abiotic H_2S oxidation or

iron-sulfur reactions, which would remove H_2S from porewaters (reviewed in Burdige 2006). The situation is reversed in sites dominated by marine OM. Low to undetectable specific rates of H_2S production are observed in carbonate dominated and ocean sites, which we attribute to the substantially smaller quantities of OM buried below the anoxic redox boundary in these sediments (Figure 4.5a), and/or the rapid recycling of H_2S via oxidation pathways.

Rates of OM remineralization calculated using porewater NH_4^+ represent the cumulative effect of OM degradation over time. Specific rates of NH_4^+ accumulation display similar trends to O_2 consumption rates, with higher rates observed at the ocean site, becoming progressively slower as sites become more dominated by terrestrial OM along the transect, culminating in the lowest specific rates of NH_4^+ production at the mangrove site (Table 4.3). The specific remineralization rates calculated using integrated NH_4^+ buildup are minimum rates because they do not consider consumption pathways (e.g., nitrification) or loss of NH_4^+ via benthic efflux or sorptive removal onto clays. Additionally, in the carbonate dominated and ocean sites post-incubation porewater NH_4^+ profiles display a reversal at depth (Figure 4.6). Accumulation rates of NH_4^+ were calculated using integrated profiles of the entire sediment core. For these two sites, the production of NH_4^+ due to OM remineralization will be underestimated because processes causing the consumption of NH_4^+ at depth, resulting in the observed gradient reversal, were not considered.

The observed reversals in porewater NH_4^+ are intriguing, and may reflect a number of processes, including anoxic nitrification, ammonium oxidation, annamox activity (reviewed

Table 4.3 Metabolic rates estimated from whole core incubations. OC standing crop and NH_4^+ production rate are calculated from integrated porewater profiles (Equations 4.2 and 4.3, respectively). O_2 consumption and H_2S production rates are calculated from time course microelectrode data at discrete depths where microelectrodes were situated (0 cm and 13 cm, respectively; see Figure 2), as illustrated in Figure 4.7c.

Site	Mangrove	Terrestrial Dominated	Carbonate Dominated	Ocean
OC standing crop (μmole C * cm^{-2})	17.60×10^4	7.84×10^4	7.94×10^4	2.08×10^4
NH_4 production rate (mmole NH4 * μmole OC^{-1} * hr^{-1})	1.08	b.d.l.*	2.34	6.31
O_2 consumption rate (mM O_2 * μM OC^{-1} * hr^{-1})	-19.6	-4.0	-71.1	-121.4
H_2S production rate (mM H_2S * μM OC^{-1} * hr^{-1})	1.2	4.3	1.2	b.d.l.*

* b.d.l. Below Detection Limit

in Burdige, 2006), and/or ammonium adsorption onto clays or humic material (Boatman and Murray 1982; Rosenfeld 1979). Sediments from carbonate-dominated and ocean sites show no evidence of becoming anoxic (as indicated by the lack of H_2S detection using microelectrodes), which suggests that anoxic nitrification is not an important process at these sites. Ammonium oxidation with O_2 is also unlikely because the NH_4^+ reversals occur below the oxygenated layer in the sediments; ammonium oxidation via reactions with oxidants other than O_2 in the suboxic sediment cannot be ruled out, however. Annamox activity and adsorption of ammonium by the solid phase could well explain the reversals we observe. Data that would confirm that one or both of these processes were operant are not available as part of this study, however, so the processes responsible for consumption of NH_4^+ in the anoxic zones of sediment at these sites remain an avenue for future research.

Accumulation of NH_4^+ in sediment porewaters due to remineralization of OM throughout the 3-day incubation (filled symbols, Figure 4.6) can result in a diffusional flux of NH_4^+ across the sediment-water interface (Table 4.2). Benthic efflux of NH_4^+ from porewaters to the overlying water occurred in all cores, with higher fluxes in post-incubation sediment cores. Post-incubation diffusional NH_4^+ fluxes ranged from 301 μmoles m^{-2} d^{-1} at the mangrove site to 187 μmoles m^{-2} d^{-1} at the ocean site (Table 4.2). These values are consistent with previously published estimates of benthic NH_4^+ efflux in Kane'ohe Bay, with a mean value estimated at 490 μmoles m^{-2} d^{-1} (Stimson and Larned 2000). Although the benthic NH_4^+ efflux in the post-incubation core at the terrigenous-dominated site was significantly lower than at other sites (Table 4.2), we are skeptical that this estimate is robust due to the sparse NH_4^+ porewater data at this site. Thus, for the purposes of this discussion we will not further consider the calculated fluxes of NH_4^+ at the terrigenous-dominated site.

A systematic trend of decreasing benthic NH_4^+ efflux is observed from a high at the mangrove site, with progressively lower fluxes observed at the carbonate-dominated and ocean sites, in both pre- and post- incubation cores (Table 4.2). This may seem to contradict the previous argument that more rapid rates of respiration occur in the ocean site; however, this apparent paradox can be resolved by considering the question of OM quantity versus OM quality. Larger quantities of OM are available for remineralization at the mangrove site, with progressively less OM available at the carbonate-dominated and ocean sites (Figure 4.5a). Larger quantities of OM deposition result in greater accumulation of regenerated inorganic

nutrients during sedimentary OM remineralization in a given amount of time, even if the specific remineralization rates are lower (Table 4.2 and 4.3). Thus, while the quantity of OM present at each site determines the absolute quantity of metabolite (such as NH_4^+) that escapes the sediment via benthic efflux, the efficiency with which OM remineralization occurs, based on specific rates, displays a clear trend of higher metabolic rates in sediments dominated by labile OM of marine origin (Table 4.3).

The concept of stoichiometric nutrient regeneration stipulates that the concentrations of dissolved carbon, nitrogen (NH_4^+) and phosphorus (PO_4^{3-}) in porewaters should accumulate at a ratio equivalent to the carbon, nitrogen and phosphorus ratio in the OM undergoing remineralization (Eq. 4.5 and 4.6) (Berner 1977). Thus, we would expect to observe an accumulation of DIP in

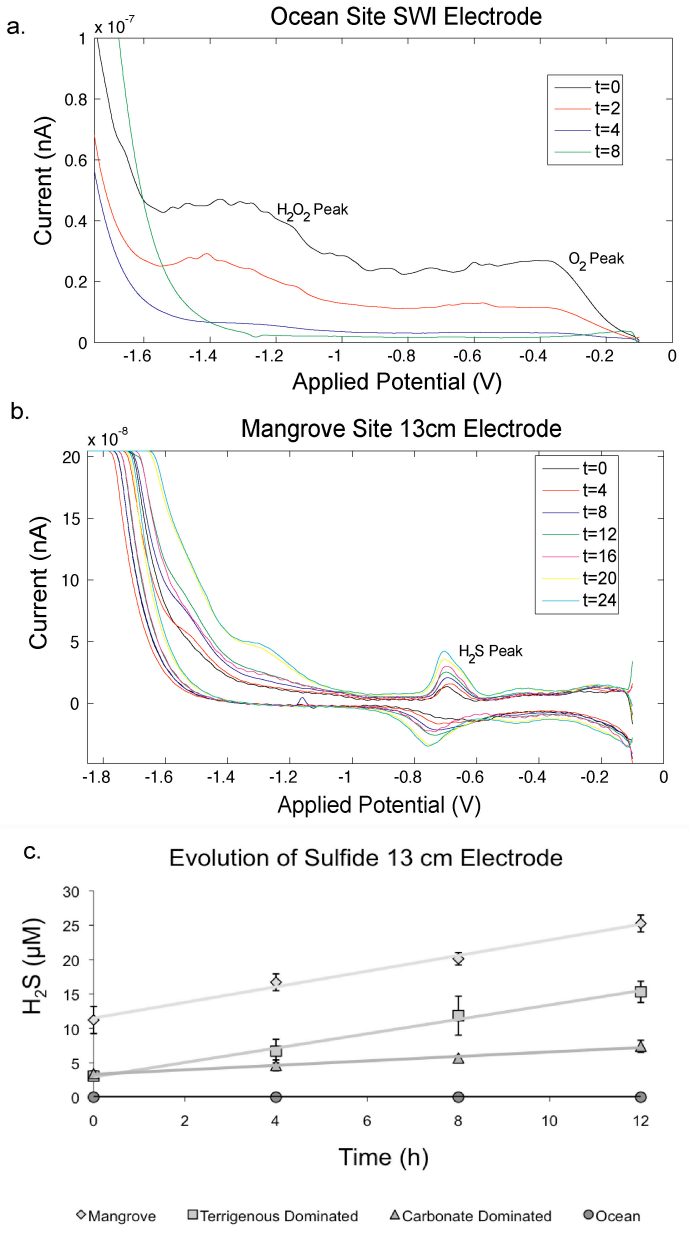

Figure 4.7 Representative raw voltammetric data illustrating (a) O_2 scans from the ocean site at the SWI throughout the incubation; consumption of O_2 at the -0.3V peak is evident, and (b) H_2S scans at the mangrove site from 13 cm below SWI throughout the incubation; production of H_2S is evident at the -0.62V peak. Conversion of raw voltammetric data (as in (a) and (b)) to concentrations allows progressive consumption or build-up of redox species over time to be visualized, as is shown in (c), the time-course H_2S accumulation at all sites from the electrodes positioned 13 cm below SWI.

sediment porewaters, as well as a benthic DIP efflux, similar to NH_4^+, but offset by the stoichiometric ratio set by the decomposing OM. Contrary to these expectations, we observe no DIP accumulation in porewaters of post-incubation sediment cores, with the exception of the mangrove site. The absence of DIP accumulation occurring in tandem with NH_4^+ accumulation suggests that the sediments sequester liberated porewater DIP produced during OM remineralization. In the absence of more detailed solid-phase P speciation data, it is not possible to ascertain the pathway(s) responsible for removing DIP. However, the fact that sediments in this study site are enriched in ferric iron (Fe) minerals suggests that sorptive removal onto reactive Fe phases may be an important pathway for removal of DIP liberated to porewaters during OM remineralization (Roden and Edmond 1997; Rozan et al. 2002). Although typically a process restricted to the surface oxidized layer, previous work has shown that in depositional environments receiving large quantities of reactive Fe minerals, reactive Fe can persist at depth (Aller et al. 2004; Canfield 1989) and thus have the potential to maintain porewater DIP at low levels below the redox boundary. It is also possible that authigenic carbonate-fluorapatite, the primary sink for phosphate in marine sediments (Ruttenberg 2003), may precipitate in these sediments, facilitated by the high carbonate content in the carbonate dominated and ocean sites (Ames 1959; Ruttenberg and Berner 1993).

4.7 Conclusions

1. Our study confirms earlier work (Ruttenberg and Goñi 1994a; Ruttenberg and Goñi 1994b) that suggested that the use of $\delta^{13}C$ of OC in conjunction with OC:OP ratios, the multi-tracer approach to OM source assessment, is more robust than use of elemental ratios or carbon isotope composition alone. OC:OP ratios are less commonly reported than OC:TN ratios due to the additional analytical work (beyond CHN analysis) required for OP determination (an observation supported by the relative dearth of OC:OP ratios in previously published end member values summarized in Table 4.1). However, OC:TN ratios are not as robust an indicator of OM source to marine sediments as OC:OP ratios, principally for two reasons: (i) the more restricted dynamic range of OC:TN ratios prevents clear distinction of terrestrial- from marine-derived OM, and (ii) post-depositional changes in OC:TN ratios occur that occur during diagenesis obscure the source signature of initially deposited OM.

Our work suggests that quantifying OP in sediments will provide important constraints for assessments of sedimentary OM source and reactivity, and will provide an objective basis for understanding OM reactivity and preservation potential.

2. Indices of OM source (elemental ratios and isotopic signatures) can be linked to measured rates of bulk OM decomposition in order to determine the effects of OM type on remineralization rates. Four independent approaches were undertaken to examine the efficiency of sedimentary OM remineralization: (i) calculating O_2 consumption and (ii) H_2S production during the incubation using voltammetric microelectrode detection, (ii) determining whole sediment-core integrated NH_4^+ production rates, and (iii) calculating rates of benthic efflux of NH_4^+. By examining specific rates, as opposed to net rates, we were able to systematically compare rates between study sites and relate these rates to the inherent lability of OM at each site.

3. Higher remineralization rates observed at the ocean site are linked to the more labile, marine-dominated OM that characterizes sediments at this site. Progressively slower remineralization rates were observed as the fraction of terrestrial OM increased in sites along the transect culminating in the lowest specific remineralization rates observed at the mangrove site, which is dominated by terrestrial, and therefore more refractory, sources of OM. This trend is revealed in estimates of both specific rates of O_2 consumption and of NH_4^+ accumulation in porewaters over the depth of the incubated cores, which suggests that lability of OM not only drives the rapid consumption of O_2 and remineralization efficiency in surface sediments during the first stages of diagenesis, but also influences rates of OM remineralization over more protracted time intervals.

4. NH_4^+ benthic flux estimates and specific rates of H_2S production illustrate the importance of OM quantity in different depositional environments. Larger quantities of OM (i.e., at the mangrove site) result in larger quantities of regenerated inorganic nutrients in a given amount of time, and consequently generate greater benthic nutrient fluxes, even when the specific remineralization rate is lower. Additionally, larger quantities of OM buried below the oxic respiration zone result in OM available for respiration via sulfate reduction, as indicated by higher specific rates of H_2S production in sediments characterized by larger quantities of OM.

5. Downcore porewater NH_4^+ and DIP profiles display several intriguing features. Marked reversals observed in porewater NH_4^+ gradients in the carbonate dominated and ocean sites may reflect several pathways of nitrogen recycling in these coastal sediments, the most likely of which are annamox activity (reviewed in Burdige, 2006) and/or ammonium adsorption onto clays or humic material (Boatman and Murray 1982; Rosenfeld 1979). Additionally, in violation of behavior predicted by stoichiometric nutrient regeneration, DIP did not accumulate in sediment porewaters in tandem with NH_4^+ accumulation. Fractionation of regenerated DIP from NH_4^+ suggests one or more processes in the study sites that actively sequester porewater DIP liberated during OM remineralization; rapid surface sorption onto mineral surfaces and uptake in authigenic mineral precipitation are suggested as two possible DIP sequestration pathways.

Acknowlegements

We are grateful to In Chieh Chen who assisted with field preparations, sample collection and laboratory analyses. We thank Craig Glenn for access to his coulometer and Philip Rapoza for aiding in the construction of the incubation setup. This research was supported by a grant/cooperative agreement from the National Oceanic and Atmospheric Administration; project R/EL-42, which is sponsored by the University of Hawai‘i Sea Grant College Program, SOEST, under Institutional Grant NA05OAR4171048 from NOAA Office of Sea Grant, Department of Commerce. The views expressed herein are those of the authors and do not necessarily reflect the views of NOAA or any of its subagencies. UNIHI-SEAGRANT-xxxx. This is SOEST contribution #xxxx.

Chapter 5

Impact of *Montipora capitata* coral spawning events on Hawaiian coastal biogeochemistry

with Padilla-Gamiño, J. L., Bidigare, R. R., Gates, R. D., Ruttenberg, K. C.

Abstract

This study examines a *Montipora capitata* coral spawning event in Kane‘ohe Bay, Hawai‘i, which supplies labile, spawn derived organic matter (SDOM) to the water column and has a cascading series of related effects on the biogeochemistry of the system. Specifically, we have quantified the isotopic signatures and nutrient ratios of spawning material (egg, sperm, and bundle) and coral colonies, and utilized these signatures to track pathways of SDOM incorporation into this coral-dominated ecosystem. We observe: (1) rapid transfer of SDOM into higher trophic levels as indicated by a shift in the $\delta^{15}N$ of water column particulate organic matter (POM), which promotes enhanced deposition of POM to the sediment surface, (2) enhanced sediment efflux of NH_4^+ after the spawning event that provided sufficient nutrients to fuel a phytoplankton bloom in the overlying water, (3) drawdown of dissolved water column nutrient inventories after spawning that coincide with the occurrence of a water column phytoplankton bloom. We were able to conclude that the SDOM-triggered phytoplankton bloom was dominated by diatoms based on both pigment (fucoxanthin) enrichments in water column POM and a systematic drawdown of water column $Si(OH)_4$ that was observed during the bloom period. These observations, when taken together, are consistent with an SDOM-triggered phytoplankton bloom, similar to those that have been documented in other coral-dominated environments, such as the Great Barrier Reef.

5.1 Introduction

Coral reefs are characterized by exceedingly high rates of productivity and biodiversity, yet are typically situated in nutrient-poor (oligotrophic) waters (e.g. Furnas et al. 2005). Consequently, perturbations in inventories of essential nutrients can influence coral growth and physiology, and affect population dynamics and community composition of coral reefs (Szmant 2002). It is important to understand the biogeochemical processes that supply nutrients to these systems, as the nature of these processes and the magnitude of their impact on essential nutrient inventories will affect the productivity and biodiversity of coral reef ecosystems. Here, we quantify the effect of release of labile organic matter during spawning by *Montipora capitata* on nutrient supply to a coral reef in Kane‘ohe Bay, Hawai‘i, and identify subsequent ecosystem responses to this event.

Montipora capitata is one of the most abundant and important reef building coral species in the main Hawaiian Islands (Jokiel et al. 2004), and is an hermaphroditic broadcast-spawner (Hodgson 1985; Hunter 1988; Kolinski and Cox 2003) that releases gametes to the water column for external fertilization (Baird et al. 2009; Guest 2008; Richmond and Hunter 1990). A few hermaphroditic spawners release gametes independently, but the majority, like *M. capitata*, package and release gametes as positively buoyant egg-sperm bundles (Arai et al. 1993; Kinzie 1996; Padilla-Gamino et al. 2011). The magnitude and synchronicity of coral spawning can vary regionally (Richmond and Hunter 1990). In areas such as Hawai‘i, in the central Pacific, or in the Red Sea, the spawning of ecologically dominant species occurs in different seasons, months and lunar phases (Kolinski and Cox 2003; Richmond and Hunter 1990; Shlesinger and Loya 1985). For example, *Montipora capitata* releases egg-sperm bundles during the new moon of summer months in Hawai‘i, while *Pocillopora meandrina* and *Porites compressa* release their gametes during the full-third quarter moon in the spring and summer months, respectively (Kolinski and Cox 2003). By contrast, mass spawning events in the Great Barrier Reef (GBR) are multi-specific, and can include over 130 species. GBR spawning events occur during 1-2 months in the spring and release enormous quantities of eggs and larvae to the reef ecosystem (Harrison and Wallace 1990; Willis et al. 1985).

Spawning events result in the influx of large quantities of labile organic material into the water column, hereafter described as Spawn Derived Organic Matter (SDOM, Fig. 1). Nutrient release from SDOM to the water column has the potential to significantly influence tropic interactions (Baird et al. 2001; Pratchett et al. 2001; Westneat and Resing 1988), biogeochemical processes in oligotrophic reef systems (Eyre et al. 2008; Glud et al. 2008; Wild et al. 2008), and in rare occasions cause extensive mortality of corals and other reef animals (Simpson et al. 1993). SDOM that is not fertilized in the water column has several potential fates: (1) abiotic or biotic decomposition within the water column, (2) direct sedimentation of unfertilized SDOM, or (3) ingestion of SDOM by higher tropic level organisms and subsequent sinking of fecal matter to the sediments (Wild et al. 2008; Wild et al. 2004a).

Figure 5.1 Flow chart processes that potentially influence the biogeochemistry of coral reef ecosystems during spawning events.

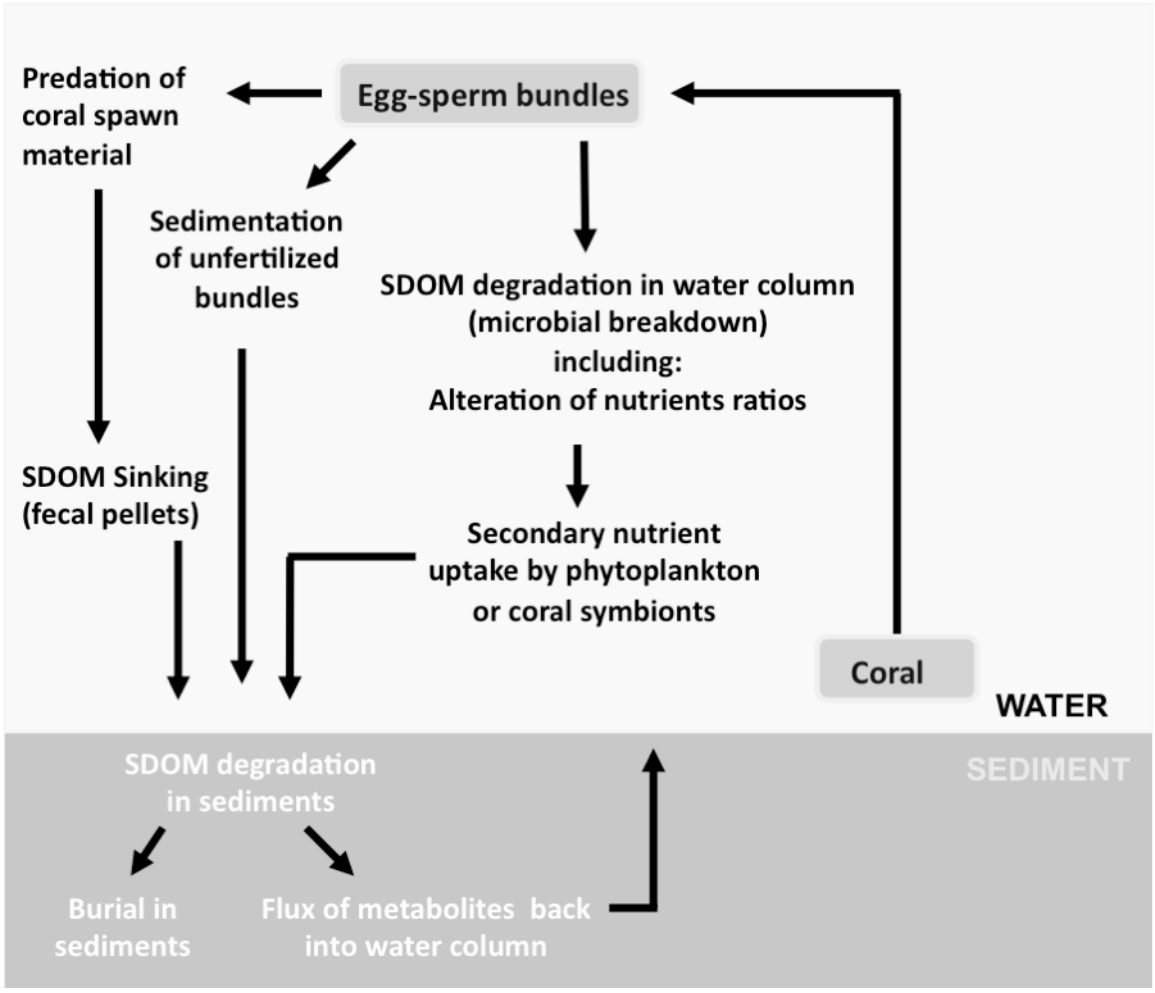

The purpose of this study was to examine how SDOM produced by *M. capitata* spawning events in Kane‘ohe Bay, Hawai‘i, alter nutrient budgets and influence water column productivity. Specifically, we quantified the isotopic signatures and nutrient ratios of spawning material (egg, sperm and bundle) and coral colonies, and utilized these signatures to track pathways of SDOM incorporation into the coral ecosystem. Additionally, we evaluated the impact of SDOM on dissolved nutrient inventories, identified nutrient recycling pathways, and tracked the impact of SDOM-driven elevated nutrient inventories on phytoplankton biomass. Finally, we compared the quantity of SDOM nutrient and organic carbon input during spawning events in Kane‘ohe Bay, Hawai‘i to SDOM-driven nutrient loading in the GBR, and consider the importance of physical factors in controlling the magnitude of the ecosystem response to SDOM-driven nutrient perturbations.

5.2 Methods

Study site: This study was conducted in June 2008 at Gilligan’s lagoon (21° 25.973’N; 157° 47.392’W) on the western side of Moku O Lo‘e Island (Coconut Island) in Kane‘ohe Bay (O‘ahu, Hawai‘i). Kane‘ohe Bay, located on the windward side of O‘ahu, Hawai‘i, is the largest sheltered body of water in the main Hawaiian Islands, with a total surface area at mean low tide of 61 x 10^6 m^2 (Jokiel et al. 2004). Coral covers approximately 20% of Kane‘ohe Bay, with ~12% of that coral being *Montipora capitata* (Hunter and Evans 1995). At our study site, Gilligan’s Lagoon, *M. capitata* is the dominant coral species.

Instrumentation: A multi-parameter YSI 6600V2 Sonde® and a LiCor 193 Spherical Quantum Sensor® were deployed within 2 m of the sampling location to monitor real-time water conditions throughout the study. The YSI sonde measured temperature, salinity, turbidity, conductivity, pH, and pressure (depth). The LiCor sensor measured photosynthetically active radiation (PAR), and was adapted with a small cup on the lower side of the spherical sensor to avoid reflective radiation from the sediment water interface. A bottom-mounted 600 kHz RD Instruments acoustic Doppler current profiler (ADCP)® was placed in the lagoon to monitor water motion throughout the study. In addition to underwater sensors, data from the Hawai‘i Institute of Marine Biology Weather Station provided information on weather conditions, including precipitation, wind direction, wind speed, solar irradiation, water temperature, and air temperature.

Coral host tissue and spawn material collection and on-shore processing: Tissue samples from adult coral colonies were obtained before (pre) and after (post) spawning during 2007 and 2008 (pre: 9 June 2007 and 27 May 2008; post: 30 September 2007 and 21 September 2008). Coral host tissue samples were obtained by breaking a small fragment of the parental colony from regions where polyps were anticipated to be reproductively active (at least 4 cm away from tips and edges) (Wallace 1985). Samples were placed immediately on dry ice and stored at -80°C until further analysis.

Gametes were collected upon release to the water column during the spawning event of summer 2007 and 2008 from colonies located in ~1-2 m of water. The gametes were collected on the fringing reef using a novel net system that caused minimal damage to both adult coral colonies and released gametes (Padilla-Gamiño and Gates, *submitted*). The cylindrical nets were placed on coral colonies 1-2 hours before spawning commenced and were removed every night after the spawning events. The collected egg-sperm bundles were rinsed with filtered (0.2 μm polycarbonate filter) seawater and aliquots placed immediately in aluminum foil capsules for carbon and nitrogen analysis. An additional aliquot of egg-sperm bundles was rinsed with filtered seawater to break apart the bundles and isolate the sperm packets from eggs. Sperm packets were placed in aluminum capsules for carbon and nitrogen analysis and eggs were placed in Eppendorf® tubes. Egg-sperm bundles, eggs, and sperm samples were stored at -80°C until analyzed.

Coral host tissue and spawn material processing and analysis: All elemental, isotopic, and biochemical measurements of coral tissue were obtained using collected whole coral samples including coral host tissue, coral symbionts (*Symbiodinium)*, and skeleton (for adults). Skeleton was removed and the remaining sample, which consisted of a combination of host tissue plus the algal *Symbiodinium* (referred to hereafter as host tissue sample), was filtered onto pre-combusted 25 mm glass fiber filters for organic carbon (OC) and total nitrogen (TN) analysis (Whatman® GF/F, 0.7 μm nominal pore size). Eggs collected during spawning were also filtered onto pre-combusted GF/F filters for analysis. Adult coral host tissue material on GF/F filters was acidified to remove inorganic carbon (IC) by slowly adding 3N HCl, drop wise, to each filter and drying after acidification was complete. Host tissue and egg samples on GF/F filters, as well as aluminum capsules that were prepared in the field with whole bundle and sperm samples, were analyzed for carbon and nitrogen

concentrations and isotopic values at the Isotope Biogeochemistry Laboratory at the University of Hawaii, Manoa. Carbon and nitrogen isotopic values are reported using conventional δ-notation with respect to VPDB and atmospheric N_2, respectively. Total phosphorus was determined on eggs and host tissue using a modified high-temperature ashing/hydrolsis method (Aspila et al. 1976), and analyzed via the molybdenum blue method (Grasshoff et al. 1983); phosphorus content of whole bundle and sperm samples was not determined. Inorganic phosphorus content of corals and gametes was below detectable levels, and thus we report total phosphorus only, which is equivalent to organic phosphorus (OP) in this data set. All filtered samples were normalized to total ash-free dry host tissue biomass of the organic fraction according to Grottoli et al. (2004) to account for residual skeleton material. Total lipids of coral fragments were extracted according to Rodrigues and Grottoli (2007). In brief, lipids were extracted from ground samples (skeleton + host tissue + symbiont cells) in a 2:1 chloroform/methanol solution, the organic phase was washed using 0.88% KCl and the extract dried to a constant weight.

Prior to analysis the $\delta^{13}C$ (per mil), OC:OP (mol mol^{-1}), OC:TN (mol mol^{-1}) and total lipid (g g^{-1} dry matter) values were normalized (if necessary) using a logarithmic transformation to achieve homogeneity of variances and normality. Data were analyzed using a general linear model, with year, pre/post spawning and colony as fixed factors. Colony was nested within the pre/post spawning category to account for the repeated measurements between periods before and after spawning.

Water and sediment sample collection: Water and sediment samples were collected pre-, post-, and during spawning in June 2008 over a 19-day time period. Samples collected pre- and post-spawn event were collected at noon (12:00) and midnight (00:00). On the three days over which spawning occurred (3- 5 June 2008), samples were collected at noon (00:00), at the start of bundle release (~21:00), at the end of bundle release (~22:00), and 1 hour after spawning ceased (~23:30). Surface and bottom water samples were collected at each time point in acid-washed, sample-rinsed 1-L HDPE bottles and immediately transferred to shore for filtration. Water samples were also collected for pigment analysis using a soap-washed and sample rinsed 250-mL amber bottle. Small sediment push cores were collected at each sampling time point from a sediment patch surrounded by coral heads using a modified 60-cc syringe as a coring device.

Sediment sample processing and analysis: Sediment push cores were sectioned into 3 intervals (0-2 cm, 2-4 cm and 4-6 cm) under an inert (N_2) atmosphere to prevent oxidation artifacts (Bray et al. 1973; Krall et al. 2009). Porewater was separated from bulk sediment via centrifugation. In order to maximize porewater collection in sandy sediments, Whatman VectaSpin 20 ® centrifuge tubes were adapted to allow filtration during centrifugation by replacing the manufactured installed polypropylene filter with a coarse 24 mm glass fiber filter (VWR ® Grade 696, 1.2 μm nominal pore size). The coarse glass fiber filter allowed maximum recovery of sediment porewater, which was subsequently filtered using a 0.4 μm Pall Life Sciences GHP acrodisc® filters. Filtered porewater was split into two subsamples: a frozen, untreated split and a refrigerated-acidified split. Samples were analyzed for dissolved phosphate (PO_4^{3-}), ferrous iron (Fe^{2+}), and ammonium (NH_4^+) using well-established colorimetric protocols (Grasshoff et al. 1983) on a BioTek Synergy HT Multi-Mode Microplate Reader; all reported data have a 2% standard error associated with them. The microplate reader permits colorimetric detection on small porewater sample volumes (300-μL), allowing for the analysis of multiple dissolved constituents on a single porewater interval, despite the small volumes of porewater collected from each interval. We used Nunc 96-well Optical Bottom Plates ®, which have a 1-cm path length, comparable to that of standard spectrophotometric detection. Total dissolved phosphorus (TDP) was determined on porewaters using a modified high-temperature ashing-hydrolysis method and analyzed via the molybdenum blue method; Dissolved organic phosphorus (DOP) is calculated as the difference between TDP and DIP (Monaghan and Ruttenberg 1999). Porewater concentrations of PO_4^{3-} and NH_4^+ are the focus of this paper; other data are available upon request.

After removal of porewater, sectioned sediments were frozen under an inert atmosphere until freeze-dried under vacuum to prevent oxidation artifacts (Krall et al. 2009). Sediments were ground with an agate mortar and pestle, sieved (<125 μm) and stored in sealed vessels prior to analysis. Sediment inorganic phosphorus (IP) was determined utilizing acid hydrolysis and sediment total phosphorus (TP) was determined using high-temperature ashing/hydrolysis; OP was calculated as the difference between TP and IP (Aspila et al. 1976). Total carbon (TC), OC, IC, and TN, as well as carbon and nitrogen isotope values ($\delta^{13}C$ and $\delta^{15}N$, respectively) were determined on sediments using a combined

coulometric-elemental analyzer-mass spectrometry method adapted for high-carbonate sediments (Briggs et al. 2011, *submitted*). Carbon and nitrogen isotopic values are reported using conventional δ-notation with respect to VPDB and atmospheric N_2, respectively. Samples were analyzed for carbon and nitrogen values at the Isotope Biogeochemistry Laboratory at the University of Hawaii, Manoa.

Water sample processing and analysis: A 700-ml split of surface and bottom water collected in the 1-L HDPE bottles was filtered through a pre-weighed 47 mm polycarbonate filter (Whatman®, 0.2 µm nominal pore size), which was acid-washed and rinsed with MQ-H_2O prior to use. Filtrate was split into two subsamples: a frozen, untreated split and a refrigerated-acidified sample. Frozen, untreated splits were analyzed for dissolved PO_4^{3-}, $Si(OH)_4$, NO_3^-, NO_2^-, NH_4^+, total dissolved nitrogen (TDN), and total dissolved phosphorus (TDP) on a Technicon AutoAnalyzer II® following well-established analytical methods at The Water Center at the University of Washington. DOP was determined as the difference between TDP and PO_4^{3-} (dissolved inorganic phosphorus, DIP).

A 250-ml split of the remaining sample water was filtered through pre-combusted 25 mm GF/F filter for the analysis of particulate OC and TN, as well as carbon and nitrogen isotope values ($\delta^{13}C$ an $\delta^{15}N$, respectively). Filters were acidified and analyzed according to the same procedures outlined for host tissue samples (see above).

Sample water collected in the amber bottle was filtered through a 25 mm GF/F filter to collect suspended particulates for photosynthetic pigment. Samples were frozen at -80ºC prior to analysis and were extracted and analyzed by reverse-phase high-performance liquid chromatography (HPLC) as described by Bidigare et al. (2005).

Benthic nutrient efflux calculations: Sediment porewater profiles were used to calculate diffusive nutrient fluxes across the sediment water interface using Fick's first law of diffusion. The fluxes were calculated based on the difference between the peak concentration of porewater NH_4^+ and PO_4^{3-} at depth (within the top 6 cm sampled) and the NH_4^+ and PO_4^{3-}concentration in the overlying bottom water, respectively. The whole molecular diffusion constant for seawater (D_{sw}) based on values from Boudreau (1997) ($NH_4^+$and PO_4^{3-}, 1.85×10^{-9} and 8.9×10^{-10}, respectively). Sediment tortuosity (θ^2) was calculated from the porosity of sediments using the assumptions outlined in Boudreau (1997).

5.3 Results

Coral spawning and physical conditions: Spawning of *M. capitata* occurred between 20:45 and 21:15 for three days during the first quarter of the new moon in June, July and August of 2007 and 2008. The spawning events in both years occurred when tidal amplitudes were at their greatest, and tide was going out. Spawning dynamics changed significantly between years. In 2007, there were both more colonies participating in the spawning events and larger reproductive output per colony (Padilla-Gamino and Gates 2011, *submitted*). In 2008, the reproductive output decreased dramatically, only 25% of the volume released in 2007 was released in 2008 (Padilla-Gamino and Gates 2011, *submitted*).

Figure. 5.2 In situ instruments were deployed within 2 m of the sampling location to monitor real-time water quality throughout the study. A multi-parameter YSI 6600V2 Sonde® provided data on (a) temperature (ºC), (b) salinity (practical salinity units) and (d) water depth (cm), and a LiCor 193 Spherical Quantum Sensor® provided data on (c) PAR (µmol m^{-2} s^{-1}). Additionally, (e) wind speed and direction (mph; positive-y is the north direction), as well as (f) precipitation (cm) data were obtained from the Hawai'i Institute of Marine Biology (HIMB) weather station. Shaded box denotes the three consecutive days of spawning.

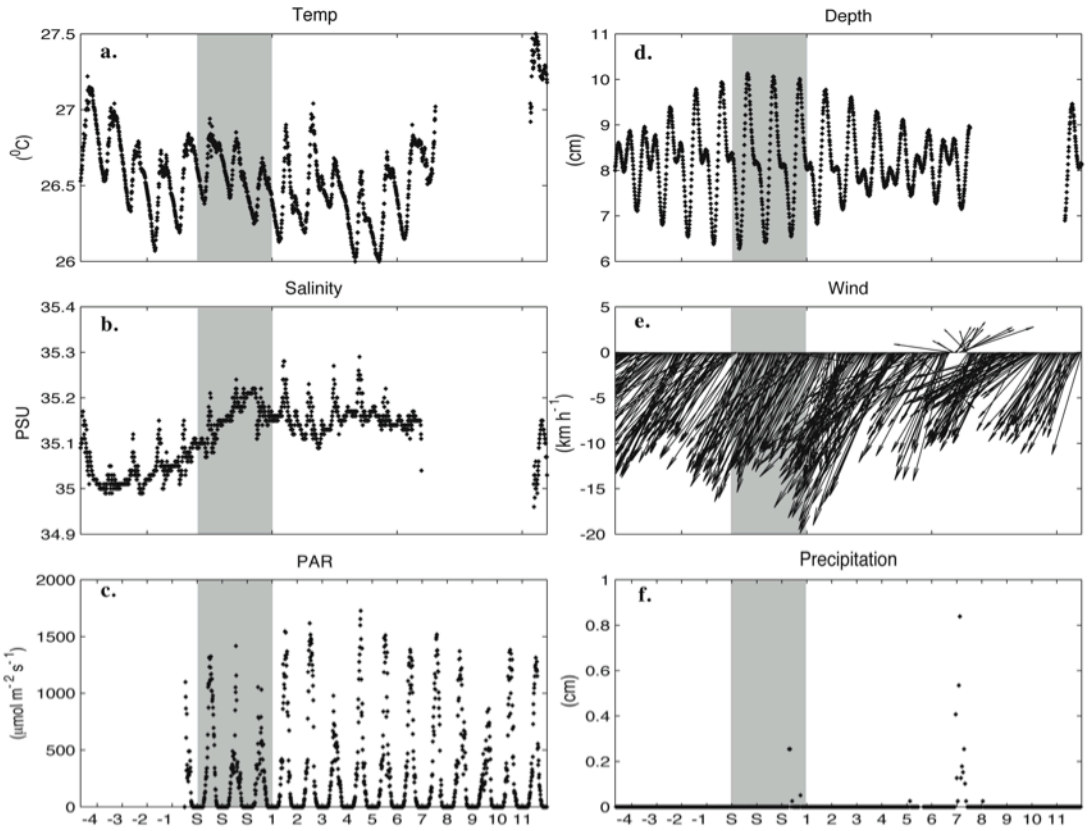

Pertinent weather and water quality data collected from in situ instrumentation (temperature, salinity, PAR and depth) and the Hawai‘i Institute of Marine Biology (HIMB) weather station (wind, precipitation) is presented for the June 2008 spawning event (Fig. 5.2). Additional data from instrument sondes and weather gauges are not shown. Average water temperature and salinity (± standard error from daytime fluctuations) were 26.6 ± 0.3˚C and 35.1 ± 0.1 over the 19-day study period, respectively (Fig. 5.2a-b), and diurnal variations in PAR were observed with peak values of 1726 (µmol m^{-2} s^{-1}) (Fig. 5.2c). YSI pressure sensor data reveal semi-diurnal tidal fluctuations, with spring tide conditions during spawning events (Fig. 5.2d). Trade-wind conditions, characterized by an absence of rainfall and NE winds at 10-20 km h^{-1}, persisted throughout the study (Fig. 5.2e), with the exception of a small rain event and wind shift that occurred 7 days after spawning ceased (Fig. 5.2f). This rain event was brief (8 hrs), and peaked at 03:00 on the morning of June 12, resulting in 0.84 cm of rain.

A 600kHz RD® Instrument acoustic Doppler current profiler (ADCP) measured water flow in Gilligan’s Lagoon during the study. The instrument measures flow in 3 directions, u

Figure 5.3 Data from a 600 kHz RD acoustic Doppler current profiler deployed in Gilligan’s lagoon during the study period. Water velocity (cm s^{-1}) is displayed on the right-hand y-axis in three directions: (a) north/south: u, (b) east/west: v, and (c) vertical motion: w. Water elevation (m) is on the left-hand y-axis and is displayed as a dark black line on each panel. Panel (f) displays the horizontal currents from 2.12 m above the seafloor as current velocity vectors, where positive-y is the northeast direction.

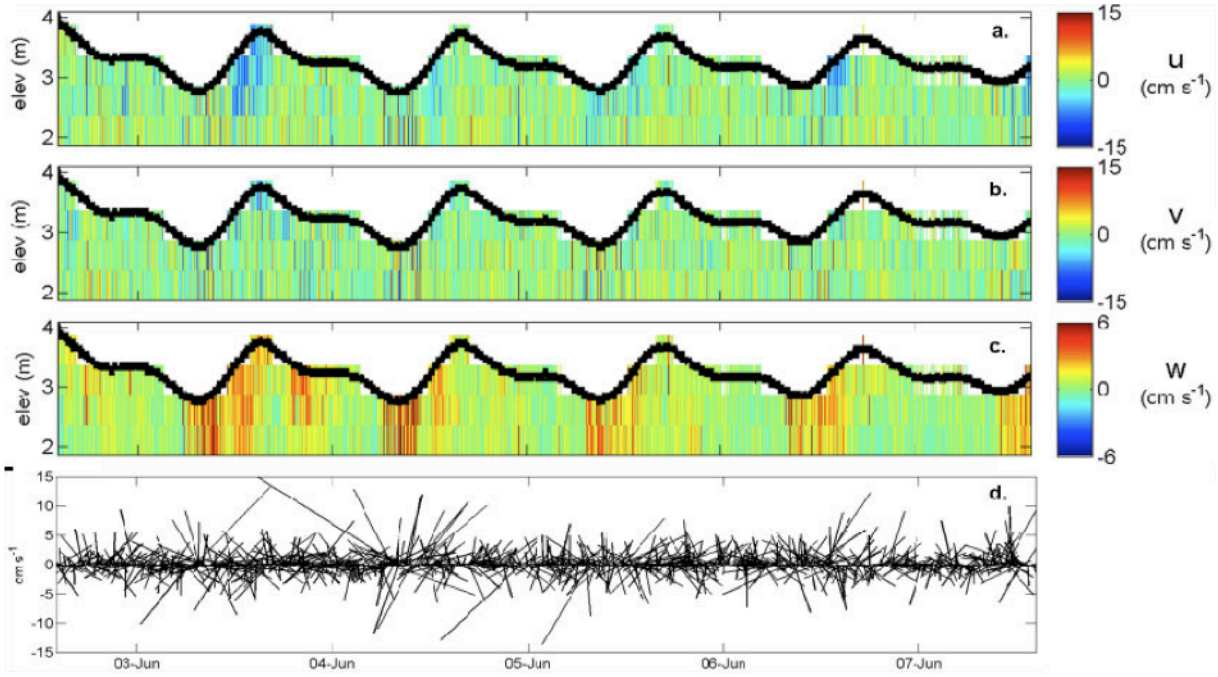

(north and south), v (east and west), and w (vertical motion) (Fig. 5.3a-c). Flow data in each direction was used to create a current velocity vector plot from 2.12 m above the seabed, with positive-y vectors in the northern direction (Fig. 5.3d). The ADCP data reveal extremely low and variable flow rates (<5 ± 2 cm s^{-1}), which register just above the error of the instrument (Fig. 5.3). In general, water elevation was tidally driven (dark line plotted on left-hand y-axis in Figs. 5.3a-c). Horizontal currents were slow and variable, yielding a velocity vector plot that indicates clearly the absence of unidirectional flow during tidal shifts (Fig. 5.3d), suggesting minimal flushing of the lagoon during the tidal cycle.

Coral host tissue and spawn material: Elemental and isotopic composition of host tissue samples from corals containing gametes prior to spawning (n=6) were compared to host tissues from corals post-spawn (n=6). The average OC:OP (mol mol^{-1}) from 2007 and 2008 pre- and post-spawning host tissue samples was 364 ± 18, significant changes were not observed between spawning years and pre- or post-spawn samples (p=0.759, p=0.814, Fig. 5.4a, Table 5.1). $\delta^{13}C$ values were heavier in the post-spawning coral tissues (p=0.001, Fig. 5.4b, Table 5.1), The average $\delta^{13}C$ values in pre and post spawning host tissue samples (both years) were -13.3 ± 0.4 and 12.2 ± 0.4, respectively (Fig. 5.4, Table 5.1). Overall, $\delta^{13}C$ values were heavier in 2008 than 2007 (p=0.001, Table 5.1) and substantial variability within colonies was observed (p=0.001, Table 5.1).

Bundles (n=10 samples) and individual components of the spawn material (n=15 egg samples and n=4 sperm samples), were analyzed for OC:TN and $\delta^{13}C$ values. Bundle and sperm material $\delta^{13}C$ values were similar to host tissue samples with $\delta^{13}C$ values of -12.1 ± 0.1 and -13.0 ± 0.1 respectively; however, eggs displayed a lighter $\delta^{13}C$ value of -14.5 ± 0.1

Table 5.1: Results of the general linear model testing the effects of year, pre/post spawning and colony on $\delta^{13}C$, OC:OP, OC:TN and lipids of *Montipora capitata*. Df=degrees of freedom, F=F-statistic, p=p-value. Significant values at 95% confidence (p<0.05) are in bold.

		Effect of Year		Effect of Pre/Post		Effect of Colony (Pre/Post)		Effect of Year*Pre/Post	
Variable	df	F	p	F	p	F	p	F	p
$\delta^{13}C$	46	13.57	**0.001**	16.19	**0.001**	4.5	**0.001**	1.06	0.314
OC:OP	46	0.10	0.759	0.06	0.814	0.71	0.781	0.46	0.506
OC:TN	46	4.89	**0.038**	2.25	0.148	1.23	0.317	5.91	**0.024**
Lipids	67	2.44	0.128	3.86	0.058	2.19	**0.015**	0.88	0.356

(Fig. 5.4b). Organic carbon to total nitrogen (OC:TN) ratios in host tissue samples pre-spawn were not significantly different from OC:TN ratios of post-spawn host tissues; the average OC:TN ratio of all host tissues was 11.0 ± 0.4. Bundle, egg, and sperm material had distinct OC:TN ratios of 19.1 ± 0.5, 21.4 ± 0.6, and 5.3 ± 0.1, respectively (Fig. 5.4b). Spawn bundles displayed a $\delta^{15}N$ value of 4.6 ± 0.1 (n = 10), and the OC:OP ratio of spawn eggs was 838 ± 198 (n = 6) (data not shown). Overall, OC:TN was lower in coral tissues from 2007 than 2008 (p=0.038, Table 5.1).

Figure 5.4 Isotopic signatures and nutrient ratios of gamete and adult host tissue from 2007 and 2008. (a) OC:OP versus $\delta^{13}C$ for 2007 and 2008 host tissue. (b) OC:TN versus $\delta^{13}C$ for host tissue, egg, sperm, and bundles. Error bars represent standard errors associated with replicate sample analysis.

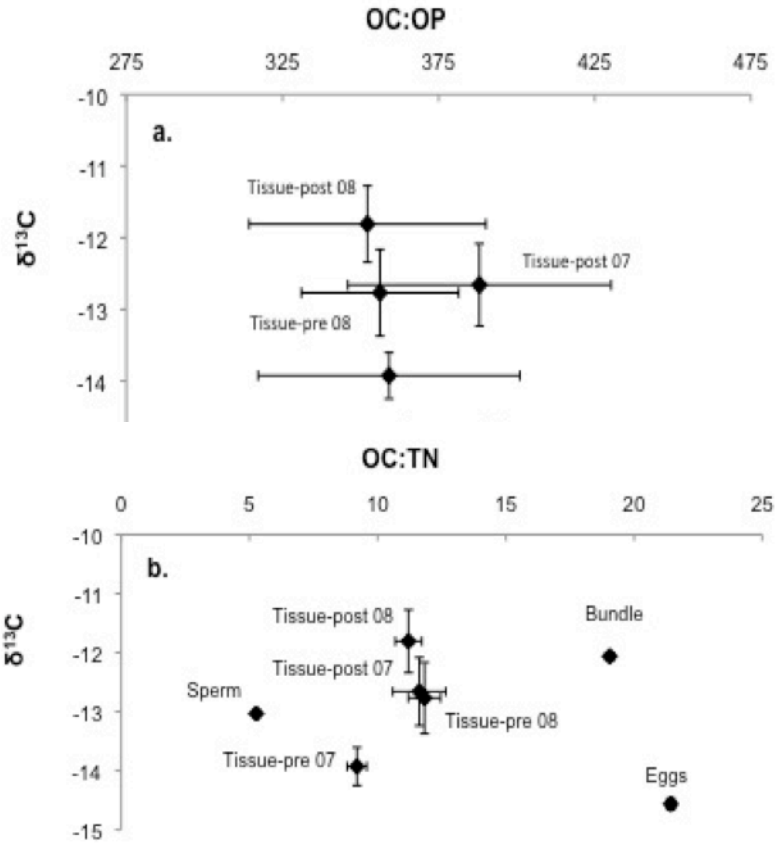

No difference in lipid content was found between years (p=0.128, Table 1). A marginally significant p-value in the lipid content before and after spawning (p=0.058, Fig. 5, Table 1), suggests that lipid concentrations in post-spawn host tissue samples collected in both years were lower compared to pre-spawn host tissue samples (Fig. 5, Table 1), Pre-spawn host tissue lipid concentrations collected in 2007 and 2008 were 0.23 ± 0.01 and 0.30 ± 0.02 g total lipids g^{-1} dry matter (n=17), respectively; post-spawning host tissue lipid concentrations collected in 2007 and 2008 were 0.20 ± 0.01 and 0.22 ± 0.02 g total lipids g^{-1} dry matter (n=17), respectively (Fig. 5). Colony had a significant effect on lipid content before and after spawning (p=0.015), indicating that there is a large variation in lipid content between colonies.

Figure 5.5 Lipid concentrations (g total lipids g^{-1} dry matter) from pre- and post-spawning adult host tissues collected in 2007 (white bars) and 2008 (black bars).

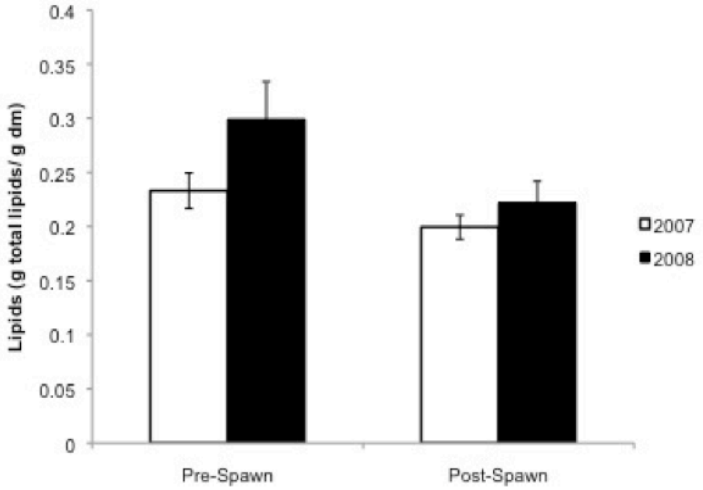

Water column and sediment: $\delta^{13}C$ values of surface water column particles prior to spawning were lighter (-19.4 ± 0.6; n=6) than samples collected 24 hours after spawning (-13.6 ± 0.8; n=3) (Fig. 5.6a); bottom water column particles displayed a similar trend towards heavier $\delta^{13}C$ values immediately following spawning. $\delta^{15}N$ values in water column particulates from surface and bottom waters increased during- and post-spawn to 7.5 ± 0.3 (n=38) (Fig. 5.6b) from pre-spawn values of 4.9 ± 0.4 (n=12). Sediments and water column particulates had OC concentrations ranging from 0.5 to 3.5 wt % (Fig. 5.6c). OC and TN concentrations and OC:TN ratios of water column particulates and surface sediments post-spawn were not different from pre-spawn sample OC and TN concentrations (Fig. 5.6c-e).

The calculated diffusive fluxes of nutrients from sediments to the water column (Fig. 5.7) are most likely minimum estimates, because only the top 6 cm of the sediment was sampled, and porewater concentrations may be higher deeper in the sediments. Nonetheless, results of these calculations indicate that sediments act as a source of NH_4^+ and PO_4^{3-} to the overlying water, with positive flux rates observed at all sampling times (Fig. 5.7). The magnitude of the PO_4^{3-} flux was relatively invariant during this study (0.78 ± 0.36 μmol m^{-2} d^{-1}). Within twenty-four hours after the last spawning event, by contrast, benthic ammonium fluxes were nearly 4-fold higher (39 μmol m^{-2} d^{-1}) than pre-spawn flux rates (Fig. 5.7).

Pre-spawn Chl *a* levels in surface and bottom waters were relatively invariant (316 ± 38 ng L^{-1}; n=12). Six days after the spawning event Chl *a* levels spiked to 1335 ng L^{-1}, 3 times the concentration observed during the pre-spawn period (Fig. 5.8a). Fucoxanthin, a biomarker pigment for diatoms, spiked to 288 ng L^{-1} synchronously with Chl *a* (Fig. 5.8b). A

total of 52 particulate water samples were collected for Chl *a* and photosynthetic pigment analysis. Because our intent was to use Chl *a* as a marker for water column phytoplankton biomass response to SDOM-derived nutrients, we excluded 4 high Chl *a* samples from the data set that also had exceedingly high concentrations of peridinin, the pigment characteristic of dinoflagellates. These high peridinin values (30-130 times background levels) most likely indicate the presence of the dinoflagellate endosymbionts present in the eggs of the bundles (*M. capitata* has vertical transmission of symbionts), and do not reflect free-living phytoplankton biomass.

Overall, dissolved inorganic and organic nutrient concentrations from surface and bottom waters were relatively similar (Fig. 5.9), indicating a well-mixed water column during most of the study. Pre-spawn water column concentrations of NH_4^+ and PO_4^{3-} averaged 0.42 ± .11 μmol L^{-1} (n=12) (Fig. 5.9a), and 0.16 ± .02 μmol L^{-1} (n=12) (Fig. 5.9b), respectively. After the spawning event had run its course, NH_4^+ and PO_4^{3-} concentrations decreased to near detection limits (0.92 and 0.07 μmole L^{-1}, respectively). $Si(OH)_4$ concentrations were ~8 μmol L^{-1} at the start of the study and steadily decreased after spawning commenced to ~2 μmol L^{-1} (Fig. 5.9c). To confirm that this decrease was not an artifact of instrument drift, these samples were rerun manually on the BioTek Plate reader (see methods) using a colorimetric molybdenum-blue method (Grasshoff 1972). Values obtained on the plate reader were within 5% of values reported from the auto-analyzer at the Water Resource Center, and displayed the same decreasing trend (data not shown). Pre-spawning NO_2 + NO_3 (NO_x) averaged 0.21 ± 0.09 μmol L^{-1} (n=12) (Fig. 5.9d); NO_x concentrations increased 2-fold after the spawning event.

With the exception of the time period during which the spawning event occurred, DON and DOP concentrations were fairly invariant throughout the study (Fig. 5.9e-f). Two samples collected during the spawning event (spawning day 1 and spawning day 2) that display high levels of DON and DOP likely reflect sampling artifacts, as samples collected 30 minutes later did not present similarly high levels of DON or DOP (Fig. 5.9h). We suspect that bundles caught on the filter may have broken apart during filtration, artificially elevating levels of dissolved organic nutrient concentrations. Dissolved inorganic nitrogen (DIN= NO_x + NH_4^+) to dissolved inorganic phosphorus (DIP= PO_4^{3-}) ratios increased after the last day of spawning (Fig. 5.9g) and DON:DOP (mol mol^{-1}) ratios averaged 39.8 ± 0.7

(n=52) throughout this study (Fig.9h). The DIN:DIP (mol mol^{-1}) in pre-spawn samples average 4.0 ± 0.3 (n=12); post-spawn the ratio increased to a maximum of 15.

5.4 Discussion

The guiding hypothesis of this study was that *M. capitata* coral spawning events in Kane‘ohe Bay supply a quantity of labile, spawn derived organic matter (SDOM) to the water column that have a cascading series of related effects on the biogeochemistry of the system. First, we considered that the elemental and isotopic composition of water column particulate matter would be altered due to the input of SDOM, and that this signature might also be visible in surface sediments that would receive sinking SDOM. Second, we anticipated that water column dissolved nutrient inventories would be enhanced due to rapid mineralization of the labile pool of SDOM, and that this in turn could trigger a water column phytoplankton bloom. Recent studies examining the biogeochemical response to mass coral spawning at the GBR found that SDOM can instigate a chain of pelagic and benthic processes which significantly influence the reef community and nutrient recycling of these systems (Eyre et al. 2008; Glud et al. 2008; Wild et al. 2008). The events reported in the GBR studies were driven by nutrient regeneration from mineralized of SDOM in both water column and sediments.

To evaluate impacts of SDOM on the biogeochemistry of our system it was necessary to (1) determine the elemental and isotopic composition of SDOM, (2) follow the evolution of dissolved nutrients and photosynthetic pigments in the water column from before the spawning event (pre-spawn), during, and for approximately 2 weeks after the spawning event (post-spawn), and (3) evaluate the contribution of remineralization of SDOM in bottom sediments to the water column nutrient inventory, including benthic nutrient fluxes pre- and post-spawn. Each of these lines of evidence is discussed below. Finally, we assess the regional impact of the coral spawn event for nutrient loading to Kane‘ohe Bay.

Characterization of coral host tissue and spawn material: Pre- and post-spawn samples of adult host tissue have similar OC:OP and OC:TN ratios (Fig. 5.4), but post-spawn host tissue samples are shifted to heavier $\delta^{13}C$ relative to pre-spawn signatures. In general, host biomass has higher concentrations of lipids in the pre-spawn samples compared to post-spawn host tissues (Fig. 5.5). The higher concentration of lipids within corals prior to

spawning is most likely due to the presence of eggs (Arai et al. 1993), and would contribute to the lighter $\delta^{13}C$ signatures (Fig. 5.4), since lipids tend to be depleted in ^{13}C (Deniro and Epstein 1977). This observation is consistent with measurements showing that *M. capitata* eggs have almost four times the quantity of lipids as compared to the tissues of adult colonies (Padilla-Gamino and Gates, *in prep*).

The observed shift in $\delta^{13}C$ values from lighter pre-spawn to heavier post-spawn adult coral host tissue samples could also be due to a switch from heterotrophic to autotrophic feeding habits. The $\delta^{13}C$ values of host tissue plus zooxanthellae can be used as indicators of the relative contribution of heterotrophy versus photosynthesis to coral metabolism (Muscatine et al. 1989). Heterotrophic feeding drives $\delta^{13}C$ signatures to lower values as more ^{13}C depleted zooplankton are incorporated into the host tissue (Muscatine et al. 1989; Rodrigues and Grottoli 2006). Post-spawn host tissue samples are characterized by heavier $\delta^{13}C$ values than pre-spawn samples, suggesting either a decrease in heterotrophic feeding habits, or an increase in autotrophy (or both) after spawning. A switch in trophic sources of carbon has been noted during bleaching events and subsequent recovery (Rodrigues and Grottoli 2006). We hypothesize that the stress associated with spawning events may similarly alter the relative importance of heterotrophy versus photosynthesis for carbon acquisition by corals. In order to distinguish between these two possible explanations for the observed shift in $\delta^{13}C$ suggested here, the isotopic composition of host tissue would need to be separately characterized, and the relative abundance of *Symbiodinium* in the coral host tissue samples quantified, as it may not be the same in pre- and post-spawn host tissue samples. A further complicating factor is that pre-spawn samples contain reproductive components that may obscure the signatures of feeding habits on bulk host tissue $\delta^{13}C$ values.

The OC:TN ratio of coral egg material (21:1) determined in this study is consistent with previously reported values for coral eggs (19:1) (Wild et al. 2004b). The OC:OP ratio, however, is substantially higher (838:1) than previously reported values (316:1) (Eyre et al. 2008).The mean OC:TN:OP (C:N:P) ratio of coral egg material from spawning events in our study site was 838:35:1. Our sampling method, which involved careful collection of individual bundles, and the scrupulous removal of sperm and egg-sperm bundle components for analysis, ensured that our samples consisted only of coral eggs, excluding any other forms of organic matter. In contrast, Eyre et al. (2008) sampled the bulk spawn slick, which likely

contained non-coral derived organic matter including plankton material, which may account for the lower OC:OP ratio reported in the GBR study.

The OC:TN values of individual spawn components (eggs, sperm) were strikingly different than the whole bundle from which they were derived (Fig. 5.4b). A simple mass balance calculation, assuming that the bundle is comprised entirely of eggs and sperm, and using the measured OC:TN ratios of these components, suggests that the bundle is comprised of 85% eggs and 15% sperm. This is consistent with our understanding of the structure of the bundle (Padilla-Gamino et al. 2011). However, the $\delta^{13}C$ values of egg and sperm components cannot be explained using these relative percentages (Fig. 5.4b), because the bundle is characterized by a heavier $\delta^{13}C$ value than each of the individual components (sperm and egg) alone, suggesting there is another source of heavy carbon in the bundle that is unrelated to the gametes. The most likely source of this heavier carbon is packaging material within the bundle, which consists of a mucus layer possibly secreted by the oocytes (Padilla-Gamino et al. 2011). In order to understand the sources of OM to coastal sediments in tropical coral reef environments, it may be necessary to evaluate the isotopic signatures and organic nutrient ratios of coral components (such as SDOM) to account for bulk sediment OM isotopic compositions. As an example, heavy $\delta^{13}C$ values observed in coastal marine sediments of Kane‘ohe Bay can only be explained when coral components are considered as a source of OM to marine sediments (Briggs et al. 2011, *submitted*).

Tracking the impact of SDOM on water column suspended and surface sediment organic matter: There are several pathways for SDOM incorporation into the ecosystem (Fig. 5.1). In this section we examine water column particulate and surface sediment carbon and nutrient concentrations, and C and N isotopic compositions, to track the impact of SDOM on these components of the system. Of all the parameters in this suite, the $\delta^{13}C$ signature of surface water particulates (Fig. 5.6a) displays the clearest and most pronounced perturbation due to the spawning event. Carbon isotopic values from surface water particulates were enriched by ~6 per mil over pre-spawn values, for 24 hours following the onset of spawning (Fig. 5.6a). Particulates collected from bottom water also display enrichment due to the spawning event, but the effect lags by 1-2 days that observed for surface water particulates. Variability is substantially more muted in surface sediments than in water column particulates, but nonetheless an enrichment of approximately 2 per mil is

Figure 5.6 (a) $\delta^{13}C$ isotopic values, (b) $\delta^{15}N$ isotopic values, (c) OC concentrations (wt percent), (d) TN concentrations (wt percent), and (e) the OC:TN ratio of surface (diamonds) and bottom water (squares) particulate samples and surface sediments (stars). Shaded box denotes the three consecutive days of spawning.

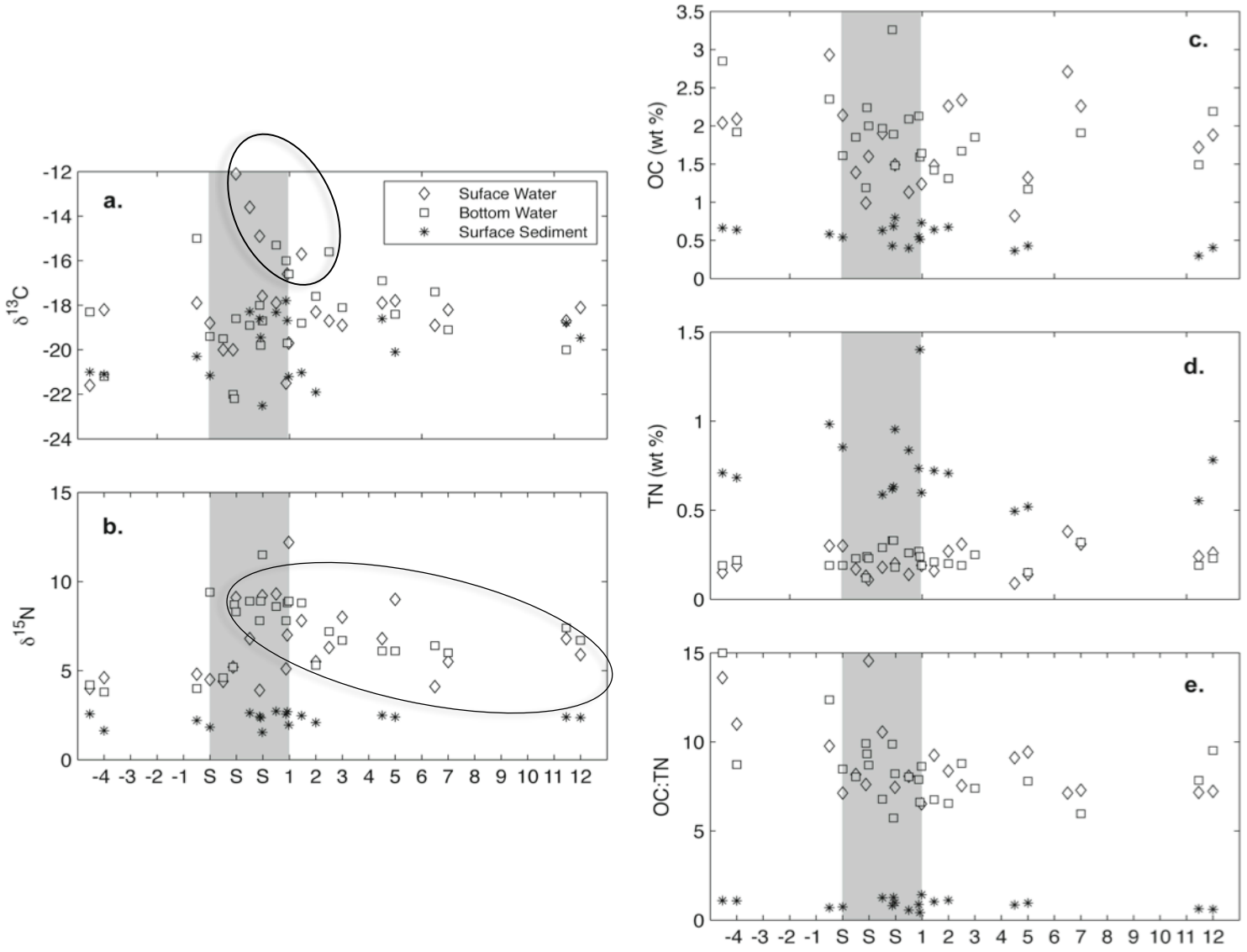

detectable in surface sediments by day-2 of the spawn event (Fig. 5.6a). A similar impact on $\delta^{15}N$ is observed in surface and bottom water particulates (enrichment of 7 and 6 per mil, respectively), but no effect is discernable in surface sediments (Fig. 5.6b).

Post-spawn, water column particulate $\delta^{13}C$ values trend relatively rapidly back to background values, while $\delta^{15}N$ values remain at enriched levels, relative to pre-spawn values (Figs. 5.6a-b). The $\delta^{15}N$ value of water column particulates can be used to examine food web dynamics, because $\delta^{15}N$ values are enriched by an average of 3.4 ± 1.1 per mil with each trophic level (reviewed in Maier et al. 2010). The $\delta^{15}N$ enrichment over pre-spawn values we observe in water column particulates (2.5 ± 0.5 per mil) reflects the cumulative effect on the isotopic composition of water column particulates as higher trophic levels feed on SDOM (Fry 1988). The rapid transfer of SDOM into higher trophic levels may increase the deposition of particulate organic matter to the sediment surface (Fig. 5.1).

While the incorporation of SDOM into the ecosystem is apparent when examining the isotopic values of water column particulates, the impact of SDOM on bulk OC concentrations of both water column particulates and surface sediments is not evident (Fig. 5.6c); there is no discernable difference in OC concentrations pre- to post-spawn in either water column particulates or surface sediments (Fig. 5.6c). We attribute the absence of post-spawn signal increases in sediment OC concentration to the dilution effect by non-organic sedimentary material (i.e. $CaCO_3$).

TN is more enriched in surface sediments (0.05 to 1.5 wt%) than in water column particulates (<0.25 wt %), in contrast to the distribution of OC between water column and surface sediments (Fig. 5.6d). The observed N-enrichment in surface sediments can be explained by microbial colonization of deposited organic matter, as bacteria are enriched in N relative to C (Rice and Hanson 1984). The elevated OC:TN ratios in surface sediments (Fig. 5.6e) are also consistent with bacterial enrichment of surface sediments over water column particulates. The fact that no discernible trend is observed pre- to post-spawn indicates that the degree of microbial colonization on SDOM is equivalent to that on non-SDOM.

Highly permeable reef sands act as biocatalytical particle filter systems where coral-derived organic matter (including SDOM) decomposes rapidly upon deposition, (Wild et al. 2005, 2008; Glud et al. 2008; Hannides and Sansone 2011, *in prep*). Although surface

Figure 5.7 Calculated benthic diffusive nutrient fluxes of NH_4^+ (dark grey) and PO_4^{3-}(light grey). Nutrient fluxes across the sediment water interface were calculated using Fick's first law of diffusion

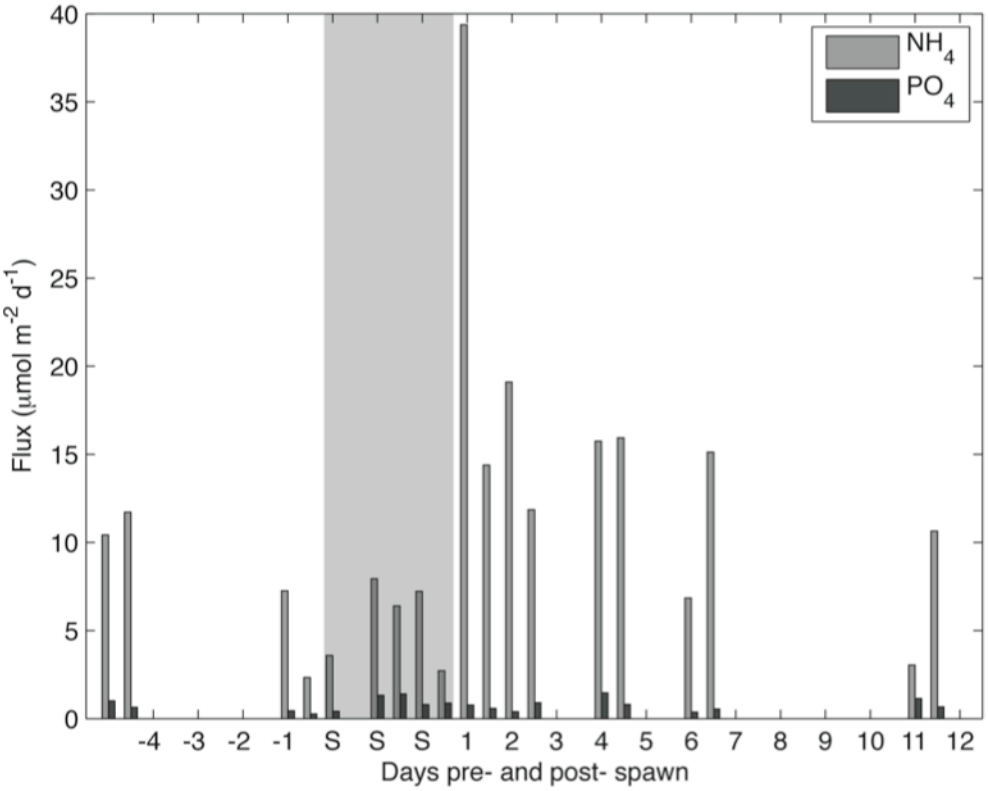

sediment concentration data do not clearly reflect the influx of SDOM (Fig. 5.6), deposited SDOM still may have a profound impact upon the system through the rapid regeneration of inorganic nutrients from this labile organic matter pool. Using sediment porewater data, we calculate a post-spawn benthic flux of NH_4^+ nearly 4 times that of pre-spawn effluxes the day after the spawning event (Fig. 5.7). Increased effluxes of porewater NH_4^+ persisted for several days after spawning, reflecting the time period over which labile SDOM was being decomposed in sediments. Previous studies have verified the significant role of sediments in recycling SDOM and have observed enhanced benthic efflux of NH_4^+ following mass spawning events, in addition to enhanced sediment oxygen consumption rates (Eyre et al. 2008; Wild et al. 2004b). The fact that no enhancement of benthic PO_4^{3-} efflux was observed can be attributed to the highly particle reactive nature of PO_4^{3-}, and indicates sediment sequestration of porewater PO_4^{3-} liberated by SDOM remineralization within the sediment (Fig. 5.7). Fractionation of benthic NH_4^+ from benthic PO_4^{3-} efflux has been observed at another study site proximal to Gilligan's Lagoon (Briggs 2011).

Figure 5.8 Photosynthetic pigment data from water column particulates. (a) Chl *a* (ng L^{-1}) and (b) fucoxanthin (ng L^{-1}) concentrations from surface (diamonds) and bottom (squares) waters. Shaded boxes denote the three consecutive days of spawning.

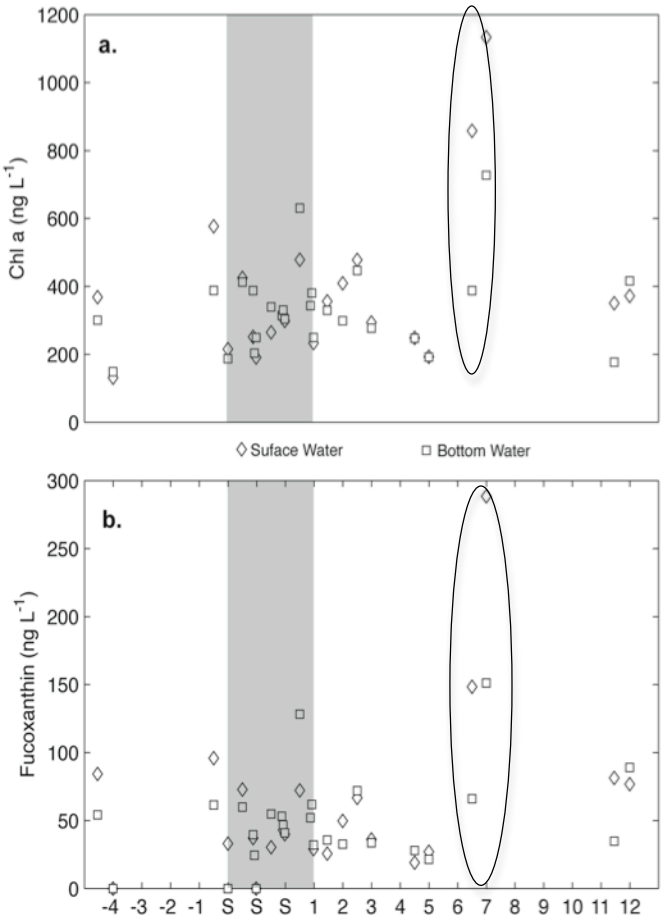

Water column dissolved nutrient perturbations by SDOM input and phytoplankton response: A phytoplankton bloom event was observed six days after the last *M. capitata* spawning in June 2007 at Gilligan's Lagoon, as evidenced by the 3-fold increase in both Chl *a* and fucoxanthin concentrations (Fig. 5.8). The rapid production of Chl *a,* and the short duration of elevated Chl *a* concentrations in the water column (Fig. 5.8a), is characteristic of the boom-bust sequence previously described by others (Eyre and Ferguson 2006; Ringuet and Mackenzie 2005). In a boom-bust sequence, rapid increases in water column productivity due to an enhanced supply of nutrients quickly collapse as nutrients are consumed and drop to limiting levels. Following coral spawn events in the GBR a boom-bust sequence was observed by Eyre et al. (2008). The bloom observed in this study may have been more protracted, however we were not able to determine the length of the bloom due to the timing of sample collection. Specifically, the bloom was first observed at noon (12:00) on 11 June 2008, and the previous sample was collected 2 days earlier, at noon (12:00) on 9 June. It is possible that the bloom initially occurred prior to 11 June, at some point during the 2-day gap in sampling (Fig. 5.8).

During coral spawning events abundant quantities of SDOM are released into the water column over several days. SDOM not respired within the water column or physically

transported out of the system, settles to the sediment, where it is degraded and chemically altered by the benthic community. A portion of degraded SDOM may be recycled into the overlying water as dissolved organic or inorganic nutrients, the products of organic matter remineralization. Our observation of enhanced benthic nutrient efflux post-spawn (Fig. 5.7) attests to the lability of SDOM, and is consistent with the rapid organic carbon degradation rates documented for broadcasting coral eggs and sperm (Wild et al. 2008). Enhanced benthic efflux of dissolved nutrients derived from SDOM mineralization will contribute to water column nutrient inventories, and have the potential to stimulate water column productivity (Eyre et al. 2008; Glud et al. 2008).

The bloom event observed in this study was similar in size and duration to storm-enhanced primary production that has been documented in other studies (Eyre and Ferguson 2006; Ringuet and Mackenzie 2005; Young 2011), suggesting that increases in water column nutrients associated with spawning events may stimulate a boom-bust water column production sequence similar to those observed with episodic fluvial inputs of nutrients (Fig. 5.8). Precipitation during our study was light (Fig. 5.3f) and the single rain event that occurred during our study happened after the Chl *a* concentrations peaked (Fig. 5.8), ruling out storm-derived nutrients as the trigger for the bloom we observed post-spawn.

The phytoplankton bloom observed post-spawn resulted in substantial drawdown of water column NH_4^+ and PO_4^{3-}, and an even more pronounced drawdown of $Si(OH)_4$ (Fig. 5.9a-c). We attribute the removal of $Si(OH)_4$ to uptake by diatoms, which dominated the bloom as evidenced by the increase in the fucoxanthin content of water column particulates (Fig. 5.8); fucoxanthin is a marker pigment for diatoms. In contrast to NH_4^+ and PO_4^{3-}, water column NO_x concentrations increased after the spawning event (Fig. 5.9d). The enhanced benthic efflux of NH_4^+ observed post-spawn could fuel water column nitrification and explain the observed increase in water column NO_x. Enhanced benthic NO_x flux could also contribute to the post-spawn water column concentrations, as has been observed to occur in the GBR (Eyre et al. 2008), but these were not quantified as part of this study. The increase

Figure 5.9 Dissolved nutrient concentrations (µmol L^{-1}) and nutrient ratios of surface (diamonds) and bottom water (squares). (a) NH_4^+ (b) PO_4^{3-} (c) $Si(OH)_4$ (d) NO_x=NO_2^- + NO_3^- (e) DON (f) DOP (g) DIN:DIP and (h) DON:DOP. Shaded box denotes the three consecutive days of spawning.

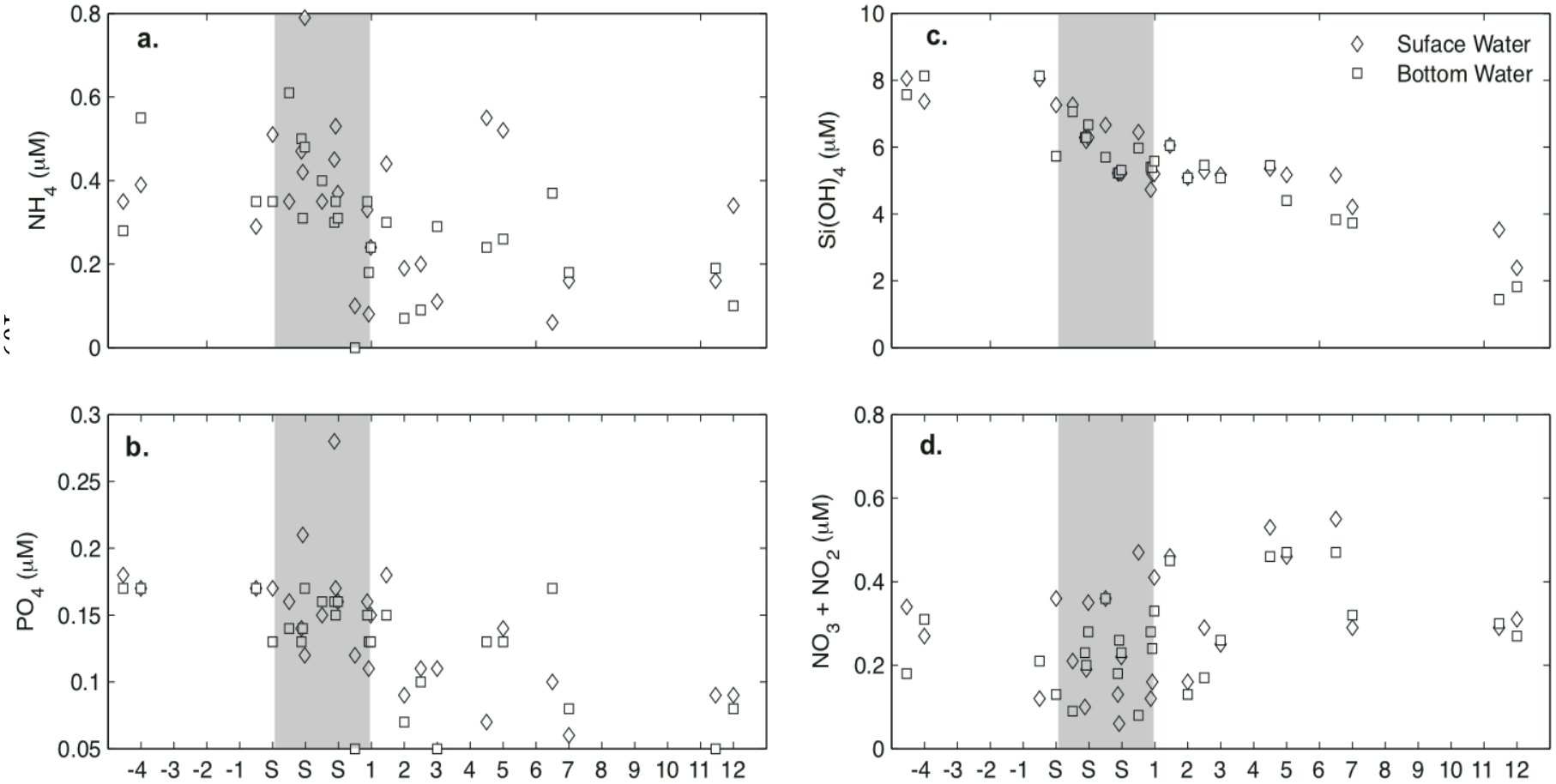

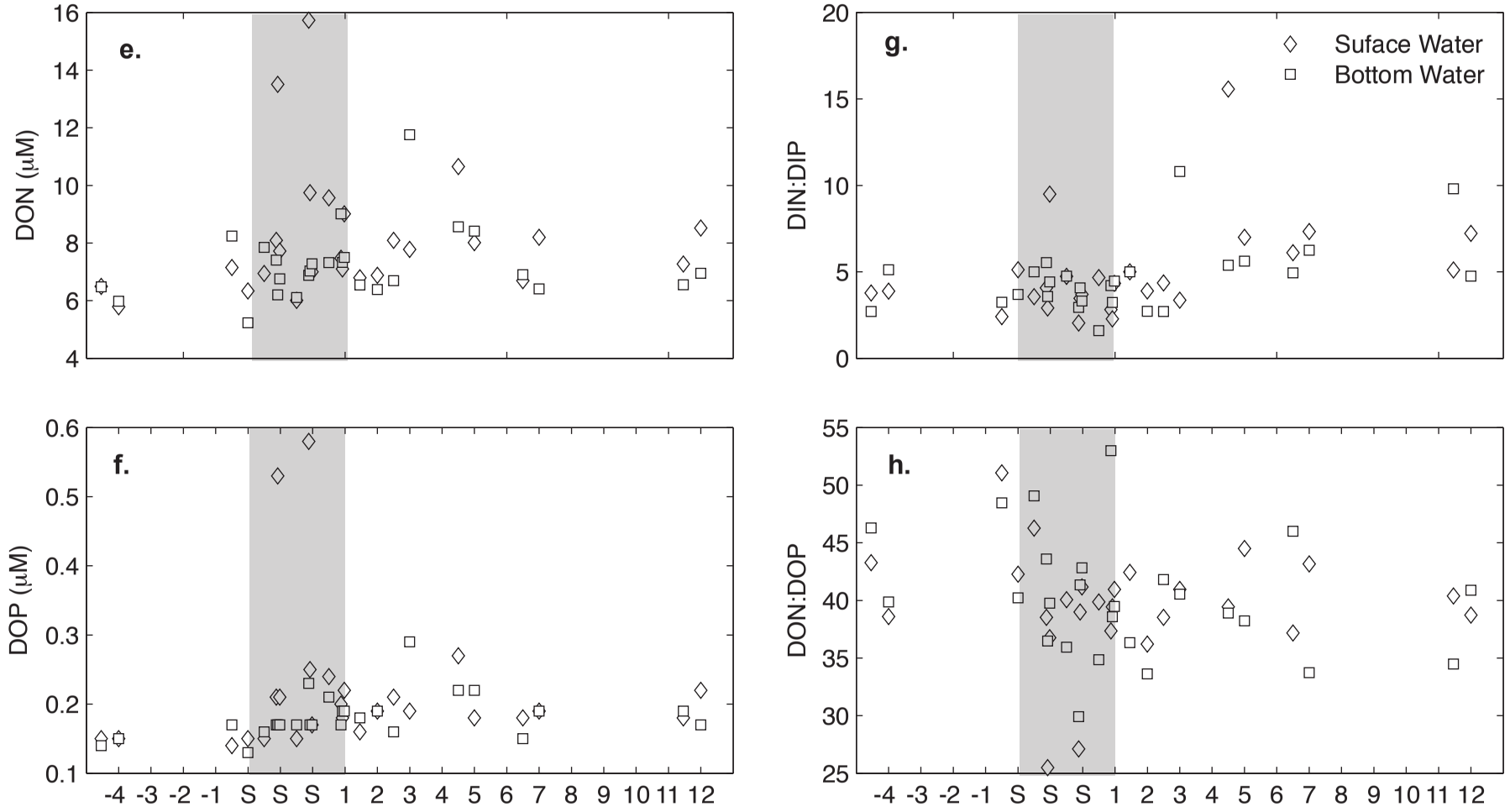
e.
DON (μM)
f.
DOP (μM)
g.
DIN:DIP
Suface Water
Bottom Water
h.
DON:DOP
-4 -3 -2 -1 S S S 1 2 3 4 5 6 7 8 9 10 11 12

in DIN:DIP ratios observed in the water column post-spawn (Fig. 5.9g) are driven both by the increase in water column NO_x (Fig. 5.9d) and the decrease in water column PO_4^{3-} (Fig. 5.9b). Concentrations of DON and DOP in surface waters were elevated above background levels on the first 2 days of the spawning event (Fig. 5.9e-f), and there appears to be an increase in DON and DOP in bottom waters during the first few days post-spawn. These elevated levels could be due either to excretion by the phytoplankton that comprise the bloom, or by sloppy feeding or excretion by zooplankton feeding on the blooming phytoplankton. DON:DOP in surface waters is depressed, relative to background ratios, during the first 2 days of the bloom (Fig. 5.9h), but are otherwise invariant throughout the time frame of the study.

Despite the large benthic efflux of porewater NH_4^+ (Fig. 5.7), dissolved water column inventories of NH_4^+ decreased following the spawning event (Fig. 5.9a). The water column inventory of NH_4^+ can be depleted by a number of factors, including (i) physical flushing of nutrients out of lagoon, (ii) biological uptake, and/or (iii) nitrification in the water column. The low and variable flow rates observed in Gilligan's Lagoon during the study period (Fig. 5.3) imply that minimal physical flushing of nutrients out of Gilligan's Lagoon occurred during the study. The low flushing rates also set up conditions that allowed for build-up of a phytoplankton bloom without disruption,
prolonging growth and biological uptake of nutrients supplied by enhanced sediment efflux. Other studies have observed primary productivity in oligotrophic reef waters in response to episodic inputs of nutrients that endure for days (Furnas et al. 2005; Ringuet and Mackenzie 2005; Wild et al. 2007).

Gilligan's Lagoon is characterized by DIN:DIP ratios well below the canonical Redfield ratio (106:16:1, C:N:P), with a increase in DIN:DIP ratios (primarily driven by increased NO_x concentrations) observed after spawning (Fig. 5.9g). Recognizing that the Redfield ratio is not a universal optimum for phytoplankton growth (Arrigo 2005), it does provide a metric for examining nutrient limitation in an ecosystem (e.g., Healey and Hendzel 1980; Hecky et. al. 1988). Oligotrophic waters surrounding coral reef ecosystems are characterized by low, often limiting nutrient concentrations (e.g., Furnas et al. 2005). Kane'ohe Bay has been described as an N-limited environment during non-storm conditions (Laws and Allen 1996; Ringuet and Mackenzie 2005), and the DIN:DIP ratios observed in

this study are consistent with the notion of an N-limited system. The post-spawn increase in DIN:DIP suggests, however, that the post-spawn bloom draws down DIP at more rapid rates than DIN, potentially shifting the system towards a more P-stressed environment. This aligns well with reports by Ringuet and Mackenzie (2005) and Young (2011) who noted shifts towards P limitation following episodic inputs of storm derived nutrients and organic matter to Kane‘ohe Bay.

Substantial differences exist in the post-spawn behavior of water column nutrients in the GBR (Eyre et al. 2008), as contrasted with our study site in Kane‘ohe Bay. In the GBR, DIN was almost completely removed from the water column, while DIP inventories were only minimally drawn down. Dissolved organic forms of N and P were important to benthic and pelagic production in GBR coral reef systems, whereas in this study the changes in the DON and DOP pool were insignificant, and therefore are considered to provide only minor sources of nutrients for the observed biomass increase (Fig. 5.9e-f). These observed differences in water column inorganic and organic nutrient inventories following a spawning event highlight the regional variations in nutrient recycling patterns that can occur in different systems. Pelagic and benthic biogeochemical responses associated with SDOM will vary between regions depending upon a number of factors, including: (1) the magnitude of the spawning event and, in particular, how many species and/or individuals participate in the event (Wild et al. 2008; Wild et al. 2004b), (2) the residence time of SDOM in the water column, which will be influenced by weather, currents, successful fertilization of eggs, and predation intensity (Oliver and Willis 1987; Pratchett et al. 2001; Simpson et al. 1993; Westneat and Resing 1988), and (3) SDOM recycling and removal processes that may be particular to each environment (Eyre et al. 2008; Simpson et al. 1993; Wild et al. 2008).

Apprill and Rappé (2011), who also studied spawning events at Gilligan’s Lagoon in 2007 (one year prior to our study), argued that no biogeochemical response was imparted to the ecosystem by the spawning event. Because no flow data was available for their study however, they could only speculate that tidal flushing was responsible for the lack of biological response. In contrast to the conditions they speculated were present during their study, we observed extremely low and variable flow rates at this site (< 5 cm/sec; Fig. 5.3), which implies low tidal flushing in the lagoon. If similar low flushing rates characterized the time-frame of the Apprill and Rappé (2011) study, their failure to detect a SDOM-triggered

bloom cannot be attributed to physical factors such as flushing rates. We suggest that it is possible that their sampling scheme was such that they may have missed a water column bloom event post-spawn. We have shown here, as have others (Eyre, Wild, etc.), that SDOM-triggered blooms are ephemeral. We have further illustrated the importance of establishing conditions immediately prior to spawning, so that perturbations to biogeochemistry of the ecosystem that follow a coral-spawning event can be resolved relative to background, pre-spawn conditions. Apprill and Rappé (2011) averaged background conditions over an extended time period, which may have included variability unrelated to spawning events (i.e. rain events, spawning by other organisms, coastal wind mixing, etc.). The expanded range of 'background' values enumerated by Apprill and Rappé (2011) may have obscured the influence of spawning events on ecosystem response in their study. Our study emphasizes how critical it is to constrain the conditions immediately prior to spawning in order to discern ephemeral responses to coral spawning events, such as the phytoplankton bloom we describe here.

In summary, we observe: (1) rapid transfer of SDOM into higher trophic levels as indicated by a shift in water column $\delta^{15}N$ (Fig. 5.6b), which increases the deposition of particulate organic matter to the sediment surface, (2) enhanced sediment efflux of NH_4^+ after spawning that provided sufficient nutrients to fuel the phytoplankton bloom event (Fig. 5.7), (3) drawdown of dissolved water column nutrient inventories after spawning that coincide with enhanced phytoplankton biomass (Figs. 5.8 and 5.9), and (4) diatom dominance within the bloom, which was verified by both pigment concentrations and $Si(OH)_4$ removal (Fig. 5.8 and 9). These observations, when taken together, are consistent with a SDOM-triggered phytoplankton bloom. Finally, we note that the timing and magnitude of the SDOM-triggered bloom event in Kane'ohe Bay is consistent with previous research that has documented phytoplankton blooms triggered by episodic nutrient loading to the coastal ocean by storm-driven river input (Ringuet and Mackenzie 2005; Young 2011), and by coral spawning events in other systems (Furnas et al. 2005; Glud et al. 2008).

Contribution of SDOM to regional carbon and nitrogen loading: The average OC:TN ratio of egg material (21.4 ± 0.6) was used to determine the yearly carbon and nitrogen loading to Kane'ohe Bay from *M. capitata* spawning in 2007 and 2008 (Table 5.2). Calculations were based upon the number of eggs caught within a known surface area of

coral (Padilla-Gamino and Gates, 2011 *submitted*), and extrapolating that value to the surface area of *M. capitata* coverage in Kane‘ohe Bay. Carbon and nitrogen loading from *M. capitata* spawning as the sole C and N source was strikingly low in both 2007 and 2008 compared to values calculated for spawning events in Heron Island, GBR. If we assume that all coral species in Hawai‘i produce levels of spawn material equivalent to *M. capitata* in 2007, we calculate that the carbon and nitrogen to Kane‘ohe Bay loading is an order of magnitude higher than the loads from *M. capitata*, alone. However, these values are still well below the nutrient loading calculated to occur at Heron Island, GBR. We can reconcile this apparent discrepancy by considering that the quantity of material released to each environment may be less important than the physical processes that dictate the residence time of this material within the ecosystem. The flushing rates in Kane‘ohe Bay were sufficiently low to retain the SDOM within the immediate system, and drive the biogeochemical cycling of SDOM and the ecosystem response.

Table 2: Input of carbon and nitrogen to the water column from coral eggs released during spawning events. Values are reported in metric tons of carbon and nitrogen per a year.

Site	Carbon	Nitrogen	Source
Kane’ohe Bay 2007 (*M. capitata* only)	0.02	.001	This study
Kane’ohe Bay 2008 (*M. capitata* only)	0.006	.0003	This study
Kane’ohe Bay (All hard corals*)	0.2	0.01	This study
Heron Island, GBR (All hard corals)	310	18	Wild et al, 2004

*This calculation utilizes the volume of eggs produced during 2007 and extrapolates to total coral coverage in Kane’ohe Bay.

To conclude, we present evidence for a water column phytoplankton bloom event triggered by the input and recycling of labile organic matter injected into the water column by the spawning of *M. capitata* at Gilligan’s Lagoon in Kane‘ohe Bay, Hawaii. Specifically, the coincidence of a spike in water column Chl *a* and fucoxanthin, with clear depletions of water column dissolved $Si(OH)_4$, NH_4^+ and PO_4^{3-} occurring in the days immediately following the spawning event, accompanied by the increase in benthic NH_4^+ flux post-spawn, create a coherent picture of sediment SDOM recycling and subsequent response by the water column phytoplankton community. The observed post-spawn biogeochemical perturbations to the ecosystem are similar to those observed in the GBR (Eyre et al. 2008; Glud et al. 2008; Wild et al. 2008), despite the fact that considerably less SDOM was supplied during the Kane‘ohe Bay spawning event relative to those reported for the GBR. This discrepancy can

be reconciled by considering the fact that low flushing rates in Gilligan's Lagoon create conditions for SDOM retention in the system for extended periods, resulting in a protracted time frame for recycled nutrient supply from microbially respired SDOM. Thus, physical processes play a critical role in determining the extent of nutrient loading from SDOM to the system, as well as the size and duration of the subsequent SDOM-triggered phytoplankton bloom.

Acknowledgements

Jeff Sevadjian supplied support with ADCP data acquisition and presentation, which we gratefully acknowledge. We thank Craig Glenn for access to his coulometer. We are grateful to Danielle Hull, Christine Pequignet, Pablo Quiroga and the numerous volunteers that assisted with instrument placement, field preparations, sample collection and laboratory analyses. Thanks to the Point Lab at HIMB and K. Rodgers for her assistance obtaining the records from the meteorological station. This research was supported by a grant/cooperative agreement from the National Oceanic and Atmospheric Administration; project R/EL-42, which is sponsored by the University of Hawai‘i Sea Grant College Program, SOEST, under Institutional Grant NA05OAR4171048 from NOAA Office of Sea Grant, Department of Commerce. JLPG was supported by a CONACYT Graduate Research Fellowship, the World Bank CRTR program and C-MORE. The views expressed herein are those of the authors and do not necessarily reflect the views of NOAA or any of its sub-agencies. UNIHI-SEAGRANT-xxxx. This is SOEST contribution #xxxx and HIMB contribution number XXXX.

Chapter 6

Diel variations in sediment redox conditions: Impacts on sediment nutrient cycling in a nearshore coastal environment

with K.C. Ruttenberg, and B.T. Glazer

Abstract

Diurnal experiments conducted in two distinct depositional environments, a fine-grained site proximal to shore and magnroves, and a sandy site distal from shore, illustrate that shoaling of sediment redox boundaries occurs in tandem with transitions from daytime benthic photosynthesis to nighttime respiration. Sediment cores collected at four time-points (11:00, 16:00, 00:00, and 07:00) were analyzed for dissolved inorganic and organic nutrients, as well as redox speciation using high-resolution voltammetric microelectrode profiles. Diurnal experiments display vertical oscillations in the depth of redox transition boundaries that are correlated to diurnal shifts between benthic photosynthesis and respiration, wherein (i) During daylight hours O_2 penetration is, and the accumulation of Fe^{2+} as well as the appearance of H_2S occurs deeper in the sediment, and (ii) nighttime cores display a shoaling of the O_2 penetration depth, Fe^{2+} accumulation is greater, and both Fe^{+} and H_2S appearance occurs at shallower depths.

The net production rates of NH_4^+ were calculated for all sediment cores. We observed higher rates of organic matter remineralization at the sandy site, dominated by more labile, marine-dominated OM, and slower remineralization rates characterized the muddy site, dominated by terrestrial, and therefore more refractory OM. The NH_4^+ build-up in porewaters reflects release of metabolites as a consequence of OM remineralization in these sediments; however, we did not observe PO_4^{3-} accumulating in porewaters indicating that one or more PO_4^{3-} removal processes was operating in these sediments. The particular PO_4^{3-} removal process appears to be dictated by site mineralogy, with the more distal site showing evidence of authigenic carbonate fluorapatite formation, while the more terrigenous-dominated site shows evidence of PO_4^{3-} sorption onto Fe-(oxy)hydroxide phases. The fact that we observe build up of dissolved organic phosphorus (DOP) in sediment porewaters, implies that DOP is not as vulnerable to uptake reactions as is phosphate. These field observations suggest differential sorption immobilization of DOP relative to phosphate, consistent with recent laboratory studies that demonstrated this same phenomenon, and suggest that benthic efflux of phosphorus from sediments at this site may be dominated by DOP and not phosphate.

6.1 Introduction

During burial and subsequent breakdown of organic matter, microbial aerobic and anaerobic respiration processes releases dissolved organic matter and inorganic nutrients (i.e. NH_4^+ and PO_4^{3-}) to sediment porewater (Klump and Martens 1987; Ruttenberg 2003 and references cited within). A portion of the dissolved metabolites generated from OM degradation may be recycled into the overlying water, which can alter water column nutrient ratios and shift phytoplankton community composition, potentially providing selective pressure for certain groups of primary producers. This, in turn, can propagate into shifts in the overall community structure. The residual degraded OM is incorporated into sediments, where it can undergo further degradation during burial.

Organic matter (OM) deposited in sediments is subjected to chemical alteration through a complex series of microbial respiratory pathways (e.g., Froelich et al 1979; Burdige 2006). Microbially mediated OM degradation proceeds by successive use of oxidants, beginning with those that yield the greatest quantity of free energy per mole of organic carbon respired,

Figure 6.1 Redox ladder schematic illustrating the progression of organic matter oxidants used during microbial respiration of organic matter in marine sediments.

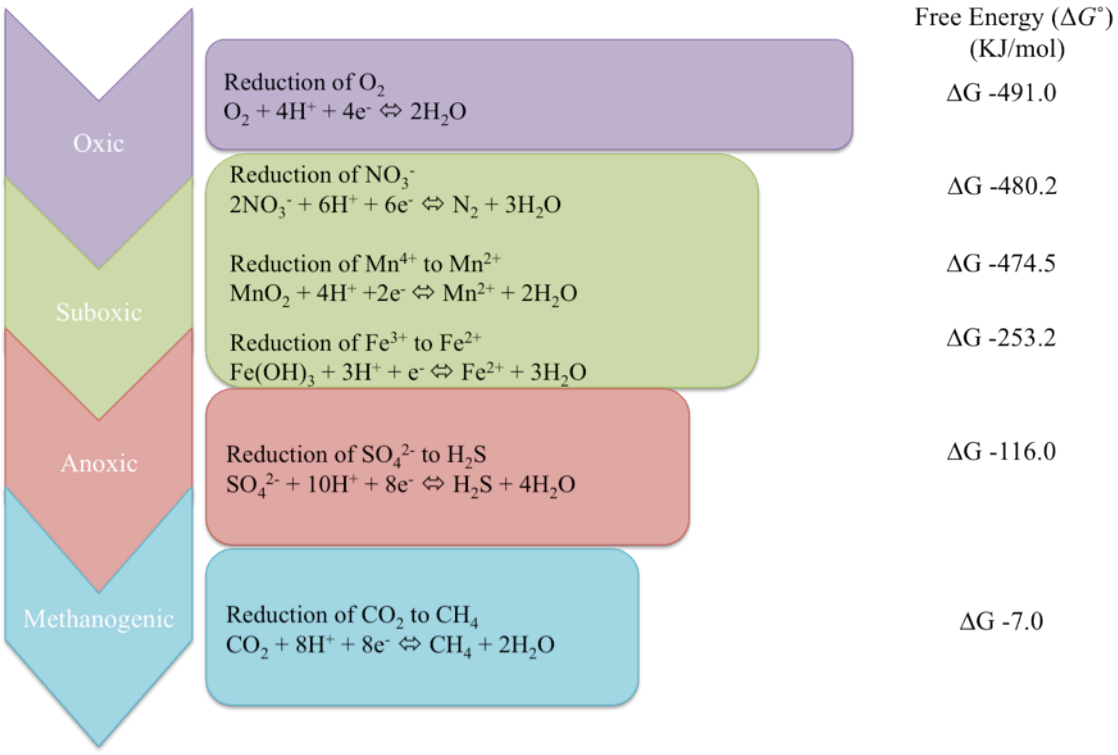

to progressively less energy efficient metabolic pathways, generally following the oxidant sequence: O_2, NO_3^-, oxides of Mn and Fe, and SO_4^{2-}. (Figure 6.1) (e.g., Froelich et al. 1979; Canfield et al. 1993; Burdige 2006). The dominant electron acceptor used during OM mineralization at a given depth dictates the spatial distribution of reduction-oxidation (redox) reactive chemical species. Oxygen, the most energetically favorable electron acceptor, will be preferentially consumed, followed by nitrate, manganese oxides, iron oxides, and sulfate (Figure 6.1). This thermodynamically-driven distribution of redox reactive chemical species, known as the redox ladder (Scott and Morgan 1990), creates distinct zones within sediments (Figure 6.1).

The depth of oxygen penetration in coastal sediments changes seasonally due to shifts in biological activity in the overlying water (Colman and Holland 2000; Jørgensen and Richardson 1996). During seasonal bloom periods, deposition of organic matter in sediments and its subsequent mineralization results in consumption of oxygen and a consequent shoaling of the depth of oxygen penetration in marine sediments (Jørgensen 1996). Transitions in sediment redox state can also occur on shorter, diurnal time scales, as a consequence of diel fluctuations in the activity of seabed organisms. In this paper we will examine shoaling of 2 transition zones on diurnal time scales (Figure 6.1): (i) the oxic redox transition boundary, which is defined as the boundary between oxic and suboxic zones; the disappearance of oxygen serves as a proxy for the depth of this boundary, and (ii) the anoxic redox transition boundary, which is defined as the depth at which sulfate reduction occurs; the presence of H_2S or aqueous FeS serves as a proxy for the depth of the anoxic redox transition boundary (Colman and Holland 2000).

6.2 Objectives and Rationale

For the purposes of this paper, redox zonations will be referred to using the classical terms, oxic (zone with detectable O_2), suboxic (zone with no detectable O_2 or H_2S), and anoxic (zone with detectable H_2S). While we recognize that broadly applying this classification scheme is somewhat simplistic due to the overlap of metabolic processes within each designated zone (Aller 1994; Canfield and Thamdrup 2009), because this study examines shoaling of transitions zones, and does not attempt to quantify rates of specific

metabolic pathways, our adherence to this classical classification of redox zonations should cause no confusion.

Transitions from daytime benthic photosynthesis to nighttime respiration are accompanied by a shoaling of the sediment oxic redox transition boundary (Briggs et al. 2007; Revsbech et al. 1983). Profiles of redox sensitive porewater constituents from sediment cores collected over a series of 24-hour studies in a coastal system within Kane‘ohe Bay, Hawai‘i, reveal that O_2 penetration depth into the sediment increases during daytime photosynthesis, but as nighttime respiration takes over, oxygen becomes depleted at the sediment water interface (Figure 6.2a) (Briggs et al. 2007). The depth of O_2 penetration influences the concentration and depth of ferrous iron (Fe^{2+}) accumulation in sediment porewaters as well as the depth at which hydrogen sulfide is detected (Figure 6.2b; noted by a star). When O_2 penetration is greatest (16:00 sediment core), Fe^{2+} and H_2S are undetectable in the sediment core; however, as nighttime respiration commences, O_2 is depleted in surface sediments, porewater Fe^{2+} accumulates, and the anoxic redox transition boundary shoals upwards. These findings illustrate that shoaling of the oxic redox transition boundary results in alterations of down core distributions of redox reactive chemical species, such as ferrous iron, and influences the depth of the anoxic redox transition boundary.

Figure 6.2 Profiles of redox sensitive porewater constituents (O_2, Fe^{2+}, and first appearance of H_2S noted by star) from sediment cores collected over a 24-hour study in a coastal system within Kane‘ohe bay Hawai‘i (adapted from Briggs et al. 2007).

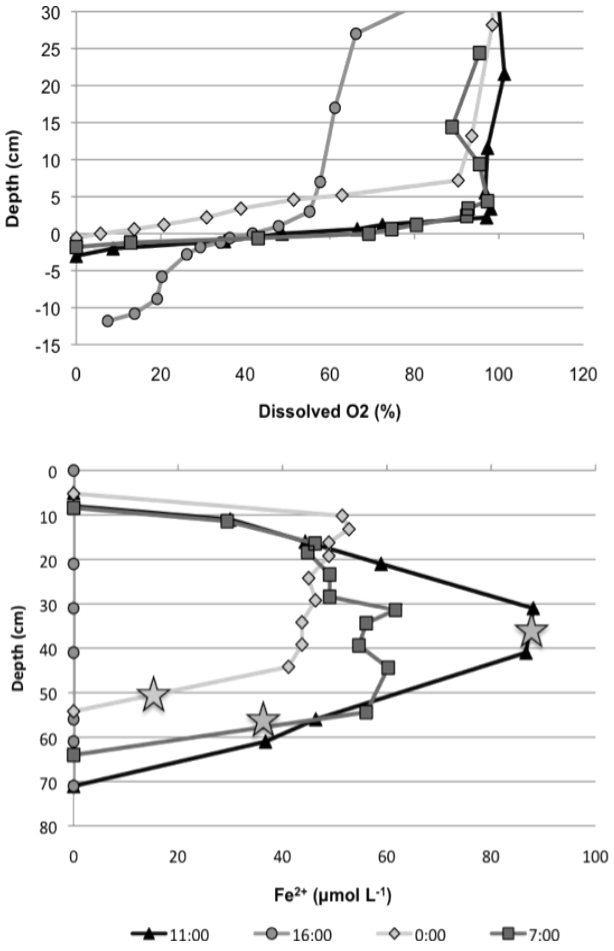

The depth and time scale over which oxygen, iron, and sulfur interact in the sediments is on the order of

several centimeters over several hours (Figure 6.2). Recent findings by Nielsen et al. (2010) suggest that flow of electron currents through sediments can couple redox reactions in the anoxic layer to those in the oxic layer, on time scales of hours, even when these layers are physically separated. Nielsen et al. (2010) also observed that changes in oxygen concentrations in the overlying seawater result in rapid changes (within 1 hour) in the depth of the suboxic zone and the anoxic transition boundary. To explain these observations, the novel hypothesis has been advanced that the rapid interaction of spatially separated chemical species occurs via bacterial networking and interactions which transmit electrons in a conductive network (Nealson 2010; Nielsen et al. 2010).

The shoaling of redox transition boundaries on diurnal time scales, during transitions from photosynthesis to respiration, may also be accompanied by shifts in the magnitude and direction of benthic fluxes of dissolved porewater constituents. During daytime hours, when oxygen concentrations penetrate below the sediment-water interface, upward diffusion of redox-active species such as Mn^{2+}, Fe^{2+}, NH_4^+, or HS^- can be oxidized effectively hindering the porewater efflux of these species. Additionally, because PO_4^{3-} has a high affinity for sorption onto Fe (oxy)hydroxide surfaces, within this oxic zone regenerated PO_4^{3-} will be rapidly adsorbed onto freshly precipitated Fe (oxy)hydroxide (Figure 6.3) (Colman and Holland 2000; Ingall and Jahnke 1997; Jahnke et al. 2000; Mcmanus et al. 1997; Slomp et al. 1996). As nighttime respiration commences, and the oxygenated sediment layer is removed, near-surface suboxic or anoxic conditions develop impeding the mobility and benthic efflux of potentially bioavailable species, such as PO_4^{3-} and NH_4^+, which exists when sediments are oxic. These diurnal shifts in redox state, location of redox horizons, and subsequent effects on benthic nutrient fluxes (Figure 6.3) are similar to those observed to accompany seasonal shifts in sediment redox state (Colman and Holland 2000; Gunnars and Blomqvist 1997; Moosmann et al. 2006; Taillefert et al. 2002b).

Figure 6.3 Schematic of diurnal oscillations in sediment redox conditions, driven by daytime benthic photosynthesis and nighttime benthic respiration, and effects on phosphorus and iron. (adapted from Rozan et al. 2002).

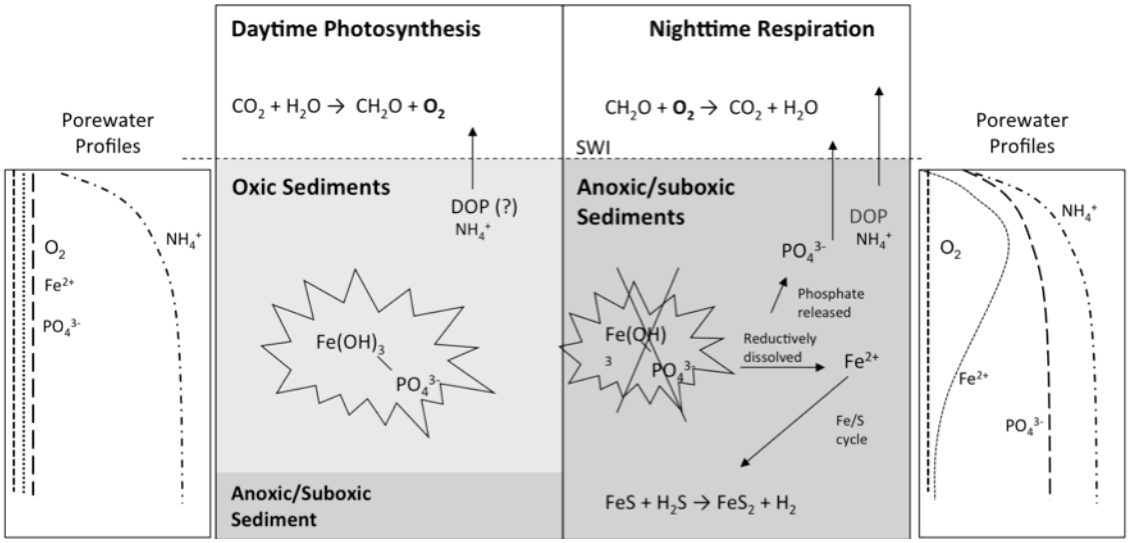

The three main objectives of this study are:

Objective 1: Examine how the shoaling of the oxic redox transition boundary alters down core distributions of redox reactive chemical species (such as ferrous iron), and influences the depth of the anoxic redox transition boundary (Figure 6.3), in sediments collected from two distinct depositional environments.

Objective 2: Determine how the expansion and contraction of the oxygenated surficial sediment layer, as a consequence of diurnal shifts between benthic photosynthesis and respiration, can influence the distribution and porewater accumulation of dissolved inorganic nutrients (Figure 6.3).

Objective 3: Determine whether, and to what extent, dissolved organic phosphorus (DOP) in sediment porewaters, generated by microbial remineralization of sedimentary OM, may also be affected by sorptive removal onto Fe (oxy)hydroxides under oxic conditions in surface sediments (Figure 6.3).

6.3 Background

Cycling of dissolved ammonium in coastal sediments: Dissolved ammonium (NH_4^+) is the by-product of microbial OM remineralization in marine sediments. As such, NH_4^+ accumulation in porewaters can serve as a proxy for the rate and quantity of OM undergoing

remineralization via multiple metabolic pathways in marine sediments. However, in order to utilize NH_4^+as a proxy for OM remineralization, removal processes, which will affect the distribution and concentration of NH_4^+ in porewaters, must be quantified.

In the presence of oxygen the removal of dissolved NH_4^+ from porewaters can be achieved by oxic nitrification of ammonium to nitrite (Grundmanis and Murray 1977):

$$NH_4^+ + 2\ O_2 \rightarrow NO_3^- + H_2O + 2\ H^+ \quad (6.1)$$

In the anoxic layers of marine sediments, in the absence of nitrification, large pools of dissolved ammonium can build up in porewaters. Other anaerobic oxidation reactions, however, may also effectively oxidize and remove NH_4^+ from porewaters. For example, metal oxides present below the anoxic redox transition boundary, such as MnO_2, may oxidize ammonium to nitrite (Bartlett et al. 2008; Hulth et al. 1999; Luther et al. 1997; Mortimer et al. 2004):

$$4\ MnO_2 + NH_4^+ + 6\ H^+ \rightarrow 4\ Mn^{2+} + NO_3^- + 5\ H_2O \quad (6.2)$$

Recent findings have also indicated that anaerobic ammonium oxidation by nitrite (anammox) may be an important pathway for NH_4^+ removal in coastal marine sediments as well (Risgaard-Petersen et al. 2004; Thamdrup and Dalsgaard 2002; Trimmer et al. 2003):

$$5\ NH_4^+ + 3\ NO_2^- \rightarrow 4\ N_2 + 9\ H_2O + 2\ H^+ \quad (6.3)$$

In addition to the aforementioned reaction pathways that can oxidize dissolved NH_4^+, and depress the accumulation of NH_4^+ in porewater, physical ionic interactions with sediments may also influence porewater NH_4^+ concentrations. Sorption onto clays and organic material in marine sediments can be an important removal pathway for dissolved NH_4^+ in some depositional environments (Boatman and Murray 1982; Mackin and Aller 1984).

Coupled iron and phosphorus cycling in coastal sediments: Phosphorus (P) and iron (Fe) are highly insoluble under oxic conditions, and tend to cycle together in aquatic systems. Microbial respiration of OM releases phosphate to porewater during burial and subsequent breakdown of organic matter (Klump and Martens 1987; Ruttenberg 2003 and references therein). Once released to porewaters, phosphate (PO_4^{3-}) can then be removed from porewaters by authigenic mineral precipitation (Ruttenberg 2003; Slomp et al. 1996), and/or sorption onto labile ferric (oxy)hydroxides (Anshutz et al. 1998; Jensen et al. 1995; Krom and Berner 1980; Rozan et al. 2002; Ruttenberg 2003; Slomp et al. 1996). Phosphate not

retained by sorption or authigenic mineral formation can diffuse upward into overlying water (Colman and Holland 2000; Klump and Martens 1987; Rozan et al. 2002) where it is available to support primary production.

Ferric (oxy)hydroxides in soils and oxic sediments typically have associated with them significant quantities of sorbed phosphate (Anshutz et al. 1998; Slomp et al. 1996). Once buried below the redox boundary, Fe-(oxy)hydroxides are subject to reductive dissolution (Figures 6.1 and 6.3), resulting in a release of dissolved, ferrous iron (Fe^{2+}) and associated phosphate (Fe-bound P) to porewaters (Anshutz et al. 1998; Colman and Holland 2000; Fox 1993; Mcmanus et al. 1997; Rozan et al. 2002; Ruttenberg 2003; Slomp et al. 1996; Slomp et al. 1998; Sundby et al. 1992). Reductively dissolved Fe^{2+} may diffuse into the oxic region and reprecipitate as Fe-(oxy)hydroxides or, in the anoxic region Fe^{2+} can react with reduced sulfur species to form pyrite (Figure 6.3). Progressive accumulation of PO_4^{3-} in porewaters as decomposition of OM continues during burial, setting up a concentration gradient that promotes upward diffusion of PO_4^{3-}, where it can be lost into the overlying waters. Alternatively PO_4^{3-} can readsorb onto freshly precipitated Fe (oxy)hydroxide surfaces in the suboxic and oxic region of sediments (Colman and Holland 2000; Ingall and Jahnke 1997; Jahnke et al. 2000; Mcmanus et al. 1997), diminishing or eliminating the benthic flux of PO_4^{3-} into overlying waters. Authigenic carbonate-fluorapatite, the primary sink for phosphate in marine sediments (Ruttenberg 2003), may ultimately form at depth, permanently removing P from porewater and sequestering it in the solid phase for long-term burial.

Dissolved organic phosphorus in sediment porewaters: Terrestrial soil studies have shown that dissolved organic phosphorus (DOP), like PO_4^{3-}, will adsorb onto Fe (oxy)hydroxides (Gjettermann et al. 2007; Lilienfein et al. 2004) and this process has recently been documented in marine systems (Ruttenberg and Sulak 2011). However, kinetic studies of $PO_4^{3-}$and DOP sorption onto Fe (oxy)hydroxides in seawater indicate that DOP compounds are far less efficiently sorbed than is PO_4^{3-}(Ruttenberg and Sulak 2011). The reduced affinity of DOP for Fe (oxy)hydroxides, relative to PO_4^{3-}, is likely due to steric effects, which inhibit the sorption of larger, more complex DOP compounds. Extrapolating the experimental results of Ruttenberg and Sulak (2011) to *in situ* marine sediments, it is expected that Fe-rich seabed sediments will immobilize phosphate more efficiently than DOP

through sorption reactions. The greater mobility of DOP in oxic sediments may allow for a DOP benthic flux at the same time that PO_4^{3-} is completely immobilized in sediments (Figure 6.3), such that DOP may play an enhanced role in supporting primary production in overlying waters.

Coupled iron and sulfur cycling in coastal sediments: Iron-sulfide mineral formation occurs via a series of complex reactions that have been of interest to the scientific community for decades (reviewed in Rickard and Morse 2005). Sedimentary reactions affecting iron-sulfide mineral formation include complex redox mechanisms involving organic and metal complexes. For the purpose of this study, a narrower focus on the Fe-S cycle was adopted: only pyrite formation as an indication of removal of dissolved iron from porewater is considered.

The co-occurrence of H_2S and Fe^{2+} in porewaters favors the formation of pyrite, which can be summarized by reactions involving sulfur and dissolved iron species (Carey and Taillefert 2005; Luther 2005; Meysman and Middelburg 2005; Rickard and Morse 2005; Taillefert et al. 2002a). The first step in pyrite formation involves reactions to form FeS:

$$Fe^{2+} + H_2S \rightarrow 2H^+ + FeS_{aq} \quad (6.4)$$

$$FeS_{aq} \rightarrow FeS_s \quad (6.5)$$

Pyrite formation then occurs via one of the following competing mechanisms:

$$FeS + S_n^{2-} \rightarrow FeS_2 + S_{n-1}^{2-} \quad (6.6)$$

or

$$FeS + H_2S \rightarrow FeS_2 + H_2 \quad (6.7)$$

FeS and H_2S are highly reactive phases that easily oxidize. While the co-occurrence of Fe^{2+} and H_2S in porewaters suggests that aqueous FeS formation may be occurring, FeS may represent a transient Fe-sink within the sediment, which can either be oxidized or converted into pyrite. Stable pyrite, on the other hand, represents a terminal, long-term sink for dissolved Fe. The removal of dissolved Fe^{2+} from porewater at depth, in conjunction with H_2S accumulation, suggests that the rate of secondary re-oxidation does not exceed the rates of sulfate reduction and pyrite formation. Accumulation of H_2S in porewaters further indicates that potentially bioavailable Fe^{2+} is efficiently removed from porewaters by pyrite formation. Iron-sulfide minerals, such as pyrite, do not readily adsorb phosphate (Huerta-Diaz and Morse 1992; Rozan et al. 2002), so that in the zone of FeS and pyrite formations

PO_4^{3-} is able to accumulate in porewaters while dissolved Fe^{2+} is effectively removed at depth.

6.4 Study Site

He‘eia fishpond is an 88-acre historical fishpond situated on the shoreline of Kane‘ohe Bay on the windward coast of O’ahu (Figure 6.4). The exact age of the pond is not known, but earliest maps of the pond date back to the 1800s (Kelly 2000). He‘eia Fishpond has been cultivated by native Hawaiians for centuries for fish and seaweed. A decline in the health of this coastal ecosystem has been observed over the past 50 years (Kelly 2000), coincident with increased urbanization of the watershed, which has been accompanied by enhanced erosion and sediment deposition in the coastal zone. Indications of a decline in ecosystem health include a reduction in the population of indigenous marine organisms, and an increase in invasive species (PaePae O He‘eia, unpubl.). One of the principal motivations for this project was to determine how the recently deposited sediment layer might contribute to changes in the nutrient regime of the system, which in turn could be responsible for the deleterious ecosystem changes that have been observed.

As is traditional in Hawaiian Fishponds (Kikuchi 1976), a wall physically encloses

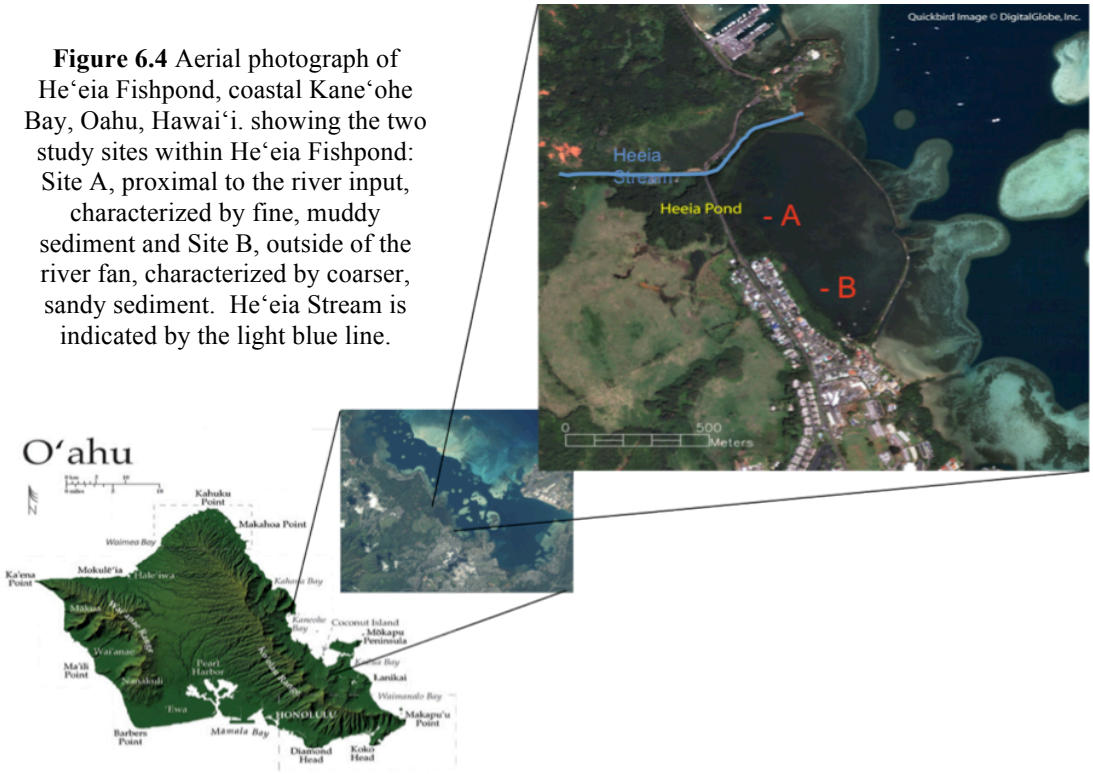

Figure 6.4 Aerial photograph of He‘eia Fishpond, coastal Kane‘ohe Bay, Oahu, Hawai‘i. showing the two study sites within He‘eia Fishpond: Site A, proximal to the river input, characterized by fine, muddy sediment and Site B, outside of the river fan, characterized by coarser, sandy sediment. He‘eia Stream is indicated by the light blue line.

He‘eia fishpond, with water movement into and out of the pond controlled by gates on both the river, and bay sides. The fishpond is characterized by shallow waters (< 2 m) and a thin sediment cover (4-35 cm). Surface sediments range from silty-mud, dominated by clay and Fe minerals near the sites of freshwater input, to coarse, coral-dominated sands, predominantly aragonite, at sites distal from river inputs. The juxtaposition of different sediment mineralogy within a semi-enclosed coastal system with similar overlying water conditions provides an ideal venue for studying the role of mineralogy in sediment biogeochemistry. He‘eia fishpond is thus an exceptionally well-suited natural laboratory to conduct cutting-edge research on the role of benthic photosynthesis on sediment nutrient cycling. The shallow environment allows light penetration to the benthic algal community throughout the day, and its semi-enclosed nature allows the fishpond to act as a large mesocosm embedded in a natural coastal environment, facilitating quantification of the overall impact of sediments, as nutrient sources or sinks, on this coastal system.

6.5 Methods

Sampling rationale and experimental setup: Diurnal experiments were conducted at two distinct depositional environments within He‘eia Fishpond, and are hereafter defined as: i) Site A: a location proximal to riverine input and characterized by fine grained, muddy sediments, and ii) Site B: a location distal from riverine input, closer to Kane‘ohe Bay, and characterized by sandy carbonate-rich sediments (Figure 6.4). In total, four diurnal experiments were conducted during the summer of 2007. Site B and A were sampled on August 12 and 14, respectively, during a neap tidal regime, and again on September 1 and 3, respectively, during a spring tidal regime. Sampling was conducted at four time-points during each diurnal experiment (11:00, 16:00, 00:00, and 07:00), chosen to capture maximum biogeochemical effects of benthic photosynthesis (16:00) and respiration (07:00) on sediment redox conditions and the corresponding transitional periods (00:00 and 11:00).

Sample collection: At each sampling point, paired cores were taken within defined sampling grids: one core (10.16 cm diameter and ~20-25 cm depth) was collected for sectioning and porewater extraction, and a second core (5.08 cm diameter an ~15-20 cm depth) was collected for microelectrode profiling of redox species and pH. Sampling grids were defined at each site by staking out a 6 x 6 foot area using PVC posts. We selected areas

at each site with visually uniform conditions that were devoid of macroalgae and appeared to be minimally affected by bioturbation. At each sampling time point, samples were collected from successive quadrants with the sampling grid to avoid coring in previously disturbed areas. Immediately after collection, cores were placed in a bucket of ice to reduce metabolic activity, and covered to inhibit photosynthetic activity during transport to shore for analysis.

Instrumentation: A multi-parameter YSI 6600V2 Sonde® was deployed within 1 m of the core sampling grid to monitor real-time water quality throughout the diurnal experiments. The YSI sonde recorded temperature, salinity, pH, pressure, and dissolved oxygen. The Hawai‘i Institute of Marine Biology Weather Station, located within Kane‘ohe Bay (in close proximity to the study location), provided information on weather conditions including precipitation, wind direction, wind speed, and solar irradiation.

Sediment and water sample analysis: After removal and collection of overlying water, sediment cores were sectioned at 0.25 to 1 cm intervals under an inert (N_2) atmosphere to prevent oxidation artifacts. A split of sectioned sediment was collected for porosity analysis, also under an inert atmostphere (Berner 1980). Porewater was separated from bulk sediment via centrifugation. In order to maximize porewater collection in sandy sediments, Whatman VectaSpin 20 ® centrifuge tubes were adapted to allow filtration during centrifugation by replacing the manufactured installed polypropylene filter with a coarse 25 mm GF/F filter (VWR ® 1.2 µm nominal poresize). The coarse GF/F filter allowed maximum recovery of sediment porewater, which was subsequently filtered using a 0.4 µm Pall Life Sciences GHP acrodisc® filters.

Filtered porewater was split into two subsamples: a frozen, untreated split (for NH_4^+ analysis) and a refrigerated-acidified split (for PO_4^{3-} and TDP analyses). Samples were analyzed for dissolved phosphate (PO_4^{3-}) and ammonium (NH_4^+) using well-established colorimetric protocols (Grasshoff et al. 1983) on a BioTek Synergy HT Multi-Mode Microplate Reader; all reported data have a 2% standard error associated with them. Dissolved organic phosphorus (DOP) was determined on porewaters using a modified high-temperature ashing/hydrolysis method and analyzed via the molybdenum blue method (Monaghan and Ruttenberg 1999). The microplate reader permits colorimetric detection on small sample volumes (300 µL), allowing for the analysis of multiple dissolved constituents on a single porewater interval, despite the small volumes of porewater collected from each

interval. The Nunc 96-well Optical Bottom Plates ® used have a 1-cm path length comparable to that of standard spectrophotometric 1-cm cuvettes but with a slightly lower detection limit than traditional spectrophotometers (0.2 μM). After removal of porewater, sectioned sediments were frozen under an inert atmosphere until freeze-dried under vacuum, to prevent oxidation artifacts, and reserved for future work (Krall et al. 2009).

Water samples from bottom and overlying water from each sediment core were filtered through pre-weighed 47 mm polycarbonate filters (Whatman ® 0.2 μm nominal poresize), which was acid-washed and rinsed prior to use. Filtrate was split into two subsamples: a frozen, untreated split and a refrigerated-acidified sample. Frozen, untreated splits were analyzed for colorimetrically dissolved inorganic nutrient concentrations (NH_4^+, ($NO_3^- + NO_2^-$), PO_4^{3-}, and H_4SiO_4) on a Seal Analytical AA3 Auto-analyzer at the USF/USGS Nutrient Biogeochemistry Laboratory in St. Petersburg, Florida. (JGOFS, 1994).

Profiling of sediment cores: Sediment profiling using pH probe voltammetric microelectrodes was conducted on the second of the paired cores, immediately after collection. Solid-state Au/Hg glass voltammetric microelectrodes are a unique tool for estimating sediment redox conditions, as they can simultaneously measure dissolved O_2, H_2S,

Table 6.1 Electrode reactions at the Au/Hg electrode vs. the Ag/AgCl reference electrode. All data were obtained with a 100 mm diameter electrode. O_2 and H_2O_2 data were collected using Linear Sweep Voltammetry; all others using Cyclic Voltammetry or Square Wave Voltammetry. (MDL – Minimum Detection Limit) (see Luther et al,. 2008 for review)

	E_p ($E_{1/2}$) (V)	**MDL (μM)**
$O_2 + 2H^+ + 2e^- \rightarrow H_2O_2$	-0.30	2
$HS^- + Hg \rightarrow HgS + H^+ + 2e^-$	adsorption onto Hg	<-0.62
$HgS + H^+ + 2e^- \leftrightarrow HS^- + Hg$	~ -0.62	< 0.1
$S^0 + Hg \rightarrow HgS$	adsorption onto Hg	< -0.60
$HgS + H^+ + 2e^- \leftrightarrow HS^- + Hg$	~ -0.62	< 0.1
$Hg + S_x^{2-} \leftrightarrow HgS_x + 2e^-$	adsorption onto Hg	< -0.60
$HgS_x + 2e^- \leftrightarrow Hg + S_x^{2-}$	~ -0.62	< 0.1
$S_x^{2-} + xH^+ + (2x-2)e^- \leftrightarrow xHS^-$	~ -0.62	< 0.1
$2\ RSH \leftrightarrow Hg(SR)_2 + 2H^+ + 2e^-$	typically more positive than H_2S/HS^-	
$2\ S_2O_3^{2-} + Hg \leftrightarrow Hg(S_2O_3)_2^{2-} + 2e^-$	-0.15	10
$S_4O_6^{2-} + 2e^- \rightarrow 2\ S_2O_3^{2-}$	-0.45	15
$FeS + 2e^- + H^+ \rightarrow Fe(Hg) + HS^-$	-1.1	molecular species
$Fe^{2+} + Hg + 2e^- \leftrightarrow Fe(Hg)$	-1.43	10
$Fe^{3+} + e^- \leftrightarrow Fe^{2+}$	-0.2 to -0.9	molecular species
$Mn^{2+} + Hg + 2e^- \leftrightarrow Mn(Hg)$	-1.55	5
$Zn^{2+} + Hg + 2e^- \leftrightarrow Zn(Hg)$	-1.02	< 0.1

Mn(II), Fe(II), $S_2O_3^{2-}$, $S_4O_6^{2-}$, S_x^{2-}, S(0) and aqueous species of Fe(III) and FeS (i.e., Luther et al. 2008 for review). Microelectrode technology enables quantification of gradients at the fine spatial resolutions critical for capturing steep near-interface gradients (Brendel and Luther 1995; Luther et al. 1998; Luther et al. 2008), and permits the measurement of dynamic, short time-scale oscillations in redox transition zones.

Custom fabricated Au/Hg working microelectrodes, constructed by sealing a 0.1 mm diameter gold wire into drawn glass tubing using a two-part epoxy (Brendel and Luther 1995), were attached to a mico-profiler to obtain high-resolution (mm-scale) profiles of multiple redox species within each sediment core. Counter (Pt) and reference (Ag/AgCl) electrodes, each of diameter 0.5 mm, were made in commercially available polyethyletherketone (PEEK^{TM}) tubing. Cyclic voltammetry was employed at scan rates of 500 mV s^{-1}. Each redox species, if present at detectable levels, produces a current peak that can be discriminated from others in one potential scan from –0.1 V to –2.0 V (Table 6.1). A conditioning step of –0.8 V was applied prior to each scan to remove any deposited Fe, Mn, or S-species (because none of these species are electroactive at this potential), followed by a second conditioning step at –0.05 V to restore the electrode surface between scans. Prior to use, electrodes were calibrated using a suite of laboratory standardization methods (Brendel and Luther 1995).

After voltammetry profiling was completed, a protected needle combination pH microelectrode from Microelectrode Inc® was used to profile the sediment core for pH. The pH probe was attached to the micro-manipulator, and at each depth interval the pH probe was allowed to stabilize prior to data collection.

6.6 Results

Study site background information: Water quality data from multi-parameter YSI 6600V2 Sonde® and weather data from the Hawai‘i Institute of Marine Biology Weather station were collected during each diurnal study. Two brief rain events occurred during the study; however, precipitation never exceeded 0.01 inches of rain and was thus considered negligible. Trade winds from the northeast persisted throughout the study and wind speeds were ~25-28 mph. Temperature, salinity, dissolved oxygen, pH, and depth (converted from YSI pressure data) from the in-situ YSI are presented in Figure 6.5. Salinity varies in concert

with tidal height in the diurnal experiments conducted during neap tides (Fig. 6.5a-b), while temperature, dissolved oxygen and pH trends correlate primarily with daytime to nighttime oscillations. These same patterns are apparent, but slightly muted, in diurnal experiments conducted during spring tidal conditions (Fig. 6.5c-d).

Porewater profiles: In this section we describe the down core trends observed in each sediment core, and compare the porewater profiles from sediment cores collected in each of the two distinct depositional environments (temporal variations during the diurnal experiment will be discussed in a later section). Site A, which is characterized by muddy, fine-grained sediments, had an average down-core porosity of 61 ± 6 %; sediment density at this Site was 2.28 g L^{-1}. Site B, which is characterized by sandy, coarse-grained sediments, had an average down-core porosity of 51 ± 3 %; sediment density at this Site was 2.48 g L^{-1}. Both Sites are characterized by saline porewaters (32.6 ± 2.0 at Site A; 32.5 ± 1.8 at Site B); down core salinity variations were minimal, indicating that fresh submarine groundwater input at these sites was unimportant.

Electrochemical profiles of sediment cores collected during spring and neap diurnals at each site display variability in the distribution and concentrations of redox reactive species (Figure 6.6). Specifically, we report data for O_2, Mn^{2+}, Fe^{2+}, and H_2S. Because data are unavailable from the 16:00 and 11:00 time points for spring Site B sediment cores, only the neap diurnal experiment from Site B will be discussed further. In all sediment cores, oxygen disappears either above the sediment water interface (SWI) or within the first cm of sediment. As a consequence, suboxic or anoxic pathways dominate all sediment cores. Manganese (Mn^{2+}) was not detected in Site A sediment cores at any time point, and in Site B cores manganese was detected only in four of the eight cores collected (Neap 11:00, Neap 16:00, Neap 00:00, and Spring 07:00). Mn^{2+} concentrations were < 80 μmol L^{-1}, and were always exceeded by iron (Fe^{2+}) concentrations. Fe reduction (Figure 6.1) is therefore considered the predominant metal oxide metabolic pathway in the suboxic zone at both Sites, and Mn^{2+} profiles will not be further discussed.

The reductive dissolution of iron oxides results in an accumulation of Fe^{2+} in sediment porewaters. In sediment cores from Site A, Fe^{2+} accumulation occurs over a broad, 5-10 cm region within each core (with the exception of Neap 07:00 core), with first

Figure 6.5 In situ water quality data from multi-parameter YSI 6600V2 Sonde® during diurnal experiments at Site A and Site B under Neap and Spring tidal conditions. Pressure (m) in green; pH in purple; dissolved oxygen (%DO) in orange; salinity (practical salinity units) in red; temperature (°C) in blue.

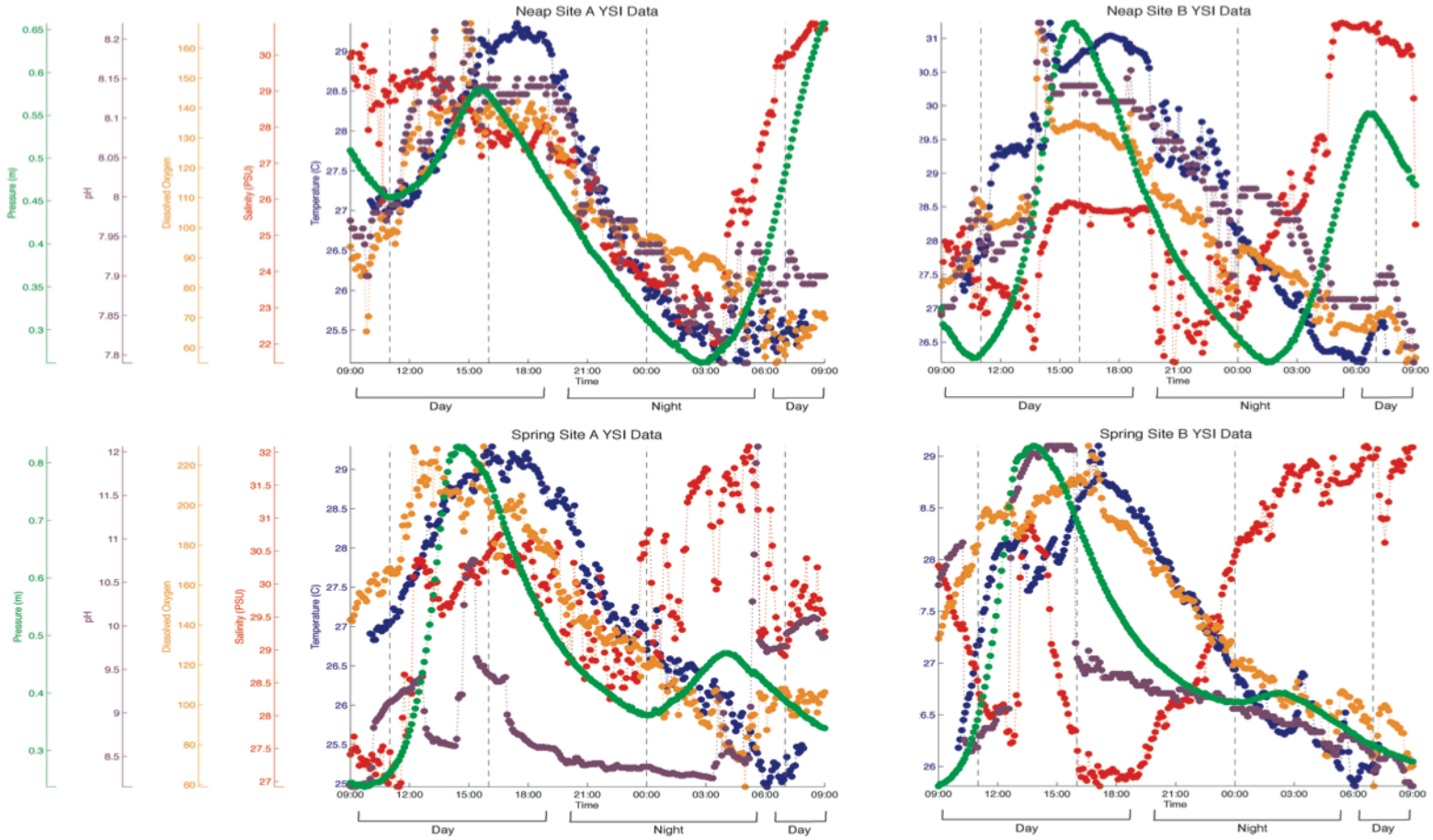

appearance occurring at approximately 1 to 5 cm below the SWI (Figure 6.6a). The disappearance of Fe^{2+} tends to occur at depths where H_2S begins to accumulate in all cores from Site A, with the exception of the Spring Site A 16:00 core, in which Fe^{2+} was still present at the deepest sediment layer analyzed and H_2S was never detected. In Site B sediment cores, Fe^{2+} accumulates in all cores analyzed, but the depth of detection and observed concentration range of Fe^{2+} was considerably more variable between cores at this site relative to Site A (Figure 6.6b).

Accumulation of H_2S occurred in all sites analyzed, with the exception of spring Site A at 16:00. On average, H_2S was usually detected at shallower depths (~2-5 cm) at Site B relative to Site A (~1-11cm), illustrating that the suboxic zone in Site B cores is significantly more expanded than in Site A cores and, in general, anoxic sediments characterize the Site B sediments.

Porewater NH_4^+ concentrations display typical diffusional profiles in all sediment cores (Figure 6.7), with lower concentrations in surface sediments building up to progressively higher concentrations at depth. On average, maximum concentrations in cores from Site B were higher (~78-167 μmol L^{-1}) than in the Site A cores (~43-100 μmol L^{-1}) (Figure 6.7). Nearly all cores display distinct NH_4^+ concentration reversals at depth. In contrast to the typical diffusional profiles observed for NH_4^+, porewater PO_4^{3-} concentrations did not display regularly increasing concentrations with depth (Figure 6.7). Porewater PO_4^{3-} concentrations were <1.5 μmol L^{-1} at both sites, and porewater
DOP concentrations exceeded PO_4^{3-} in most porewater intervals analyzed (Figure 6.7). Site B DOP data are unavailable for Spring 16:00 and 00:00.

6.7 Discussion

Biological influence on water column parameters: In order to understand fluctuations in oxygen penetration depth in surface sediments throughout the diurnal experiments, it was necessary to first examine the processes that control dissolved oxygen concentrations in the near-bottom (i.e. overlying) water. At first glance, dissolved oxygen and temperature values appear to vary systematically with transitions from daytime to nighttime conditions (Figure 6.5). During the day, both O_2 and temperature in bottom waters are substantially elevated relative to nighttime O_2 levels. This pattern is consistent with benthic photosynthetic

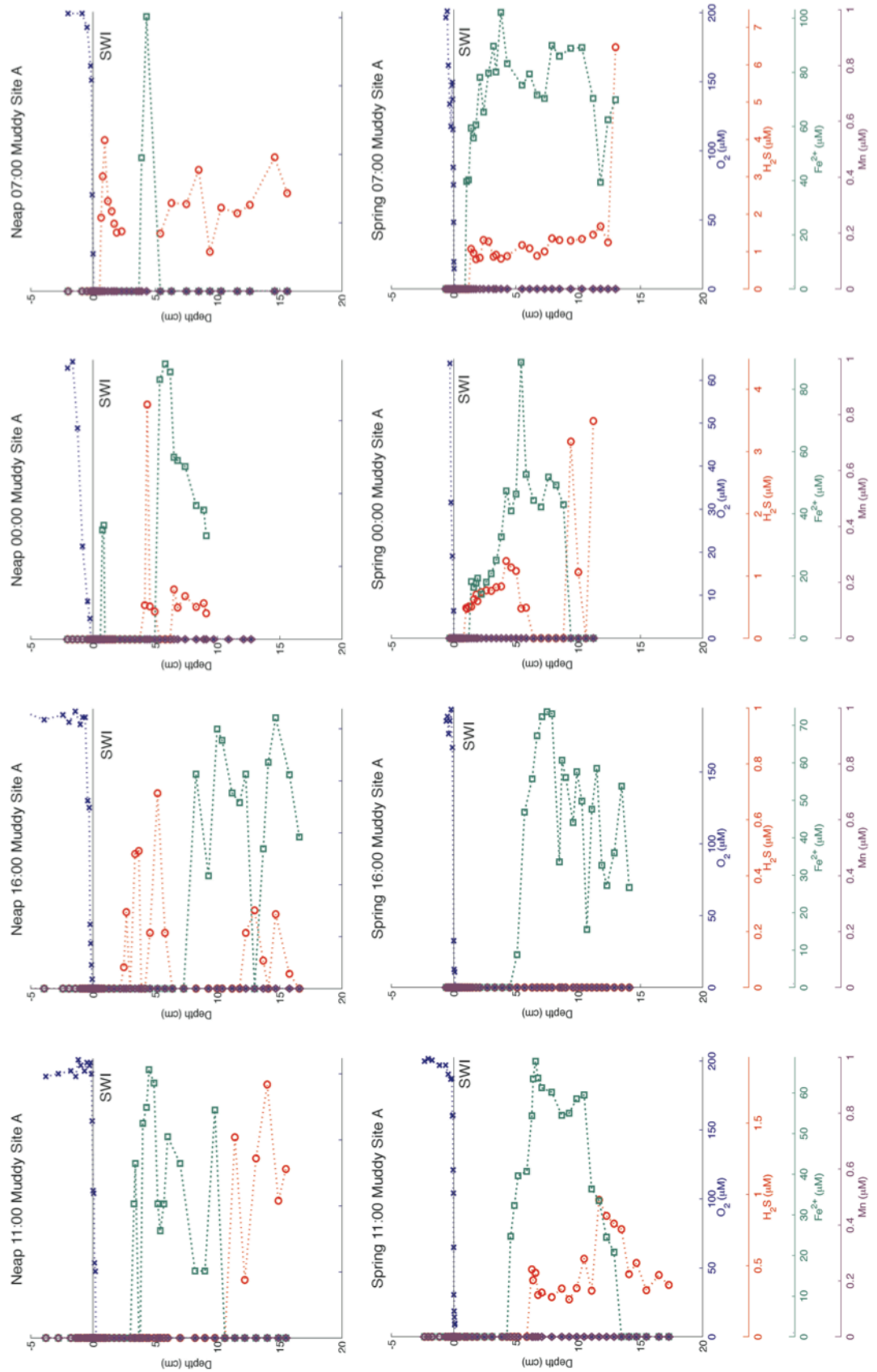

Figure 6.6 Electrochemical profiles from sediment cores collected at each tidal regime (spring and neap) during diurnal experiments at (a) Site A and (b) Site B. Depth on the y-axis is in cm, with negative values above the sediment-water interface (SWI); SWI is depicted by a black line. O_2 in blue; H_2S in orange; Fe^{2+} in green; Mn^{2+} in purple.

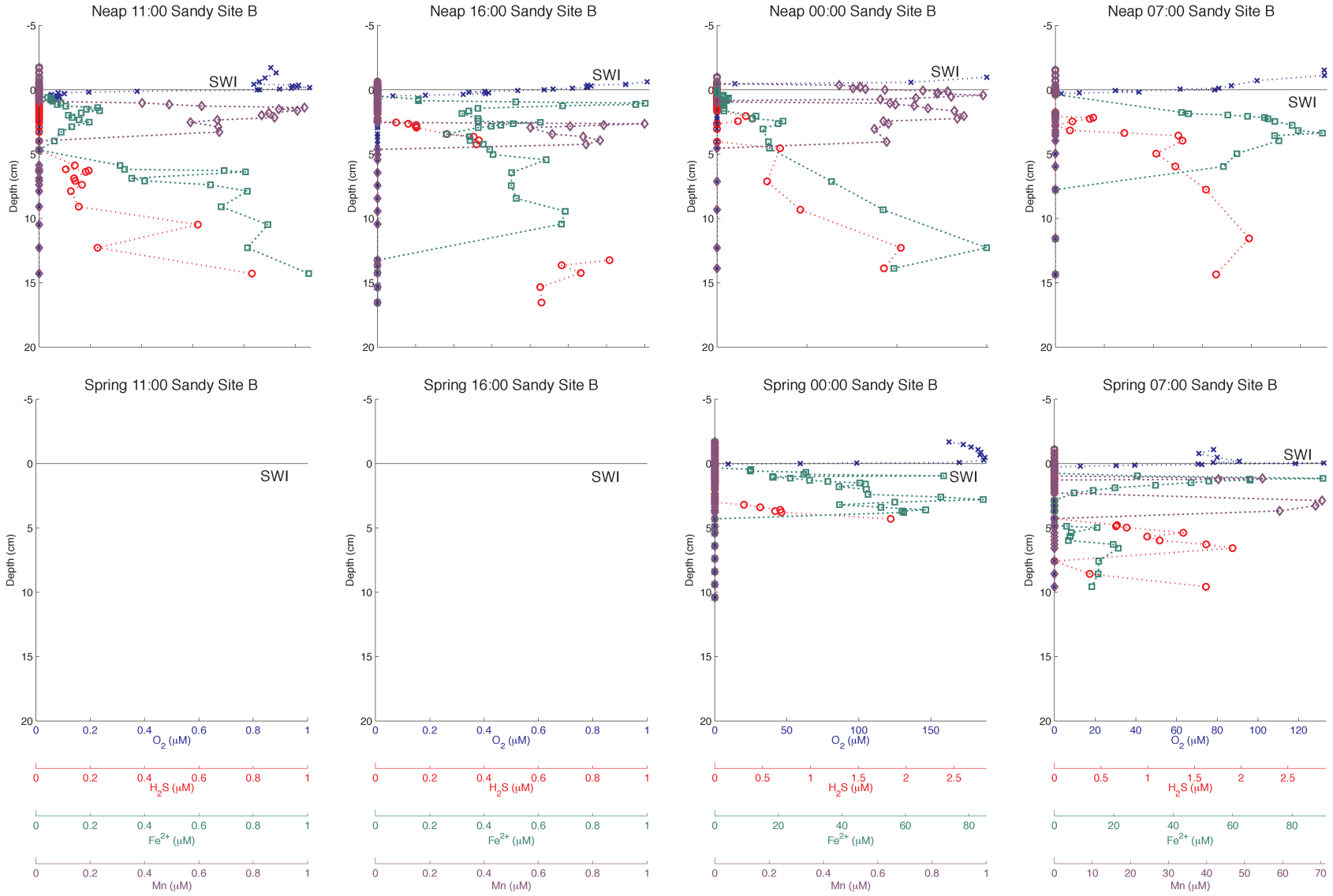
Neap 11:00 Sandy Site B
Neap 16:00 Sandy Site B
Neap 00:00 Sandy Site B
Neap 07:00 Sandy Site B
Spring 11:00 Sandy Site B
Spring 16:00 Sandy Site B
Spring 00:00 Sandy Site B
Spring 07:00 Sandy Site B
SWI
Depth (cm)
O2 (μM)
H2S (μM)
Fe2+ (μM)
Mn (μM)

Figure 6.7 Inorganic and organic nutrient profiles from sediment cores collected at each tidal regime (spring and neap) during diurnal experiments at (a) Site A and (b) Site B. Depth on the y-axis is in cm, with negative values abpve the sediment-water interface (SWI); SWI is depicted by a black line. NH_4^+ in blue; PO_4^{3-} in orange; dissolved organic phosphorus (DOP) in purple.

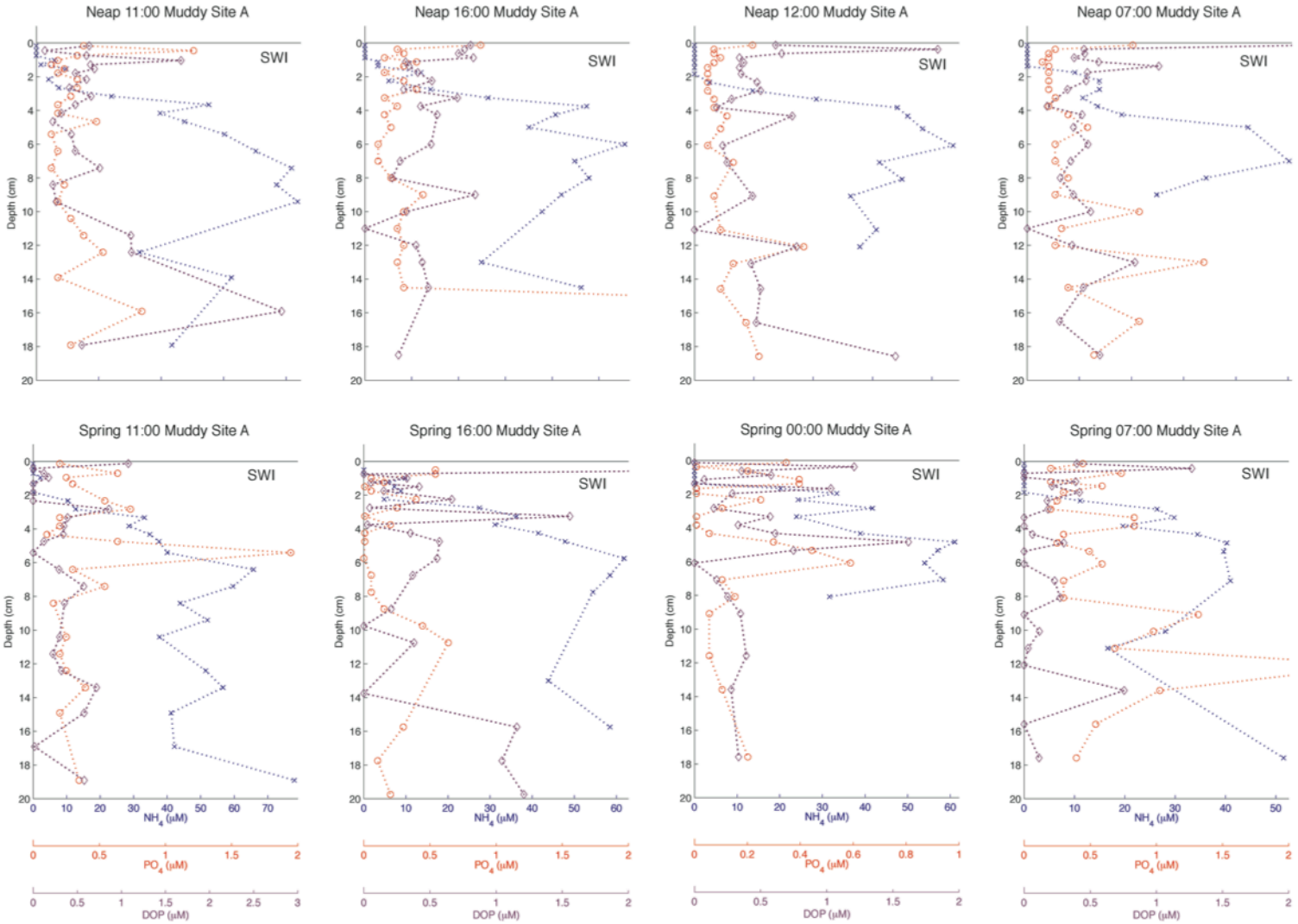

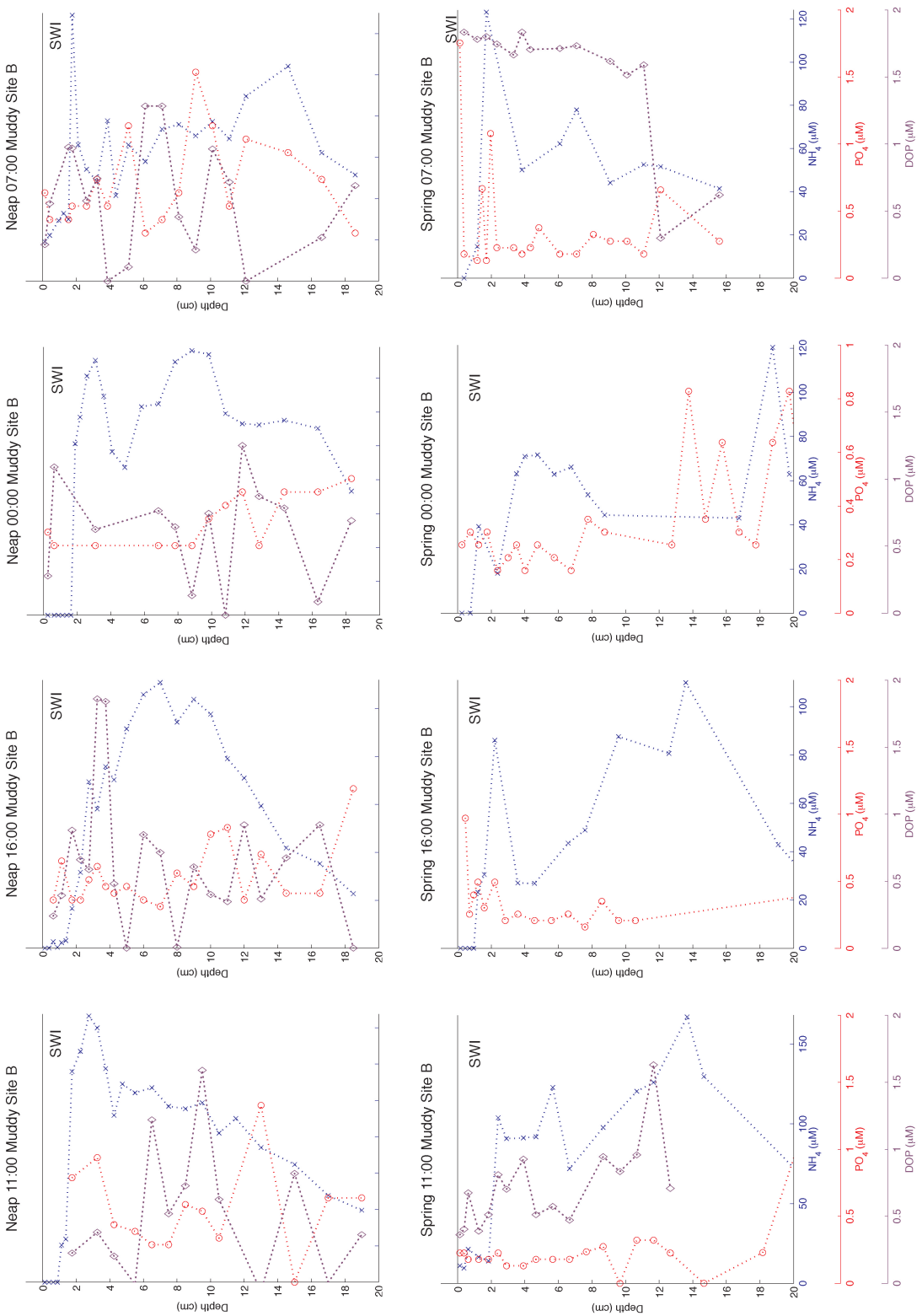
Neap 11:00 Muddy Site B
Neap 16:00 Muddy Site B
Neap 00:00 Muddy Site B
Neap 07:00 Muddy Site B
Spring 11:00 Muddy Site B
Spring 16:00 Muddy Site B
Spring 00:00 Muddy Site B
Spring 07:00 Muddy Site B
SWI
Depth (cm)
NH4 (μM)
PO4 (μM)
DOP (μM)

generation of O_2 during daylight hours and consumption via respiration at night (Figures 6.3 and 6.5). Likewise, temperature is expected to be higher during daylight hours and lower at night. To confirm that a shift from benthic photosynthesis to respiration in both the water column and sediment community is driving the observed diurnal oscillations in O_2, solar irradiance data were collected from the HIMB weather station to correlate benthic photosynthesis and respiration (light and dark conditions) with YSI data. pH is expected to be more basic when photosynthesis is active and buildup of metabolic acid due to respiration will drive pH down at night. pH appears to trend with DO, temperature, and irradiance (Figure 6.5), but the pH measurements did not statistically fall in-line with DO due to gaps in the pH measurements (Figure 6.5).

We employed principle component factor analysis using IBM SPSS Statistical Software® on water column data to examine the correlation between water column parameters and benthic photosynthesis/respiration (Figure 6.8). A two-component solution explained 88% of the variance in the data set; however when including pH into the statistical

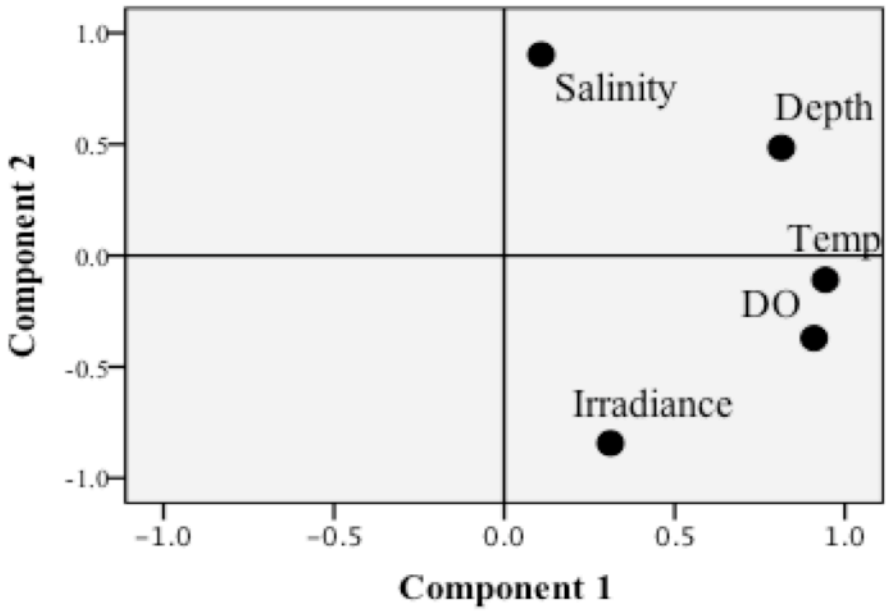

Figure 6.8 Results of principle factor analysis of water column data calculated using IBM SPSS Statistical Software®. Salinity, depth (calculated from pressure), temperature, and dissolved oxygen (DO) were collected from multi-parameter YSI 6600V2 Sonde®. Irradiance data were collected from the weather station at HIMB. A two-component solution explaining 88% of the variance is presented with varimax rotation to maximize the variance on each axis.

analysis, a third component was necessary to explain variance in the dataset. We choose to simply use the 2-component loadings (excluding pH) and employed a varimax rotation to maximize the variance on each axis in Figure 6.8. The grouping of parameters on the 2-component plot illustrates the relationship between parameters. The statistical analysis reveals that DO is related most closely to temperature. We believe the time course correlation of DO with pH (Figure 6.5), as well as the statistical analysis which correlates DO with temperature and irradiance (Figure 6.8), illustrate that the concentrations of DO in the overlying water are driven by diel, and not tidal shifts.

Diurnal trends in sediment porewaters: Transitions from daytime benthic photosynthesis to nighttime respiration are accompanied by a shoaling of sediment redox boundaries (Figure 6.6). To quantify the relationship between benthic microbial activity and sediment redox conditions, porewater profiles were compared from sediment cores collected at each time point in the diel experiment (Figure 6.9). As discussed previously, care was taken to assure lateral homogeneity within the sampling grid by selecting areas with visually uniform conditions that were devoid of macroalgae and appeared to be minimally affected by bioturbation. The assumption of lateral homogeneity affords us the opportunity to evaluate diel oscillations in porewater profiles

Table 6.2 Depth (cm) of disappearance (O_2, Fe^{2+}) and appearance (Fe^{2+}, H_2S) in porewaters throughout the diurnal experiment. Positive depth values are below the sediment-water interface; negative depth values are above the sediment-water interface.

Neap, SITE A				
	11:00	16:00	00:00	7:00
O_2 disappearance	0.24	0.00	-0.18	0.06
Fe^{2+} appearance	3.30	8.28	5.36	3.90
Fe^{2+}disappearance	9.80	-	9.10	4.30
H_2S appearance	11.40	2.48	4.16	0.66
Spring, SITE A				
	11:00	16:00	00:00	7:00
O_2 disappearance	0.12	0.12	0.02	0.08
Fe^{2+}appearance	4.58	5.10	1.42	1.04
Fe^{2+}disappearance	12.88	-	8.82	-
H_2S appearance	6.28	-	1.00	1.40
Neap, SITE B				
	11:00	16:00	00:00	7:00
O_2 disappearance	0.90	0.74	-0.36	0.36
Fe^{2+}appearance	0.60	0.74	0.42	1.76
Fe^{2+}disappearance	-	10.44	-	5.96
H_2S appearance	5.88	2.48	2.54	2.16
Spring, SITE B				
	11:00	16:00	00:00	7:00
O_2 disappearance	-	-	0.08	0.26
Fe^{2+}appearance	-	-	0.46	0.96
Fe^{2+}disappearance	-	-	3.80	-
H_2S appearance	-	-	3.20	4.78

from the series of sediment cores taken from each site throughout the diurnal experiment.

Observed diel oscillations in production and consumption of O_2 in surface sediments are driven by photosynthesis and respiration. During daylight hours benthic photosynthetic production increases bottom water oxygen concentrations (as previously discussed), and increases O_2 penetration in surface sediments (11:00 and 16:00) (Figure 6.9a and 6.10; Table 6.2). During nighttime hours benthic respiration, which lowers O_2 concentrations in the overlying waters, also reduces the depth of O_2 penetration into surface sediments (00:00 and 07:00) (Figures 6.9a and 6.10; Table 6.2). The shoaling of the oxic redox transition boundary during nighttime hours limits O_2 availability for the removal processes that utilize dissolved O_2 (Figure 6.9a; Table 6.2), such as oxidation of Fe^{2+} and its re-precipitation as Fe oxides.

The deepest O_2 penetration occurs in sediment cores taken at 11:00, and O_2 penetration depth shoals to its most shallow depth in the 00:00 sediment core. This is evident at both sites, under both spring and neap tidal conditions (Figure 6.9a and 6.10; Table 6.2). Shoaling of the O_2 penetration depth is more pronounced in the neap diurnals compared to spring tidal conditions, with O_2 disappearing above the SWI in the 00:00 neap sediment cores at both sites. O_2 concentrations in the overlying water were not driven by tidal conditions (see Figure 6.5 and 6.8 and prior discussion); however it appears that under different tidal conditions O_2 penetration depth varies. We suspect that under spring tide conditions enhanced tidal flow in overlying water may promote more vigorous mixing of overlying water, promoting deeper O_2 penetration depths, masking some of the diurnal signal of benthic O_2 production and consumption. However, under neap tidal conditions, tidal flow is suppressed, allowing for conditions of O_2 depletion to be sustained during nighttime hours, and lessening O_2 penetration into the sediments. Overlying water profiles of dissolved O_2 support the notion of mixing controlled O_2 penetration depth (Figure 6.9a), as follows. In the neap diurnal experiments, conditions of low dissolved O_2 extend higher in the water column above the SWI, and O_2 profiles reflect diffusive removal of O_2 at the SWI. During spring diurnal experiments, by contrast, bottom water O_2 is fairly well mixed right down to the SWI, with an extremely steep gradient right at the SWI indicating O_2 consumption over a more compressed depth interval occurs than during neap conditions.

The O_2 penetration depth sets the depth at which reductively dissolved Fe^{2+} that diffuses into the oxic region will oxidize and precipitate as iron-(oxy)hydroxides. Less O_2 is

Figure 6.9 Electrochemical profiles of (a) O_2, (b) H_2S and (c) Fe^{2+} from porewaters of sediment cores collected during the diurnal experiments at Site A and Site B (neap and spring tidal conditions). Depth on the y-axis is in cm, with negative values above the sediment-water interface (SWI); SWI is depicted by a black line. Sediment cores collected at 11:00 are in blue, 16:00 in red, 00:00 in green, and 07:00 in black.

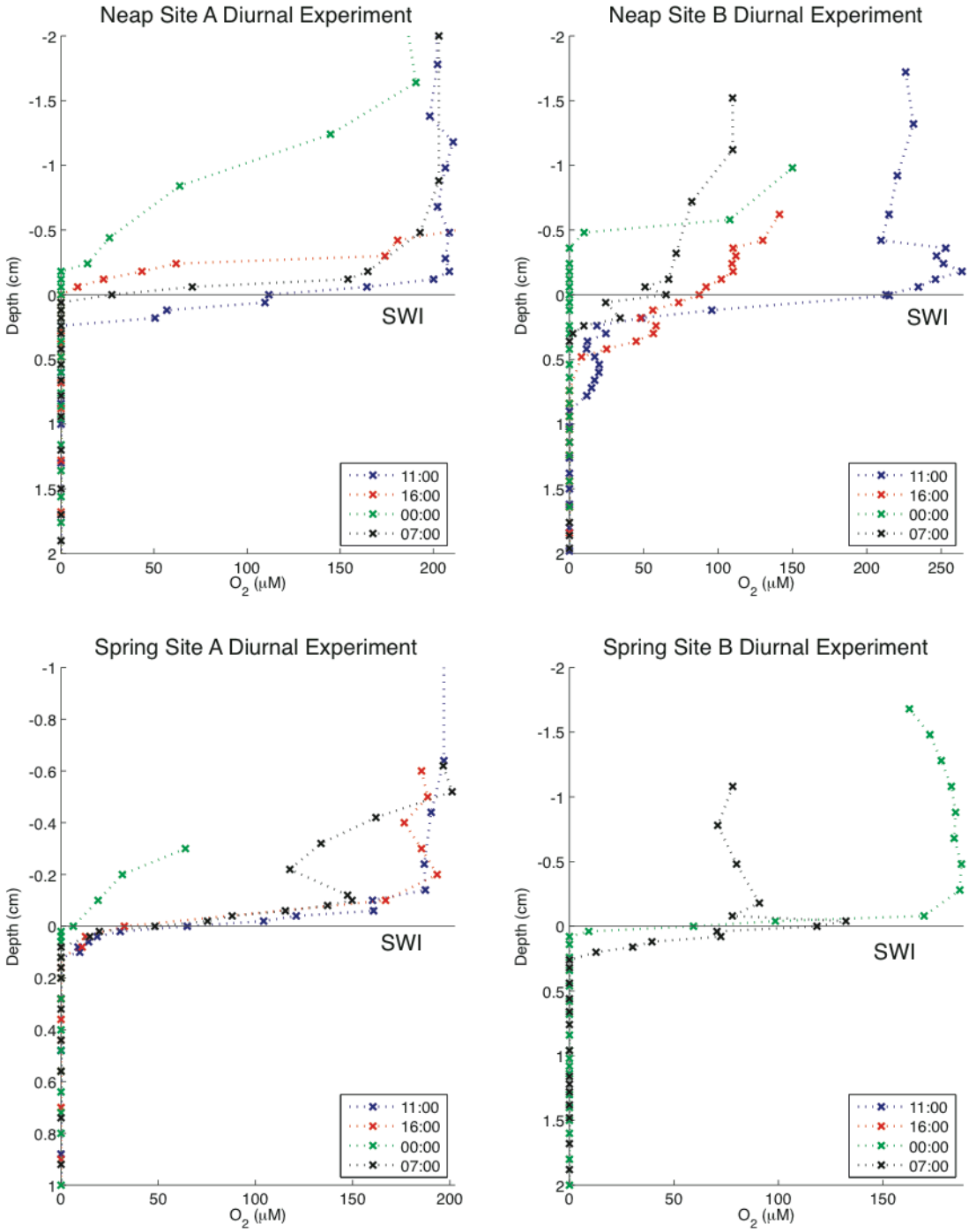

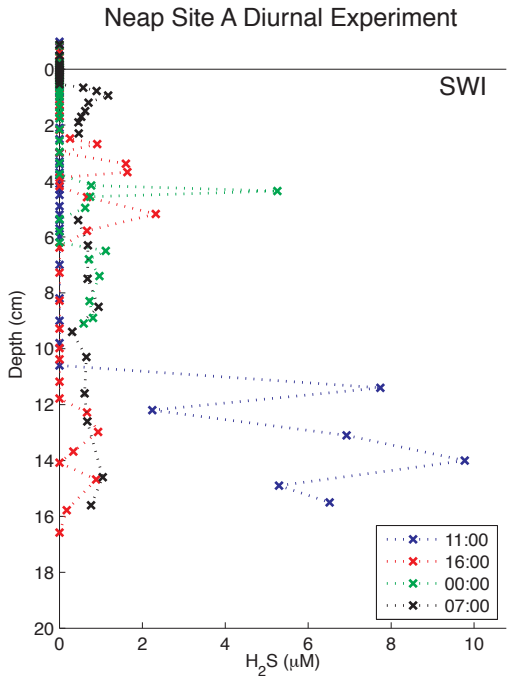
Neap Site A Diurnal Experiment
SWI
Depth (cm)
H2S (µM)
11:00
16:00
00:00
07:00

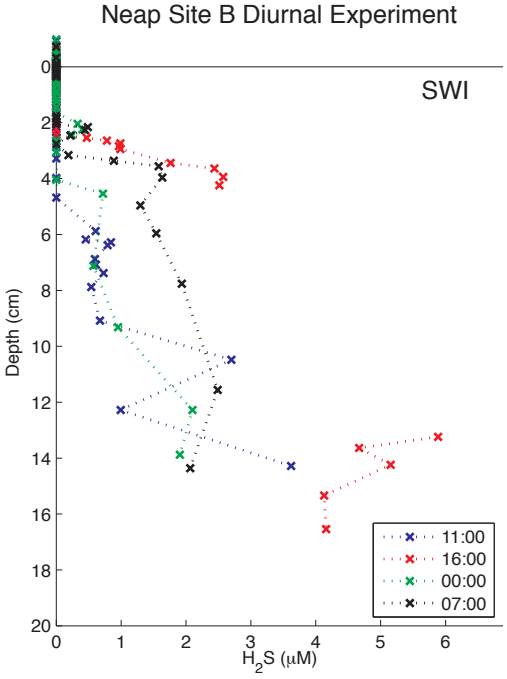
Neap Site B Diurnal Experiment
SWI
Depth (cm)
H2S (µM)
11:00
16:00
00:00
07:00

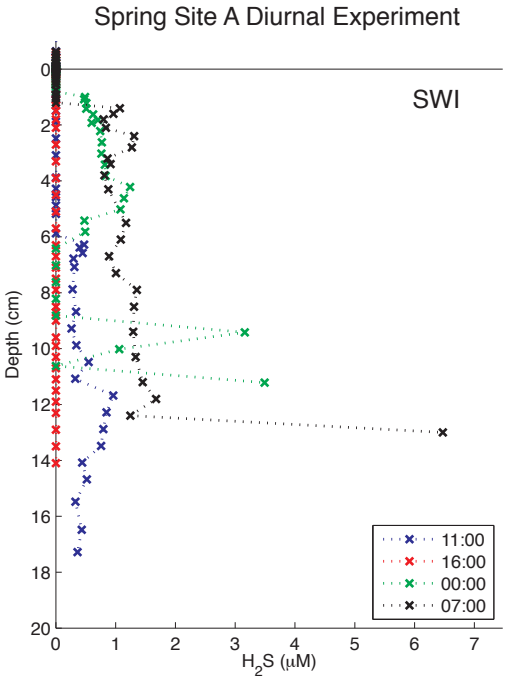
Spring Site A Diurnal Experiment
SWI
Depth (cm)
H2S (µM)
11:00
16:00
00:00
07:00

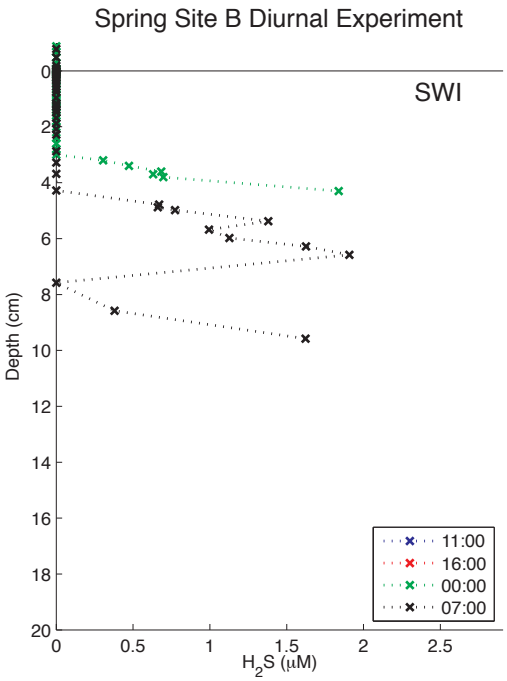
Spring Site B Diurnal Experiment
SWI
Depth (cm)
H2S (µM)
11:00
16:00
00:00
07:00

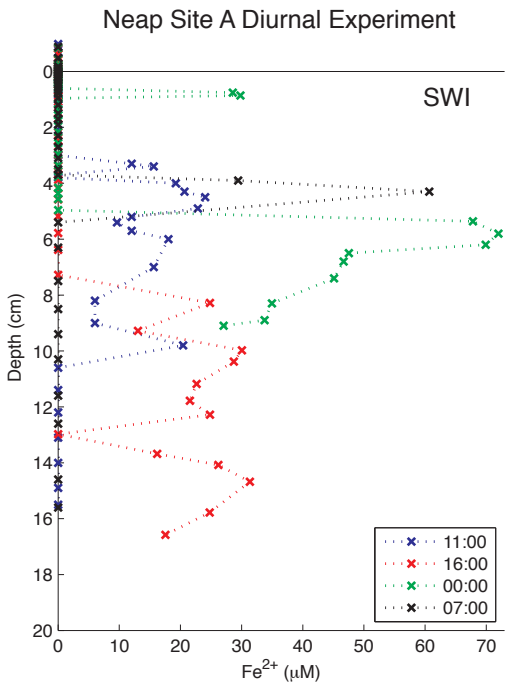
Neap Site A Diurnal Experiment
SWI
Depth (cm)
Fe2+ (μM)
11:00
16:00
00:00
07:00

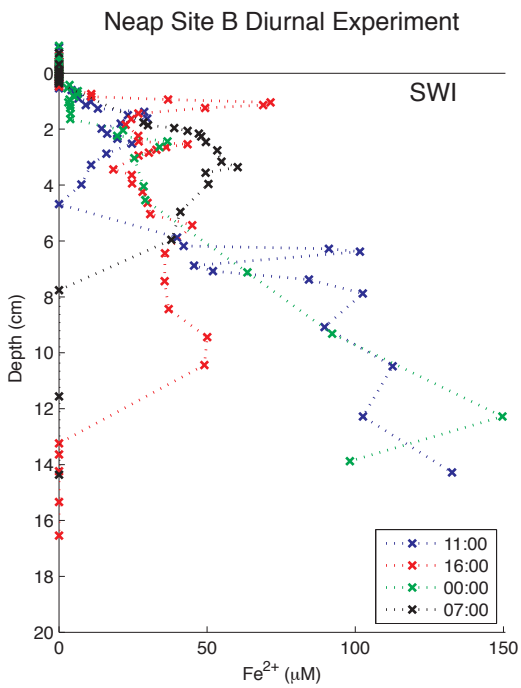
Neap Site B Diurnal Experiment
SWI
Depth (cm)
Fe2+ (μM)
11:00
16:00
00:00
07:00

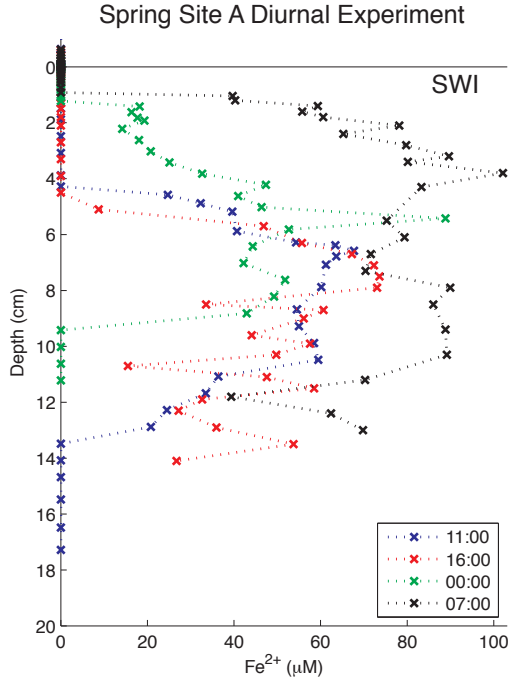
Spring Site A Diurnal Experiment
SWI
Depth (cm)
Fe2+ (μM)
11:00
16:00
00:00
07:00

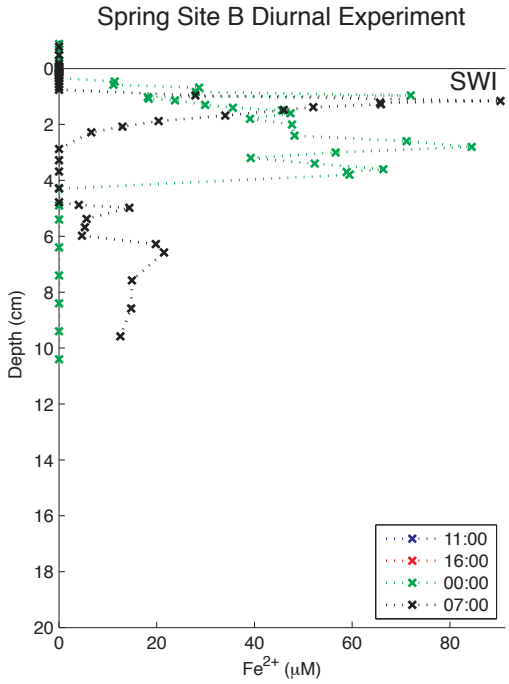
Spring Site B Diurnal Experiment
SWI
Depth (cm)
Fe2+ (μM)
11:00
16:00
00:00
07:00

available for the oxidation of reduced Fe^{2+} in sediment cores collected during nighttime hours (00:00 and 07:00), which have the lowest sediment O_2 concentrations (Figure 6.9a). Thus, in the nighttime sediment cores larger quantities of Fe^{2+} are able to accumulate at shallower depths (Figure 6.9b). Cores collected in the daytime (11:00 and 16:00) display Fe^{2+} accumulation deeper within the sediments (Figure 6.9c and 6.10; Table 6.2).

The disappearance of Fe^{2+} in the sediment cores occurs at the depth at which H_sS appears. We attribute Fe^{2+} removal to the reaction of iron with sulfur to form pyrite (Equations 6.4-6.7). The H_2S and Fe^{2+} profiles overlap in some of the cores; however Fe^{2+} only disappears in sediment cores with H_2S accumulation in porewaters, supporting the notion that coupled iron-sulfur cycling is responsible for the removal of Fe^{2+}. In spring Site A 16:00 sediment core, Fe^{2+} is present throughout the entire core, and H_2S is never detected. Sediment cores collected during the daytime, characterized by the deepest O_2 penetration (11:00 cores), also display the deepest appearance of H_2S, whereas in cores collected during nighttime hours, H_2S appears at shallower depths (Table 6.2; Figure 6.9b).

The aforementioned diel patterns are more simply and clearly seen if a single set of diel sediment cores are examined. For example, if we focus on the spring Site A diurnal experiment, O_2 penetration is deepest (-0.12 cm) in the daytime (11:00 and 16:00) sediment cores (Figure 6.9a). Fe^{2+} appearance is deepest (-4.58 to -5.10 cm), and accumulation of Fe^{2+} is <73 μmole L^{-1} (Figure 6.9c). In the 16:00 sediment core the H_2S concentrations in the are undetectable (<1 μmol L^{-1}) and in the 11:00 sediment core the first appearance of H_2S does not occur until 6.2 cm. Thus, during daytime cores H_2S is near or below detection and found deeper in the sediment cores compared to nighttime (00:00 and 07:00) sediment cores. Nighttime benthic respiration results in a shoaling of O_2 penetration depth to, -0.02 to -0.08 cm, at 00:00 and 07:00, respectively (Figure 6.9a) and Fe^{2+} appears at -1.42 to -1.04 cm, with concentrations exceeding 100 μmol L^{-1} (Figure 6.9c). In nighttime sediment cores H_2S accumulates more shallowly in the sediment porewaters (~1 cm), and concentrations are >1 μmol L^{-1} (Figure 6.9b).

Temporal oscillations in sediment redox conditions display the diel patterns previously discussed in all diurnal experiments conducted (Figure 6.10). In summary, all diurnal experiments display shoaling of redox zones during the daytime that appears to be correlated to benthic photosynthesis, and a deepening of redox boundaries at night as a

consequence of benthic respiration. Salient features of diel redox oscillations include: (i) daytime cores display deeper O_2 penetration, the accumulation of Fe^{2+}, and the appearance of H_2S occurring deeper in the sediment, (ii) in nighttime cores there is a shoaling of the O_2 penetration depth, Fe^{2+} accumulation occurs at shallower depths and in higher concentrations, and H_2S appearance occurs at shallower depths, and (iii) transitions in redox boundaries are particularly evident in cores collected during peak daytime and nighttime hours (11:00 and 00:00). These patterns are consistent in all diurnal studies described here. Any deviations from these patterns could be a result of the presence of microzones within individual sediment cores, which could be present even though care was taken to ensure lateral homogeneity within each sample site grid (see Methods). An example of such a deviation from typical diurnal patterns is seen in the neap core Site A 00:00, in which spatially (depth) isolated peaks in Fe^{2+} and H_2S concentrations (observed ~4 cm) do not correlate with expected diel patterns, and appear to reflect a small anoxic microzone in the sediment core.

Site A and Site B diurnal experiments display similar patterns of oscillation of redox transition boundaries; however, there are some noticeable differences in the characteristic depth of redox boundaries between these sites. As previously mentioned, Site A is characterized by muddy, fine-grained sediments while Site B sediments are coarser grained and sandy. Both locations are predominately driven by diffusive flow, but because Site B has larger grain size and higher porosity, advective flow may influence the surface sediments (prior to compaction) to a greater extent at this site. The depth of O_2 penetration at each site reflects these patterns, with suppressed penetration in all cores at Site A compared to Site B sediment cores (Figure 6.9 and 6.10).

The spatial separation between the depth of O_2 penetration (between -0.12 to 0.18 cm), the depth at which Fe^{2+} first appears, and the depth of H_2S appearance (at depths between 31- 62.4 cm) in porewaters precludes the possibility that O_2 directly oxides Fe^{2+} and H_2S in any of the cores analyzed; yet, we have shown in the preceding discussion that these layers deepen and shoal in a synchronous way, implying that a relationship exists between these sediment layers on a diel cycle. Although NO_3^- oxidation of Fe^{2+} remains as a possible mechanism by which Fe^{2+} can be oxidized at a depth below that of O_2 penetration, this cannot explain the interaction of oscillations in O_2 and H_2S. Using the Einstein-

Figure 6.10 Depth of O_2 disappearance (diamonds), Fe^{2+} appearance (circles), and H_2S appearance (squares) during Site A and Site B diurnal experiments. Depth on the y-axis is in cm, with negative values below the sediment-water interface (SWI).

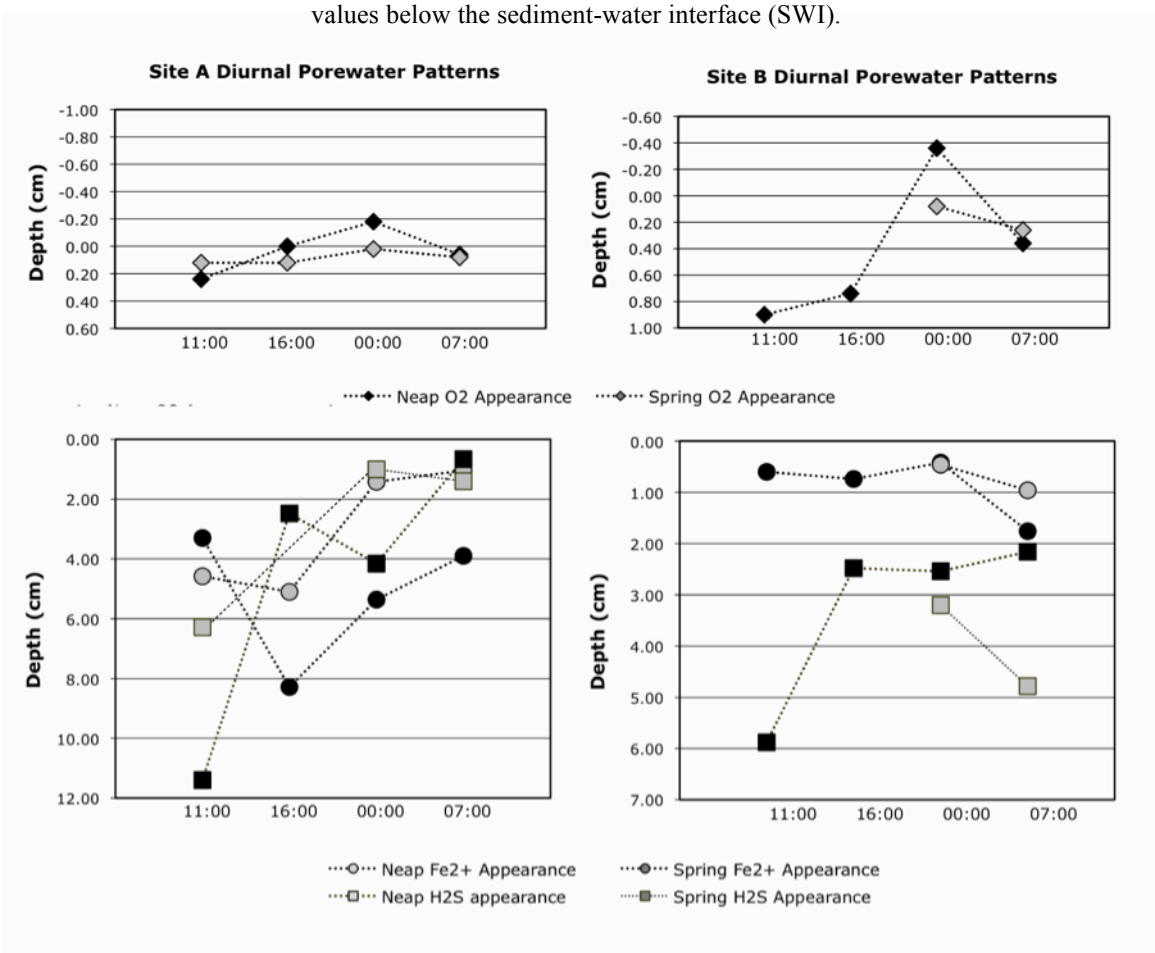

Smoluchowski equation, which is employed to describe the time and space scales over which diffusion operates, the distance an ion can travel by solute molecular diffusional transport, in 24 hours for typical bulk sediments, is ~1cm (reviewed in Burdige 2006). Thus, diffusion cannot explain the synchronous diel oscillations displayed by oxygen and other redox sensitive porewater species. Advective solute transport can exceed molecular diffusion by up to three orders of magnitude, and mix pore-waters at depths >10 cm; however a key factor important to advective porewater mixing is permeability (Jannsen et al. 2005). Sediments with high permeabilities (10-100 Darcy) are dominated by advective transport (Huettel and Gust 1992). Sediments characterized by high permeabilities in the range of 10-100 Darcy have porosities ≤ 0.4 (Bryant et al. 1975) and median grain size is typically > 0.1 mm (Shepherd 1989). We do not have permeability values for our study sites, however porosity at both sites is > 0.4 (see section 6.6) and grain size of ~50% of the sediments at both sites is <

63 microns. Thus, both study sites have a large clay component suggesting that the sediments should have permeabilities < 10 Darcy, and thus are not expected to be dominated by advective solute transport. These arguments illustrate that neither molecular diffusion nor advection could promote O_2 interaction with Fe^{2+} and H_2S in sediment porewaters, and thus cannot explain the mechanism by which these segregated redox layers deepen and shoal in tandem.

As an alternative to physical transport, Neilsen et al. (2010) suggested a novel mechanism by which spatially separated redox species can interact via electron shuttling in sediments. Organisms work together, mutually creating natural electrical currents that connect oxidation-reduction reactions in spatially segregated regions within the sediment column. Neilsen et al. (2010) illustrated, through laboratory experiments, that changes in O_2 concentrations in overlying water can alter the depth of the anoxic redox transition boundary 2 cm below the SWI. The temporal (diurnal) trends we observe in this study represent *in situ* data that are consistent with laboratory study of Neilsen et al. (2010).

Porewater profiles of NH_4^+: Net nutrient production in marine sediments can be estimated by fitting a model to the NH_4^+ porewater profiles. Porewater profiles of NH_4^+ (Figure 7) display the expected trend of smoothly increasing concentrations with depth below the SWI, reflective of OM decomposition and generation of NH_4^+ from decomposition of OM. We assumed that molecular diffusion was the most important transport process controlling the distribution of NH_4^+ concentrations in the down-core sediment porewater profile, and that steady-state conditions are present. These assumptions allow us to construct a nutrient mass conservation equation:

$$\varphi D_s (d^2C/dz^2) + R = 0 \qquad (6.8)$$

where C is the porewater concentration, z is depth, φ is porosity, D_s is the molecular diffusivity corrected for tortuosity, and R is the net rate of nutrient production per unit volume of sediment (Berner 1980; Boudreau 1997). The molecular diffusivity constant (D_s) was calculated at each interval using sediment tortuosity (calculated using the porosity of sediments at each interval) and a molecular diffusional constant for seawater NH_4^+ (1.85×10^{-9}; see Boudreau 1997 for equations). An average D_s value was taken over the entire

sediment core for use in subsequent calculations. One of the many analytical solutions to equation 6.8 is a parabolic relationship, which assumes that R is constant with depth:

$$C = -(R / 2\varphi D_s) z^2 + Az + B \quad (6.9)$$

where A and B are constants. Using Matlab Curve Fitting Toolbox™ a parabolic fitting function was applied to the gradient between the peak concentration of porewater NH_4^+ at depth and the depth and concentration where NH_4^+ becomes undetectable near the SWI. By using the fitting method, instead of a direct solution of Equation 6.8, we were able to remove the necessity of including boundary conditions for the solution of Equation 6.8 (Mcglathery et al. 2001). The parabolic function gives us three coefficients, $(R / 2\varphi D_s)$, A, and B (in Equation 6.9). Using known values of φ and D_s evaluated for each sediment core, R can be calculated. A sample NH_4^+ porewater profile from the neap Site B sediment core collected at

Figure 6.11 Ammonium porewater profile from Neap 16:00 collected at Site B (blue stars). The modeled parabolic fitting function calculated with Matlab Curve Fitting Toolbox™ is presented as a dashed black line.

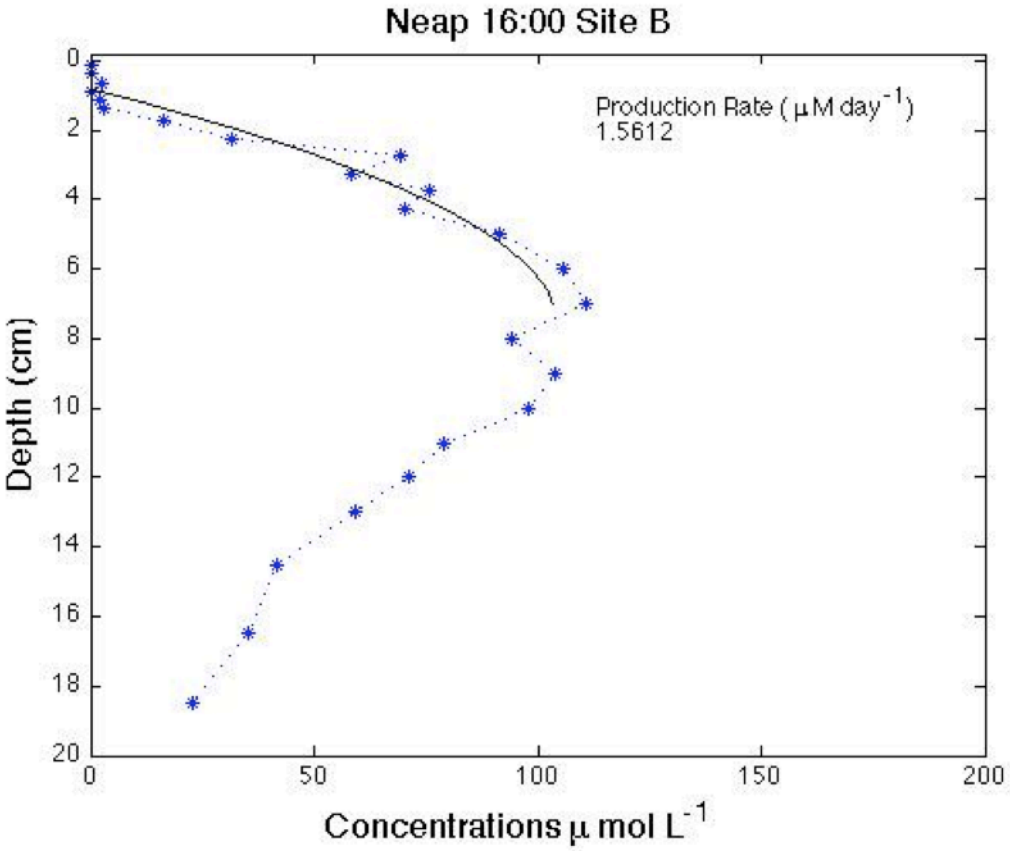

16:00 is presented in Figure 6.11 shows that the computed parabolic function fits well with the NH_4^+ concentration data. Similar fits were obtained for all other cores (data not shown).

The net production rate, calculated using the above method, provides insight into the relative production at each depositional environment. The net production of NH_4^+ calculated in all cores collected at Site B averaged 133.5 ± 36.8 μmol d^{-1} (range: 17.3-301.9 μmol d^{-1}), whereas Site A sediment cores displayed an average net production of 110.8 ± 27.8 μmol d^{-1} (range 29.0-223.7 μmol d^{-1}). These rates of production fall well in-line with previously published values of ammonium production in marine sediments, ranging from 11-395 μmol d^{-1} (Blackburn 1979; Mcglathery et al. 2001; Thamdrup and Dalsgaard 2002). Briggs et al. (2011, *submitted)* (Chapter 4) discuss how rates of OM remineralization are influenced by the quality versus quantity of OM deposited at the SWI at He'eia Fishpond. Higher remineralization rates are observed at sites dominated by more labile, marine-dominated OM, which characterize Site B sediments. Progressively slower remineralization rates are observed as the fraction of terrestrial OM increases in sites dominated by terrestrial, and therefore more refractory, sources of OM, characteristic of Site A.

Although NH_4^+ profiles from all cores display typical diffusional profiles of increasing NH_4^+ concentrations with depth, generated from OM decomposition in surface sediments, most profiles also display a concentration reversal at depth (Figure 7). To evaluate the quantity of NH_4^+ consumption at each site, we assumed that the peak NH_4^+ concentration observed in the porewater profile was equivalent to the asymptotic NH_4^+ concentration that would have been reached if no NH_4^+ removal process were operating. Profiles of NH_4^+ were integrated using the Matlab Curve Fitting Toolbox™, assuming that the maximum concentration persisted down core (i.e. the case in which no NH_4^+ consumption was occurring) (Figure 6.11). Profiles defined by the actual NH_4^+ concentration data, which show the concentration reversal and diminishing NH_4^+ concentration with depth were integrated (below peak NH_4^+) to determine the actual reservoir of NH_4^+ present in porewaters at depth (Figure 6.11). The difference between these two integrated curves was assumed to represent the quantity of NH_4^+ consumed at depth. Higher consumption of NH_4^+ was observed in Site B, with average NH_4^+ consumption of 478 ± 119 μmol m^{-2} (50% of total NH_4^+ porewater). Site A sediment cores display average NH_4^+ consumption of ~258 ± 49 μmol m^{-2} (52% of total NH_4^+ in porewater).

The observed reversals are intriguing, and may result from a number of processes, including oxic nitrification (Equation 6.1), anoxic nitrification of ammonium via Mn oxides (Equation 6.2) (Bartlett et al. 2008; Hulth et al. 1999; Luther et al. 1997; Mortimer et al. 2004), anammox activity (Equation 6.3) (Risgaard-Petersen et al. 2004; Thamdrup and Dalsgaard 2002; Trimmer et al. 2003), and/or ammonium adsorption onto clays or humic material (Boatman and Murray 1982; Mackin and Aller 1984; Rosenfeld 1979). Each of these processes will be considered in turn, and the likelihood that they could be operating to cause the NH_4^+ consumption we observe at depth in these sediments will be evaluated.

Ammonium oxidation with O_2 is unlikely to account for NH_4^+ consumption because the NH_4^+ reversals occur below the oxygenated layer in the sediments (Equation 6.1). Anoxic nitrification via Mn oxides, however, could be a likely pathway (Equation 6.2). Sediments from all sites are characterized by anoxia (as indicated by the accumulation of H_2S), which suggests that anoxic nitrification could occur at both sites. We consider this an unlikely pathway for NH_4^+ oxidation, however, because anoxic nitrification can only occur where sediment manganese levels are high (Hulth et al. 1999; Luther et al. 1997; Mortimer et al. 2004). As previously stated, the lack of Mn accumulation in porewaters suggests anoxic nitrification via Mn oxides is likely unimportant.

Thamdrup and Dalsgaard (2002) found that anaerobic oxidation of NH_4^+ via anammox (Equation 6.3) can be responsible for 24-67% of the N loss in marine sediments. Our calculations suggest that 50-52% of the total NH_4^+ produced via OM respiration is being consumed in porewaters, which falls within the range observed by Thamdrup and Dalsgaard (2002). Thus, the consumption estimates we have made based on our porewater profiles are consistent with anaerobic oxidation of NH_4^+ via anammox. In marine sediments, the proportion of NH_4^+ lost from sediments via anammox is related to water depth, and is estimated to be more important in slope and hemipelagic sediments (Risgaard-Petersen et al. 2004; Thamdrup and Dalsgaard 2002; Trimmer et al. 2003) than sediments in shallow waters. The shallow water column at our sites suggests that anammox alone, probably does not explain the total NH_4^+ consumption in observed in porewater profiles in this study.

Ammonium produced via the decomposition of organic matter (OM) can be adsorbed by clay minerals or onto solid-phase OM. The exchangeable NH_4^+ on clays is regulated by the concentration of NH_4^+ in porewaters (Berner 1980). Rosenfeld (1979) found that

adsorption of exchangeable ammonium occurred in a linear fashion when NH_4^+ was present at lower concentrations (<10 mM), but that at higher concentrations (>10 mM) adsorption behavior was exponential. Our sediment profiles display NH_4^+ concentrations much less than 10 mM, therefore would be best described by linear and not exponential adsorption. The removal of OM via adsorption on clay minerals cannot be ruled out as a possible mechanism consuming NH_4^+ in our sediment porewaters.

Figure 6.12 Predicted PO_4^{3-} concentrations, calculated from NH_4^+ porewater concentrations, calculated using a stoichiometric nutrient regeneration model (see text) plotted versus measured PO_4^{3-} concentrations at all sediment intervals at Site A (open symbols) and Site B (closed symbols). Dashed black line represents 1:1 ratio, values above this line indicate that predicted values exceed actual values, and vice versa.

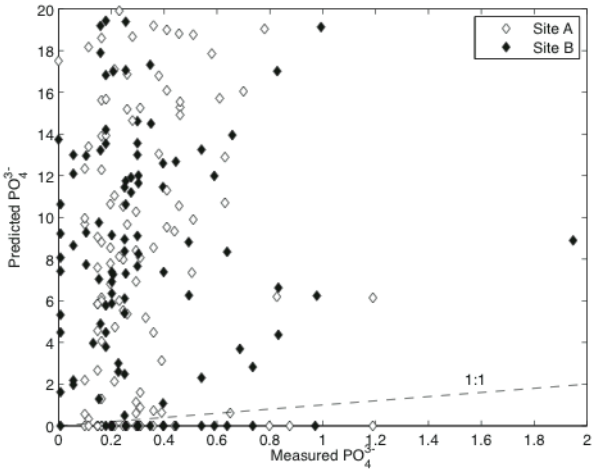

Stoichiometric nutrient regeneration: The concept of stoichiometric nutrient regeneration stipulates that the concentrations of dissolved inorganic carbon, nitrogen (NH_4^+) and phosphorus (PO_4^{3-}) in porewaters should accumulate at a ratio equivalent to the carbon, nitrogen and phosphorus ratio in the OM undergoing remineralization (Berner 1977). Thus, we would expect to observe PO_4^{3-} accumulation in sediment porewaters, in tandem with NH_4^+, but offset by the stoichiometric ratio set by the decomposing OM. The NH_4^+ build-up in porewaters, as well as net production rates, confirm the process of OM remineralization is occurring in these sediments, accompanied by release of metabolites (i.e. NH_4^+ and PO_4^{3-}). The lack of PO_4^{3-} accumulation (Figure 6.7b) indicates that one or more PO_4^{3-} uptake process is operating in these sediments.

In order to evaluate the magnitude of PO_4^{3-} uptake, we employ a stoichiometric nutrient regeneration model (Berner 1977; Ruttenberg and Berner 1993; Schuffert et al. 1998), as follows. Predicted PO_4^{3-} concentrations were calculated from NH_4^+ porewater concentrations, using average total nitrogen to organic phosphorus ratios (TN:OP) of OM from each study site (OP:TN= 4.5 Site A; 3.7 Site B) (Briggs et al. 2011). Predicted PO_4^{3-} concentrations exceeded measured PO_4^{3-} concentrations at almost all depths at both study

Figure 6.13 Solid-phase P speciation data generated using the modified SEDEX sequential extraction for Site A (blue) and Site B (red) surface sediments. The modified SEDEX method separates P into 6 reservoirs: (Pre: labile organic phosphorus, Step I: exchangeable or loosely sorbed P, Step II: iron-bound P, Step III: authigenic and biogenic apatite, as well as carbonate-bound P, Step IV: detrital apatite, and Step V: refractory organic P.

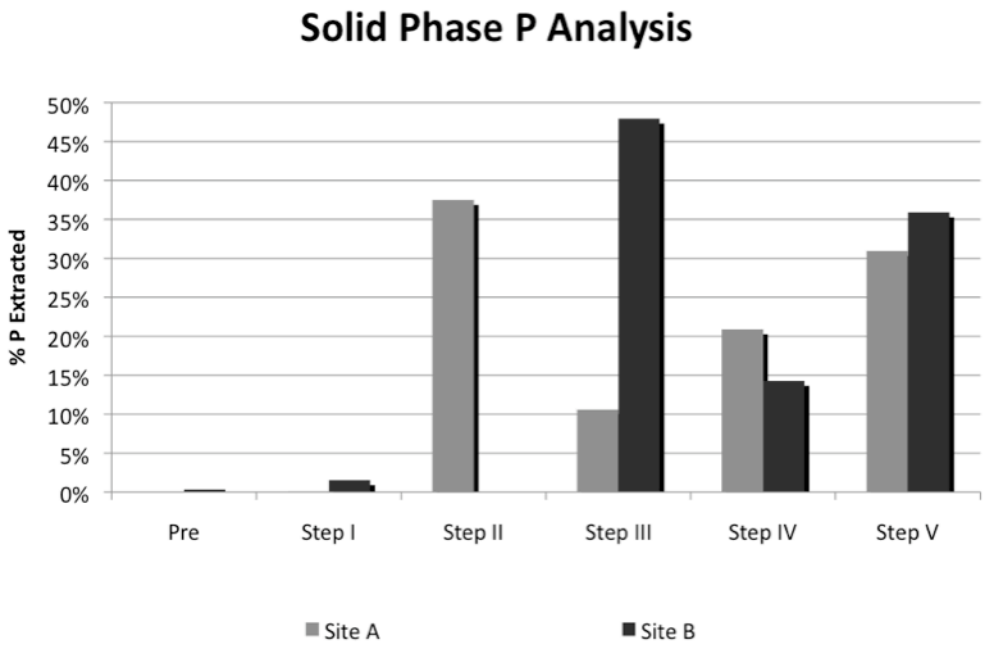

sites (Figure 6.12), an observation that implies that there is a sink for PO_4^{3-} in both depositional environments.

The missing P story: To examine the pathway(s) that may be responsible for the removal of PO_4^{3-} at each depositional site, we examined solid-phase P speciation data generated using the modified SEDEX sequential extraction technique (Chapter 3; Briggs and Ruttenberg 2011) (Figure 6.13). The modification entails insertion of a pre-extraction step to selectively and separately quantify labile organic P (Briggs and Ruttenberg 2011). The modified SEDEX method separates P into 6 reservoirs: (i) labile organic phosphorus, (ii) exchangeable or loosely sorbed P, (iii) iron-bound P, (iv) authigenic and biogenic apatite, as well as carbonate-bound P, (v) detrital apatite, and (vi) refractory organic P.

In Site B surface sediments, 48% of the solid phase P is extracted in step III, the step that selectively dissolves authigenic and biogenic apatite, as well as carbonate-bound P (Figure 6.13). Site B is characterized by sandy, coarse-grained sediments, dominated by aragonite mineralogy, and therefore high concentrations of carbonate-bound P are expected. Authigenic carbonate-fluorapatite (CFA), the primary sink for phosphate in marine sediments (Ruttenberg 2003), most likely precipitates in these sediments, facilitated by the high

carbonate content of the sediments (Ames 1959; Ruttenberg and Berner 1993). Both sites display similar concentrations of refractory OP (Step V), while labile organic P (Pre-Extraction step) is only present in Site B surface sediments. We would expect more detrital apatite in terrigenous dominated sediments, and the close proximity of Site A to the river outflow most likely explains the higher concentrations of detrital apatite (Step IV) at Site A compared to Site B. Surface sediments from Site A are characterized by a large pool of P associated with reactive iron-oxyhydroxides, which is reasonable considering the close proximity to the river input. At Site A, therefore, we would expect coupled iron-phosphate cycling to be active resulting in the formation of iron-bound P in the surface sediments (Figure 6.13) (Roden and Edmond 1997; Rozan et al. 2002; Slomp et al. 1996). When nighttime respiration commences, reductive solubilization of iron-oxyhydroxides becomes favorable as O_2 concentrations drop (Figure 6.9a), and dissolved Fe^{2+} is liberated to porewaters. The dissolved Fe^{2+} could reasonably be expected to be accompanied by elevated phosphate due to the large pool of Fe-bound P in Site A sediments (Figure 6.13). However, porewater profiles from all diurnal sediment cores showed no evidence of PO_4^{3-} accumulation (Figure 6.7), implying a decoupling of porewater dissolved Fe^{2+} and PO_4^{3-}. We believe this decoupling is due to higher levels of iron-oxyhydroxides in these sediments. Iron-bound PO_4^{3-} may be liberated to the sediment during Fe reduction; however, if sufficient iron-oxyhydroxides remain intact to re-adsorb dissolved PO_4^{3-}, this could prevent PO_4^{3-} build-up in porewaters.

PO_4^{3-} concentrations tend to increase in deeper intervals of several sediment cores (Figure 6.7). Below the redox transition boundary, in the anoxic zone of sediments, sulfur will influence the coupled Fe-P cycle by removing dissolved iron from porewaters through the formation of solid phase iron-sulfide minerals (Equations 6.4-6.8). Solid iron-sulfide minerals, such as pyrite, do not readily adsorb phosphate (Huerta-Diaz and Morse 1992; Rozan et al. 2002). Therefore, deeper within the anoxic zone of sediments, the sequestration of Fe^{2+} as FeS removes the possibility of iron-oxyhydroxides as an active sink for PO_4^{3-}.

Despite the fact that there is no discernable accumulation of PO_4^{3-} in sediment porewaters, build-up of dissolved organic phosphorus (DOP) in porewaters occurs in all sediment cores examined in this study (Figure 6.7). Although studies that have quantified DOP in marine porewaters are rare, it has been recognized that DOP may play an important

role in P cycling in coastal waters (Mcglathery et al. 2001; Monbet et al. 2009). A plot of DOP versus PO_4^{3-} from all intervals in all sediment cores illustrates the degree of enrichment of DOP over PO_4^{3-} in these sediments (Figure 6.14). Fractionation of PO_4^{3-} from DOP in porewaters can be explained because PO_4^{3-} is more rapidly and efficiently removed onto iron-oxyhydroxides in seawater than is DOP, due to differential sorption of PO_4^{3-} versus DOP onto iron-oxyhydroxides (Ruttenberg and Sulak 2011). Additionally, uptake of PO_4^{3-} during carbonate-fluoroapatite formation can remove PO_4^{3-} leaving behind DOP. Greater mobility of DOP relative to PO_4^{3-} in these sediments will potentially support an enhanced DOP benthic flux relative to PO_4^{3-}. DOP may thus play a disproportionately important role in supporting primary production in waters overlying Fe-(oxy)hydroxide enriched coastal sediments.

DOP plays a particularly important role in supporting primary production where phosphate is present at limiting levels. This has been suggested to occur in both open ocean

Figure 6.14 Porewater DOP versus PO_4^{3-} concentrations from all sediment intervals at Site A (open symbols) and Site B (closed symbols). Dashed black line represents 1:1 ratio, values above this line indicate enrichment of DOP over PO_4^{3-} in sediment porewater intervals, and vice versa.

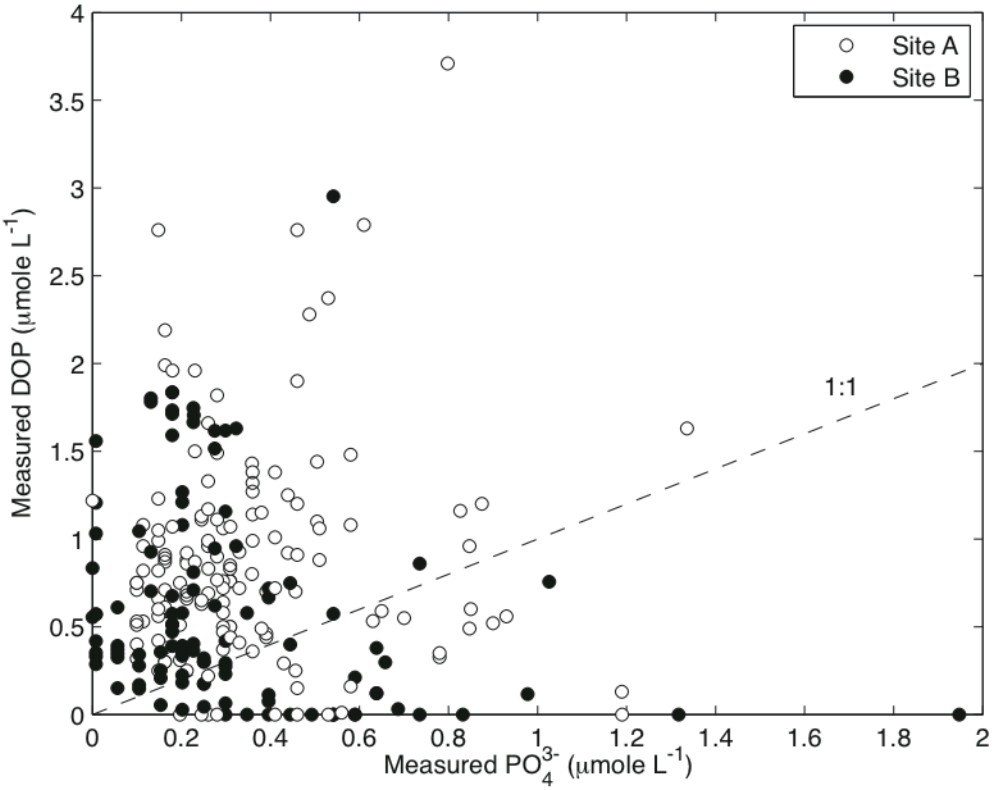

(Karl et al. 1998; Wu et al. 2000) and near shore environments (Dyhrman and Palenik 1999; Monaghan and Ruttenberg 1999; Ruttenberg and Dyhrman 2005). The potential of DOP as a nutrient source depends upon its chemical composition and the ability of organisms to access different DOP compounds. Organisms employ phosphohydrolytic enzymes, such as alkaline phosphatase, to access P from DOP through hydrolytic cleavage of phosphate from DOP (Cembella et al. 1984; Dyhrman and Ruttenberg 2006). Due to the energy requirement for this process, alkaline phosphatase activity (APA) is only present in environments characterized by P-stress or P-limitation. Thus the presence of APA can be used as a indictor of metabolic P stress (Cembella 1984; Dyhrman and Ruttenberg 2006). In He'eia Fishpond, the prevalence of APA throughout the fishpond indicates that the biological community is experiencing some degree of P- stress, and possible P-limitation (Young 2011). A substantial benthic flux of DOP may play an important role in sustaining primary-producers in this coastal system.

6.8 Conclusions

1. All diurnal experiments display depth oscillations of redox zones throughout the diel experiment that appear to be correlated to day-night shifts between benthic photosynthesis and respiration. Diel patterns include: (i) daytime cores exhibit deeper O_2 penetration, the accumulation of porewater Fe^{2+}, and the appearance of H_2S occurs deeper in the sediment, and (ii) in nighttime cores there is a shoaling of the O_2 penetration depth, Fe^{2+} accumulation occurs at shallower depths and is present at high concentrations, and H_2S appearance occurs at shallower depths. The spatial separation between the depth of O_2 penetration, the depth at which Fe^{2+} first appears, and the depth of H_2S appearance in porewaters precludes the possibility that O_2 directly oxides Fe^{2+} and H_2S in any of the cores analyzed; yet, we have shown that a relationship exists between these sediment layers on a diel cycle. Diffusive flow cannot explain the interaction of redox species spatially segregated in these layers, and advective flow is suppressed in our study sites due to the low permeability at these sites, which was based on small grain size and low porosity values. Thus, we hypothesize that the mechanism proposed by Nielsen et al. (2010) may be operating in these sediments, wherein organisms work together to mutually create natural electrical

currents to connect oxidation-reduction reactions in spatially segregated regions within the sediment column.

2. The net production of NH_4^+ calculated in all cores collected at Site B averaged 133.5 ± 36.8 μmol d^{-1} (range: 17.3-301.9 μmol d^{-1}), whereas Site A sediment cores displayed average net production of 110.8 ± 27.8 μmol d^{-1} (range 29.0-223.7 μmol d^{-1}). The quality versus quantity of OM deposited at the SWI at each site influence the production rates observed in this study. Higher remineralization rates are observed at sites dominated by more labile, marine-dominated OM (Site B). Progressively slower remineralization rates are observed as the fraction of terrestrial OM increases in sites dominated by terrestrial, and therefore more refractory, sources of OM (Site A). Although NH_4^+ profiles from all cores display typical diffusional profiles generated from OM decomposition in surface sediments, most profiles also display a concentration reversal at depth. The observed reversals most likely are not the result of oxidation directly with O_2 (Equation 6.1), or anoxic nitrification of ammonium via Mn oxides (Equation 6.2). We hypothesize that anammox activity (Equation 6.3), and/or ammonium adsorption onto clays or humic material may explain the reversals observed in NH_4^+ porewater profiles.

3. The NH_4^+ build-up in porewaters, as well as net production rates, confirm that the process of OM remineralization is occurring in these sediments, accompanied by release of metabolites (i.e. NH_4^+ and PO_4^{3-}) to porewater. The fact that PO_4^{3-} build-up does not occur in tandem with NH_4^+ accumulation in porewaters suggests that the sediments sequester the porewater PO_4^{3-} produced during OM remineralization. We hypothesize that rapid surface sorption onto mineral surfaces and uptake in authigenic minerals are two possible PO_4^{3-} sequestration pathways. SEDEX data suggest that sorption on iron-(oxy)hydroxides dominates at Site A, and formation of CFA at Site B. This is a direct consequent of the mineralogy at each depositional environment.

4. The results presented here illustrate that porewater DOP builds up in oxic surface sediments whereas PO_4^{3-}concentrations remain below detection, a result consistent with the idea of differential sorption immobilization of DOP versus phosphate. The greater mobility of DOP in oxic sediments may allow for a DOP benthic flux at the same time that $PO_4^{3-}$is completely immobilized in sediments, such that DOP may play an enhanced role in supporting primary production in overlying waters.

Acknowledgements

We thank Iuri Herzfeld and James Krest for access to, and assistance with the segmented flow auto-analyzer for nutrient analysis. We are grateful to In Chieh Chen, Amanda Ricardo Marcie Grabowski, Dan Sulak, Kahoa Keahi and the numerous additional volunteers that assisted with extensive field preparations, sample collection throughout the diurnal experiments and laboratory analyses. This work could not have been accomplished without the aid and support of Paepae o He‘eia, the local nonprofit group, who maintain the historical and structural integrity of He‘eia Fishpond. This research was supported by a grant/cooperative agreement from the National Oceanic and Atmospheric Administration; project R/EL-42, which is sponsored by the University of Hawai‘i Sea Grant College Program, SOEST, under Institutional Grant NA05OAR4171048 from NOAA Office of Sea Grant, Department of Commerce. The views expressed herein are those of the authors and do not necessarily reflect the views of NOAA or any of its subagencies. UNIHI-SEAGRANT-xxxx. This is SOEST contribution #xxxx.

Chapter 7

Conclusions

Organic matter preservation and burial in marine sediments plays a crucial role in the global carbon cycle (Berner 1989), and can be described by the following simplified equation:

$$CO_2 + H_2O \rightarrow CH_2O + O_2 \quad (7.1)$$

Equation 7.1 illustrates that OM burial not only affects the global carbon cycle through carbon preservation, but also leads to CO_2 removal from and O_2 input to the atmosphere (reviewed in Burdige 2007). Continental margins and coastal sediments are the major sites of organic matter (OM) burial and preservation (reviewed Hedges and Keil 1995 and Burdige 2007) and many research efforts focus on these areas. While the importance of OM remineralization and burial in marine sediments is widely recognized, our knowledge of the factors that determine preservation of organic carbon in sediments is still limited (Hedges and Keil 1995).

The research presented in this dissertation focuses primarily on OM remineralization in coastal sediments. To fully understand OM preservation, one must focus on both the source and lability of OM delivered to marine sediments (Hedges and Keil 1995). We have developed new techniques that permit identification of OM sources to marine sediments, which will be informative to OM preservation studies (Chapters 1-3). In the latter portion of this dissertation, particular aspects of early diagenetic pathways of OM remineralization are examined.

In the simplest sense, OM remineralization in sediments is controlled by: (i) the quantity and lability of OM deposited at the SWI (Figure 7.1; blue) and, (ii) the concentration and availability of oxidants within sediments (Figure 7.1; red) (Burdige 2006). Microbial aerobic and anaerobic respiration of sediment organic matter releases dissolved organic matter and inorganic nutrients (i.e., NH_4^+ and PO_4^{3-}) to porewater during burial and subsequent breakdown of organic matter (Klump and Martens 1987; Ruttenberg 2003). Thus, the processes operating during OM remineralization determine the depth distribution below the SWI of redox species utilized in metabolic pathways, and the products of OM

Figure 7.1 Schematic illustrating OM burial and remineralization in sediments, and areas of interest associated with each overall process (italics) that are targeted for study in this dissertation.

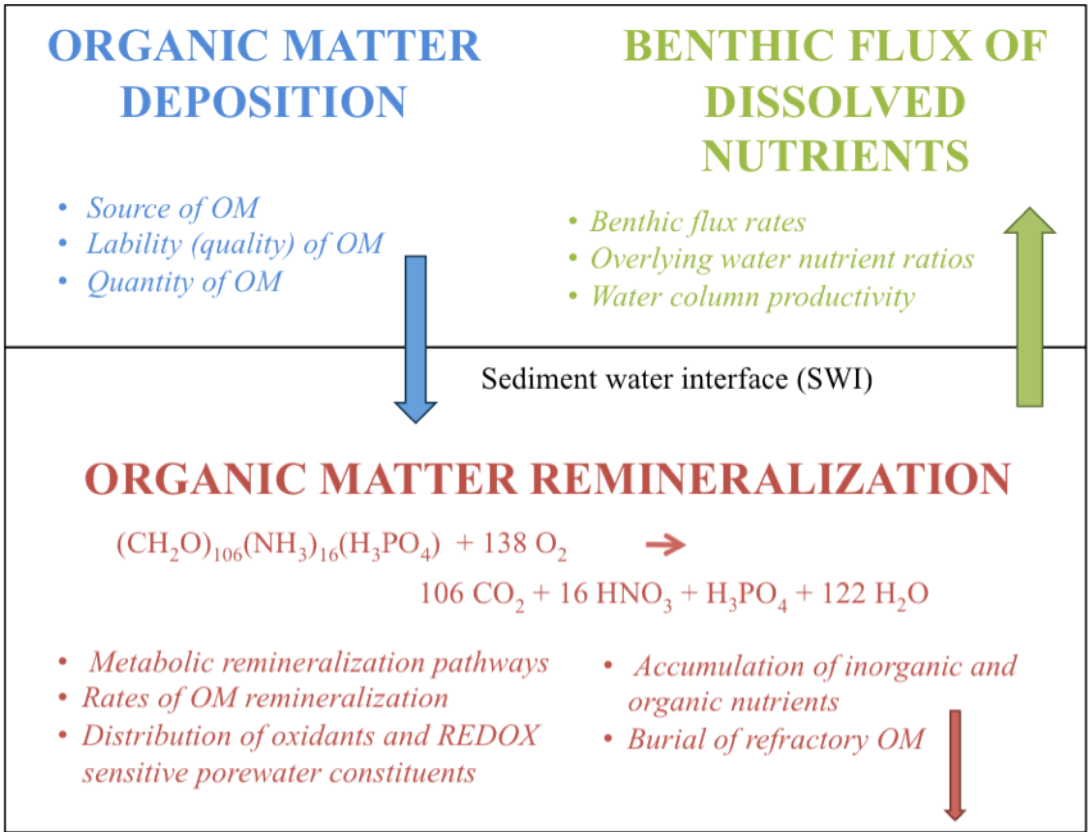

degradation that are released to marine sediment porewaters (Figure 7.1; red). Additionally, sediment degradation of OM impacts nutrient cycles in waters overlying sediments via the burial or release of dissolved nutrients (Figure 7.1; green). In the following discussion, we explain how this dissertation research provides unique insight into each of the aforementioned processes that influence OM remineralization in coastal sediments.

The principle tools for distinguishing marine versus terrestrial OM are elemental ratios and isotopic composition. Marine derived OM is generally more labile than its refractory, terrestrial counterpart (Aller et al. 1996; Cowie and Hedges 1992), so being able to differentiate sources of OM allows us to understand relative lability of OM deposited at different sediment locations. The traditional two-end member notion of OM sources to marine sediments can be imperfect due to overlap in the parameters (elemental ratios and isotopic compositions) utilized to distinguish terrestrial and marine end member material (Chapter 4). The OM reservoir in sediments in our study sites could not be explained by two end-members alone, and only when a new source of OM was recognized as a contributor to

sedimentary OM. We found that OM associated with coral reef components, not previously recognized as an important contributor of OM to marine sediments, could adequately explain the C:N:P and C- and N-isotopic composition of the bulk OM pool in He‘eia Fishpond and Kane‘ohe Bay sediments (Chapter 4). Further detailed study of individual components of coral (i.e. tissue, mucus, gametes) revealed unique and complex signatures of coral derived OM (Chapter 5).

One of the important outcomes of our study was a recognition that organic carbon to total nitrogen (OC:TN) ratios were not as robust an indicator of OM source to marine sediments as organic carbon to organic phosphorus (OC:OP) ratios, principally for two reasons: (i) the more restricted dynamic range of OC:TN ratios prevents clear distinction of terrestrial- from marine-derived OM, and (ii) post-depositional changes in OC:TN ratios occurring during diagenesis obscure the source signature of initially deposited OM (Chapter 4). Quantifying OP in sediments affords important constraints for assessments of sedimentary OM source and reactivity, and provides an objective basis for understanding OM reactivity and preservation potential.

In addition to quantifying bulk sedimentary OP, we introduce a novel selective extraction method for separately identifying labile OP in marine sediments (Chapter 3). This extraction step can be combined with the more standard SEDEX method for separate quantification of different forms of P in marine sediments (Ruttenberg 1992), and allows accurate quantification of labile OP as distinct from more refractory OP quantified in the final step of the SEDEX method. The ability to separately quantify labile OP is essential for quantifying living biomass P and labile non-living OP, the pools most likely to generate mineralized P to support new cycles of primary production. The selectivity and efficiency Pre-extraction technique we describe may be particularly important for application to aquatic suspended particulates or newly deposited bottom sediments, which may be dominated by labile, cellular material.

In order to quantify the organic carbon content of the carbonate-rich sediments of our study sites, we found it necessary to modify well-established methods for carbon and nitrogen quantification and isotopic analysis (Chapter 2). Once developed, this method allowed us to examine the lability of OM delivered to differing depositional environments along a land-to-sea transect that included sites characterized by carbonate rich sediments

(Chapter 4-6). The high permeability of the carbonate-rich reef sands that characterize sites at the distal end of our transect act as biocatalytical particle filter systems that rapidly decompose OM and support high rates of water column productivity (Chapter 5), features that were only apparent once the ability to accurately quantify OC in these carbonate sediments was secured.

The contrast between the OM content, OM source and lability at the sites arrayed along the land-to-sea transect occupied in this study afforded insight into understanding the importance of organic matter source on rates of OM remineralization. Rates of O_2 consumption, H_2S production, and NH_4^+ accumulation were used as proxies for microbial OM remineralization, and these rates were systematically compared between sediment cores collected along a shore-perpendicular transect (Chapter 4). Our findings demonstrate that higher remineralization rates are observed at sites characterized by more labile, marine-dominated OM, and progressively slower remineralization rates are observed as the fraction of terrestrial, and therefore more refractory, OM increases. Thus, lability and OM source plays an integral role in OM decomposition rates and production of porewater metabolites. Similar findings were obtained in our coral-spawning study, wherein episodic inputs of labile OM resulted in rapid remineralization of OM and benthic efflux of nutrients (Chapter 5).

Microbially mediated OM degradation proceeds by successive use of oxidants beginning with those that yield the greatest quantity of free energy per mole of organic carbon respired, to progressively less energy efficient metabolic pathways, generally following the oxidant sequence: O_2, NO_3^-, oxides of Mn and Fe, and SO_4^{2-}. (Figure 6.1) (e.g., Froelich et al. 1979; Canfield et al. 1993; Burdige 2006). The presence of oxygen plays an important role in OM remineralization, both as an oxidant in the OM remineralization processes, and as an oxidant for reduced diagenetic products. The depth of oxygen penetration into sediments is controlled by the source and transport of OM and dissolved O_2 to marine sediments, as well as the consumption processes within sediments (Chapter 4 and 6). In Chapter 6, we show that the depth of O_2 penetration influences the concentration and depth of ferrous iron accumulation in sediment porewaters as well as the depth at which hydrogen sulfide is detected. The influence of O_2 on porewater redox reactions has been well documented on seasonal time-scales (Colman and Holland 2000; Jørgensen 1996), however we have illustrated that these processes can oscillate on short, diurnal times-scales. Benthic

photosynthesis and respiration influence the distribution of redox reactive chemical species; O_2 penetration is greatest during daylight hours and both Fe^{2+} and H_2S are undetectable in the sediment core; however, as nighttime respiration commences, O_2 is depleted in the surface sediments, porewater Fe^{2+} accumulates and the anoxic redox transition boundary shoals upwards (Chapter 6). Our work illustrates the coupling of redox boundaries spanning spatial scales of cm, and we hypothesize that these boundaries are connected via biologically mediated electrical currents, as has recently been proposed by Nielsen et al. (2010).

The quantity of OM deposited within a given site plays an important role in the net production rate of porewater metabolites. Larger quantities of OM deposited at a given site results in larger quantities of regenerated inorganic nutrients in a given amount of time, and consequently can generate larger benthic nutrient fluxes, even if the specific remineralization rate was lower. This was illustrated in all three field studies: the benthic flux calculations of the incubation cores (Chapter 4) and sediments influenced by the deposition of labile coral spawn-derived OM (Chapter 5), as well as the net production rates calculated at each study site in the diurnal experiments (Chapter 6). At all study sites examined in this research, NH_4^+ profiles were used to estimate metabolite production, whereas a lack of PO_4^{3-} accumulation was observed in sediment porewaters. We hypothesize that the sediments sequester liberated porewater PO_4^{3-} produced during OM remineralization, and that the sequestration pathway (Fe-bound P versus authigenic Ca-P) depends upon sediment mineralogy. Despite the absence of PO_4^{3-} accumulation, we observed that porewater DOP builds up in oxic surface sediments, a result consistent with the idea of differential sorption immobilization of DOP versus phosphate (Chapter 6). These results suggest that organic nutrients may play a crucial role in sediment nutrient cycling, and should be investigated in tandem with inorganic nutrient analyses of sediment porewaters.

Nutrient cycles in shallow, near shore environments can be profoundly influenced by sediments, via the burial or release of nutrients through diagenetic OM remineralization. Depending upon the relative loading of different nutrients that escape sediments and enter overlying waters, the relative proportion of essential nutrients (reflected by nutrient ratios) that efflux into overlying waters can shift phytoplankton community composition, selecting for certain phytoplankton over others. This process is evident in the coral spawn project (Chapter 5), wherein efflux of nutrients from sediment degradation of labile OM resulted

triggered a diatom bloom in the overlying water column. Other episodic events that deliver large qualities of OM to coastal sediments, such as storm events and resultant fluvial inputs, will also increase the rate of OM degradation and benthic efflux, and have the potential to influence primary production in the water column.

The outcomes of this work contribute significantly to our understanding of OM remineralization and preservation in coastal waters. This study places constraints on sources and sinks of bioavailable nutrient inventories in coastal sediments, and subsequent influence on coastal water nutrient ratios and productivity. As such, the processes examined throughout this dissertation can shed light on delivery of bioavailable nutrients from coastal waters to the open ocean.

References

Aller, R. C. 1994. Bioturbation and remineralization of sedimentary organic matter: effects of redox oscillation. Chem. Geol. **114:** 331-345.

Aller, R. C., N. E. Blair, Q. Xia, and P. D. Rude. 1996. Remineralization rates, recycling, and storage of carbon in Amazon shelf sediments. Continental Shelf Research **16:** 753-786.

Aller, R. C., A. Hannides, C. Heilbrun, and C. Panzeca. 2004. Couplilng of early diagenetic processes and sedimentary dynamics in tropical shelf environments: the Gulf of Papua deltaic complex. Continental Shelf Research **24:** 2455-2486.

Ames, J., L.L. 1959. The genesis of carbonate apatites. Economic Geology **54:** 829-841.

Anderson, G. M. 1976. Error propagation by the Monte Carlo method in geochemical calculations. Geochimica et Cosmochimica Acta **40:** 1533-1538.

Anderson, W. T., and J. W. Fourqurean. 2003. Intra- and interannual variability in seagrass carbon and nitrogen stable isotopes from south Florida, a preliminary study. Organic Geochemistry **34:** 185-194.

Anshutz, P., S. Zhong, B. Sunby, A. Mucci, and C. Gobeil. 1998. Burial efficiency of phosphorus and the geochemistry of iron in continental margin sediments. Limnology and Oceanography **43:** 53-64.

Apprill, A., and M. S. Rappè. 2011. Response of the microbial community to coral spawning in lagoon and reef flat environments of Hawaii, USA. Aquatic Microbial Ecology **62:** 251-266.

Arai, T., M. Kato, A. J. Heyward, Y. Ikeda, T. Iizuka, and T. Maruyama. 1993. Lipid-composition of positively buoyant eggs of reef building corals. Coral Reefs **12:** 71-75.

Arrigo, K. R. 2005. Marine microorganisms and global nutrient cycles. Nature **437:** 349-355.

Aspila, K. I., H. Agemian, and A. S. Y. Chau. 1976. A semi-automated method for the determination of inorganic, organic and total phosphate in sediments. Analyst **101:** 187-197.

Atkinson, M. J., and S. V. Smith. 1983. C:N:P ratios of benthic marine plants. Limnology and Oceanography **28:** 568-574.

Baird, A. H., J. R. Guest, and B. L. Willis. 2009. Systematic and biogeographical patterns in the reproductive biology of scleractinian corals. Annual Review of Ecology Evolution and Systematics **40:** 551-571.

Baird, A. H., M. S. Pratchett, D. J. Gibson, N. Koziumi, and C. P. Marquis. 2001. Variable palatability of coral eggs to a planktivorous fish. Marine and Freshwater Research **52:** 865-868.

Baldwin, D. S., J. K. Beattie, M. L. Coleman, and D. R. Jones. 1995. Phosphate ester hydrolysis facilitated by mineral phases. Environ. Sci. and Tech. **29:** 1706-1709.

Bartlett, R., R. J. G. Mortimer, and K. Morris. 2008. Anoxic nitrification: Evidence from Humber Estuary sediments (UK). Chemical Geology **250:** 29-39.

Berner, R. A. 1977. Stoichiometric models for nutrient regeneration in anoxic sediments. Limnology and Oceanography **22:** 781-786.

---. 1980. Early diagenesis: A theoretical approach. Princeton University Press.

---. 1982. Burial of organic carbon and pyrite sulfur in the modern ocean: its geochemical and environmental significance. American Journal of Science **282:** 451-473.
---. 1989. Biogeochemical cycles of carbon and sulfur and their effect on atmospheric oxygen over phanerozoic time. Palaeoceanography, Palaeoclimatology, Palaeoecology **75:** 97-122.
Bidigare, R. R., L. Van Heukelem, and C. C. Trees. 2005. Analysis of algal pigments by high-performance liquid chromatography, p. 327-344. *In* R. Andersen [ed.], Algal Culturing Techniques. Academic Press.
Blackburn, T. H. 1979. Method for measuring rates of NH_4^+ turnover in anoxic marine sediments, using ^{15}N-NH_4^+ dilution technique. Applied and Environmental Microbiology **37:** 760-765.
Bladwin, D. S., J. K. Beattie, and D. R. Jones. 1996. Hydrolysis of an organic phosphorus compound by iron-oxide impregnated filter papers. Water Research **30:** 1123-1126.
Bligh, E. G., and W. J. Dyer. 1959. A rapid method of total lipid extraction and purificiation. Can. J. Physiol. Pharmacol. **37:** 911-917.
Boatman, C. D., and J. W. Murray. 1982. Modeling exchangeable NH_4^+ adsorption in marine sediments: Process and controls of adsorption. Limnology and Oceanography **27:** 99-110.
Boudreau, B. P. 1997. Diagenetic models and their implementation, 1 ed. Springer.
Bray, J. T., O. P. Bricker, and B. N. Troup. 1973. Phosphate in interstitial waters of anoxic sediments: Oxidation effects during sampling procedure. Science **180:** 1362-1364.
Brendel, P. J., and G. W. Luther. 1995. Development of a gold amalgam voltammetric microelectrode for the determination of dissolved Fe, Mn, O_2, and S(-II) in porewaters of marine and freshwater sediments. Environmental Science and Technology **29:** 751-761.
Briggs, R. A. 2011. Organic matter remineralization in coastal sediments in and around Kane‘ohe Bay, Hawai‘i. University of Hawai‘i.
Briggs, R. A., and K. C. Ruttenberg. 2011. Labile organic phosphorus pre-extraction: an adaptation to the SEDEX method.
Briggs, R. A., K. C. Ruttenberg, and B. T. Glazer. 2007. Diurnal shifts in surficial oxygen in sandy versus muddy sediments. ASLO Aquaitc Sciences Meeting.
Briggs, R. A., K. C. Ruttenberg, A. E. Ricardo, and B. T. Glazer. 2011. Linking source, abundance, and lability of organic matter to sediment remineralization rates and redox conditions. Marine Chemistry **in prep**.
Bryant, W. R., W. Hoffman, and P. T. Trabant. 1975. Permeability of unconsolidated and consolidated marine sediments, Gulf of Mexico. Marine Geotechnology **1:** 1-13.
Burdige, D. J. 2006. Geochemistry of marine sediments. Princeton University Press.
---. 2007. Preservation of organic matter in marine sediments: Controls, mechanisms, and an imbalance in sediment organic carbon budgets? Chemical Review **107:** 467-485.
Canfield, D. E. 1989. Reactive iron in marine sediments. Geochimica et Cosmochimica Acta **53:** 619-632.
Canfield, D. E. and others 1993. Pathways of organic carbon oxidation in three continental margin sediments. Marine Geology **113:** 27-40.
Canfield, D. E., and B. Thamdrup. 2009. Towards a consistent classification scheme for geochemical environments, or, why we wish the term ‘suboxic’ would go away. Geobiology **7:** 385-392.

Carey, E., and M. Taillefert. 2005. The role of soluble Fe(III) in cycling of iron and sulfur in coastal marine sediments. Limnology and Oceanography **50:** 11129-11141.
Cembella. 1984. Environmental (extracellular) phosphorus compounds and their utilization. from: Cembella et al. 1984 CRC Crit Rev. Microbiol. **10:** 319-327.
Cembella, A. D., N. J. Antia, and P. J. Harrison. 1984. The utilization of inorganic and organic phosphorous compounds as nutrients by eukaryotic microalgae: A multidisciplinary perspective: Part I. In: CRC Critical Reviews in Microbioogy **10:** 317-391.
Cloern, J. E., E. A. Canuel, and D. Harris. 2002. Stable carbon and nitrogen isotope composition of aquatic and terrestrial plants of the San Francisco Bay estuarine system. Limnology and Oceanography **47:** 713-729.
Colman, A. S., and H. D. Holland. 2000. The global diagenetic flux of phosphorus from marine sediments to the ocean: redox sensitivity and the control of atmospheric oxygen levels. Marine Authigenesis: From Global to Microglobal, SEPM, special publication **66:** 53-75.
Cornelisen, C. D., S. R. Wing, K. L. Clark, M. H. Bowman, R. D. Frew, and C. L. Hurd. 2007. Patterns in the d13C and d15N signature of Ulva pertusa: Interaction between physical gradients and nutrient source pools. Limnology and Oceanography **52:** 820-832.
Cowie, G. L., and J. I. Hedges. 1992. Sources and reactivities of amino acids in a coastal marine environment. Limnology and Oceanography **37:** 703-724.
Decottignies, P., P. G. Beninger, Y. Rince, R. Robins, J. , and P. Riera. 2007. Exploitation of natural food sources by two sympatric, invasive suspension-feeders: Crassostrea gigas and Crepidula fornicata. Marine Ecology Progress Series **334:** 179-192.
Deniro, M. J., and S. Epstein. 1977. Mechanisms of carbon isotope fractionation associated with lipid synthesis. Science **197:** 261-263.
Dyhrman, S. T., and B. P. Palenik. 1999. Phosphate stress in cultures and field populations of the dinoflagellate *Prorocentrum minimum* detected by a single-Cell alkaline phosphatase assay. Applied and Environmental Microbiology **65:** 3205-3212.
Dyhrman, S. T., and K. C. Ruttenberg. 2006. Presence and regulation of alkaline phosphatase activity in eukaryotic phytoplankton from the coastal ocean: Implications for dissolved organic phosphorus remineralization. Limnology and Oceanography **51:** 1381-1390.
Eyre, B. D., and J. P. Ferguson. 2006. Impact of a flood event on benthic and pelagic coupling in a sub-tropical east Australian estuary (Brunswick). Estuarine, Coastal and Shelf Science **66:** 111-112.
Eyre, B. D., R. N. Glud, and N. Patten. 2008. Mass coral spawning: A natural large-scale nutrient addition experiment. Limnology and Oceanography **53:** 997-1013.
Fourqurean, J. W., J. C. Zieman, and G. V. N. Powell. 1992. Relationships between porewater nutrients and seagrasses in a subtropical carbonate environment. Marine Biology **114:** 57-65.
Fox, L. E. 1993. The chemistry of aquatic phosphate: inorganic processes in rivers. hydrobiologia **253:** 1-16.
Freudenthal, T., T. Wagner, F. Wenzhöfer, M. Zabel, and G. Wefer. 2001. Early diagenesis of organic matter from sediments of the eastern subtropical Atlantic: evidence from

stable nitrogen and carbon isotopes. Geochimica et Cosmochimica Acta **65:** 1795-1808.
Froelich, P. 1980. Analysis of organic carbon in marine sediments. Limnology and Oceanography **25:** 564-572.
Froelich, P. N. and others 1979. Early oxidation of organic matter in pelagic sediments of the eastern equatorial Atlantic: suboxic diagenesis. Geochim et Cosmochim Acta **43:** 1075-1090.
Furnas, M., A. Mitchell, M. Skuza, and J. Brodie. 2005. In the outer 90%: Phytoplankton responses to enhanced nutrient availability in the Great Barrier Reef Lagoon. Marine Pollution Bulletin **51:** 253-263.
Gearing, P., F. E. Plucker, and P. L. Parker. 1977. Organic carbon stable isotope ratios of continental sediments. Marine Chemistry **5:** 251-266.
Gibbs, R. J. 1977. Effects of combustion temperature and time, and of the oxidation agent used in organic carbon and nitrogen analysis of marine sediment and dissolved organic material. Journal of Sedimentary Petrology **47:** 547-550.
Gjettermann, B., M. Styczen, S. Hansen, O. K. Borggaard, and H. C. B. Hansen. 2007. Sorption and fractionation of dissolved organic matter and associated phosphorus in agricultural soil. J. Environ. Qual. **36:** 753-763.
Glud, R. N., B. D. Eyre, and N. Patten. 2008. Biogeochemical responses to mass coral spawning at the Great Barrier Reef: Effects on respiration and primary production. Limnology and Oceanography **53:** 1014-1024.
Goni, M. A. 1997. 32. Record of terrestrial organic matter composition in Amazon fan sediments. *In* R. D. Flood, Piper, D.J. W., and Peterson, L.C. [ed.], Proceedings of the Ocean Drilling Program , Scientisif Results.
Goñi, M. A., and J. I. Hedges. 1995. Sources and reactivities of marine-derived organic matter in coastal sediments as determined by alkaline CuO oxidation. Geochim Cosmochim Acta **59:** 2965-2981.
Goñi, M. A., K. C. Ruttenberg, and T. I. Eglinton. 1997. Sources and contributions of terrigenous organic carbon to surface sediments in the Gulf of Mexico. Nature **389:** 275-278.
---. 1998. A reassessment of the sources and importance of land-derived organic matter in surface sediments from the Gulf of Mexico. Geochimica et Cosmochimica Acta **62:** 3055-3075.
Grasshoff, K., M. Ehrhardt, and K. K. (Eds). 1983. Methods of seawater analysis, 2nd ed. Verlag Chemie.
Grottoli, A. G., L. J. Rodrigues, and C. Juarez. 2004. Lipids and stable carbon isotopes in two species of Hawaiian corals, *Porites compressa* and *Montipora verrucosa*, following a bleaching event. Marine Biology **145:** 621-631.
Grundmanis, V., and J. W. Murray. 1977. Nitrification and denitrification in marine sediments from Puget Sound. Limnology and Oceanography **22:** 804-813.
Guest, J. 2008. How reefs respond to mass coral spawning. Science **320:** 621-623.
Gunnars, A., and S. Blomqvist. 1997. Phosphate exchange across the sediment-water interface when shifting from anoxic to oxic conditions an experimental comparison of freshwater and brackish-marine systems. Biogeochemistry **37:** 203-226.

Harrison, P. L., and C. C. Wallace. 1990. Reproduction, dispersal and recruitment of scleractinian corals, p. 133-207. *In* Z. Dubinsky [ed.], Ecosystems of the world, coral reefs. Elsevier Science Publishers B.V.

He, Z. L., V. C. Baligar, D. C. Martens, and K. D. Ritchey. 1998. Determination of soluble phosphorus in the presence of organic ligands or fluoride. Soil Scienc Society of America **62:** 1538-1541.

Healey, F. P., and L. L. Hendzel. 1980. Physiological indicators of nutrient deficiency in lake phytoplankton. Can. J. Fish. Aquat. Sci. **37:** 442-453.

Heath, R. T., T. C. Moore, and J. P. Dauphin. 1977. Organic carbon in deep-sea sediments, p. 605-625. *In* N. R. Anderson and A. Malanhoff [eds.], The fate of fossil fuel CO2 in the oceans. Plenum Press.

Hecky, R. E., and P. Kilham. 1988. Nutrient limitation of phytoplankton in freshwater and marine environments: a review of recent evidence on the effects of enrichment. Limnology and Oceanography **33:** 796-822.

Hedges, J., and J. Stern. 1984. Carbon and nitrogen determinations of carbonate-containing solids. Limnology and Oceanography **29:** 657-663.

Hedges, J. I., and R. G. Keil. 1995. Sedimentary organic matter preservation: an assessment and speculative synthesis. Marine Chemistry **49:** 81-115.

Hedges, J. I., and P. L. Parker. 1976. Land-derived organic matter in surface sediments from the Gulf of Mexico. Geochimica et Cosmochimica Acta **40:** 1019-1029.

Hemminga, M. A., and M. A. Mateo. 1996. Stable carbon isotopes in seagrasses: variability in ratios and use in ecological studies. Marine Ecology Progress Series **140:** 285-298.

Hemminga, M. A., F. J. Slim, J. Kazungu, G. M. Ganssen, J. Nieuwenhuize, and N. M. Kruyt. 1994. Carbon outwelling from a mangrove forest with adjacent seagrass beds and coral reefs (Gazi Bay, Kenya). Marine Ecology Progess Series **106:** 291-301.

Hillebrand, H., and U. Sommer. 1999. The nutrient stoichiometry of benthic microalgal growth: Redfield proportions are optimal. Limnology and Oceanography **44:** 440-446.

Hodgson, G. 1985. Abundance and distribution of planktonic larvae in Kane'ohe Bay, Oahu, Hawaii. Marine Ecology Progess Series **26:** 61-71.

Hoegh-Guldberg, O., L. Muscatine, C. Goiran, D. Siggaard, and G. Marion. 2004. Nutrient-induced perturbations to delta13C and delta15N in symbiotic dinoflagellates and their coral hosts. Marine Ecology Progress Series **280:** 105-114.

Huerta-Diaz, M. A., and J. W. Morse. 1992. Pyritization of trace metals in anoxic marine sediments. Geochim et Cosmochim **56:** 2681-2702.

Huettel, M., and G. Gust. 1992. Impact of bioroughness on interfacial solute exchange in permeable sediments. Marine Ecology Progess Series **89:** 253-267.

Hulth, S., R. C. Aller, and F. Gilbert. 1999. Coupled anoxic nitrification/manganese reduction in marine sediments. Geochimica Cosmochimica Acta **63:** 49-66.

Hunter, C. L. 1988. Environmental cues controlling spawning in two Hawaiian corals, *Montipora verrucosa* and *M. dilatata*. Proc 6th Int Coral Reef Symp **2:** 727-732.

Hunter, C. L., and C. W. Evans. 1995. Coral Reefs in Kaneohe Bay, Hawaii: Two centuries of western influence and two decades of data. Bulletin of Marine Science **57:** 501-515.

Hyacinthe, C., and P. Van Cappellen. 2004. An authigenic iron phosphate phase in estuarine sediments: composition, formation and chemical reactivity. Marine Chemistry **91:** 227-251.

Ingall, E., and R. Jahnke. 1997. Influence of water-column anoxia on the elemental fractionation of carbon and phosphorus during sediment diagenesis. Marine Geology **139:** 219-229.

Ingall, E. D., P. A. Schroeder, and R. A. Berner. 1990. The nature of organic phosphorus in marine sediments: New insights from 31P NMR. Geochim Cosmochim Acta **54:** 2617-2620.

Jahnke, R., M. Richards, J. Nelson, C. Robertson, A. Rao, and D. Jahnke. 2005. Organic matter remineralization and porewater exchange rates in permeable South Atlantic Bight continental shelf sediments. Continental Shelf Research **25:** 1433-1452.

Jahnke, R. A., J. R. Nelson, R. L. Marinelli, and J. E. Eckman. 2000. Benthic flux of biogenic elements on the Southeastern US continental shelf: influence of pore water advective transport and benthic microalgae. Continental Shelf Research **20:** 109-127.

Jannsen, F., M. Huettel, and U. Witte. 2005. Pore-water advection and solute fluxes in permeable marine sediments (II): Benthic respiration at three andy sites with different permeabilities (German Bight, North Sea). Limnology and Oceanography **50:** 779-792.

Jensen, H. S., P. B. Mortensen, F. O. Andersen, E. Rasmussen, and A. Jensen. 1995. Phosphorus cycling in a coastal marine sediment, Aarhus Bay, Denmark. Limnology and Oceanography **40:** 908-917.

Jensen, H. S., and B. Thamdrup. 1993. Iron-bound phosphorus in marine sediments as measured by bicarbonate-dithionite extraction. hydrobiologia **253:** 47-59.

Jokiel, P. L., E. K. Brown, A. Friedlander, S. K. Rodgers, and W. R. Smith. 2004. Hawaii Coral Reef Assessment and Monitoring Program: Spatial patterns and temporal dynamics in reef coral communities. Pacific Science **58:** 145-158.

Jorgensen, B. B. 1983. Processes at the sediment - water interface, p. 478-509. *In* B. Bolin and R. Cook [eds.], In: The Major Biogeochemical Cycles and Their Interactions, SCOPE 21,.

Jørgensen, B. B. 1996. Material flux in the sediment, p. 115-135. *In* B. B. Jørgensen and K. Richardson [eds.], Eutrophication in coastal marine ecosystems. American Geophysical Union.

Jørgensen, B. B., and K. Richardson. 1996. Eutrophication in coastal marine ecosystems. American Geophysical Union, Coastal and Estuarine Studies.

Karl, D. M., D. V. Hebel, K. Bjorkman, and R. M. Letelier. 1998. The role of dissolved organic matter release in the productivity of the oligotrophic North Pacific Ocean. Limnology and Oceanography **43:** 1270-1286.

Kelly, M. 2000. Loko I'a O He'eia, p. 50. Bernice Pauahi Bishop Estate.

Kennett, J. P. 1982. Marine Geology. Prentice Hall.

Kikuchi, W. 1976. Prehistoric Hawaiian Fishponds. Science **193:** 295-299.

Kinzie, R. A. 1996. Modes of speciation and reproduction in Archaeocoeniid corals. Galaxea **13:** 47-64.

Klump, J. V., and C. S. Martens. 1987. Biogeochemical cycling in an organic-rich coastal marine basin; 5, Sedimentary nitrogen and phosphorus budgets based upon kinetic

models, mass balances, and the stoichiometry of nutrient regeneration. Geochimica et Cosmochimica Acta **51:** 1161-1173.
Kolinski, S. P., and E. F. Cox. 2003. An update on modes and timing of gamete and planula release in Hawaiian scleractinian corals with implications for conservation and management. Pacific Science **57:** 17-27.
Komada, T., M. R. Anderson, and C. L. Dorfmeier. 2008. Carbonate removal from coastal sediments for the determination of organic carbon and its isotopic signatures, $\delta^{13}C$ and $\Delta^{14}C$: comparison of fumigation and direct acidification by hydrochloric acid Limnology and Oceanography Methods **6:** 254-262.
Kostka, J. E., B. Thamdrup, R. N. Glud, and D. E. Canfield. 1999. Rates and pathways of carbon oxidation in permanently cold Arctic sediments. Marine Ecology Progess Series **180:** 7-21.
Krall, P., C. P. Slomp, A. Forster, M. M. M. Kuypers, and A. Sluijs. 2009. Pyrite oxidation during sample storage determines phosphorus fractionation in carbonate-poor anoxic sediments. Geochim Cosmochim Acta **73:** 3277-3290.
Krom, M. D., and R. A. Berner. 1980. Adsorption of phosphate in anoxic marine sediments. Limnology and Oceanography **25:** 797-806.
Laarkamp, K. 2000. Organic phosphorus in marine seidments: Chemical structure, diagenetic alteration, and mechanisms of preservation. Massachusetts Institute of Technology.
Lapointe, B., M. Littler, and D. Littler. 1992. Nutrient availability to marine macroalgae in siliciclastic versus carbonate-rich coastal waters. Estuaries and Coasts **15:** 75-82.
Larned, S. T. 1998. Nitrogen- versus phosphorus-limited growth and sources of nutrients for coral reef macroalgae. Marine Biology **132:** 409-421.
Laws, E. A., and C. B. Allen. 1996. Water quality in a subtropical embayment more than a decade after sewage discharges. Pacific Science **50:** 194-210.
Lee, M., W. Bae, J. Chung, H.-S. Jung, and H. Shim. 2008. Seasonal and spatial characteristics of seawater and sediment at Youngil bay, Southeast Coast of Korea. Marine Pollution Bulletin **57:** 325-334.
Lehmann, M. F., S. M. Bernasconi, A. Barbieri, and J. A. Mckenzie. 2002. Preservation of organic matter and alteration of its carbon and nitrogen isotope composition during simulated and in situ early sedimentary diagenesis. Geochimica et Cosmochimica Acta **66:** 3573-3584.
Levasseur, M. E., P. J. Harrison, and J.-C. Theriault. 1990. Simultaneous nitrogen and silicate deficiency of a phytoplankton community in a coastal jet-front. Marine Biology **104:** 329-338.
Likens, G. E., F. H. Bormann, and N. M. Johnson. 1981. Interaction between major biogeochemical cycles in terrestrial ecosystems, p. 93-112. *In* G. E. Likens [ed.], Some Perspectives of the Major Biogeochemical Cycles-SCOPE 17. Wiley.
Lilienfein, J., R. G. Qualls, S. M. Uselman, and S. D. Bridgham. 2004. Adsorption of dissolved organic and inorganic phosphorus in soils of a weathering chronosequence. Soil Sci Soc Am J **68:** 620-628.
Loneragan, N. R., S. E. Bunn, and D. M. Kellaway. 1997. Are mangroves and seagrasses sources of organic carbon for penaeid prawns in a tropical Australian estuary? A multiple stable-isotope study. Marine Biology **130:** 289-300.

Lukkari, K., H. Hartikainen, and M. Leivuori. 2007. Fractionation of sediment phosphrus revisited: I fraction steps and their biogeochemical basis. Limnology and Oceanography Methods **5:** 433-444.

Luther, G. W. 2005. Acid volatile sulfide-A comment. Marine Chemistry **97:** 198-205.

Luther, G. W. and others 1998. Simultaneous measurement of O_2 , Mn, Fe, I^-, and S^{2-} in marine pore waters with a solid-state voltammetric microelectode. Limnology and Oceanography **43:** 325-333.

---. 2008. Use of voltammetric solid-state (micro)electrodes for studying biogeochemical processes: Laboratory measurements to real time measurements with an in situ electrochemical analyzer (ISEA). Marine Chemistry **108:** 221-235.

Luther, G. W., B. Sundby, B. L. Lewis, P. J. Brendel, and N. Sliverberg. 1997. Interactions of manganese with the nitrogen cycle: alternative pathways to dinitrogen. Geochimica Cosmochimica Acta **61:** 4043-4052.

Luther Iii, G. W. and others 2008. Use of voltammetric solid-state (micro)electrodes for studying biogeochemical processes: Laboratory measurements to real time measurements with an in situ electrochemical analyzer (ISEA). Marine Chemistry **108:** 221-235.

Mackin, J. E., and R. C. Aller. 1984. Ammonium adsorption in marine sediments. Limnology and Oceanography **29:** 250-257.

Maier, C., M. G. Weinbauer, and J. Patzoid. 2010. Stable isotopes reveal limitations in C and N assimilation in the Caribbean reef corals *Madracis aurentenra, M. carmabi* and *M. formosa*. Marine Ecology Progess Series **412:** 103-112.

Mcglathery, K. J., P. Berg, and R. Marino. 2001. Using porewater profiles to assess nutrient availability in seagrass-vegetatd carbonate sediments. Biogeochemistry **56:** 239-263.

Mcgroddy, M. E., T. Daufresne, and L. O. Hedin. 2004. Scaling of C:N:P stoichiometry in forests worldwide: Implications of terrestrial Redfield-type ratios. Ecology **85:** 289-302.

Mckee, K. L., I. C. Feller, M. Poppe, and W. Wanek. 2002. Mangrove isotopic ($\delta^{15}N$ and $\delta^{13}C$) fractionation across a nitrogen vs. phosphorus limitation gradient. Ecology **83:** 1065-1075.

Mcmanus, J., W. M. Berelson, K. H. Coale, K. S. Johnson, and T. E. Kilgore. 1997. Phosphorus regeneration in continental margin sediments. Geochimica et Cosmichimica Acta **61:** 2891-2907.

Meyers, P. A. 1994. Preservation of elemental and isotopic source identification of sedimentary organic matter. Chemical Geology **114:** 289-302.

---. 1997. Organic geochemical proxies of paleoceanographic, paleolimnologic, and paleoclimatic processes. Organic Geochemistry **27:** 213-250.

Meysman, F. J. R., and J. J. Middelburg. 2005. Acid-volatile sulfide (AVS)-A comment. Marine Chemistry **7:** 206-212.

Middelburg, J. J., and J. Nieuwenhuize. 1998. Carbon and nitrogen stable isotopes in suspended matter and sediments from the Schelde Estuary. Marine Chemistry **60:** 217-225.

Mills, G. L., and J. G. Quinn. 1979. Determination of organic carbon in marine sediments by persulfate oxidation. Chemical Geology **25:** 155-162.

Monaghan, E., and K. C. Ruttenberg. 1999. Dissolved organic phosphorus in the coastal ocean: Reassessment of available methods and seasonal phosphorus profiles from the Eel River Shelf. Limnology and Oceanography **44:** 1702-1714.

Monbet, P., I. D. Mckelvie, and P. J. Worsfold. 2009. Dissolved organic phosphorus speciation in the waters of the Tamar estuary (SW England). Geochimica et Cosmochimica Acta **73:** 1027-1038.

Moosmann, L., R. Gachter, B. Muller, and A. Wuest. 2006. Is phosphorus retention in autochthonous lake seidmnets controlled by oxygen or phosphorus? Limnology and Oceanography **51:** 763-771.

Morse, J., and F. T. Mackenzie. 1990. Geochemistry of sedimentary carbonates. Elsevier Publishing Co.

Mortimer, R. J. G. and others 2004. Anoxic nitrification in marine sediments. Marine Ecology Progess Series **276:** 37-51.

Muller-Parker, G., C. B. Cook, and C. F. D'elia. 1994. Elemental composition of coral Pocillopora damicornis exposed to elevated seawater ammonium. Pac Sci **48:** 234-246.

Muscatine, L., C. Goiran, L. Land, J. Jaubert, J.-P. Cuif, and D. Allemand. 2004. Stable isotopes (d13C and d15N) of organic matrix from coral skeleton. Proceedings of the National Academy of Sciences **102:** 1525-1530.

Muscatine, L., J. W. Porter, and L. R. Kaplan. 1989. Resource partitioning by reef corals as determined from stable isotope com- position. I. δ13C of zooxanthellae and animal tissue versus depth. Marine Biology **100:** 185-193.

Nealson, K. H. 2010. Geomicrobiology: Sediment reactions defy dogma. Nature **463:** 1033-1034.

Nedwell, D. B., R. J. Parkes, A. C. Upton, and D. J. Assinder. 1993. Seasonal fluxes across the sediment-water interface, and processes within sediments. Philosophical Transactions of the Royal Society of London. Series A: Physical and Engineering Sciences **343:** 519-529.

Nielsen, L. P., N. Risgaard-Petersen, H. Fossing, P. B. Christensen, and M. Sayama. 2010. Electric currents couple spatially separated biogeochemical processes in marine sediment Nature **463:** 1071-1074.

Ogrinc, N., G. Fontolan, J. Faganeli, and S. Covelli. 2005. Carbon and nitrogen isotope compositions of organic matter in coastal marine sediments (the Gulf of Trieste, N Adriatic Sea): indicators of sources and preservation. Marine Chemistry **95:** 163-181.

Oliver, J. K., and B. L. Willis. 1987. Coral spawn slicks in the Great Barrier Reef: preliminary observations. Marine Biology **94:** 521-529.

Padilla-Gamino, J. L., T. Weatherby, R. G. Waller, and R. D. Gates. 2011. Formation and structural organization of the egg-sperm bundle of the scleractinian coral *Montipora capitata*. Coral Reefs **30:** 371-380.

Peterson, B. J., and R. W. Howarth. 1987. Sulfur, carbon, and nitrogen isotopes used to trace organic matter flow in the salt-marsh estuaries of Sapelo Island, Georgia. Limnology and Oceanography **32:** 1195-1213.

Pratchett, M. S., N. Gust, G. Goby, and S. O. Klanten. 2001. Consumption of coral propagules represents a significant trophic link between corals and reef fish. Coral Reefs **20:** 13-17.

Redfield, A. C., B. H. Ketchum, and F. A. Richards. 1963. The influence of organisms on the composition of sea-water, p. 26-77. *In* M. N. Hill [ed.], The Sea. Interscience.
Revsbech, N. P., B. B. Jørgensen, T. H. Blackburn, and Y. Cohen. 1983. Microelectrode studies of the photosynthesis and O_2, H_2S, and pH profiles of a microbial mat. Limnology and Oceanography **28:** 1062-1074.
Rice, D. L., and R. B. Hanson. 1984. A kinetic model for detritus nitrogen: The role of the associated microflora in nitrogen accumulation. Bulletin of Marine Science **35:** 326-340.
Richmond, R. H., and C. L. Hunter. 1990. Reproduction and recruitment of corals - comparisons among the Caribbean, the Tropical Pacific, and the Red-Sea. Marine Ecology Progess Series **60:** 185-203.
Rickard, D., and J. W. Morse. 2005. Acid volatile sulfide (AVS). Marine Chemistry **97:** 141-197.
Ringuet, S., and F. T. Mackenzie. 2005. Controls on nutrient and phytoplankton dynamics during normal flow and storm runoff conditions, Southern Kaneohe Bay, Hawaii. Estuaries **28:** 327-337.
Risgaard-Petersen, N. and others 2004. Anaerobic ammonium oxidation in an estuarine sediment. Aquatic Microbial Ecology **36:** 293-304.
Roden, E. E., and J. M. Edmond. 1997. Phosphate mobilization in iron-rich anaerobic sediments: microbial Fe(III) oxide reduction versus iron-sulfide formation. Arch. Hydrobiol. **139:** 347-378.
Rodrigues, L. J., and A. G. Grottoli. 2006. Calcification rate and the stable carbon, oxygen, and nitrogen isotopes in the skeleton, host tissue, and zooxanthellae of bleached and recovering Hawaiian corals. Geochimica Cosmochimica Acta **70:** 281-2789.
---. 2007. Energy reserves and metabolism as indicators of coral recovery from bleaching. Limnology and Oceanography **52:** 1874-1882.
Rosenfeld, J. K. 1979. Ammonium adsoption in nearshore anoxic sediments. Limnology and Oceanography **24:** 356-364.
Rozan, T. F. and others 2002. Iron-sulfur-phosphorus cycling in the sediments of a shallow coastal bay: Implications for sediment nutrient release and benthic macroalgal blooms. Limnology and Oceanography **47:** 1346-1354.
Ruttenberg, K. C. 1992. Development of a sequential extraction method for different forms of phosphorus in marine sediments. Limnology and Oceanography **37:** 1460-1482.
---. 2003. The global phosphorus cycle, p. 585-643. Treatise on Geochemistry. Elsevier.
Ruttenberg, K. C., and R. A. Berner. 1993. Authigenic apatite formation and burial in sediments from non-upwelling, continental margin environments. Geochim Cosmochim Acta **57:** 991-1007.
Ruttenberg, K. C., and S. T. Dyhrman. 2005. Temporal and spatial variability of dissolved organic and inorganic phosphorus, and metrics of phosphorus bioavailability in an upwelling-dominated coastal system. Journal of Geophysical Research **110:** C10S13.
Ruttenberg, K. C., and M. A. Goñi. 1995. Characterization of organic carbon:phosphorus ratios in arctic, temperate, and tropical coastal sediments, p. 1147-1149. 17th International Meeting on Organic Geochemistry.
---. 1997a. Depth trends in phosphorus distribution and C:N:P ratios of organic matter in Amazon fan sediments: Indices of organic matter source and burial history. Proceedings of the Ocean Drilling Program Scientific Results **155:** 505-517.

---. 1997b. Phosphorus distribution, C:N:P ratios, and $\delta^{13}C_{oc}$ in arctic, temperate, and tropical coastal sediments: tools for characterizing bulk sedimentary organic matter. Marine Geology **139:** 123-145.
Ruttenberg, K. C., N. O. Ogawa, F. Tamburini, R. A. Briggs, N. D. Colasacco, and E. Joyce. 2009. Improved, hgh-throughout approach for phosphorus speciation in natural sediments via the SEDEX sequential extraction method. Limnology and Oceanography Methods **7:** 319-333.
Ruttenberg, K. C., and D. J. Sulak. 2011. Sorption and desorption of dissolved organic phosphorus onto iron (oxyhydr)oxides in seawater. Geochimica et Cosmochimica Acta **75:** 4095-4112.
Rysgaard, S., K. Finster, and H. Dahlgaard. 1996. Primary production, nutrient dynamics and mineralisation in a northeastern Greenland fjord during the summer thaw. Polar Biology **16:** 497-506.
Sanudo-Wilhelmy, S. A., A. Tovar-Sanchez, F.-X. Fu, D. G. Capone, E. J. Carpenter, and D. A. Hutchins. 2004. The impact of surface-adsorbed phosphorus on phytoplankton Redfield stoichiometry. **432:** 897-901.
Schuffert, J. D., M. Kastner, and R. A. Jahnke. 1998. Carbon and phosphorus burial associated with modern phosphorite formation. Marine Geology **146:** 21-31.
Scott, M. J., and J. J. Morgan. 1990. Energetics and conservative properties of redox systems, p. 368-378. Chemical Modeling of Aqueous Systems II. ACS Symposium Series. American Chemical Society.
Shchenau, S. J., and G. J. De Lange. 2000. A novel chemical method to quanitfy fish debris in marine sediments. Limnology and Oceanography **45:** 963-971.
Shepherd, R. G. 1989. Correlations of permeability and grain size. Groundwater **7:** 633-638.
Shlesinger, Y., and Y. Loya. 1985. Coral community reproductive patterns: Red Sea versus the Great Barrier Reef. Science **228:** 1333-1335.
Silverman, S. R., R. K. Fuyat, and J. D. Weiser. 1952. Quantitative determination of calcite associated with carbonate-bearing minerals. American Mineralogist **37:** 211-222.
Simpson, C. J., J. L. Cary, and R. J. Masini. 1993. Destruction of corals and other reef animals by coral spawn slicks on Ningaloo Reef, Western Australia. Coral Reefs **12:** 185-191.
Slomp, C. P., E. H. G. Epping, W. Helder, and W. Van Raaphorst. 1996. A key role for iron-bound phosphorus in authigenic apatite formation in North Atlantic continental platform sediments. Journal of Marine Research **54**.
Slomp, C. P., J. F. P. Malschaert, and W. Van Raaphorst. 1998. The role of adsorption in sediment-water exchange of phosphate. Limnology and Oceanography **43:** 832-946.
Stimson, J., and S. T. Larned. 2000. Nitrogen efflux from the sediments of a subtropical bay and the potential contribution to macroalgal nutrient requirements. Journal of Experimental Marine Biology and Ecology **252:** 159-180.
Stumm, W., and J. J. Morgan. 1981. Aquatic chmistry. Wiley Interscience.
Sundby, B., C. Gobeil, N. Silverberg, and A. Mucci. 1992. The phosphorus cycle in coastal marine sediments. Limnology and Oceanography **37:** 1129-1145.
Suzumura, M., and I. Koike. 1995. Application of solid-phase extraction technique for determination of phosphorus in sediment extract. Geochemical Journal **29:** 331-335.
Szmant, A. M. 2002. Nutrient enrichment on coral reefs: Is it a major cause of coral reef decline? Estuaries **25:** 743-766.

Taillefert, M., V. C. Hover, T. F. Rozan, S. M. Theberge, and G. W. Luther. 2002a. The influence of sulfides on soluble organic-Fe(III) in anoxic sediment porewaters. Estuaries **25:** 1088-1096.

Taillefert, M., T. F. Rozan, B. T. Glazer, J. Herszage, R. E. Trouwborst, and G. W. Luther. 2002b. Seasonal variations of soluble organic-Fe(III) in sediment porewaters as revealed by voltammetric microelectrodes, p. 247-264. *In* M. Taillefert and T. F. Rozan [eds.], Environmental Electrochemistry: Analysis of trace element biogeochemistry. American Chemical Society Symposium Series.

Thamdrup, B., and D. E. Canfield. 1996. Pathways of carbon oxidation in continental margin sediments off central Chile. Limnology and Oceanography **41:** 1629-1650.

Thamdrup, B., and T. Dalsgaard. 2002. Production of N_2 through anaerobic ammonium oxidation coupled to nitrate reduction in marine sediments. Applied and Environmental Microbiology **68:** 1312-1318.

Trimmer, M., J. C. Nicholls, and B. Deflandre. 2003. Anaerobic ammonium oxidation measured in sediments along the Thames Estuary, United Kingdom. Applied and Environmental Microbiology **69:** 6447-6454.

Tsandev, I. 2010. The global marine phosphorus cycle: response to climate change and feedbacks on ocean biogeochemistry. Doctor of Philosophy. Utrecht University.

Verardo, D., P. Froelich, and A. Mcintyre. 1990. Determination of organic carbon and nitrogen in marine sediments using the Carolo Erba NA-1500 Analyzer. Deep-Sea Research **37:** 157-165.

Vink, S., R. M. Chambers, and S. V. Smith. 1997. Distribution of phosphorus in sediments from Tomales Bay, California. Marine Geology **139:** 157-179.

Wallace, C. C. 1985. Reproduction, recruitment and fragmentation in nine sympatric species of the coral genus *Acropora*. Marine Biology **88:** 217-233.

Westneat, M. W., and J. M. Resing. 1988. Predation on coral spawn by planktivorous fish. Coral Reefs **7:** 89-92.

Wild, C., A. Haas, M. Naumann, C. Mayr, and M. El-Zibday. 2008. Comparative investigation of organic matter release by corals and benthic reef algae-implications for pelagic and benthic microbial metabolism. Proceedings of the 11th Inernational Coral Reef Symposium.

Wild, C., M. Huettel, A. Klueter, S. G. Kremb, M. Y. M. Rasheed, and B. B. Jørgensen. 2004a. Coral mucus functions as an energy carrier and particle trap in the reef ecosystem. Nature **428:** 66-70.

Wild, C., C. Jantzen, U. Struck, O. Hoegh-Guldberg, and M. Huettel. 2007. Biogeochemical responses following coral mass spawning on the Great barrier Reef: pelagic-benthic coupling. Coral Reefs **DOI 10.1007/s00338-007-0298-7**.

Wild, C., R. Tollrian, and M. Huettel. 2004b. Rapid recycling of coral mass-spawning products in permeable reef sediments. Marine Ecology Progess Series **271:** 159-166.

Wild, C., H. Woyt, and M. Huettel. 2005. Influence of coral mucus on nutrient fluxes incarbonate sands. Marine Ecology Progress Series **287:** 87-98.

Willis, B. L., R. C. Babcock, P. L. Harrison, and J. K. Oliver. 1985. Patterns in the mass spawning of corals on the Great Barrier Reef from 1981 to 1984, p. 343-348. Proceedings of the Fifith International Coral Reef Congress.

Wooller, M., B. Smallwood, U. Scharler, M. Jacobson, and M. Fogel. 2003. A taphonomic study of $\delta^{13}C$ and $\delta^{15}N$ values in Rhizophora mangle leaves for a multi-proxy approach to mangrove palaeoecology. Organic Geochemistry **34:** 1259-1275.

Wu, J., W. Sunda, E. A. Boyle, and D. M. Karl. 2000. Phosphate depletion in the western North Atlantic Ocean. Science **289:** 759-762.

Yamamuro, M., H. Kayanne, and M. Minagawa. 1995. Carbon and nitrogen stable isotopes of primary producers in coral reef ecosystems. Limnology and Oceanography **40:** 617-621.

Young, C. W. I. 2011. Perturbation of nutrient inventories and phytoplankton community composition during sotrm events in a tropical coastal system: He'eia Fishpond, O'ahu, Hawai'i. Master of Science. University of Hawaii at Manoa.